BASEMENT TECTONICS 12

Proceedings of the International Conferences on Basement Tectonics

VOLUME 6

The titles published in this series are listed at the end of this volume.

BASEMENT TECTONICS 12

Central North America and Other Regions

Proceedings of the Twelfth International Conference on Basement Tectonics, held in Norman, Oklahoma, U.S.A., May 1995

Edited by

JOHN P. HOGAN
and
M. CHARLES GILBERT

School of Geology and Geophysics,
University of Oklahoma,
Norman, Oklahoma, U.S.A.

SPRINGER SCIENCE+BUSINESS MEDIA, B.V.

A C.I.P. Catalogue record for this book is available from the Library of Congress.

ISBN 978-94-010-6141-4 ISBN 978-94-011-5098-9 (eBook)
DOI 10.1007/978-94-011-5098-9

Printed on acid-free paper

Originally published by Kluwer Academic Publishers in 1998
Softcover reprint of the hardcover 1st edition 1998

CONTENTS

Conference committees xi

Trustees xiii

Sponsors xv

Foreword xvii

Part I Selected Articles

Petrologic constraints on the tectonic evolution of the Llano uplift
W.D. Carlson 3

Geologic provinces of Oklahoma
R.A. Northcutt and J.A. Campbell 29

The Southern Oklahoma Aulacogen: a Cambrian analog for Mid-Proterozoic AMCG (Anorthosite-Mangerite-Charnockite-Granite) complexes?
J.P. Hogan and M.C. Gilbert 39

Surface and near-surface investigation of the alteration of the Mount Scott Granite and geometry of the Sandy Creek Gabbro pluton, Hale Spring area, Wichita Mountains, Oklahoma
J.D. Price, J.P. Hogan, M.C. Gilbert and J. Payne 79

Multiple reactivations of rigid basement block margins: examples in the northern Reading Prong, U.S.A.
A.E. Gates and R.E. Costa 123

The Variscan geodynamic cycle in the Sardinian-Corsican Massif, according to the most recent data
N. Minzoni 155

Geological and geophysical exploration for uranium mineralization in the El-Eredyia prospect area, Central Eastern Desert, Egypt
S.I. Rabie, A.A. Abdel-Meguid and A.S. Assran 169

Seismic imaging beneath thrust blocks
Z.M. Liu and R.A. Young 191

Part II Abstracts

Petrology and tectonic significance of the Polly Wright Cove pluton, Blue Ridge Province, Virginia: an extension-related, multiply-intrusive magmatic system of anorogenic origin
W.J. Abbey, R.P. Tollo and J.N. Aleinikoff 209

Basement-involved and detached phases of deformation in the evolution of fold-thrust belts: examples from the southern Cordilheira do Espinhaço and the Paramirim deformation corridor, Brazil
F.F. Alkmim and A. Danderfer Fº 211

Evolution of the Late Proterozoic basement in the northern Appalachian orogenic system and implications for the Ouachita system
P.J. Barosh 213

The north-trending swarm of Mesozoic dikes in the southern Appalachians: its map pattern and significance for Mesozoic extension
M.J. Bartholomew 215

Crustal tectonic controlling metallogenies from Paleozoic to Tertiary in the North Patagonian region, Argentina
H.G.L. Bassi 217

Early Proterozoic ductile reworking of Archean basement in the central Laramie range: a complex response to the Cheyenne belt, trans-Hudson and central plains orogens
R.L. Bauer, D.A. Gresham and J.D. Edson 219

Propagation of high angle, dip-slip basement fault zones into overlying sedimentary rocks
L.A. Boldt 223

Geologic provinces of Oklahoma
J.A. Campbell and R.A. Northcutt 225

Evidence from the stratigraphic record for basement deformation in southeastern Nebraska, midcontinent U.S.A.
M.P. Carlson 227

Petrologic constraints on the tectonic evolution of the Llano uplift
W. Carlson 229

Proterozoic evolution of the Llano uplift, central Texas: evidence for high-pressure metamorphism from the Oxford mafic body
J. Davidow and W. Carlson 231

Dikes in the Precambrian of the eastern Arbuckle mountains
R.E. Denison 233

Neoproterozoic continental-scale transpression megazone in eastern Brazil
I. Endo and R. Machado 235

Multiple reactivations of major fault zones in the northern Reading prong, U.S.A.
A.E. Gates and R. Costa 239

Structural evolution of Cima termine area, Val Venosta (northern Italy)
G.O. Gatto and N. Minzoni 241

On fracture development in rock subjected to compression
L.N. Germanovich, K.K. Lee, J-C. Roegiers and A.V. Dyskin 243

The characteristics and tectonic evolution of the basement of the collision orogenic belt on the southeastern margin of the Yangtze plate
X. Guizhong and W. Yifen 245

Revised granite-gabbro age relationships, southern Oklahoma aulacogen, U.S.A.
W.E. Hames, J.P. Hogan and M.C. Gilbert 247

Late Precambrian strike-slip fault system of the Wichita-Amarillo mountains as delineated by detailed aeromagnetic data
B.W. Hawley and S.P. Gay, Jr. 251

Crustal growth during continental rifting: an example from the southern Oklahoma aulacogen
J.P. Hogan, M.C. Gilbert, J.E. Wright and M. Deggeller 253

Integrated petrologic and sedimentologic studies of a late Neoproterozoic rift basin within the Grenvillian basement of Virginia
F.E. Hutson and R.P. Tollo 257

Structural imprint of the Wichita mountains frontal zone on overlying sediments
A.C. Lambert and R.A. Young 259

Plastic deformation as a factor of material transformation of rocks (southern Tien Shan)
M.G. Leonov 261

Evolution of Proterozoic granitoids, eastern Arbuckle mountains, Oklahoma
E.G. Lidiak 265

Seismic imaging beneath thrust blocks
Z. Liu and R.A. Young 267

Seismicity and tectonic relationships of north central Oklahoma
K.V. Luza 269

Distribution of Phanerozoic faulting and folding, seismicity, and ore deposits in the midcontent region, U.S.A.: a reflection widespread Proterozoic rifting in the North American craton?
S. Marshak and T.S. Paulsen 271

The Variscan geodynamic cycle in the Sardinian-Corsican massif
N. Minzoni and M. Minzoni 275

The influence of structural position and lithology on the fracture distribution in the east Kaibab monocline southeastern Utah: implications for fluid flow properties
P.N. Mollema, A. Aydin and D.D. Pollard 277

Evolution of Grenville tectonic provinces, southeastern Llano uplift, central Texas
S. Mosher, R.C. Roback and J.F. Reese 279

Anatomy of the Grenville orogen in west Texas
K.C. Nielsen, K. Soegaard and M.E. Bickford 281

Halokinetic associated crustal stretching in the southern Red Sea: new observations of the basement and sedimentary cover from refraction constrained reflection seismic stratigraphy
J.D. Pigott, E.S. Gebretsadik and A. Alahdahl 283

Partial melting of Mount Scott granite at 850°C and 500 bars
J.D. Price, J.P. Hogan, G.B. Morgan VI, D. London and M.C. Gilbert 285

Investigation of the Mount Scott granite drill core, Wichita mountains, Oklahoma
J.D. Price, J.P. Hogan, J. Payne and M.C. Gilbert 287

Geological and geophysical exploration for uranium mineralization on Ei-Erediya prospect area, central eastern desert, Egypt
S.I. Rabie, A.A.A. Meguid and A.S. Assran 289

Nature and age of ductile deformation associated with the "anorogenic" Town Mountain granite, Llano uplift, central Texas
R.M. Reed, R.C. Roback and M.A. Helper 291

Interdependency of mechanical and chemical processes during the evolution of chloritic breccia, Sacramento mountains, southeastern California
J. Schweitzer 293

Factors affecting limiting angles for fault reactivation in basement rocks
T.B. Scott, Jr. 295

Lead isotope mapping of crustal reservoirs within the Grenville superterrane: central and southern Appalachians
A.K. Sinha 297

Petrology and geochemistry of a late proterozoic anorgenic supersuite, Laurentian Appalachians, Virginia and North Carolina: implications for magma-generation associated with cratonic extension
R.P. Tollo and F.F. Hutson 299

The role of recurrent tectonics in the formation of the Nemaha uplift and Cherokee-Forest City basins and adjacent structural features in eastern Kansas and contiguous states, U.S.A.
F.W. Wilson and P. Berendsen 301

COCORP southwestern Oklahoma siesmic lines revisited
R.A. Young and A.C. Lambert 305

CONFERENCE ORGANIZING COMMITTEES

CHAIR

M. Charles Gilbert
School of Geology and Geophysics, University of Oklahoma, Norman, Oklahoma 73019-0628 USA

FIELD TRIP CHAIR

John P. Hogan
School of Geology and Geophysics, University of Oklahoma, Norman, Oklahoma 73019-0628 USA

FIELD TRIP LEADERS

S. Mosher, M. Helper, D. Barker, and R. Reed
Department of Geological Sciences, University of Texas at Austin, Austin, Texas 78712 USA

R. E. Denison
Department of Geosciences, University of Texas at Dallas, Richardson, Texas 75083 USA

E. G. Lidiak
Department of Geology and Planetary Science, University of Pittsburgh, Pittsburgh, Pennsylvania 15260 USA

M. C. Gilbert and J. P. Hogan
School of Geology and Geophysics, University of Oklahoma, Norman, Oklahoma 73019-0628 USA

MEETING MANAGER

Sara Moody
School of Geology and Geophysics, University of Oklahoma, Norman Oklahoma 73019-0628 USA

CONFERENCE THEMES AND ORGANIZING COMMITTEES

Fracture Development, Reactivation, and Mineralization

M. J. Bartholomew
Earth Sciences and Resources Institute, University of South Carolina, Columbia, South Carolina 29802 USA
S. Marshak
Department of Geology, University of Illinois, Urbana, Illinois 61801 USA

Evolution of the Basement of the North American Plate (with special emphasis on its southern margin)

R. E. Denison
Department of Geosciences, University of Texas at Dallas, Richardson, Texas 75083 USA
E. G. Lidiak
Department of Geology and Planetary Science, University of Pittsburgh, Pittsburgh, Pennsylvania 15260 USA

Probing of Basement: Geophysical and Geochemical Methods

R. A. Young
School of Geology and Geophysics, University of Oklahoma, Norman Oklahoma 73019-0628 USA
G. R. Keller
Department of Geological Sciences, University of Texas at El Paso, El Paso, Texas 79968-0555 USA

Response of Cover Rocks to Basement Deformation

P. Berendsen
Kansas Geological Survey, University of Kansas, Lawrence Kansas 66047 USA
M. P. Carlson
Nebraska Geological Survey, University of Nebraska, Lincoln, Nebraska 68588-0517 USA

INTERNATIONAL BASEMENT TECTONICS ASSOCIATION, Inc.
675 South 400 East, Salt Lake City, Utah 84111 USA

TRUSTEES
(1994-1996)

CHAIR
Mervin J. Bartholomew
Earth Sciences and Resources Institute
University of South Carolina
Columbia, South Carolina 29802
USA

VICE CHAIR
M. Charles Gilbert
School of Geology and Geophysics
University of Oklahoma
Norman, Oklahoma 73019-0628
USA

TREASURER
William. J. Hinze
Department of Earth and Atmospheric Sciences
Purdue University
West Lafayette,Indiana 49707
USA

SECRETARY
Donald U. Wise
Department of Geosciences
Franklin and Marhshall College
Lancaster, Pennsylvania 17604
USA

TRUSTEE
Stephen Marshak
Department of Geology
University of Illinois
Urbana, Illinois 61801
USA

SPONSORS

The 12th international conference on "Basement Tectonics" held in Norman Oklahoma USA, from May 21st to May 26th 1995 was sponsored by the School of Geology and Geophysics of the University of Oklahoma and the Oklahoma Geological Survey.

FOREWORD

The 12th International Basement Tectonics Conference was hosted by the School of Geology and Geophysics and the Oklahoma Geological Survey in the Sarkeys Energy Center on the campus of the University of Oklahoma, Norman, Oklahoma, U.S.A., from May 21st through May 26th, 1995. A total of 52 individuals were in attendance, 9 of which were attending from 6 different foreign countries.

Four days of oral and poster presentations were divided into four technical sessions with the following themes: 1) Fracture Development, Reactivation, and Mineralization, organized by M. J. Bartholomew and S. Marshak; 2) Evolution of the Basement of the North American Plate (with special emphasis on its southern margin), organized by R. E. Denison and E. G. Lidiak; 3) Probing of Basement: Geophysical and Geochemical Methods, organized by R. A. Young and G. R. Keller; and 4) Response of Cover Rocks to Basement Deformation, organized by P. Berendsen and M. P. Carlson. Seventy-five presentations were made during the course of the meeting, which was organized by Program Chairman M. Charles Gilbert and professionally managed by Sara Moody.

Preceding the meeting was a two day field trip to examine the mode and kinematics of terrane accretion during closure of an ocean basin, as preserved in the Precambrian geology of the eastern Llano Uplift, Texas, U.S.A. The field trip leaders Sharon Mosher, Mark Helper, Don Barker, and Robert Reed provided an excellent and comprehensive guidebook, and shared their considerable expertise in many discussions at one spectacular exposures after another. All registrants participated in the mid-conference field trip guided by R. E. Denison, E. G. Lidiak, M. C. Gilbert, and John P. Hogan to examine the Precambrian and Cambrian basement terranes exposed in the Arbuckle Mountains uplift in southern Oklahoma, U.S.A. Evidence for a possible continental arc setting for the southern margin of the ~1.4 Ga Granite-Rhyolite Terrane, the opening of the Cambrian Southern Oklahoma Aulacogen as evidenced by a spectacular exposure of a diabase dike swarm, and the role of earlier tectonic fabrics in the development of younger structures were some of the topics of discussion. The two day post conference field trip to the Wichita Mountains uplift, southwestern Oklahoma, U.S.A. was led by M. Charles Gilbert, and John P. Hogan. This trip highlighted the Cambrian Southern Oklahoma Aulacogen. The trip had several focal points: 1) rock response to stress in the brittle regime at high and low temperature; 2) shallow (low pressure) magma emplacement and crystallization, including the formation of subhorizontal sheet-like batholiths; 3) layered mafic complexes; 4) rift-related magmatism, including A-type granites; and the character of the aulacogen basement.

The conference volume is divided into two parts: submitted proceedings papers, of which two were rejected; and abstracts of papers and posters presented at the meeting. The papers represent various aspects of the themes of the meeting, and represent important contributions demonstrating the pivotal role "basement" studies play in understanding the evolution of the lithosphere and in better management of resources. The editors acknowledge the considerable effort and patience of the conference participants, authors, reviewers, as well as S. Moody, in bringing this volume to completion, and thank the sponsors for their kind and generous support.

PART I

SELECTED ARTICLES

PETROLOGIC CONSTRAINTS ON THE TECTONIC EVOLUTION OF THE LLANO UPLIFT

WILLIAM D. CARLSON
University of Texas at Austin
Department of Geological Sciences
Austin Texas 78712 USA

1. Abstract

Tectonic models for the Proterozoic evolution of the Llano Uplift must account for a polymetamorphic history dominated by two kinematically distinct events. Early dynamothermal metamorphism took place at moderate to high pressures and decreased in intensity from southwest to northeast across the uplift. Late largely static metamorphism at lower pressures resulted from a thermal event linked to regionally widespread emplacement of granitic intrusions at relatively shallow levels in the crust.

Relict mineral assemblages that provide thermobarometry for the early event are preserved only in a few localities, but regional patterns of prograde growth zoning in garnet demonstrate that the Uplift as a whole underwent early high-grade metamorphism at elevated pressure. The dominant mineral assemblages in the uplift, characteristic of low-pressure metamorphism in the middle amphibolite facies, commonly overprint deformational fabrics with static recrystallization textures. In key calc-silicate localities, these later assemblages are genetically linked by evidence from phase equilibria and stable-isotope compositions to the widespread intrusion of granitic plutons.

The petrologic evidence is consistent with emerging tectonic models that invoke southwestward subduction of the Proterozoic margin of the continent. Subsequent uplift of deeply buried rocks to shallow crustal levels, where major pulses of granitic intrusion took place as deformation waned, was more pronounced in the southwest than in the northeast.

2. Introduction

At present, petrologic information relevant to basement tectonics in the Llano Uplift of central Texas (USA) is widely scattered throughout the literature. This article is a synoptic review of metamorphism in the Uplift,

providing a synthesis of the data that yield constraints on regional tectonics during the mid-Proterozoic along the southern margin of the North American continent. In some instances, earlier data are reinterpreted here in light of revised thermobarometric calibrations and in consideration of new field and petrographic observations made since the original work appeared.

2.1 GEOLOGIC SETTING

The Precambrian rocks of the Llano Uplift (Figure 1) are best regarded as the metamorphic core of a collisional orogen in which island-arc, oceanic, and arc-flank / continental slope assemblages were accreted to the southern margin of North America (Mosher *in* Rankin et al., 1993). These Middle Proterozoic rocks are part of the westward extension into Texas of the Grenville terrane that stretches from the Grenville province of Canada through the Adirondacks of New York to outliers within the Appalachians (Rankin et al., 1993). Like these other regions, the Llano Uplift underwent orogeny ca. 1100-1200 Ma and experienced a largely post-tectonic thermal event ca. 1000-1100 Ma (Walker, 1992; Roback et al., 1994; Reese, 1995; Rougvie et al., 1996).

Recent geochronologic work, principally U-Pb dating of zircon, has demonstrated that strongly deformed metamorphic units defined on the basis of lithologic similarity are made up of multiple components that have formed at different times in unrelated tectonic settings, with precursor ages that span a range from 1324 Ma to 1215 Ma (Walker, 1992; Roback et al., 1994; Reese, 1995). These metamorphic rocks are dominantly comprised of reworked older crust, with both igneous and sedimentary precursors, to which tonalitic and granitic intrusives were added during synkinematic magmatic activity. The rocks display strongly transposed layering and multiple generations of structures and fabrics, but these features are heavily overprinted in most cases by static recrystallization textures (Carter, 1989; Nelis et al., 1989; Reese, 1995).

During a protracted period of relatively shallow intrusion, numerous large granitic plutons were emplaced whose crystallization ages range from 1133 Ma to 1070 Ma (Walker, 1992). Although a few of the older of these plutons exhibit some ductile deformation features, most do not, suggesting that the intrusive episode began as regional deformation waned (Reed et al., 1995).

The age of the youngest precursor to the strongly deformed metamorphic units and the age of the oldest (largely) non-deformed granitic pluton constrain the timing of orogenesis to the period between 1215 Ma and 1133 Ma.

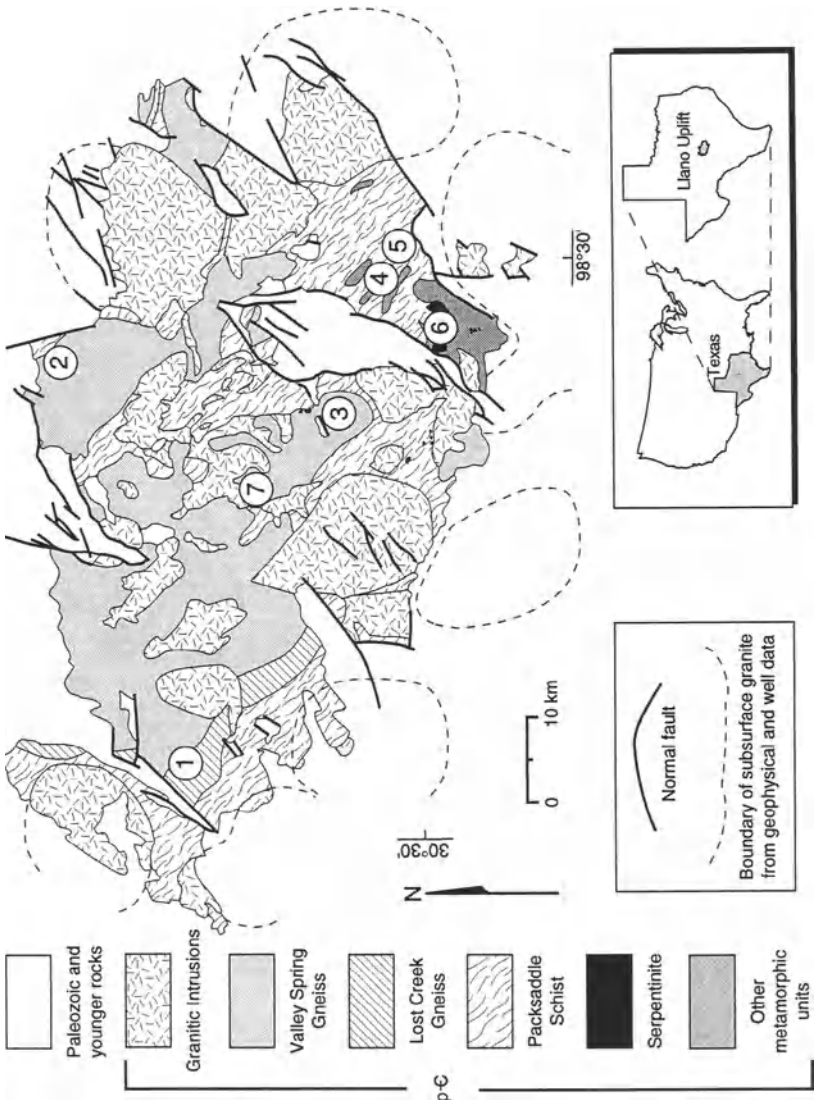

Figure1. Generalized geologic map of the Llano Uplift, showing localities described in text.

2.2 OVERVIEW OF METAMORPHISM IN THE LLANO UPLIFT

Two sequential, kinematically distinct, thermal episodes are now recognized as dominantly responsible for metamorphism in the Llano Uplift. Early metamorphism was synchronous with regional deformation during the contractional phase of orogeny, but reheating and hydration synchronous with late-syn- to post-orogenic granitic intrusion has strongly overprinted the early event by modifying textures, mineral assemblages, and mineral compositions. In most rocks, recrystallization in the later episode has markedly obscured or even obliterated the petrologic character of the early event.

Most studies undertaken prior to the mid-1980s did not recognize the existence of two discrete metamorphic episodes, did not discriminate clearly between mineral assemblages produced in each episode, or did not consider partial re-equilibration of early-formed assemblages during later metamorphism. As a result, early estimates of metamorphic conditions in the Llano Uplift range widely and are sometimes mutually inconsistent. Most petrologic work over the last decade has been directed toward segregating the mineralogic effects of the two metamorphic events, to permit meaningful thermobarometric analysis. These efforts have recently quantified the pressures and temperatures that characterize each event, thereby placing constraints on tectonic models for the region.

The picture that has emerged is that much, and probably all, of the Uplift was affected by early Barrovian-series metamorphism under conditions in the transitional region of overlap among the amphibolite, granulite, and eclogite facies. Mineral assemblages produced in this event, however, have survived only in rare localities scattered about the Uplift because of widespread and intense overprinting during a subsequent amphibolite-facies Buchan-series event.

To distinguish between the two events, they have been referred to conventionally as the *early high-pressure dynamothermal event* and the *late low-pressure static event*, although the latter designation may be somewhat misleading because recrystallization was not wholly static (Reed et al., 1995), and the "event" probably consists of a long series of scattered incidents of recrystallization that vary in their intensity according to proximity to intrusions, and that are probably asynchronous across the Uplift, occurring over a span of a few tens of millions of years.

Recent work has identified a very early deformation accompanied by metamorphic recrystallization that is apparently confined to the Coal Creek domain in the southeasternmost part of the Uplift (Roback et al., 1994). Unfortunately, metamorphic assemblages that are demonstrably relict from this event and diagnostic of metamorphic conditions have not yet been identified. Consequently, the discussion here is limited to the two metamorphic events that have affected the entire uplift, and the implications

that they hold for basement tectonics in the region.

3. Evidence for Early High-P Dynamothermal Metamorphism

Unambiguous relics of the early high-pressure dynamothermal metamorphism are quite rare. Those that are known invariably display partial re-equilibration to later low-pressure conditions. Well-preserved high-pressure assemblages are also most common in particular (often unusual) bulk compositions, or are localized in the unreacted cores of bodies that are strongly retrogressed at their margins, or are confined to relatively massive or unfractured parts of bodies that elsewhere show significant back-reaction. These modes of occurrence for the high-pressure relics suggest that mineral assemblages diagnostic of such conditions may once have been far more widespread, but were largely obliterated by late low-pressure recrystallization.

This section summarizes first the evidence at individual localities for early synkinematic metamorphism at high pressures, and then the data supporting the hypothesis that the entire Uplift once experienced moderate- to high-pressure metamorphism under a range of conditions corresponding to the region of transition and overlap among the upper-amphibolite facies, the lower-granulite facies, and the medium-T eclogite facies.

3.1 ECLOGITIC REMNANTS

The most conclusive evidence for high pressures during the early event comes from remnants of eclogitic mafic rocks in three localities in the western, northern and south-central parts of the Uplift (Figure 2). To emphasize their high-pressure origin, these rocks are here loosely termed eclogites, using a broad definition to designate mafic rocks that were originally plagioclase-free and dominantly comprised of omphacitic clinopyroxene and pyropic garnet at the peak of metamorphism. Because assemblages are transitional to those of the amphibolite and granulite facies, clinopyroxene in these rocks is more commonly sodian augite than true omphacite, and garnet often contains high spessartine component (Wilkerson et al., 1988; Carlson and Johnson, 1991; Davidow, 1996). The intensity of retrogression varies markedly within and among localities, so many of the more retrogressed rocks that retain little of their original mineralogy are perhaps more properly described as garnet amphibolites — although garnet always appears to be unstable, and therefore not part of the low-pressure equilibrium assemblage.

In this section, petrologic data from each of the three localities are summarized, and contrasts among the localities that have tectonic significance are highlighted.

3.1.1 Mason County

The best-preserved eclogite relics are found in scattered outcrops and as float restricted to small areas on the surface in two locations in Mason County in the western uplift (locality 1 on Figure 1). Wilkerson et al. (1988) described two metamafic bodies, the Jordan Ranch body and the Purdy Hill body. Of these, only the Purdy Hill body remains exposed, as a house has recently been built atop the Jordan Ranch body. The two bodies are petrologically very similar, with only very slight differences in mineral chemistry to differentiate them, so they are discussed here in tandem.

Assemblages and textures. The least-retrogressed samples from Mason County preserve the assemblage pyropic garnet + sodian augite + low-Al enstatite + subsilicic ferroan pargasite + rutile (Figure 2A). The pyrope content of garnet and the jadeite content of clinopyroxene classify these rocks among the "Group B" eclogites of Coleman et al. (1965), and clinopyroxene has ratios of jadeite to Tschermak's components that exceed 1:2, the minimum value used by Lovering and White (1969) to differentiate "eclogitic" from "granulitic" clinopyroxene. In contrast to the localities described below, inclusions within garnet are components of the preserved high-pressure assemblage, namely sodian augite, low-Al enstatite, pargasitic amphibole, and rutile. This inclusion assemblage indicates that garnet grew from a plagioclase-absent matrix, *i.e.*, that garnet crystallization took place entirely within the eclogite facies.

Retrogression in these rocks has produced coronal textures in which symplectitic reaction zones of andesine + pargasite + magnetite ± hypersthene separate garnet from original sodian augite; the sodian augite is typically replaced by a symplectite of oligoclase + augite (Figure 2B).

Thermobarometry. Thermobarometry based on exchange equilibria for garnet-clinopyroxene, garnet-orthopyroxene, garnet-amphibole, and clinopyroxene-orthopyroxene pairs yields consistent results indicating equilibration at approximately 750 (±50) °C. These high temperatures are supported by the relative abundance in nearby quartzofeldspathic gneisses of indicators of highly ductile modes of deformation, migmatization, and melt migration.

Pressure estimates, however, are more problematical. Pressures are based on the Al-content of orthopyroxene equilibrated with garnet, but Al is inhomogeneously distributed in orthopyroxene grains. Rims of orthopyroxene crystals (~50 μm thick) often contain 2-4 wt.% Al_2O_3, whereas cores commonly contain just under 1 wt.% Al_2O_3. In the original work (Wilkerson et al., 1988), pressures were calculated from these measurements using the calibration published in Harley (1984). The calculations yielded pressures for rims in the range 8-11 kbar at 750 °C,

and pressures for cores near 30 kbar at 750 °C (and near 20 kbar even at temperatures as low as 500 °C). These estimates were interpreted as recording two successive stages in the high-pressure history of the rocks.

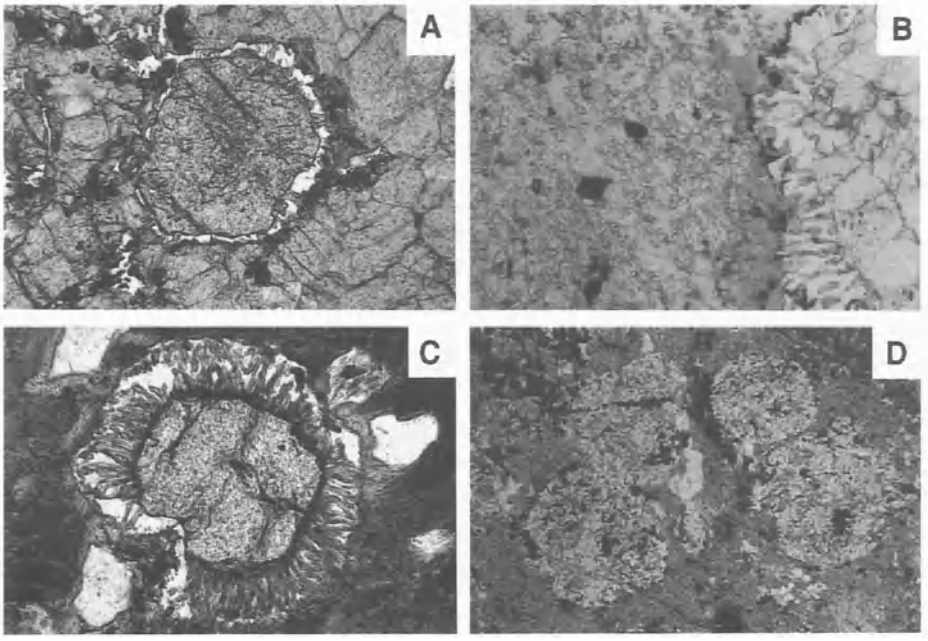

Figure 2. Photomicrographs in plane-polarized light of eclogitic rocks from the Llano Uplift. (**A**) Eclogite from Mason County, western uplift (Sample LU81-24). Pyropic garnet in center shows slight resorption at margins, with development (particularly along right side) of inner zone of plagioclase with minor amphibole surrounded by rim of magnetite + dark-green hornblende. Surrounding sodian augite shows little evidence of retrogression. Long dimension of photograph is 1.2 mm. (**B**) Partially retrogressed eclogite from Mason County, western uplift (same sample as in part A). Garnet (right) is surrounded by sequential coronal reaction rims of amphibole (gray) + plagioclase (white), magnetite (black), and orthopyroxene + amphibole (dark gray). Original sodian augite at left of photo has been partly replaced by a symplectitic intergrowth of oligoclase + augite. Long dimension of photograph is 0.6 mm. (**C**) Strongly retrogressed eclogite from Whitt Ranch, northern uplift. Garnet at center is surrounded by radial symplectite of plagioclase + amphibole, rimmed by a narrow zone of amphibole (medium gray). Matrix is composed of very fine-grained symplectite (dark gray mottled areas) of oligoclase + augite [after omphacite], plus coarse blebs of quartz rimmed by clinopyroxene. Long dimension of photograph is 1.2 mm. (**D**) Fully retrogressed eclogite from Oxford, central uplift. Round patches (light gray) consist of intergrown plagioclase + amphibole + magnetite [after garnet]; surrounding matrix (dark gray) is intimately intergrown oligoclase + augite [both after sodic clinopyroxene] ± hornblende. Long dimension of photograph is 5.9 mm.

Recently, a typographical correction to the Harley (1984) barometer has appeared (Fitzsimons and Harley, 1994) that has forced a re-evaluation of our earlier interpretation. When the corrected equations are used, pressures calculated from orthopyroxene rims adjacent to garnet come out close to 5 kbar — a value so low that it is difficult to reconcile with the eclogitic mineral assemblage, and one not much greater than that assigned to the late low-pressure event (see section 4, below). Corrected pressures calculated from orthopyroxene cores are 15 to 20 kbar at 750 °C.

In light of these results, we have re-examined the distribution of Al in orthopyroxene by generating X-ray maps of entire crystals and by analyzing across orthopyroxene rims at contacts with various other minerals (Davidow, 1996). The results show that high Al contents are present at the margins of orthopyroxene grains where they are adjacent to high Al phases such as garnet, but that at contacts with less aluminous phases, the Al-content of orthopyroxene rims is only slightly enriched relative to core values. Moreover, Al-content in orthopyroxene is slightly enriched in the vicinity of fractures that transect entire grains, whether infilled with later minerals or not. These observations lead to the interpretation that the Al-enrichment represents late-stage equilibration between neighboring grains and between orthopyroxene crystals and fluids in the surrounding matrix. Consequently, the best estimates for pressure of equilibration for the eclogitic assemblage are probably those provided by orthopyroxene core compositions, which range from 15 to 20 kbar at 750 °C (or from 12 to 14 kbar at 500 °C).

3.1.2 Whitt Ranch

A large body (~0.5 km diameter) of mafic rock with petrologic characteristics very similar to the Mason County eclogites is found in the northern uplift, near the community of Babyhead (locality 2 on Figure 1). Known informally as the "Whitt Ranch metagabbro," this intensely studied body preserves its high-pressure history in more subtle ways than do the Mason County rocks. In particular, the Whitt Ranch rocks have been more thoroughly retrogressed. Garnet is abundant, yet surrounded by coronal reaction zones ~200 μm thick, and original omphacitic clinopyroxene is preserved only as rare inclusions within garnet (Carlson and Johnson, 1991). All other original clinopyroxene has back-reacted to very fine-grained symplectites of oligoclase + augite.

Assemblages and textures. Mineral assemblages, mineral compositions, and reaction textures have been documented by Carlson and Johnson (1991). As in the Mason County eclogites, the peak prograde mineral assemblage was dominated by garnet and clinopyroxene (Figure 2C). In the Whitt Ranch body, however, garnet is less magnesian and clinopyroxene is more sodic, whereas blue amphibole inclusions tend to be

somewhat less sodic and more silicic. Although low-Al enstatite is not present in the Whitt Ranch rocks, rare inclusions of rutile are found in garnet rims.

Retrogression in the Whitt Ranch rocks is more widespread and more intense than in the Mason County rocks, and has produced spectacular coronal textures that are chemically, mineralogically and often texturally identical to those in the Mason County occurrence (Carlson and Johnson, 1991). Although no sodic clinopyroxene is preserved except as inclusions within garnets, the matrix surrounding garnets in Whitt Ranch rocks is made up of patches of symplectitic augite + oligoclase (± hornblende) in optical continuity, with mineral chemistry and modes nearly indistinguishable from those that partially replace sodian augite in the Mason County rocks. Because of this similarity and the presence of rare omphacite inclusions in Whitt Ranch garnets, the augite + oligoclase symplectites are interpreted as retrogressive replacements of original crystals of omphacite.

The inclusion suite within garnets of the Whitt Ranch rocks is distinctly different from that of the Mason County rocks. Monomineralic inclusions of quartz, andesine, clinozoisite, pargasitic amphibole, and ilmenite are common in garnet cores, indicating that garnet crystallization began in a matrix with a typical high-pressure amphibolite-facies mineral assemblage. Near the rim of one garnet, however, a few inclusions of omphacite were discovered, and rutile inclusions are also found in garnet rims. This inclusion assemblage near garnet rims, combined with textural evidence for a plagioclase-free matrix rich in sodic clinopyroxene, demonstrates that peak metamorphic conditions were probably within the eclogite facies.

Worthy of special note are polymineralic inclusions within garnet displaying a spatial organization that mimics the sequence of reaction zones that extend outward from garnet, with identical mineral compositions. These "internal corona" features are invariably linked by fractures to the matrix surrounding the garnet. We interpret them as former inclusions of omphacite that reacted with garnet and metamorphic fluids in retrogressive reactions identical to those affecting omphacite at garnet margins.

Thermobarometry. Thermometry based upon Fe-Mg exchange between garnet and clinopyroxene yields 585 (±50) °C; results from garnet-amphibole Fe-Mg exchange thermometry scatter widely about that value. Assemblages suitable for quantitative barometry are absent, but a comparison of inclusion suites, temperatures, and mineral assemblages and chemistry with those for the Mason County rocks suggests that lower pressures of about 6-8 kbar (but perhaps as high as 10 kbar) are reasonable for the Whitt Ranch rocks.

3.1.3 Oxford

Rocks with many similarities to those just discussed are found near the town of Oxford, in the south-central uplift (locality 3 in Figure 1). Originally mapped and described by Collins (1978), this occurrence has recently been subjected to field and petrologic study by Davidow (1996). Lost Hollow Creek contains several excellent exposures of heavily to completely retrogressed metamafic rocks that show strong textural and mineralogical affinity to better preserved eclogitic remnants, particularly those at Whitt Ranch (Figure 2 D).

Assemblages and textures. The Oxford body is chemically distinct in two respects from other occurrences of remnant eclogites in the uplift. In addition to relict pyropic garnet and symplectitic intergrowths of oligoclase + augite after sodic clinopyroxene, Oxford samples contain abundant quartz that appears texturally to have been part of the high-pressure assemblage. The Oxford rocks also have elevated Ti and P contents, with abundant ilmenite and titanite and appreciable apatite present both in the matrix and as inclusions within garnet porphyroblasts.

Matrix symplectites, garnet compositions, and inclusion suites within garnet are very similar to those in the Whitt Ranch rocks, except for the absence at Oxford of omphacite inclusions within garnet, and the rarity of amphibole inclusions. Retrogression at this locality is far more advanced, however, with garnet resorption zones that are 0.5 to 5 mm wide; thus all late-crystallizing garnet (which hosts omphacite and rutile at Whitt Ranch) has been removed by backreaction at Oxford. Although polymineralic inclusions connected by fractures to the matrix are numerous, none bear orthopyroxene, and none show the spatial organization characteristic of the "internal coronas" at Whitt Ranch. The interpretation that garnet crystallization spanned both amphibolite- and eclogite-facies conditions is therefore logical, but less well-supported for the Oxford rocks than for those at Whitt Ranch.

Thermobarometry. Thermometry for the early event at the Oxford locality is restricted to a single determination from an amphibole inclusion inside an originally large but now strongly resorbed garnet. Fe-Mg exchange thermometry yields a temperature, presumably along the prograde path, of 620 (±50?) °C, which should probably be regarded a minimum value for peak metamorphic conditions, insofar as considerable garnet crystallization took place after incorporation of the amphibole inclusion. This temperature implies that peak metamorphic conditions were intermediate between those at Whitt Ranch and those in Mason County. Consequently, based again on mineral assemblages and comparison of inclusion suites and thermometry between this locality and the others, a pressure near 8-10 kbar is assigned for peak metamorphism at Oxford.

3.1.4 Summary

Three known occurrences of eclogite remnants in the uplift appear to span a range of peak metamorphic conditions, from ~750 °C at about 15 kbar in Mason County in the western uplift down to ~585 °C at perhaps 6-8 kbar at the Whitt Ranch in the northern uplift; conditions in the south-central uplift at Oxford appear to be intermediate. Inclusion suites in garnet indicate that the Whitt Ranch and Oxford rocks began crystallizing garnet under upper-amphibolite-facies conditions, then completed crystallization in the eclogite facies, whereas the Mason County rocks reached pressures sufficient to destabilize plagioclase and stabilize sodian augite before the onset of garnet crystallization.

Retrogression, while highly variable in intensity and ubiquity within and between localities, nevertheless appears to have produced nearly identical mineral assemblages and compositions in all three of the eclogite occurrences.

3.2 GEOGRAPHIC PATTERNS OF GARNET HOMOGENIZATION

Homogenization of prograde garnet growth zoning by intracrystalline diffusion occurs over a narrow range of temperature near the transition from the amphibolite to the granulite facies (e.g., Anderson and Olimpio, 1977; Woodsworth, 1977; Yardley, 1977). Because peak metamorphic conditions inferred from the eclogite remnants span this range of temperature, Carlson and Schwarze (1993, 1997) were able to draw petrologic inferences from the geographic patterns of partial homogenization of garnet distributed regionally throughout the uplift (Figure 3).

Geographically systematic variations in the extent of garnet homogenization indicate that the eclogitic bodies are *not* tectonic anomalies that were metamorphosed at greater depths than the rest of the uplift and subsequently emplaced into surrounding rocks that experienced an exclusively low-pressure history. Instead, there is clear evidence that the eclogites formed *in situ*, implying that the uplift as a whole underwent high-pressure metamorphism.

3.2.1 Principles

During prograde metamorphism, unequal partitioning of elements between garnet and coexisting minerals commonly combines with sluggish intracrystalline diffusion to produce compositional zoning in garnet crystals growing at low grade. In the uppermost amphibolite facies, however, diffusion becomes rapid enough to partially or wholly homogenize any zoning produced by garnet growth at lower temperatures.

Quantitative diffusion models demonstrate that only very minor relaxation of compositional profiles in almandine-rich garnet could have

occurred during the late static metamorphism, which reached peak temperatures of only 550 ± 75 °C (section 4, below). Thus the distribution of wholly homogenized, partially homogenized, and unhomogenized growth zoning records regional differences in peak temperatures during the early dynamothermal event.

3.2.2 Systematic Variations in Homogenization across the Uplift

The extent of garnet homogenization varies systematically across the uplift, as shown in Figure 3. In the western uplift, flat interior profiles in the eclogite remnants of Mason County (B) are matched by flat profiles in garnets from nearby calc-schists (A) and pelitic schists (C). In the northern uplift, garnets in the eclogitic remnant at Whitt Ranch (E) and in

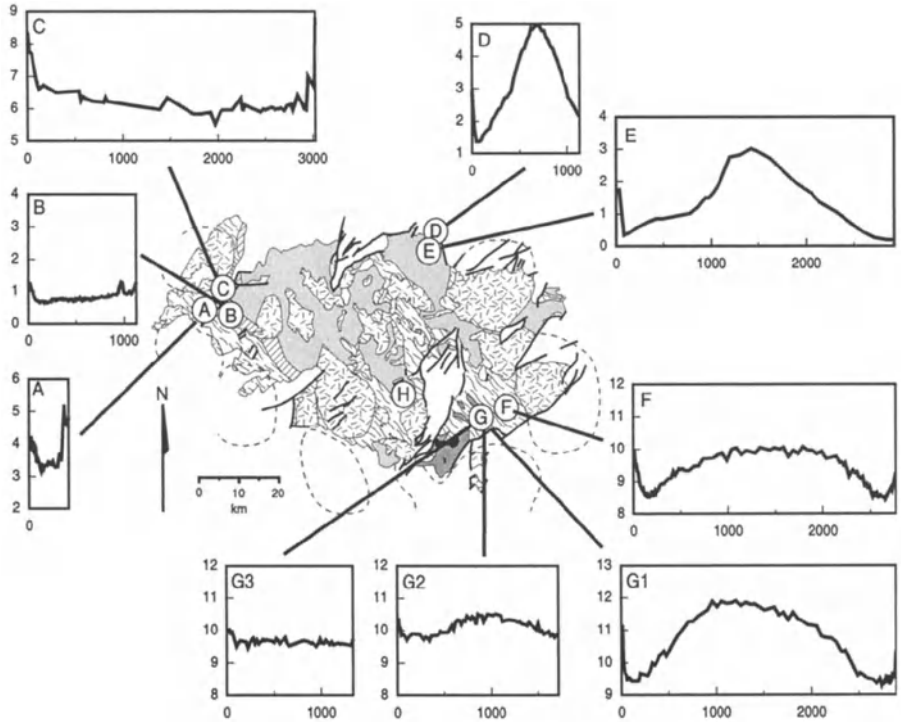

Figure 3. Geographic variation in Mn-zoning profiles for garnet in the Llano Uplift. [from Carlson and Schwarze, 1997]. Horizontal scales (in μm) and vertical scales (in wt.% MnO) are equivalent in all diagrams. The effects of late static metamorphism are seen as sharp reversals in composition near the garnets' outer margins; these effects are restricted to the outermost 50-100 μm of the crystals. In the western uplift, all garnets have virtually flat interior profiles, regardless of size or lithology. In the northern uplift, all garnets have steep gradients in their interiors, regardless of size. In the southeastern uplift, large garnets have moderately steep interior gradients, and smaller crystals display progressively shallower interior gradients.

nearby garnet amphibolites (D) preserve steep growth zoning in the interiors of crystals of all sizes. In the central and southeastern uplift, garnets in the eclogitic remnant at Oxford (H) and in semi-pelitic schists (F, G) retain zoning profiles that differ according to size: larger garnets systematically preserve steeper profiles, consistent with partial homogenization at the culmination of the early dynamothermal event.

3.2.3 Implications

Because relict zoning profiles differ systematically across the uplift but are similar at each locality for both the eclogitic remnants and the rocks nearby, it is unlikely that the eclogitic rocks from which high pressures are inferred are tectonic anomalies. Instead, it seems clear that the eclogites and their surrounding rocks have shared identical metamorphic histories. Thus it is likely that the entire Llano Uplift underwent early metamorphism at high pressures, despite the very limited preservation of mineral assemblages diagnostic of that early history.

3.3 HIGH-H STAUROLITE AND ITS PROGRADE BREAKDOWN

Staurolite was originally reported as absent from the Llano Uplift (e.g., McGehee, 1979, p. 29; Garrison et al., 1979, p. 361), and its absence was regarded as evidence for an exclusively low-pressure metamorphic history for the region. But since 1986, two localities have been discovered in the southeastern Llano Uplift where staurolite is present in pelitic metasediments that are part of the supracrustal sequence north of the boundary with the Coal Creek domain (Roback et al., 1994). The two staurolite discoveries differ importantly in their mineral chemistry and occurrence, in ways that reinforce the emerging picture of a polymetamorphic history in which early dynamothermal metamorphism at high pressure was followed by static recrystallization at low pressure.

3.3.1 Fe-Mg Staurolite at Sandy Creek

Staurolite was first discovered (Carlson and Nelis, 1986) exclusively as inclusions in a spessartine-rich garnet from Sandy Creek (locality 4 in Figure 1). This staurolite is compositionally unexceptional, and has a typical Fe:Mg ratio. Staurolite is absent from the matrix of quartz + biotite + oligoclase + microcline that surrounds the garnet porphyroblasts in this rock.

3.3.2 Fe Staurolite at White Creek

More recently, Carlson and Reese (1994) reported very nearly pure Fe-staurolite as an abundant component of two lithologic layers in an uncommon suite of pelitic metasediments at White Creek (locality 5 in Figure 1). Peak metamorphic conditions for this rock appear to have been

very close to the limit of thermal stability for staurolite in the presence of quartz: textural evidence (Figure 4) for the incomplete reaction of staurolite + quartz to produce almandine + sillimanite is unambiguous. The same reaction in a contrasting texture is illustrated in Figure 3b of Carlson and Reese (1994). Development of almandine + sillimanite is limited and highly localized, suggesting that the reaction boundary was overstepped only slightly.

Because of this staurolite's unusual composition and the textural evidence that it equilibrated very near its breakdown curve, its hydrogen content can be compared with reasonable confidence to thermodynamic calculations of staurolite stability in the FASH system (Holdaway et al., 1995) to estimate the temperature and pressure at which the staurolite last equilibrated. The hydrogen content, calculated according to the method of Holdaway et al. (1991), is 3.7 ± 0.4 apfu. That corresponds to a range of peak metamorphic conditions along the staurolite breakdown curve from 700 °C at 7 kbar to 650 °C at 12 kbar. Because the breakdown assemblage includes not kyanite but sillimanite, which is stable with staurolite + almandine only at pressures below 8 kbar, the simplest interpretation of these data is that prograde metamorphism in the southeastern uplift peaked at temperatures just above 700 °C at pressures between 7 and 8 kbar. It is possible, however, that fibrolitic sillimanite formed metastably within the kyanite field, given the minimal overstepping and limited extent of reaction observed. If this is the case, then the H-content of 3.7 apfu implies a pressure of 10 kbar at 680 °C, and pressures as high as 12 kbar fall within the range of uncertainty of measurement.

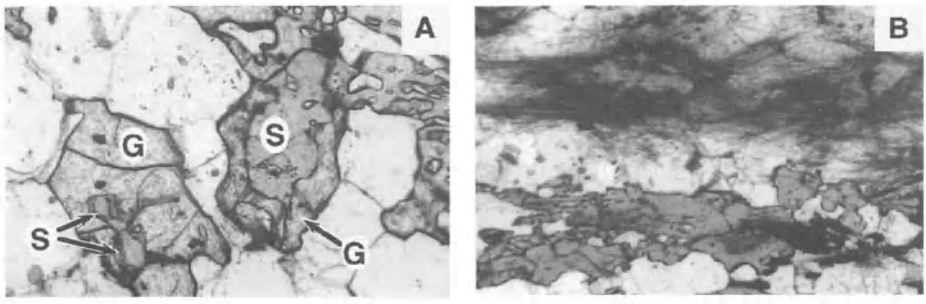

Figure 4. Prograde breakdown reactions for staurolite at White Creek. (**A**) At right center, a basal section through a formerly euhedral staurolite crystal (S) is engulfed and embayed by almandine garnet (G) at the boundary along which staurolite and quartz were formerly in contact. Garnet crystal at left center (G) encompasses large inclusion of staurolite (S, arrows). Long dimension of field of view is 1 mm. (**B**) Localized reaction of staurolite to fibrolitic sillimanite. Staurolite occupies core of felted mass of sillimanite in layer in upper half of photo; staurolite in adjacent layer in bottom half of photograph is unreacted. Long dimension of field of view is 2 mm.

3.3.3 Implications

The abundance of nearly pure Fe-staurolite at White Creek contrasts strongly with evidence at Sandy Creek for the early crystallization and later elimination of staurolite with a typical Fe:Mg ratio. These observations can be reconciled to one another, however, by recognizing that conditions during the late static metamorphism were near the lower limit of pressure stability for Fe-Mg staurolite, but above that limit for nearly pure Fe-staurolite (Carlson and Reese, 1994). Thus the occurrences at White Creek and Sandy Creek are consistent with the hypothesis that staurolite spanning a range of Fe:Mg ratios grew during an early high-pressure dynamothermal metamorphism, but that only Fe-rich staurolite survived later low-pressure static metamorphism.

3.4 RELICT ENSTATITE + FORSTERITE

Garrison (1981) reported a relict metamorphic assemblage of enstatite + forsterite + anthophyllite in the Coal Creek Serpentinite, located in the southeastern Llano Uplift (locality 6 in Figure 1). The enstatite and forsterite are small bits of relict crystals whose preferred dimensional orientation originally defined multiple deformation fabrics, which remain evident in the elongate outlines of serpentinized grains.

Equilibrium for enstatite + forsterite + anthophyllite requires a temperature of ~700°C at pressures ranging from about 2 kbar to a maximum of 8 kbar (the upper limit of anthophyllite stability), given unit activity of H_2O (Greenwood, 1963; Day et al., 1985). The assumption of high H_2O activity is validated by synkinematic crystallization of hydrous amphibole in mafic dikes within the complex (Gillis, 1989). (Anthophyllite in these rocks is commonly found in decussate sprays that crosscut the dominant pre-serpentinization fabrics, suggesting that it may not represent equilibrium with enstatite + forsterite, but instead may have formed during the late static event. If that is the case, then 700 °C is a minimum temperature, and pressure may exceed 8 kbar.)

An estimated temperature of 700°C during prograde, syn-kinematic crystallization of enstatite + forsterite in the Coal Creek Serpentinite corresponds well with temperature estimates derived from the nearby staurolite occurrence at White Creek.

4. Evidence for Late Low-P Static Metamorphism

The predominant mineral assemblages in the Llano Uplift reflect metamorphism at low to moderate pressures in the middle-amphibolite facies (McGehee, 1979). Minerals making up these low-pressure parageneses grew late in the metamorphic and deformational history of the

uplift, in most cases after deformation had ceased. Decussate porphyroblasts of minerals stable at low pressure overgrow metamorphic foliations (e.g., andalusite: Carlson and Rossman, 1988; cordierite: Nelis et al., 1989; wollastonite, vesuvianite, and grossular/andradite: Bebout and Carlson, 1986); minerals unstable at low pressures are replaced by low-pressure equivalents (e.g., garnet and sodic clinopyroxene: Carlson and Johnson, 1991); and deformational fabrics in rocks made up of minerals stable over large ranges of pressure are modified by static recrystallization textures (e.g., feldspathic gneisses and amphibolites: Carter, 1989; Nelis et al., 1989).

These features are now commonly attributed to widespread recrystallization accompanied by hydration at low pressures (Bebout and Carlson, 1986; Carlson and Nelis, 1986; Nelis et al., 1989; Carlson, 1992; Letargo and Lamb, 1993). This episode of recrystallization is ascribed to a thermal event that was coincident in time with voluminous granitic intrusion and that is genetically linked by isotopic and petrologic evidence to pluton emplacement (Bebout and Carlson, 1986; Letargo et al., 1995).

In this section, thermobarometric data for the low-pressure static metamorphic event are compiled, and the evidence linking this event to granitic plutonism is reviewed.

4.1 METAMORPHIC CONDITIONS

Thermobarometric results from a variety of techniques have produced a mutually consistent set of data that can be summarized as indicating pressures just below 3 kbar and temperatures from 475 to 625 °C. Although there are indications that higher temperatures generally characterize rocks in closer proximity to large plutons, estimates of temperatures and pressures are closely similar at localities distributed widely across the uplift, suggesting general geographic uniformity in metamorphic conditions during the late static event.

4.1.1 Thermometry

Many common Fe-Mg exchange thermometers are based upon equilibria involving almandine-rich garnet. This is problematic in the Llano Uplift because such garnet is scarce, and virtually all extant almandine-rich garnet has been partially resorbed at its margins (e.g., Figs. 2A and 2C). Re-equilibration of garnet rims appears to have been rapid, however, so use of garnet rim compositions has produced generally self-consistent thermometric data in good agreement with temperature estimates from other techniques.

Garnet-biotite thermometry yields 550 ± 75 °C from localities distributed widely across the uplift (Carlson and Nelis, 1986; Carlson and

Reese, 1994; Letargo et al., 1995; Carlson and Schwarze, 1997). Temperatures from *garnet-cordierite* thermometry from two localities are 545 and 625 ℃ (Carlson and Schwarze, 1997). *Garnet-ilmenite* thermometry yields values from 590 to 629 °C (Letargo and Lamb, 1992).

Results from *calcite-dolomite thermometry* span 475-600 ℃ (Letargo et al., 1995). *Oxygen isotopic exchange* at Blount Mountain in the central Llano Uplift is consistent with equilibration in the range 550-650 ℃ (Bebout and Carlson, 1986); *fluid-inclusion* and *carbonate phase-equilibria* studies of calc-silicates at the same locality suggest temperatures of 500-560°C (Letargo and Lamb, 1993). A detailed analysis of *carbonate-silicate phase equilibria* across the uplift produced temperature estimates in the range 475-630 °C (Letargo et al., 1995).

4.1.2 Barometry

Assemblages suitable for quantitative exchange barometry are scarce, and the apparent instability of almandine-rich garnet during the late static metamorphism again complicates the application of equilibria involving garnet. Consequently, barometric estimates have so far been obtained only from the southeastern uplift and the central uplift. Extrapolation of these results to the remainder of the uplift is therefore risky, but probably justified on the basis of the distinct uniformity throughout the uplift of Buchan-series mineral assemblages and compositions, as well as the very slight geographic variation in temperature estimates.

GASP barometry at one locality adjacent to a large granitic pluton in the southeastern uplift yields 3.0 ± 0.8 kbar; and *phase equilibrium* for the assemblage quartz + muscovite + orthoclase + sillimanite for a garnet-biotite temperature of 590 ± 50 °C and unit H_2O activity yields 2.80 ± 0.5 kbar at the margin of a large pluton in the southern uplift (Carlson and Schwarze, 1997). Likewise, *phase equilibrium* for the assemblage quartz + muscovite + orthoclase + sillimanite + andalusite for unit H_2O activity yields 2.8 ± 0.3 bars at the margin of a pluton in the southeastern uplift (Letargo and Lamb, 1991). *Fluid-inclusion* studies at Blount Mountain in the central uplift, however, yield pressures of 1 and 2 kbar (Letargo and Lamb, 1993).

4.2 RELATIONSHIP OF LOW-P METAMORPHISM TO INTRUSION

Crystallization during the late static event of decussate minerals that crosscut deformational fabrics has been linked by petrologic and isotopic evidence to granitic intrusion in key localities in the central uplift (Bebout and Carlson, 1986), and subtle gradients in temperatures of equilibration of carbonate and silicate assemblages away from plutons have been documented across the uplift (Letargo et al., 1995). These findings lead to the interpretation that late metamorphism in the uplift occurred during an

episode of regional heating consisting of numerous thermal pulses associated with widespread and voluminous emplacement of granitic plutons. In this episode, interaction of the metamorphic pile with aqueous fluids was ubiquitous but locally variable in intensity.

4.2.1 Petrologic links between static crystallization and plutonism

At Blount Mountain in the central uplift (locality 7 on Figure 1), Bebout and Carlson (1986) demonstrated that an original strongly deformed assemblage containing calcite + plagioclase + quartz was converted to an assemblage with decussate textures containing grossular/andradite + wollastonite + vesuvianite by the infiltration of aqueous fluids channelized along lithologic layering. Evidence for this conclusion came from: (1) a series of petrographic replacement textures in which minerals requiring high activities of CO_2 in the metamorphic fluid were sequentially replaced by minerals requiring successively higher activities of H_2O in the metamorphic fluid; (2) lithologic layers with assemblages requiring very high activity of H_2O, outward from which were symmetrically disposed assemblages requiring successively lower H_2O activities; and (3) similar changes in mineral assemblage away from Blount Mountain along strike, with more proximal assemblages requiring higher H_2O activities.

Analysis of carbon and oxygen isotopes confirmed that assemblages requiring higher H_2O activities also exhibited more marked isotopic depletions. Those isotopic shifts are too large to be accounted for by simple decarbonation reactions; instead, they require infiltration of a low-$\delta^{18}O$ fluid, such as that which would have been in equilibrium with measured isotopic compositions of quartz in nearby granites and in pegmatites and aplites that transect the outcrops at Blount Mountain.

From these data and observations, the conclusion was reached that static recrystallization during the late low-pressure metamorphism was intimately connected with granitic intrusion. Because late granite plutons make up nearly half of the present Precambrian surface exposures, that conclusion was logically extended to rocks throughout the uplift.

4.2.2 Thermal aureoles around plutons

One difficulty with attributing late recrystallization throughout the uplift to heating and hydration associated with plutonism is the absence of well-defined thermal aureoles around plutons. Sillimanite occurrences are commonly (but not exclusively) adjacent to major intrusive bodies, although andalusite is widely encountered elsewhere (McGehee, 1979). Retrogressive diffusion in garnet *interiors* during the late metamorphic event is pronounced in rocks adjacent to intrusions, although it is negligible elsewhere (Carlson and Schwarze, 1997). But distinct sequences of mineral assemblages indicating decreasing temperatures away

from plutons were undocumented prior to the study of Letargo et al. (1995).

That study combined results of calcite-dolomite thermometry with phase equilibria in carbonates and silicates to demonstrate the existence of subtle variations in temperatures of equilibration near pluton margins. Mineral assemblages requiring ~630 °C all lie within 1 km of large granitic plutons; rocks yielding higher calcite-dolomite temperatures tend to be closer to intrusive bodies, although exceptions exist; and talc-bearing assemblages, which require temperatures below 475 °C and for which low calcite-dolomite temperatures are calculated, tend to lie at greater distances from intrusive margins. Overall, the data suggest that gradients in equilibration temperature exist outward from large plutons, spanning at most 150 °C.

5. Constraints on Tectonic Models

Given the data and observations summarized above, it is clear that tectonic models for the Proterozoic evolution of the Llano Uplift must account for a two-part metamorphic history characterized by early dynamothermal metamorphism at high pressure that decreases in intensity from southwest to northeast, followed by later, largely static metamorphism at lower pressures associated with widespread emplacement of granitic intrusions at relatively shallow levels in the crust.

5.1 EARLY TECTONISM DURING CONTRACTIONAL OROGENY

Constraints on the early tectonic evolution of the Llano Uplift are provided by: (1) the set of pressure-temperature conditions determined from eclogite remnants in the western, northern, and central parts of the uplift, together with estimates from staurolite equilibria and equilibria in ultramafic mineral assemblages in the southeastern uplift; and (2) the geographic variation in the extent of homogenization of prograde growth zoning.

To recapitulate, thermobarometric and mineral assemblage data indicate peak metamorphic conditions near 585 °C and 6-8 kbar at Whitt Ranch; above 620 °C and near 8-10 kbar at Oxford; near 700 °C and 7-8 kbar at White Creek and Coal Creek; and near 750 °C and 15 kbar in Mason County. The extent of garnet homogenization in each of these areas is qualitatively consistent with these inferred temperatures, and local equivalence in degree of homogenization for all lithologic types demonstrates that the eclogitic rocks shared a common metamorphic history with their surrounding rocks.

These estimates of metamorphic conditions appear systematic when viewed in structural context by projecting them onto a line of section with a general SW-NE trend (Figure 5). That trend is parallel to the regional direction of bulk tectonic transport, as inferred from the vergence of major folds and the sense of motion along large-scale thrusts (Carter, 1989; Nelis et al., 1989; Reese, 1995). Emerging tectonic models for the Llano Uplift (e.g., Mosher in Rankin et al., 1993; Reese, 1993; Reese, 1995) account for these data by invoking southwestward-directed underthrusting of the North American continental margin during and following collision with a southerly continental-scale block. In this scenario, deformed rocks in the southwestern part of the uplift were carried to the deepest structural levels as they were overridden by a southerly continent and by overthrust portions of an intervening arc and accretionary complex.

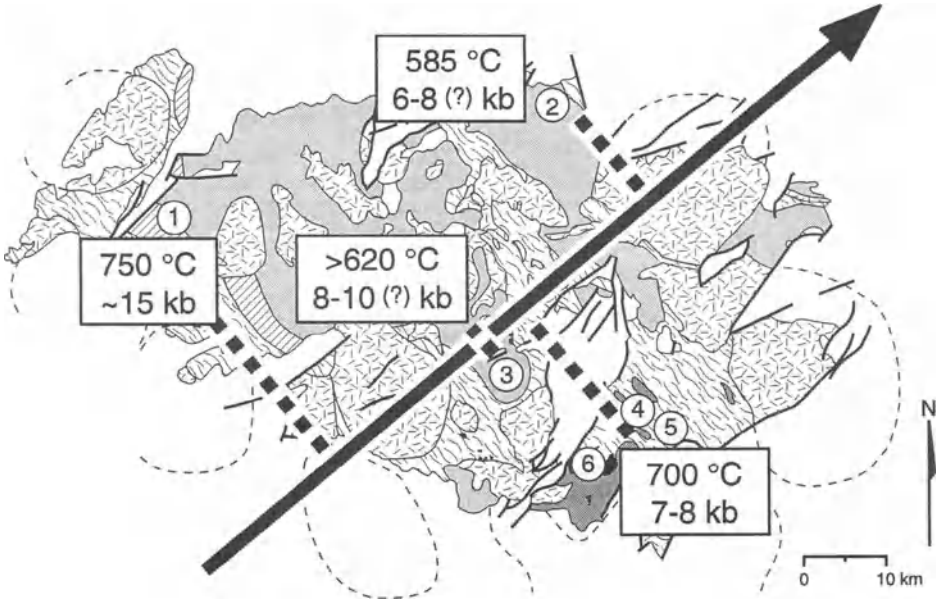

Figure 5. Geographic variation in conditions of early dynamothermal metamorphism in the Llano Uplift, in relation to direction of bulk tectonic transport, represented by arrow. When projected onto a line of section parallel to the arrow, inferred *P-T* conditions for early metamorphism decrease systematically from southwest to northeast, consistent with tectonic models invoking southwestward-directed underthrusting of the mid-Proterozoic margin of the North American continent beneath an unidentified southerly crustal block.

5.2 UPLIFT AND INTRUSIVE MAGMATISM

The marked difference between pressures determined for the early event and for the later event requires regional uplift on the order of 20-40 km between the time that peak metamorphic conditions were reached and the time that regional granitic magmatism reached its thermal peak. Given the uniformity of *P-T* conditions inferred for the late static metamorphism, the rocks now at the surface must have been at nearly uniform depths during granite intrusion. Because deformed rocks to the southwest were more deeply buried during orogenesis, uplift between the two metamorphic events was more pronounced in the southwest than in the northeast.

Analysis of the nature of the thermal event(s) responsible for metamorphism at low pressure in the Llano Uplift is a fertile area for further investigation. The regional low-pressure facies-series metamorphism in the Llano Uplift shares many characteristics with low-pressure belts elsewhere, and may have originated in similar fashion. Barton and Hanson (1989) argue convincingly that in the Cordillera of the western United States, and in many other low-pressure belts, advection of magmatic heat in a prolonged intrusive episode is required to achieve the observed metamorphic *P-T* conditions. They discount deep heat sources and advection of heat by fluids as effective causes, while acknowledging that rapid uplift during extension or erosion following thickening might be plausible mechanisms in non-Cordilleran settings.

But the Llano Uplift is distinct from the Cordilleran low-pressure metamorphic belt in ways that suggest that rapid uplift and erosion in an extensional environment following continental collision might be likely. Barton and Hanson (1989, p. 1060) emphasize the importance of the volumetric abundance of magma chambers to the magma-advection model, and indicate that in their numerical models, intrusions must occupy at least 50% of the volume of the upper crust in order for coalescence of thermal aureoles to produce low-pressure regional metamorphism. The Llano granites represent a smaller fraction of the Precambrian surface exposures, rendering the magma-advection model less likely. Barton and Hanson (1989, p. 1061) also note that uplift-induced low-pressure metamorphism: (1) requires hot, deep rocks to rise more than 10 km to produce significant thermal effects; (2) should be distinctly retrograde in character; and (3) should produce relatively small horizontal gradients. Each of these characteristics is noted above for rocks of the Llano Uplift. Moreover, north-south extension during the final deformational stages has been documented at least locally in the Llano Uplift (Carter et al., 1993).

At present, available evidence seems to favor a hybrid model in which rapid upward transport of the region following collisional orogeny brought relatively hot rocks to shallow depths, so that the heat advected upward by subsequent intrusion produced small horizontal gradients at pluton

margins, resulting in only subtle thermal aureoles. Contribution of additional heat from sources at depth, perhaps from the same sources that generated the granitic melts, may also be required to account for the geographically widespread late thermal event in shallow crust that appears regionally across the Llano Uplift in the petrologic record.

6. Acknowledgments

Research on metamorphism in the Llano Uplift has been supported by the Geology Foundation of the University of Texas at Austin, by NSF Grant EAR-8804717 to William Carlson, Sharon Mosher and Nicholas Walker, and by NSF Grant EAR-9219484 to William Carlson and Sharon Mosher. The Geology Foundation also helped to defray costs of publication. I am grateful to all of the many graduate and undergraduate students whose dissertation and thesis work in the Llano Uplift has laid the foundation for this effort. Special thanks are due to Sharon Mosher for continual encouragement and invaluable arguments in the field. Robert Roback is thanked for his insistence that dogma be challenged and for enlightening discussions, and Joel Davidow is thanked for his help in final preparation of the manuscript.

References

Anderson, D.E., and Olimpio, J.C. (1977) Progressive homogenization of metamorphic garnets, South Morar, Scotland: evidence for volume diffusion. Canadian Mineralogist, 15, 205-216.

Barton, M.D., and Hanson, R.B. (1989) Magmatism and the development of low-pressure metamorphic belts: Implications from the western United States and thermal modeling. Geological Society of America Bulletin, 101, 1051-1065.

Bebout, G.E., and Carlson, W.D. (1986) Fluid evolution and transport during metamorphism: Evidence from the Llano Uplift, Texas. Contributions to Mineralogy and Petrology, 92, 518-529.

Carlson, W.D. (1992) Polymetamorphism in the Llano Uplift. Geological Society of America Abstracts with Programs, South-Central Section, 24, 6.

Carlson, W.D., and Johnson, C.D. (1991) Coronal reaction textures in garnet amphibolites of the Llano Uplift. American Mineralogist, 76, 756-772.

Carlson, W.D., and Nelis, M.K. (1986) An occurrence of staurolite in the Llano Uplift, central Texas. American Mineralogist, 71, 682-685.

Carlson, W.D., and Reese, J.F. (1994) Nearly pure iron staurolite in the Llano Uplift and its petrologic significance. American Mineralogist, 79, 154-160.

Carlson, W.D., and Rossman, G.R. (1988) Vanadium- and chromium-bearing andalusite: Occurrence and optical-absorption spectroscopy. American Mineralogist, 73, 1366-1369.

Carlson, W.D., and Schwarze, E.T. (1993) Petrologic and tectonic significance of geographic variations in garnet growth zoning in the Llano Uplift. Geological Society of America Abstracts with Programs, 25, 101-102.

Carlson, W.D., and Schwarze, E.T. (1997) Petrologic significance of prograde homogenization of growth zoning in garnet: An example from the Llano Uplift. Journal of Metamorphic Geology, 15.

Carter, K.E. (1989) Grenville orogenic affinities in the Red Mountain area, Llano Uplift, Texas. Canadian Journal of Earth Sciences, 26, 1124-1135.

Carter, K.E., Reese, J., and Helper, M.A. (1993) Precambrian extension in the Llano Uplift. Geological Society of America Abstracts with Programs, 25, 5.

Coleman, R.G., Lee, D.E., Beatty, L.B., and Brannock, W.W. (1965) Eclogites and eclogites: their differences and similarities. Geological Society of America Bulletin, 76, 483-508.

Collins, E. (1978) Precambrian Geology of the Grape Creek area, Llano County, central Texas. M.S. thesis, Stephen F. Austin State University, 112 p.

Davidow, J.S. (1996) Proterozoic evolution of the Llano Uplift, central Texas: Evidence for high-pressure metamorphism from the Oxford mafic body. M.A. thesis, University of Texas at Austin, 172 p.

Day, H.W., Chernosky, J.V., and Kumin, H.J. (1985) Equilibria in the system MgO-SiO_2-H_2O: A thermodynamic analysis. American Mineralogist, 70, 237-248.

Fitzsimons, I.C.W., and Harley, S.L. (1994) The influence of retrograde cation exchange on granulite P-T estimates and a convergence technique for the recovery of peak metamorphic conditions. Journal of Petrology, 35, 543-576.

Garrison, J.R., Jr. (1981) Coal Creek serpentinite, Llano Uplift, Texas: A fragment of an incomplete Precambrian ophiolite. Geology, 9, 225-230.

Garrison, J.R., Jr., Long, L.F., and Richman, D.L. (1979) Rb-Sr and K-Ar geochronologic and isotopic studies, Llano Uplift, central Texas. Contributions to Mineralogy and Petrology, 69, 361-374.

Gillis, G.M. (1989) Polyphase deformation and metamorphism of the Middle Proterozoic Coal Creek Serpentinite, Gillespie County, Texas. M.A. thesis, University of Texas at Austin, 103 p.

Greenwood, H.J. (1963) The synthesis and stability of anthophyllite. Journal of Petrology, 4, 317-351.

Harley, S.L. (1984) The solubility of alumina in orthopyroxene coexisting with garnet in FeO-MgO-Al_2O_3-SiO_2 and CaO-FeO-MgO-Al_2O_3-SiO_2. Journal of Petrology, 25, 665-696.

Holdaway, M.J., Mukhopadhyay, B., and Dutrow, B.L. (1995) Thermodynamic properties of stoichiometric staurolite $H_2Fe_4Al_{18}Si_8O_{48}$ and $H_6Fe_2Al_{18}Si_8O_{48}$. American Mineralogist, 80, 520-533.

Holdaway, M.J., Mukhopadhyay, B., Dyar, M.D., Dutrow, B.L., and Rumble, D., III. (1991) A new perspective on staurolite crystal chemistry: Use of stoichiometric and chemical end-members for a mole-fraction model. American Mineralogist, 76, 1910-1919.

Letargo, C.M.R., and Lamb, W.M. (1991) Granite emplacement pressures and metamorphism in the Llano Uplift of central Texas. Geological Society of America Abstracts with Programs, 23, 446.

Letargo, C.M.R., and Lamb, W.M. (1992) Comparative thermometry on pelitic rocks and marbles of the Llano Uplift, Texas. Geological Society of America Abstracts with Programs, 24, 219.

Letargo, C.M.R., and Lamb, W.M. (1993) P-T-X conditions of calc-silicate formation: evidence from fluid inclusions and phase equilibria; Llano Uplift, central Texas, USA. Journal of Metamorphic Geology, 11, 89-100.

Letargo, C.M.R., Park, J.S., and Lamb, W.M. (1995) Comparison of calcite + dolomite thermometry and carbonate + silicate equilibria: Constraints on the conditions of metamorphism of the Llano uplift, central Texas, U.S.A. American Mineralogist, 80, 131-143.

Lovering, J.F., and White, A.J.R. (1969) Granulitic and eclogitic inclusions from the basic pipes at Delegate, Australia. Contributions to Mineralogy and Petrology, 21, 9-52.

McGehee, R.V. (1979) Precambrian rocks of the southeastern Llano region, Texas. University of Texas Bureau of Economic Geology Publication 79-3, 36.

Nelis, M.K., Mosher, S., and Carlson, W.D. (1989) Grenville-age orogeny in the Llano Uplift of central Texas: Deformation and metamorphism of the Rough Ridge Formation. Geological Society of America Bulletin, 101, 876-883.

Rankin, D.W., Chiarenzelli, J.R., Drake, A.A., Jr., Goldsmith, R., Hall, L.M., Hinze, W.J., Isachsen, Y.W., Lidiak, E.G., McLelland, J., Mosher, S., Ratcliffe, N.M., Secor, D.T., Jr., and Whitney, P.R. (1993) Proterozoic rocks east and southeast of the Grenville front. In J.C. Reed, Jr., M.E. Bickford, R.S. Houston, P.K. Link, D.W. Rankin, P.K. Sims, and W.R. Van Schmus, Eds. The Geology of North America, Precambrian: Conterminous U.S., C-2, p. 335-461. Geological Society of America, Boulder, Colorado.

Reed, R.M., Roback, R.C., and Helper, M.A. (1995) Nature and age of ductile deformation associated with the "anorogenic" Town Mountain Granite, Llano Uplift, central Texas. Twelfth International Conference on Basement Tectonics, Norman Oklahoma.

Reese, J.F. (1993) The tectonic evolution of the southeastern Llano Uplift, central Texas: A summary of recent results from structural and U-Pb geochronological studies. Geological Society of America Abstracts with Programs, 25, 297-298.

Reese, J.F. (1995) Structural evolution and geochronology of the southeastern Llano Uplift, central Texas. Ph.D. dissertation, University of Texas at Austin, 172 p.

Roback, R., Mosher, S., and Carlson, W.D. (1994) Evolution of the ~1.3 Ga Coal Creek island-arc terrane, Llano Uplift, central Texas. Geological Society of America Abstracts with Programs, 26, 405.

Rougvie, J.R., Carlson, W.D., Connelly, J.N., Roback, R.C., and Copeland, P. (1996) Late thermal evolution of Proterozoic rocks in the northeastern Llano Uplift, central Texas. Geological Society of America Abstracts with Programs, 28, 376-377.

Walker, N. (1992) Middle Proterozoic evolution of the Llano Uplift, Texas: Evidence from U-Pb zircon geochronometry. Geological Society of America Bulletin, 104, 494-504.

Wilkerson, A., Carlson, W.D., and Smith, D. (1988) High-pressure metamorphism during the Llano orogeny inferred from Proterozoic eclogite remnants. Geology, 16, 391-394.

Woodsworth, G.J. (1977) Homogenization of zoned garnets from pelitic schists. Canadian Mineralogist, 15, 230-242.

Yardley, B.W.D. (1977) An empirical study of diffusion in garnet. American Mineralogist, 62, 793-800.

GEOLOGIC PROVINCES OF OKLAHOMA

ROBERT A. NORTHCUTT
Independent Geologist, Oklahoma City, OK;
JOCK A. CAMPBELL
Oklahoma Geological Survey, Norman, OK

The geologic provinces of Oklahoma are mainly the product of tectonics and attendant sedimentation of Pennsylvanian age. Most boundaries are structural; thus, the provinces map is a generalized tectonic map. Permian and post-Paleozoic strata tend to mask those structures, but most of those strata have been removed by erosion, except in the Anadarko Basin and the Wichita Uplift provinces. The location of most of Oklahoma's oil and gas resources are either influenced by, or are the direct result of Pennsylvanian tectonics and sedimentation patterns. Therefore, the present study also defines provinces in the subsurface on the basis of geological criteria. The authors have attempted to use the originally published names for the recognized provinces. However, we also have used the most *geologically correct* names; i.e., we recommend abandonment of the term Nemaha "ridge," because it is not a geologic term, nor does it describe the feature accurately.

Oklahoma is separated into five major uplifts and six major basins, or low areas on which a significant accumulation of sedimentary rocks occur. Most of these have subprovinces, which sum to 19 additional identified geologic units. The Gulf Coastal Plain is not included in this study because it is a veneer of Cretaceous cover that masks significant structures. Faults are the most common boundary element. Although their precise age commonly is known only approximately, their geographic location is less controversial, except in detail. Stratigraphic/structural boundaries are based on less precise geological information. Such boundaries interpreted at the surface are influenced by both geology and geomorphology, and are therefore strongly influenced by the present level of erosion. The major example of a surface stratigraphic/structural boundary is the southwestern limit of the Ozark Uplift in eastern Oklahoma. Stratigraphic/structural boundaries in the subsurface are commonly based on structural or isopachous contours from well or geophysical data, or on a structural trend, as well as the experience of the authors. Basement structure is preferred. An example is the boundary that separates the Marietta Basin from adjacent geologic elements.

Important subsurface boundaries in the Anadarko and Arkoma Basins have been neglected in previous studies: The Anadarko Basin/Shelf boundary is placed near the 700-ft isochore of the Atokan and Desmoinesian Series (Rascoe, 1962), at which there is a marked rate of change of thickening southward into the basin. The northern limit of the Arkoma Basin, which is in part the shelf area of the Arkoma Basin, has been variously drawn by a number of authors. It merges imperceptibly into the southern part of the Cherokee Platform, which is in part the shelf area of the Arkoma Basin. For the purpose of this study the boundary is modified from the "hinge line" of the Atokan

GEOLOGIC PROVINCES OF OKLAHOMA

Compiled by

Robert A. Northcutt and Jock A. Campbell

1995

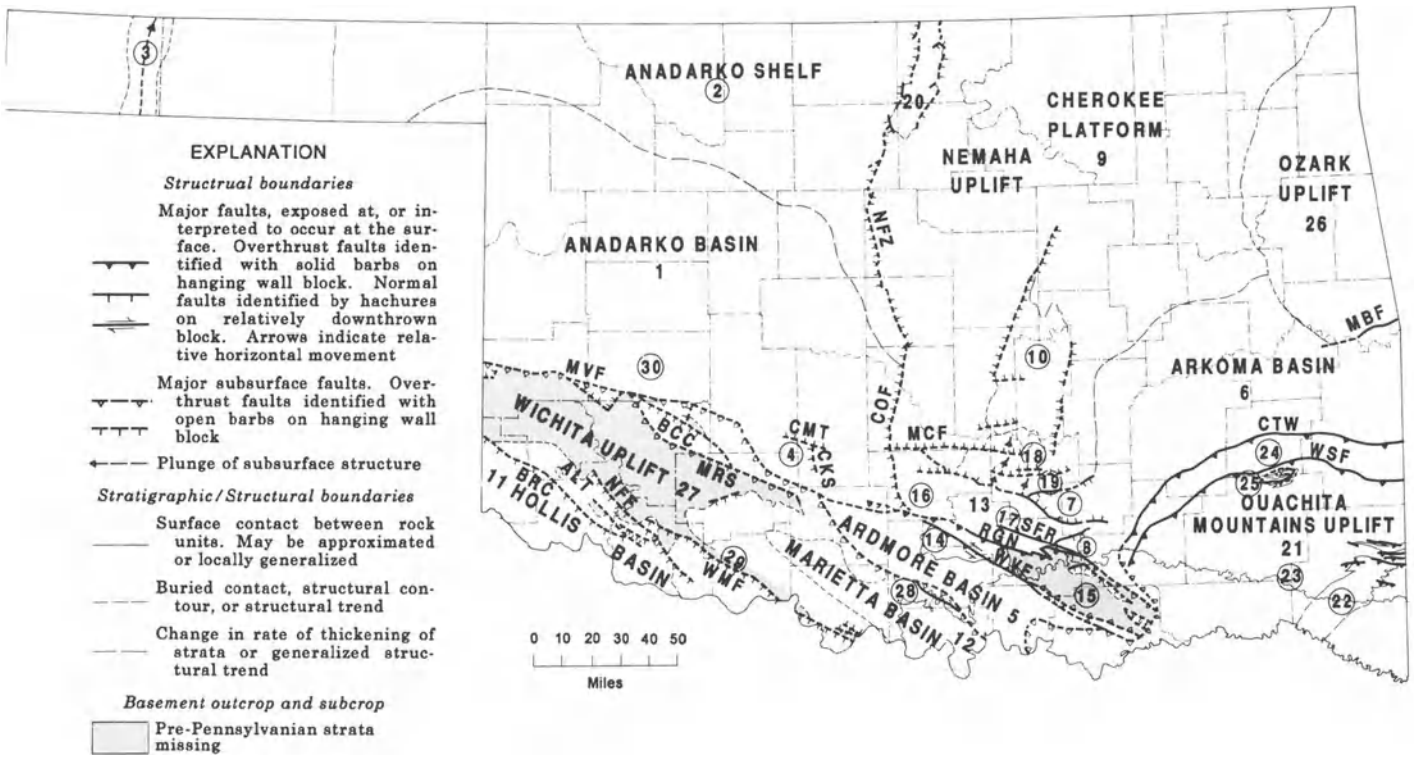

Figure 1. Map of the geologic provinces and sub provinces for the State of Oklahoma, U.S.A.

MAJOR GEOLOGIC PROVINCES AND SUBPROVINCES OF OKLAHOMA

Anadarko Basin	**1**
Anadarko Shelf	②
Cimarron Arch	③
Cyril Basin	④
Ardmore Basin	**5**
Arkoma Basin	***6***
Franks Graben	⑦
Wapanucka Graben	⑧
Cherokee Platform	**9**
Seminole Structure	⑩
Hollis Basin	**11**
Marietta Basin	**12**
Arbuckle Uplift	**13**
Arbuckle Mountains	⑭
Tishomingo-Belton Horst	⑮
Pauls Valley-Hunton Horst	⑯
Clarita Horst	⑰
Ada High	⑱
Lawrence Horst	⑲
Nemaha Uplift	**20**
Ouachita Mountain Uplift	**21**
Broken Bow Uplift	㉒
Ouachita Central Region	㉓
Ouachita Frontal Thrust Belt	㉔
Potato Hills	㉕
Ozark Uplift	**26**
Wichita Uplift	**27**
Criner Uplift	㉘
Waurika-Muenster Uplift	㉙
Wichita Frontal Fault Zone	㉚

MAJOR FAULT BOUNDARIES

Altus Fault	ALT	Central Oklahoma Fault Zone	COF	North Fork Fault	NFF
Blue Creek Canyon Fault	BCC	McClain County Fault	MCF	Reagan Fault	RGN
Burch Fault	BRC	Meers Fault	MRS	Sulphur Fault	SFR
Cement Fault	CMT	Mountain View Fault	MVF	Washita Valley Fault	WVF
Chickasha Fault	CKS	Mulberry Fault	MBF	Waurika-Muenster Fault	WMF
Choctaw Fault	CTW	Nemaha Fault Zone	NFZ	Windingstair Fault	WSF

Figure 1 continued. Nomenclature of the geologic provinces and sub provinces for the State of Oklahoma, U.S.A.

Table 1. Index to references for the geologic provinces and sub provinces of the State of Oklahoma, U.S.A.

INDEX TO REFERENCES FOR GEOLOGIC PROVINCES OF OKLAHOMA

Robert A. Northcutt and Jock A. Campbell

1995

AUTHOR	Year	1 ANADARKO BASIN	2 Anadarko Shelf	3 Cimarron Arch	4 Cyril Basin	5 ARDMORE BASIN	6 ARKOMA BASIN	7 Franks Graben	8 Waparucka Graben	9 CHEROKEE PLATFORM	10 Seminole Structure	11 HOLLIS BASIN	12 MARIETTA BASIN	13 ARBUCKLE UPLIFT	14 Arbuckle Mountains	15 Tishomingo-Belton Horst	16 Pauls Valley-Hunton Horst	17 Clarita Horst	18 Ada High	19 Lawrence Horst	20 NEMAHA UPLIFT	21 OUACHITA MOUNTAIN UPLIFT	22 Broken Bow Uplift	23 Ouachita Central Region	24 Ouachita Frontal Thrust Belt	25 Potato Hills	26 OZARK UPLIFT	27 WICHITA UPLIFT	28 Criner Uplift	29 Waurika-Muenster Uplift	30 Wichita Frontal Zone	31 Regional and historical
		PROVINCE NUMBER CODE																														
Allen	1994																															
Amsden	1975																															
ANRAN	1988																															
Arbenz	1956																															
Arbenz	1989																															
Branson	1956																															
Branson	1962																															
Brown	1984																															
Cline	1960																															
Cohee	1962																															
Davis & Northcutt	1989																															
Denison	1982																															
Donovan	1986																															
Fath	1920																															
Fenneman	1938																															
Frederickson	1957																															
Fritz	1978																															
Gatewood	1985																															
Ham, et al	1954																															
Ham, et al	1964																															
Hardie	1990																															
Harlton	1951																															
Harlton	1956																															
Harlton	1963																															
Harlton	1972																															
Hart	1974																															
Herrmann	1961																															
Hicks	1971																															
Jacobsen	1949																															
Johnson, et al	1988																															
Jordan	1959																															
Jordan	1962																															
Jordan	1967																															
Krone & Luza	1986																															
Laing	1964																															
Lang	1957																															
Levorsen	1929																															
Luza & Lawson	1981																															
Marcher & Bergman	1983																															
McConnell	1989																															
McDaniel	1959																															
Miser	1954																															
Monnett	1954																															
Moore & Haynes	1917																															
NRCC	1944																															
Paschal	1941																															
Raisz	1939																															
Rascoe	1962																															
Rascoe & Adler	1983																															
Rascoe & Hyne	1988																															
Roth	1955																															
Sears	1951																															
Suneson, et al	1990																															
Totten	1956																															
Weirich	1953																															
Wheeler	1953																															
PROVINCE NUMBER CODE		1	2	3	4	5	6	7	8	9	10	11	12	13	14	15	16	17	18	19	20	21	22	23	24	25	26	27	28	29	30	31

Series (Weirich, 1953). This boundary approximates the striking rate of change of thickness of Atokan strata southward into the Arkoma Basin.

The Nemaha Uplift province is defined by a horst-block complex in north-central Oklahoma, and continuing northward. South of the Nemaha Uplift, two northerly-trending fault zones separate the Anadarko Basin and Cherokee Platform provinces. These are the Nemaha Fault Zone, and Central Oklahoma Fault zone.

The Cyril Basin is a well-known deep segment of the greater Anadarko Basin. It is defined by the Cement and Chickasha faults on the north and northeast (Herrmann, 1961), and by the Wichita Uplift on the south (Harlton, 1972). Wheeler (1953) developed structural contours on the Desmoinesian unconformity in the subsurface.

The Arbuckle Uplift is extended northward in this study, to include the newly named, but long recognized Ada High. This structure is apparently the northern, faulted extension of a high that is part of the Pauls Valley-Hunton, and Lawrence Horst blocks (Ham and others, 1964).

The Seminole Structure was originally identified, but not named by Levorsen (1929), as an apparent positive structural feature underlying the Seminole District. The best information available to the writers is that the feature is a partial horst, tilted eastward, and bounded on the west by a northeast-trending fault system that is over 50 miles long (Wheeler, 1953). It is structurally lower than the Ada High to the south, and is separated from it, at least locally, by faults. Therefore, we include it as part of the Cherokee Platform province.

Map References

R. A. Northcutt and J. A. Campbell, compilers

Note: Numbers in parentheses refer to province index numbers on small-scale map.

Allen, Mark W., 1994, Structural analysis and tectonic history of the Potato Hills, Ouachita Mountains, Oklahoma, *in* Suneson, N. H., and Hemish, L. A., eds., Geology and Resources of the eastern Ouachita Mountains frontal belt and southeastern Arkoma Basin, Oklahoma: Oklahoma Geological Survey Guidebook 29, p. 253–261. (25)

Amsden, Thomas W., 1975, Hunton Group (Late Ordovician, Silurian, and Early Devonian) in the Anadarko Basin of Oklahoma: Oklahoma Geological Survey Bulletin 121, 214 p. (1, 9)

ANRAN Corporation, 1988, unpublished subsurface mapping and seismic profiles. (27, 30)

Arbenz, J. Kaspar, 1956, Tectonic map of Oklahoma: Oklahoma Geological Survey Map GM–3, 1 sheet, 1:750,000. (31)

Arbenz, J. Kaspar, 1989, The Ouachita system, *in* Bally, A. W., and Palmer, A. B., eds., The Geology of North America – an overview, Vol. A, p. 371–396: The Geological Society of America. (21, 22, 24)

Branson, Carl C., 1956, Pennsylvanian history of northeastern Oklahoma: Tulsa Geological Society Digest, v. 24, p. 83–86. (6)

Branson, Carl C., 1962, Pennsylvanian System of the Mid-Continent, *in* Branson, C. C., ed, Pennsylvanian System in the United States, a symposium: American Association of Petroleum Geologists, p. 431–460. (9)

Brown, W. G., 1984, Washita Valley fault system – a new look at an old fault, *in* Borger, John G., II, ed., Technical proceedings of the 1981 meeting of the AAPG Mid-Continent section: Oklahoma City Geological Society, p. 68–82. (13, 14)

Cline, Lewis M., 1960, Stratigraphy of the late Paleozoic rocks of the Ouachita Mountains, Oklahoma: Oklahoma Geological Survey Bulletin 85, 113 p. (23)

Cohee, G. V. (Chairman), 1962, Tectonic map of the United States: U.S. Geological Survey and American Association of Petroleum Geologists, 2 sheets, 1:2,500,000. (31)

Davis, Herbert G., and Northcutt, Robert A., 1989, The greater Anadarko basin: an overview of petroleum exploration and development, *in* Johnson, K. S., ed., Anadarko basin symposium: Oklahoma Geological Survey Circular 90, p. 13–24. (1, 31)

Denison, Rodger E., 1982, Geologic cross-section from the Arbuckle Mountains to the Muenster arch, southern Oklahoma and Texas: Geological Society of America Map and Chart Series, MC–28R. (13, 14, 28, 29)

Donovan, R. Nowell, 1986, Geology of the Slick Hills, *in* Donovan, R. N., ed., The Slick Hills of southwestern Oklahoma – fragments of an aulacogen?: Oklahoma Geological Survey Guidebook 24, p. 1–12. (4)

Fath, A. E., 1920, The origin of the faults, anticlines, and buried "granite ridge" of the northern part of the Mid-Continent oil and gas field: U.S. Geological Survey Professional Paper, no. 128, p. 75–84. (20)

Fenneman, Nevin M., 1938, Physiography of the eastern United States: McGraw-Hill, 691 p., 7 fold-out plates. (31)

Frederickson, E. A., 1957, Geologic map of the Criner Hills area Oklahoma: Oklahoma Geological Survey Map GM–4, 1 sheet, 1:20,000 (approx.). (28)

Fritz, Richard D., 1978, Structural contour map of Oklahoma on the Pennsylvanian Wapanucka Limestone, Oswego limestone, base of the Hoxbar Group, and Checkerboard limestone: Unpublished M.S. Thesis, Oklahoma State University, 47 p., 1 sheet, 1:500,000. (1, 2, 9, 20)

Gatewood, Lloyd E., 1985, Arbuckle structure map: Privately published and copyrighted, 1 sheet, 1:380,160 (approximately 1 inch to 32,000 feet). (4, 5, 10, 18, 31)

Ham, W. E., McKinley, M. E., and others, 1954 (revised by K. S. Johnson, 1990), Geologic map and sections of the Arbuckle Mountains, Oklahoma: Oklahoma Geological Survey Map GM–31, 1 sheet, 1:100,000. (7, 8, 10, 13, 14, 16, 17, 19)

Ham, W. E., Denison, R. E., and Merritt, C. A., 1964, Basement rocks and structural evolution southern Oklahoma: Oklahoma Geological Survey Bulletin 95, 302 p. (5, 11, 12, 13, 14, 27, 28, 29, 30)

Hardie, William E., 1990, Subsurface structural study of the buried Ouachita thrust front, southeastern Oklahoma: Shale Shaker, v. 41, no. 2, p. 32–55. (15, 24)

Harlton, Bruce H., 1951, Faults in sedimentary part of Wichita Mountains of Oklahoma: American Association of Petroleum Geologists Bulletin, v. 36, no. 5, p. 988–999. (30)

Harlton, Bruce H., 1956, The Harrisburg Trough, Stephens and Carter Counties, Oklahoma, *in* Hicks, I. C., ed., Petroleum geology of southern Oklahoma, a symposium: American Association of Petroleum Geologists, vol. 1, p. 135–143. (5, 27)

Harlton, Bruce H., 1963, Frontal Wichita fault system in southwestern Oklahoma: American Association of Petroleum Geologists Bulletin, v. 47, no. 8, p. 1552–1580. (30)

Harlton, Bruce H., 1972, Faulted fold belts of the southern Anadarko basin adjacent to frontal Wichitas: American Association of Petroleum Geologists Bulletin, v. 56, no. 8, p. 1544–1551. (4, 27, 30)

Hart, Donald L., Jr., 1974, Reconnaissance of the water resources of the Ardmore and Sherman quadrangles, southern Oklahoma; Sheet 1, geologic map, 1:250,000: Oklahoma Geological Survey Hydrologic Atlas 3, 4 plates. (6, 15, 21, 24)

Herrmann, Leo A., 1961, Structural geology of Cement-Chickasha area, Oklahoma: American Association of Petroleum Geologists Bulletin, v. 45, p. 1971–1993. (4)

Hicks, I. C., 1971, Southern Oklahoma folded belt, *in* Cram, I. H., ed., Future Petroleum Provinces of the United States—their geology and potential: American Association of Petroleum Geologists Memoir 15, v. 2, p. 1070–1077. (5, 12)

Jacobsen, Lynn, 1949, Structural relations on the east flank of the Anadarko basin, Cleveland and McClain Counties, Oklahoma: American Association of Petroleum Geologists Bulletin, v. 33, no. 5, p. 695–710. (1, 9, 13, 16)

Johnson, K. S., Amsden, T. W., Denison, R. E., Dutton, S. P., Goldstein, A. G., Rascoe, Bailey, Jr., Sutherland, P. K., and Thompson, D. M., 1988, Southern Midcontinent region, *in* Sloss, L. L., ed., Sedimentary cover – North American craton, U.S.:

Geological Society of America, Boulder, Colorado, The Geology of North America, v. D–2, p. 307–359. Reprinted *as* Oklahoma Geological Survey Special Publication 89-2, 53 p., 2 plates, 1989. (31)

Jordan, Louise, 1959, Arkoma Basin: Oklahoma Geology Notes, v. 19, no. 11, p. 235–236. (6)

Jordan, Louise, 1962, Geologic map and sections of pre-Pennsylvanian rocks in Oklahoma: Oklahoma Geological Survey Map GM–5, 1 sheet, 1:750,000. (12, 29)

Jordan, Louise, 1967, Geology of Oklahoma—a summary: Oklahoma Geology Notes, v. 27, no. 12, p. 215–228. (10, 18)

Krone, Anthony J., and Luza, Kenneth V., 1986, Holocene deformation associated with the Meers fault, southwestern Oklahoma, *in* Donovan, R. N., ed., The Slick Hills of southwestern Oklahoma: Oklahoma Geological Survey Guidebook 24, p. 68–74. (27, 30)

Laing, William E., 1964, Southwestern Oklahoma—a geophysical case history of a basin: Geophysics, v. 29, no. 6, p. 968–984. (11)

Lang, Robert C., III, 1957, The Criner Hills: a key to the geologic history of southern Oklahoma, *in* Kempf, J. H., ed., Criner Hills field conference, Lake Murray Area, Southern Oklahoma Guidebook: Ardmore Geological Society, p. 18–25. (28)

Levorsen, A. I., 1929, Greater Seminole district, Seminole and Pottawatomie Counties, Oklahoma, *in* Powers, Sidney, ed., Structure of typical American oil fields: American Association of Petroleum Geologists, v. 2, p. 315–361. (10, 18)

Luza, Kenneth V., and Lawson, James E., Jr., 1981, Seismicity and tectonic relationships of the Nemaha Uplift in Oklahoma: Oklahoma Geological Survey Special Publication 81–3, 70 p. (20)

Marcher, Melvin V., and Bergman, DeRoy L., 1983, Reconnaissance of the water resources of the McAlester and Texarkana quadrangles, southeastern Oklahoma; Sheet 1, geologic map, 1:250,000: Oklahoma Geological Survey Hydrologic Atlas 9, 4 plates, 1:250,000. (6, 21, 23, 24)

McConnell, David A., 1989, Determination of offset across the northern margin of the Wichita uplift, southwestern Oklahoma: Geological Society of America Bulletin, v. 101, no. 10, p. 1317–1332. (27, 30)

McDaniel, Gary A., 1959, Isopachous and paleogeologic studies of southwest Oklahoma: Shale Shaker, v. 10, no. 3, p. 4–27. (11)

Miser, Hugh D., 1954, Geologic map of Oklahoma: U.S. Geological Survey and Oklahoma Geological Survey, 1 sheet, 1:500,000. (22, 23, 26)

Monnett, V. E., 1954, The geological architecture of Oklahoma: Shale Shaker, v. 4, no. 8, p. 28–29. (31)

Moore, Raymond C., and Haynes, Winthrop P., 1917, The crystalline rocks of Kansas, *in* Oil and gas resources of Kansas: State Geological Survey of Kansas Bulletin 3, p. 140–173. (20)

National Research Council Commission on Tectonics, Division of Geology and Geography, C. R. Longwell and P. B. King (co-chairs), 1944, Tectonic map of the United States: American Association of Petroleum Geologists, Tulsa, Oklahoma, 1:2,500,000. (31)

Paschal, E. A., 1941, Major tectonic provinces of southern Oklahoma and their relation to oil and gas fields: American Association of Petroleum Geologists Bulletin, v. 25, no. 1, p. 1–22. (31)

Raisz, Erwin, 1939, Landforms of the United States: Harvard University Press, Cambridge, Mass., 1 sheet, approximately 1:4,625,000. (31)

Rascoe, Bailey, Jr., 1962, Regional stratigraphic analysis of Pennsylvanian and Permian rocks in western Mid-Continent, Colorado, Kansas, Oklahoma, Texas: American Association of Petroleum Geologists Bulletin, v. 46, no. 8, p. 1345–1370. (1, 2)

Rascoe, Bailey, Jr., and Adler, Frank J., 1983, Permo-Carboniferous hydrocarbon accumulations, Mid-Continent, U.S.A.: American Association of Petroleum Geologists Bulletin, v. 676, no. 6, p. 979–1001. (31)

Rascoe, Bailey, Jr., and Hyne, Norman J., eds., 1988, Petroleum geology of the Mid-Continent: Tulsa Geological Society Special Publication No. 3, 162 p. (31)

Roth, Robert, 1955, Paleogeology of the Panhandle of Texas: American Association of Petroleum Geologists Bulletin v. 39, no. 4, p. 422–443. (3)

Sears, Joe M., 1951, Southwestern Oklahoma—the Hollis basin: Shale Shaker, v. 2, no. 1, p. 4–6, 9–12, & 16. (11)

Suneson, N. H., Campbell, J. A., and Tilford, M. J., eds., 1990, Geology and resources of the frontal belt of the western Ouachita Mountains, Oklahoma: Oklahoma Geological Survey Special Publication 90–1, 196 p. (23, 24)

Totten, Robert B., 1956, General geology and historical development, Texas and Oklahoma Panhandles: American Association of Petroleum Geologists Bulletin, v. 40, no. 8, p. 1945–1967. (3)

Weirich, Thomas E., 1953, Shelf principal of oil origin, migration, and accumulation: American Association of Petroleum Geologists Bulletin, v. 37, no. 8, p. 2027–2045. (6)

Wheeler, Robert R., 1953, Structural map of Oklahoma: Privately published, 1 sheet, 1:380,160 (approximately 1 inch to 32,000 feet). (4, 10, 18)

Note: A version of this paper is in Transactions of the 1995 AAPG Mid-Continent Section Meeting, D.L. Swindler and C.P. Williams, compilers; Tulsa Geological Society, 1996, p. 128-134.

The Southern Oklahoma Aulacogen: A Cambrian analog for Mid-Proterozoic AMCG (Anorthosite-Mangerite-Charnockite-Granite) complexes?

JOHN P. HOGAN AND M. CHARLES GILBERT
University of Oklahoma, School of Geology and Geophysics
Norman, Oklahoma 73069-0628
email: jhogan@ou.edu

ABSTRACT

Comparison of the Cambrian Southern Oklahoma Aulacogen and the distinctive anorthosite-mangerite-charnockite-granite (AMCG) complexes of the Mid-Proterozoic reveal striking similarities in the temporal and spatial association of igneous rock types in these provinces that suggests a commonality in their petrogenesis. Igneous rocks that comprise the Cambrian Southern Oklahoma Aulacogen include: 1) voluminous anorthositic gabbros, 2) Fe-rich, Ti-rich, and P-rich, biotite-bearing gabbros, 3) A-type leucocratic alkali-feldspar rhyolite and granites (some with rapakivi textures, see Price *et al.*, 1996a), and 4) a suite of "late" diabase dikes. Nearly all of these igneous units have counterparts that occur within AMCG complexes. A noticeable exception in the Southern Oklahoma Aulacogen is the absence of coarse grained massif-type anorthosites, with their characteristic high-Al orthopyroxene megacrysts. This important distinction is interpreted to reflect differences in the conditions of crystallization and emplacement of magmas giving rise to these two provinces. AMCG complexes develop at significantly deeper levels in the crust where assimilation of aluminous continental crust may operate more efficiently due to higher ambient temperatures. In contrast, the epizonal to volcanic conditions of crystallization, and lack of evidence for significant contributions of ancient crust in either mafic or felsic igneous rocks, suggest that parent magmas to the igneous rocks of the Southern Oklahoma Aulacogen were rapidly transported to the emplacement level, where they cooled quickly, thus inhibiting opportunities for large scale crustal assimilation. We further speculate that, if exposed, the large mid-crustal mafic root beneath the Southern Oklahoma Aulacogen, inferred from geophysical and petrologic arguments, would have the appearance of a typical Mid-Proterozoic AMCG complex. Conversely, penecontemporaneous tectono-magmatic provinces, such as the Southern Oklahoma Aulacogen, may have overlain Mid-Proterozoic AMCG complexes and have been subsequently removed by erosion.

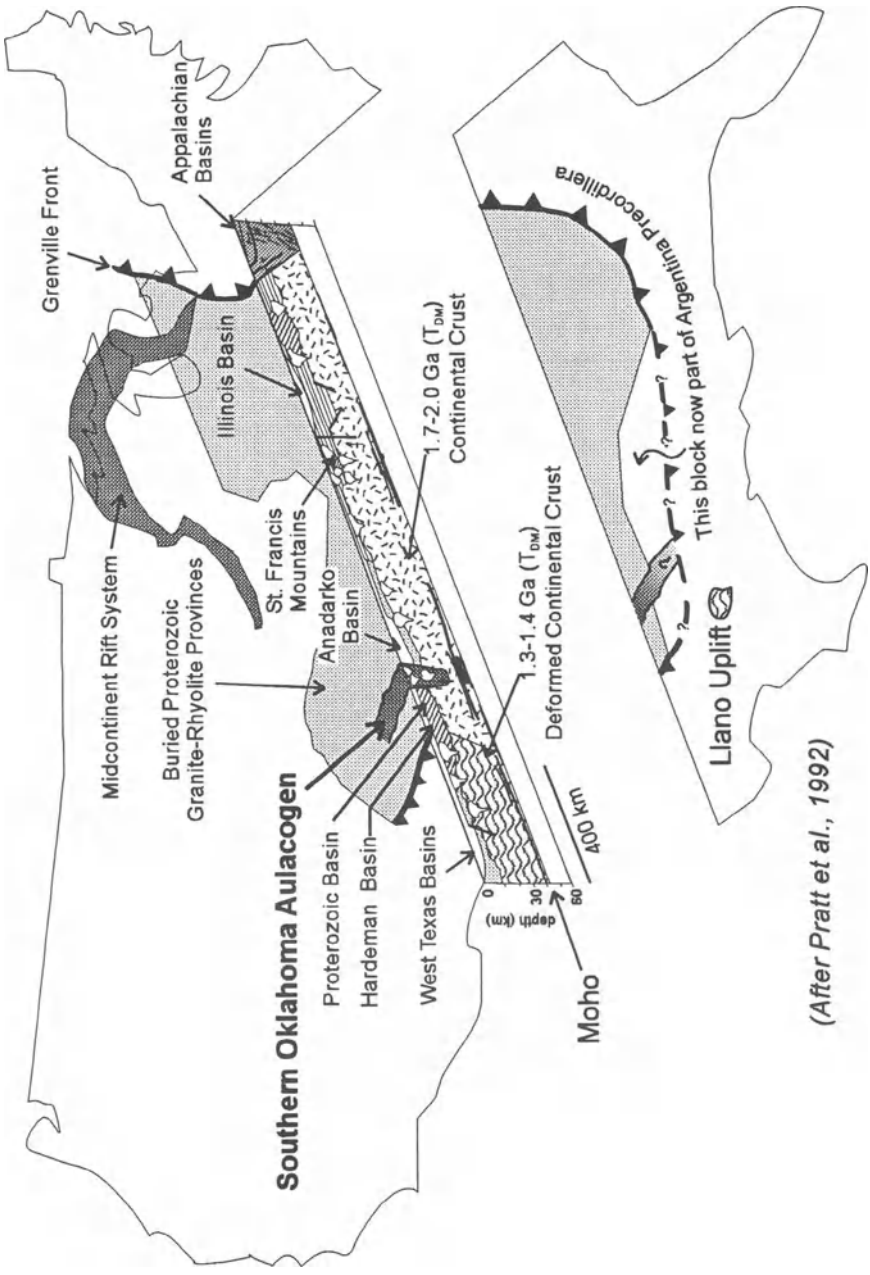

Figure 1. Location of the Southern Oklahoma Aulacogen with respect to the Grenville Front and other prominent geologic features of the Mid-continent.

1. Introduction

The Southern Oklahoma Aulacogen (SOA) is the best exposed and documented of the several aulacogens that formed within the North American craton during breakup of the Laurentian Supercontinent in Late Proterozoic to Cambrian time. Igneous rocks that comprise the Cambrian SOA include: 1) voluminous anorthositic gabbro, 2) Fe-Ti-P rich, biotite-bearing gabbro, 3) A-type leucocratic alkali-feldspar rhyolite and granite (some with rapakivi textures, see Price *et al.*, 1996a), and 4) a suite of "late" diabase dikes. This igneous assemblage is strikingly similar to the anorthosite-mangerite-charnockite-granite provinces or "AMCG" complexes (Emslie and Hunt, 1990) that are a hallmark of Mid-Proterozoic magmatism. The possibility that the SOA is a younger Paleozoic analog of AMCG magmatism warrants closer inspection. A comparative study of some of the major characteristics of igneous rocks of the SOA and of AMCG complexes is presented here with the aim of elucidating petrogenetic processes significant to one or both igneous provinces.

2. Regional Geology

The SOA (Hoffman *et al.*, 1974) is one of several aulacogens that developed during rifting of the Laurentian Supercontinent in Late Proterozoic to Cambrian time. The aulacogen formed at a relatively high angle to the incipient continental margin and appears to transect an older crustal suture between the 1.3-1.4 Ga Granite-Rhyolite Terrane of the Midcontinent and the 1.3-1.2 Ga Llano or "Texas Craton" to the south (Fig. 1). Subsequent to Cambrian rifting, a large interior basin developed over the SOA and igneous rocks of the rifting event were buried by up to 4-5 km of Cambrian to Mississippian sediments (Gilbert, 1992). During late Mississippian to early Pennsylvanian time, igneous rocks of the SOA were uplifted as large fault-bounded blocks as a result of plate collisions associated with the Ouachita Orogeny (for a review see Granath, 1989; Perry, 1989). The igneous rocks were subsequently reburied by locally derived sediment as well as sediment transported from the ancestral Ouachita Mountains to the east. The absence of significant Mesozoic and Cenozoic deformation in the Midcontinent ensured preservation of the rift assemblage (McConnell and Gilbert, 1990). More recent erosion has reexposed a cross-section through the volcanic and plutonic rocks that floored this Cambrian aulacogen (Fig. 2). Thus, in North America, the SOA is one of the best preserved and best exposed examples of igneous activity associated with an ancient rifting event.

Bimodal igneous activity and tectonism accompanied formation of the SOA. Based on field relationships, and sparse geochronology, previous studies proposed two temporally distinct magmatic episodes (Ham *et al.*, 1964; Powell and Phelps, 1977). The early phase of igneous activity was dominated by intrusion of a substantial volume of gabbroic magma with possible eruptive equivalents. The later phase of igneous

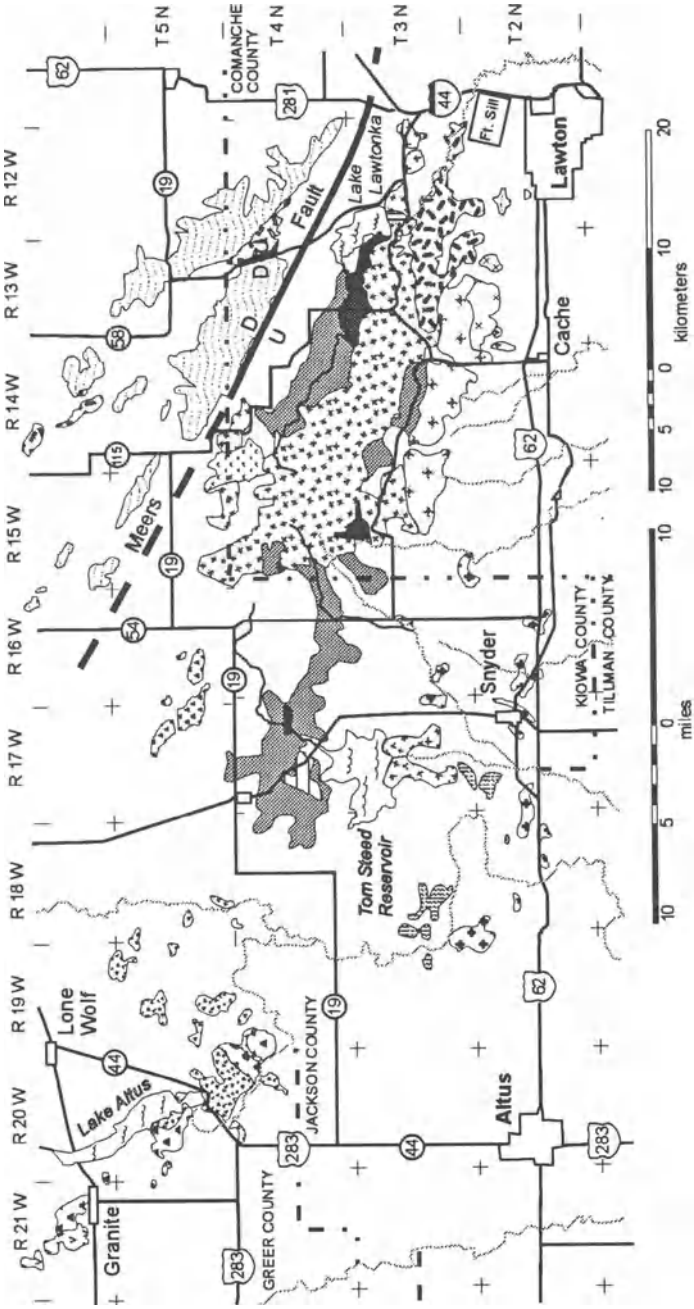

Figure 2a. Geologic Map of the Wichita Mountains Igneous Province of the Southern Oklahoma Aulacogen, southwestern Oklahoma, U.S.A.

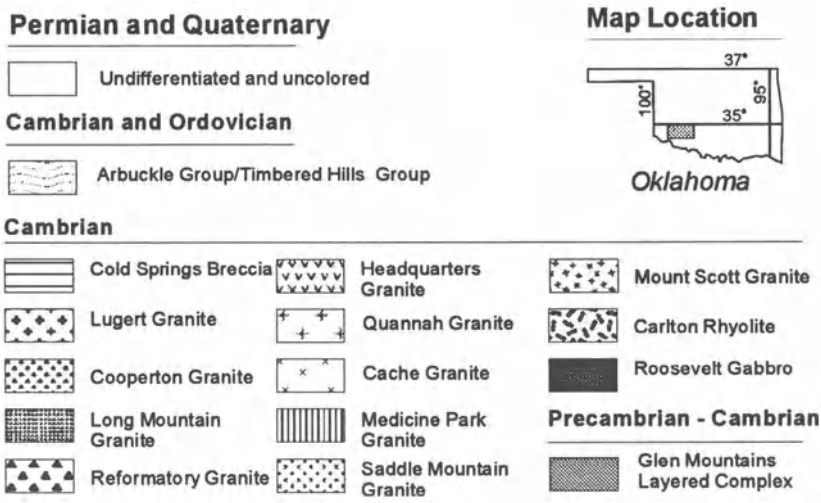

Figure 2b. Map explanation for the Wichita Mountains Igneous Province (Fig. 2a).

activity was dominated by extrusion of voluminous rhyolite and intrusion of large sheet-granites at the base of the rhyolite pile. Mafic magmatism during the later stages of rifting is limited to intrusion of diabase dikes (Gilbert and Hughes, 1986). Unequivocal field evidence for coeval mafic and felsic magmatism is present locally (*e.g.,* Vidrine and Fernandez, 1986; Hogan, unpublished mapping). However, at the present erosional level, rock types owing their origin to magma mingling are a volumetrically minor component the igneous assemblage of the SOA. Generalized stratigraphic relationships for the major surface and subsurface lithodemic units are presented in Figure 3.

A period of substantial uplift and erosion is postulated to have coincided with the hiatus that is postulated to have separated mafic and felsic igneous activity (Ham *et al.,* 1964; Powell and Phelps, 1977). Ham *et al.* (1964) argue that the subaerial Carlton Rhyolite Group rests unconformably on marine basalts and spilite of the Navajoe Mountains Group. Locally this erosional event is interpreted to have been extensive enough to have exposed underlying gabbro (see Figure 4 for relationships of *exposed* igneous units). Thus, after crystallization of the Raggedy Mountains Gabbro Group (*i.e.,* the Glen Mountains Layered Complex and the Roosevelt Gabbros) and prior to extrusion of most of the Carlton Rhyolite Group, 1-3 km of overburden were stripped off by erosion (Ham *et al.,* 1964; Powell and Phelps, 1977). McConnell and Gilbert (1990) suggested that erosion may have been accentuated by normal faulting associated with uplift and extension of the brittle crust during rifting. However, the extent of this unconformity remains problematical as more recent geochronologic and geophysical investigations indicate at least some of the Roosevelt Gabbro plutons are coeval with or postdate crystallization of the granite-sheets (Hogan *et al.,* 1996; Price *et al.*, this volume). Thus, mafic and felsic igneous activity associated with the rifting event may have a closer temporal relationship than previously thought.

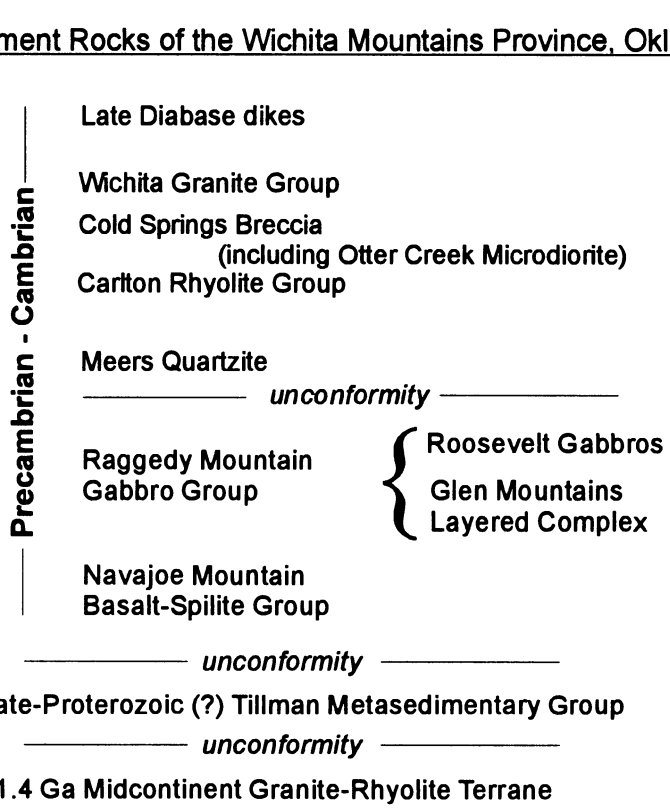

Figure 3. Generalized stratigraphic relationships of major surface and subsurface lithodemic units in the Wichita Mountains Province, Oklahoma, U.S.A.

3. MAFIC ROCKS

3.1 RAGGEDY MOUNTAIN GABBRO GROUP

The Raggedy Mountain Gabbro Group has been subdivided into two distinct suites on the basis of field mapping and petrographic investigations (Powell *et al.*, 1980a,b; Powell, 1986). A series of basalt spilites, the Navajoe Mountain Group, has been tentatively correlated with the gabbros (Ham *et al.*, 1964). However, information about these basalts is scant, as they are only known from subsurface well studies. Geochemical investigations of well-cuttings substantiate this correlation for some wells but refutes it for others (Aquilar, 1988). Thus, the relationship of these rocks to the SOA remains enigmatic and they will not be discussed further.

3.1.1. Glen Mountains Layered Complex

The Glen Mountains Layered Complex is presumed to be the oldest exposed unit in the SOA (Ham *et al.*, 1964; Powell *et al.*, 1980a,b;). In the past, the crystallization age of the Glen Mountains Layered Complex has been subject to controversy and at one time was suggested to be an extension of the Proterozoic Midcontinent Rift rather than being related to the SOA (Powell and Phelps, 1977). A more recent geochronologic investigation of this unit by Lambert *et al.*, (1988) yielded a Rb-Sr isochron age of 577±165 Ma and a Sm-Nd isochron age of 528±29 Ma. Although large uncertainties are associated with these age determinations, they appear to confirm the temporal association of the Glen Mountains Layered Complex with formation of the SOA.

The Glen Mountains Layered Complex is a well layered anorthositic gabbro complex that forms the substrate to the uplifted SOA. It occupies an area of at least 2000 km^2 and is comparable to other mid-sized layered intrusions (see Ashwal, 1993; Table 4.1). At least three major cyclic units, in which a layer of plagioclase-olivine cumulate is overlain by plagioclase-olivine-pyroxene, plagioclase-pyroxene, and plagioclase cumulate, have been recognized in the Glen Mountains Layered Complex

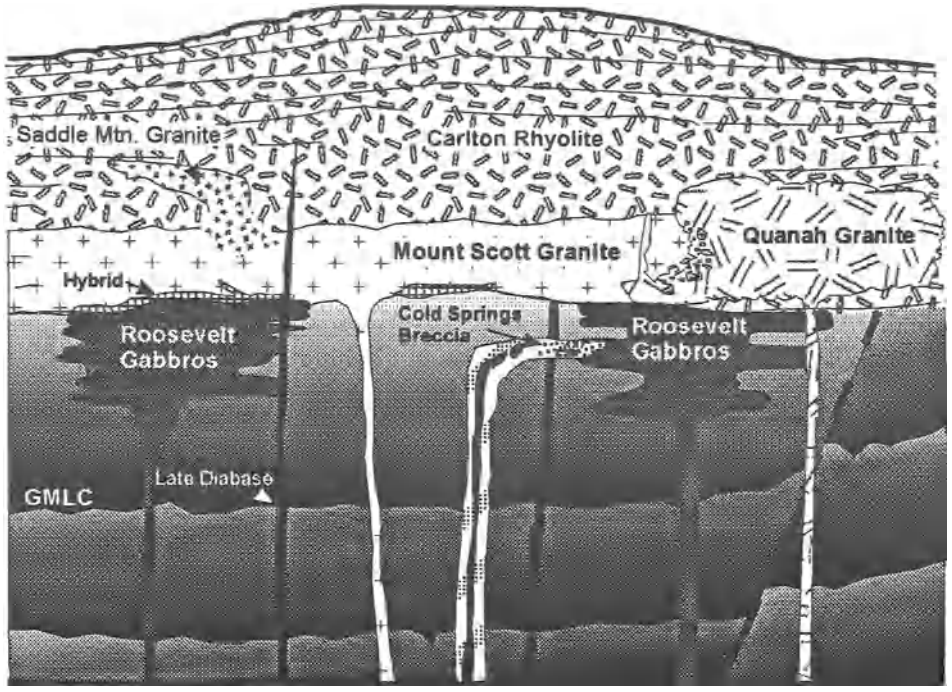

Figure 4. Schematic cross-section of the spatial relationships of the major igneous units of the Wichita Mountains Igneous Province during the late Cambrian.

Table 1. Whole Rock Compositions of the Glen Mountains Layered Complex and Selected Anorthosites.

	GMLC			Massif Anorthosites			Anorthosites from Layered Mafic Intrusions							
				Harp Lake	Nain	Laramie	Duluth		Bushveld (Critical Zone)				Still-water	Sept Isles
	1	2	3	4	5	6	7	8	9	10	11	12	13	14
SiO_2	47.39	46.42	47.57	53.02	54.56	54.15	52.20	54.30	48.72	48.46	47.97	49.56	47.95	50.10
TiO_2	0.15	0.03	0.12	0.27	0.18	0.31	0.57	0.25	0.00	0.08	0.06	0.17	0.13	0.76
Al_2O_3	32.63	30.25	29.25	28.07	25.54	27.34	27.48	27.90	32.09	30.09	31.00	28.61	28.35	27.15
Fe_2O_3	0.91	2.48	2.33	0.42		0.44	0.73	0.40	1.04	1.91	2.06	2.56	3.01	1.60
FeO				1.38	1.73	0.91	1.53	0.66						3.20
MnO	0.03	0.04	0.04	0.02	0.03	0.03	0.03	0.01	0.01	0.01	0.01	0.04	0.07	n.d.
MgO	0.39	2.81	3.11	0.98	1.44	0.39	0.88	0.19	0.72	1.04	1.38	2.64	2.24	2.78
CaO	14.72	13.96	14.63	11.02	9.98	10.39	12.24	11.50	15.11	15.08	14.82	14.16	14.70	9.74
Na_2O	2.83	2.47	2.31	4.29	4.85	4.86	3.84	4.30	2.16	2.35	2.39	2.00	2.15	4.18
K_2O	0.15	0.12	0.11	0.44	0.40	0.91	0.41	0.45	0.12	0.15	0.31	0.24	0.10	0.77
P_2O_5	0.11	0.08	0.12	0.06	0.03	0.09	0.05	0.02	0.03	0.03	n.d.	0.03	0.05	0.09
LOI	0.28	0.11	0.27		1.19								1.55	
Total	99.57	98.98	99.86	99.97	99.93	100.79	99.94	99.99	100.00	100.01	100.00	100.01	100.15	100.04

1. Average of 16 anorthosites from the Glen Mountains Layered Complex, Oklahoma (Scofield, 1968).
2. Average of 13 olivine anorthosites from the Glen Mountains Layered Complex, Oklahoma (Scofield, 1968).
3. Average of 4 gabbros from the Glen Mountains Layered Complex, Oklahoma (Scofield, 1968).
4. Average of 26 anorthosites from the Harp lake Complex, Labrador (Emslie, 1980).
5. Average of 13 anorthosites from the Nain Complex, Labrador (Wiebe, 1978).
6. Average of 15 anorthosites from the Laramie Complex, Wyoming (Fountain et al., 1981).
7. Average of 5 olivine anorthosites from the Duluth Complex, Minnesota (Miller and Weiblen, 1990).
8. Anorthosite from the Duluth Complex, Minnesota (Miller and Weiblen, 1990).
9. Average of 3 anorthosites from the UG1 Footwall, Bushveld Complex, South Africa (Eales et al., 1986).
10. Average of 3 anorthosites from the Merensky Footwall, Bushveld Complex, South Africa (Eales et al., 1986).
11. Average of 3 anorthosites from the Merensky Unit, Bushveld Complex, South Africa (Eales et al., 1986).
12. Average of 3 anorthosites from the Bastard Unit, Bushveld Complex, South Africa (Eales et al., 1986).
13. Average of 25 anorthosites from the AZIII and AZV of the Stillwater Complex, Montana, (Czamanske and Scheidle, 1985).
14. Average of 2 anorthosites from the Sept Isles Complex, Quebec, (Higgins and Doig, 1986).

(Cooper, 1991). The base of each cycle is characterized by adcumulate textures and grades upward to orthocumulate, and to mesocumulate, textures at the top.

Plagioclase comprises greater than seventy-five modal percent in all rock types (Cooper, 1991) and commonly exceeds ninety percent in many exposed units (*e.g.*, Scofield, 1968; Taylor, 1978; Stockton, 1984). Anorthositic layers exhibit orthocumulate to adcumulate textures and commonly consist of highly laminated plagioclase crystals 1-5 mm in size. However, the An content of plagioclases crystals from the Glen Mountains Layered Complex (typically An_{70} and range An_{57} to An_{80}) are substantially higher than those reported for massif-type anorthosites which generally fall in the range of An_{40} to An_{65} (see Aswhal, 1993). This difference is reflected in the compositions of whole rock samples from the Glen Mountains Layered Complex, which have substantially higher Al_2O_3 (29.2-32.6 wt%), CaO (14.0-14.7 wt%) and lower SiO_2 (46.4-47.6 wt%), and Na_2O (2.3-2.8 wt%) than massif-type anorthosites Al_2O_3 (25.5-28.1wt%), CaO (10.0-11.0 wt%), SiO_2 (53.0-54.6 wt%), and Na_2O (4.3-4.9 wt%) (see Table 1). The normative An content of anorthositic rocks from the Glen Mountains Layered Complex is considerably greater than anorthositic rocks from massif type anorthosites, and is more comparable to anorthosites from other layered mafic complexes such as the Bushveld or Stillwater Complex (Fig. 5).

The Glen Mountains Layered Complex exhibits many characteristics typical of layered complexes (*e.g.*, Stillwater, Duluth, Bushveld). Clinopyroxene occurs as both a cumulus and intercumulus phase and locally forms large (10's cms) ophitic crystals. High-Al orthopyroxene megacrysts typical of massif-type anorthosites have not yet been found. In fact, orthopyroxene is relatively scarce in the Glen Mountains Layered Complex, in contrast with typical layered complexes. It occurs primarily as a peritectic reaction rim around cumulus olivine and is less abundant as an intercumulus phase. Plagioclace cumulates (*i.e.*, anorthosites) in the Glen Mountains Layered Complex can form trough or "pothole" structures (see Irvine, 1987; Cooper, 1991) in which underlying cumulate layers have been scoured out and infilled by deposition of plagioclase (Fig. 6). These structures have been identified in the Bushveld Complex and are of considerable interest due to their close spatial association with mineralized reefs (*e.g.*, Farquhar, 1986). Mineralization in the Glen Mountains Layered Complex is also spatially associated with pothole structures (Cooper 1991).

3.1.2. The Roosevelt Gabbros

The Glen Mountains Layered Complex is intruded by a series of smaller hydrous biotite-bearing gabbro plutons (<20 km^2) and dikes of the Roosevelt Gabbros. Contact relationships are unequivocal: 1) plutons of the Roosevelt Gabbros can exhibit a narrow (cm's) chill zone against the Glen Mountains Layered Complex, 2) rocks of the Glen Mountains Layered Complex are commonly altered adjacent to the contacts with Roosevelt Gabbro plutons, 3) Glen Mountains Layered Complex xenoliths can be found within Roosevelt Gabbro plutons, and 4) dikes of biotite-bearing gabbro intruding the

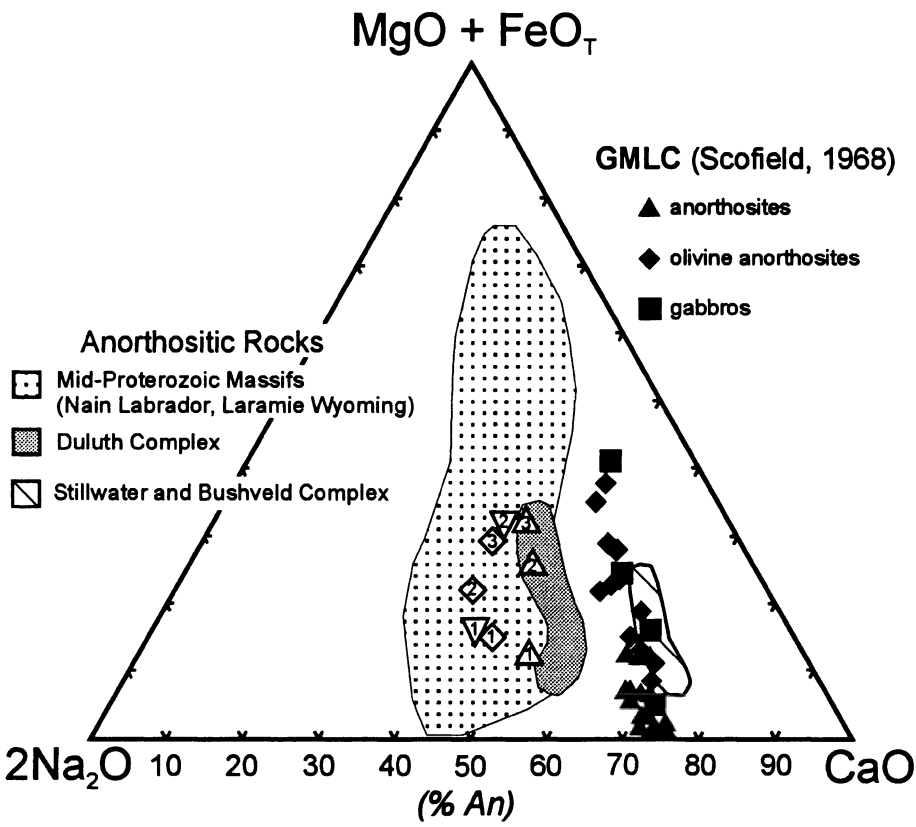

Figure 5. Triangular composition diagram $2Na_2O$-CaO-($MgO+FeO_{(total)}$) (*mol.%*) for anorthositic rocks from selected Mid-Proterozoic massif anorthosite complexes, layered mafic complexes, and the Glen Mountains Layered Complex, OK. Sources of data are the same as those given in table one. Open diamonds are from the Nain Complex: #1-average of 13 anorthosites, #2-average of 7 leuconorite dikes, and #3-average of 17 leuconorites (Wiebe, 1978). Upright open triangles are from the Harp Lake Complex: #1-average of 26 anorthosites, #2-average of 15 leuconorites and gabbros, and #3-average of 18 leucotroctolite including olivine leucogabbro and olivine leuconorite (Emslie, 1980). Inverted open triangles are from the Laramie Anorthosite Complex: #1-average of 20 anorthosites, and #2-average of 18 leucogabbros (Scoates and Chamberlain, *in press*).

Glen Mountains Layered Complex are locally abundant (Powell and Gilbert, 1982). Layering in Roosevelt Gabbros is subparallel but discordant to layering in the Glen Mountains Layered Complex (Gilbert, 1983). McConnell and Gilbert (1990) interpreted this to indicate an episode of faulting tilted the Glen Mountains Layered Complex prior to intrusion of Roosevelt Gabbro. U-Pb studies of zircon from the Mount Sheridan Gabbro, one of the Roosevelt Gabbros, have been interpreted to record a crystallization age of 552±7 Ma (Bowring and Hoppe, 1982). However, the isotopic systematics of these zircons are complicated by both the presence of an older inherited component and subsequent Pb-loss. More recent $^{40}Ar/^{39}Ar$ laser probe study of primary biotite and amphibole from this Roosevelt Gabbro recorded similar ages of 535±8 Ma (late

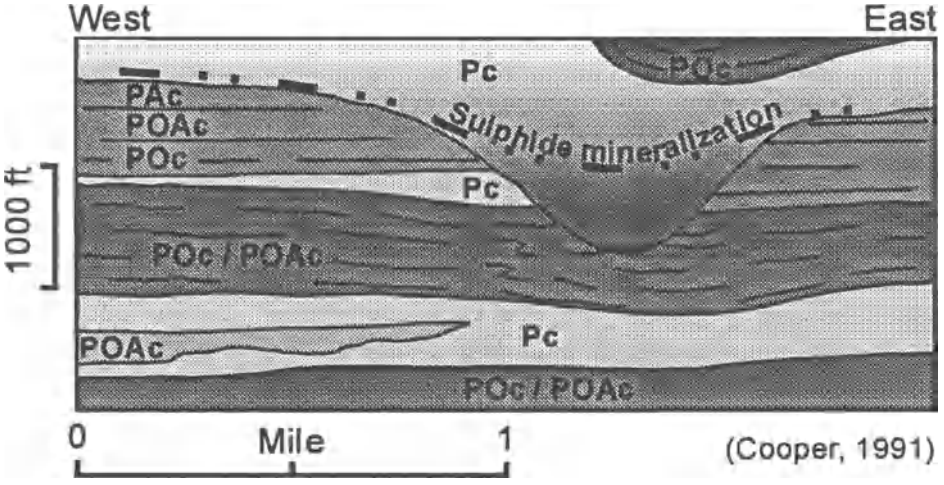

Figure 6. Stratigraphic cross-section of the major cyclic units within the Glen Mountains Layered Complex exhibiting a prominent "pot-hole" structure with spatially associated sulphide mineralization (Cooper, 1991). POc = Plagioclase - Olivine cumulate; POAc = Plagioclase - Olivine - Augite cumulate, PAc = Plagioclase - Augite cumulate; Pc = Plagioclase cumulate.

amphibole from a pegmatite), 533±2 Ma (amphibole from the gabbro) and 533±4 (biotite from the gabbro) (Hames *et al.*, 1995). The close agreement between amphibole and biotite ages are consistent with rapid cooling of a shallow intrusive and are interpreted to represent the crystallization age of this pluton.

In marked contrast to the anhydrous primary mineralogy of the Glen Mountains Layered Complex, Roosevelt Gabbros contain primary biotite and amphibole in addition to plagioclase, two pyroxenes, and ±olivine (Powell *et al.*, 1980a,b; Diez de Medina, 1988; Aquilar, 1988). Primary biotite and amphibole can be common, typically 2-6 modal%. Biotite compositions exhibit Mg/Mg+Fe from 0.4 to 0.8. Amphiboles range in composition from magnesio-hornblendes to ferro-hornblendes. Alkali feldspar and quartz occur only in the more evolved rock types within the Roosevelt Gabbro plutons.

Roosevelt Gabbro plutons are layered and display internal differentiation fractionating from olivine gabbro to Fe-rich biotite-hornblende-quartz diorites and tonalites. Pegmatite, variably comprised of amphibole, pyroxene, Fe-Ti oxides, biotite, plagioclase, granophyric alkali feldspar and quartz, and abundant apatite, titanite, zircon, occurs as dikes and pods, and locally contain miraolitic cavities. These pegmatites can exhibit extensive deuteric alteration. Such features are consistent with crystallization of an intrinsically hydrous gabbroic magma at relatively shallow crustal levels. Powell (1986) argued convincingly on the basis of mineral compositional variations, mineral paragenesis, and whole rock compositions, that the Roosevelt

Gabbros and the Glen Mountains Layered Complex crystallized from distinct magmas: the Roosevelt Gabbros from an intrinsically *hydrous* olivine tholeiite, and the Glen Mountains Layered Complex from an intrinsically *anhydrous* high-Al_2O_3 tholeiite.

Coeveal biotite-gabbro intrusives, primarily dikes, are also associated with AMCG complexes, such as Laramie (Kolker *et al.*, 1990; Mitchell *et al.*, 1995), Harp Lake (Emslie, 1980), and Nain (de Waard and Wheeler, 1971). Whole rock compositions of Roosevelt Gabbros are broadly similar to whole rock compositions of such rocks (Table 2), and display some geochemical similarities in terms of abundances of distinctive elements such as TiO_2, Al_2O_3, and P_2O_5 (Fig. 7). However, more direct comparisons are obscured by the cumulate nature of the Roosevelt Gabbro samples. Mitchell *et al.*, (1995) interpreted high-Al biotite-gabbro dikes from the Laramie Anorthosite Complex to represent samples of mantle-derived melts that may be compositionally similar to the parental magmas that eventually formed the massif anorthosite plutons.

3.2 LATE DIABASE DIKES

Igneous rocks of the SOA are cross-cut by numerous dikes of basaltic composition known collectively as Late Diabase (Ham *et al.*, 1964; Gilbert and Hughes, 1986). Some of these dikes intrude parallel to the structural grain of the rift (≈300°) which has been inherited from an older basement terrane (Denison, 1995). Late diabase dikes can be found to intrude nearly all other igneous rocks types, and thus must represent the last phase of igneous activity associated with the rift (*e.g.*, Powell *et al.*, 1980a,b). However, the presence of partially melted Mount Scott Granite adjacent to the margin of a small (<1m wide) Late Diabase dike requires a relatively high ambient temperature for the Mount Scott Granite (>300°) at the time of intrusion (see Price *et al.*, 1996b). This suggests intrusion of the Mount Scott Granite magma was followed very closely by intrusion of this Late Diabase dike. This and the presence of fragments of disaggregated basaltic dikes within other members of the Wichita Granite Group, and a basaltic dike within a xenolith of Carlton Rhyolite in the Reformatory Granite (Hogan, unpublished mapping), indicates intrusion of basaltic magma is likely to have accompanied the entire rifting event rather than representing a distinct late magmatic episode.

Late diabase dikes are fine-grained and porphyritic. Plagioclase (labradorite) phenocrysts are set in a subophitic groundmass of labradorite, augite, ±hypersthene, ±magnetite, ±ilmenite. Powell *et al.* (1980a,b) report sporadic occurrences of primary hornblende and biotite, and rare olivine in Late Diabase dikes. However, Gilbert and Hughes (1986) recognize three classes of dikes of basaltic chemistry: 1) "microgabbro", 2) "microdiorite", and 3) "Late Diabase". Microgabbro dikes contain primary olivine and biotite and are typically spatially associated with Roosevelt Gabbro plutons and are thus interpreted to be related to these intrusions. Microdiorite dikes are difficult to distinguish from Late Diabase in the field, but typically contain primary amphibole and a more sodic plagioclase (andesine), ±augite, in contrast to Late Diabase which is charaterized by augite and a more calcic plagioclase (labradorite), ±hypersthene. Microdiorite dikes appear to be spatially associated with an occurrence of intimately

Table 2. Whole Rock Compositions of Biotite Gabbros from the Southern Oklahoma Aulacogen and from Anorthosite Massifs.

	Roosevelt Gabbro Group, Oklahoma						Massif-Type					
	Sandy Creek				Mount Baker		Nain	Harp Lake		Laramie		
	1	2	3	4	5	6	7	8	9	10	11	12
SiO_2	45.78	47.95	54.73	43.45	48.93	50.66	49.61	51.03	49.19	48.22	48.26	48.10
TiO_2	1.36	2.88	2.83	5.67	3.12	2.39	1.25	1.64	2.99	1.57	0.94	1.57
Al_2O_3	16.24	14.95	13.22	11.36	14.14	17.77	16.18	17.05	14.20	18.02	17.36	16.26
Fe_2O_3	11.88	13.44	12.76	18.76	13.79	10.41	1.55	1.88	2.85	12.45	11.86	12.77
FeO							10.76	9.25	12.95			
MnO	0.16	0.19	0.20	0.26	0.19	0.15	0.18	0.18	0.23	0.19	0.15	0.17
MgO	12.96	6.91	3.49	6.26	6.10	4.23	7.87	6.28	3.35	7.61	9.19	7.89
CaO	9.09	10.16	7.08	10.84	9.50	8.90	8.23	8.24	7.90	9.31	9.17	9.79
Na_2O	2.03	2.60	3.51	2.19	2.88	3.02	2.84	2.95	3.25	2.64	2.54	2.56
K_2O	0.30	0.58	1.64	0.33	0.58	1.05	0.35	0.51	1.19	1.09	0.46	0.58
P_2O_5	0.18	0.34	0.54	0.90	0.49	0.56	0.12	0.15	0.73	0.24	0.17	0.20
LOI	0.44	0.73	0.12	0.03	0.57	0.91		0.91	0.72		0.01	0.13
Total	100.42	100.73	100.12	100.02	100.29	100.01	98.94	100.05	99.55	101.34	100.07	100.01

1. Average of 9 High MgO gabbros from the Sandy Creek Gabbro, Oklahoma (Diez de Medina, 1988).
2. Average of 13 Moderate MgO gabbros from the Sandy Creek Gabbro, Oklahoma (Diez de Medina, 1988).
3. Low MgO gabbro from the Sandy Creek Gabbro, Oklahoma (Diez de Medina, 1988).
4. Average of 2 High Ti gabbros from the Sandy Creek Gabbro, Oklahoma (Diez de Medina, 1988).
5. Average of 9 Moderate MgO gabbros from the Mount Baker Gabbro, Oklahoma (Aquilar, 1988).
6. Average of 2 Low MgO gabbros from the Mount Baker Gabbro, Oklahoma (Aquilar, 1988).
7. Biotite bearing norite form the Nain Complex Labrador (de Waard and Wheeler, 1971).
8. Average of 4 biotite gabbros from the Harp Lake Complex, Labrador (Emslie, 1980).
9. Average of 17 ferrodiorites from the Harp Lake Complex, Labrador (Emslie, 1980).
10. Average of 4 biotite gabbros from the Laramie Anorthosite Complex, Wyoming (Kolker et al., 1990).
11. Average of 29 high-Al biotite gabbro dikes from the Greaser intrusion, Laramie Anorthosite Complex, Wyoming (Mitchell et al., 1995).
12. Average of 14 other high-Al biotite gabbro dikes from the Laramie Anorthosite Complex Wyoming (Mitchell et al., 1995).

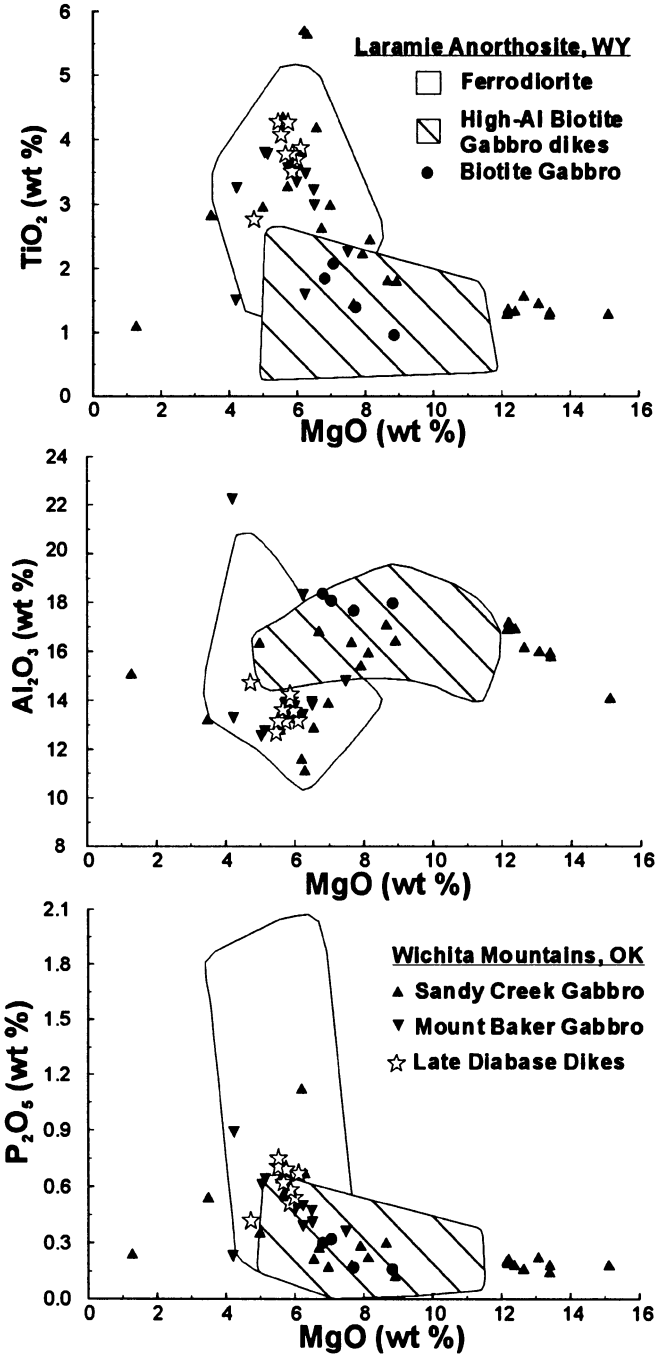

Figure 7. Variation diagrams for Roosevelt Gabbro and Late Diabase dikes from the Wichita Mountains, OK, and ferrodiorite dikes, biotite gabbros, and high-Al biotite gabbro dikes from the Laramie Anorthosite Complex, WY. Sources of data are listed in tables 2 and 3.

mingled mafic and felsic rocks known as the Cold Springs Breccia (see Vidrine and Fernandez, 1986) and thus may be related to the mafic component (*i.e.*, Otter Creek Microdiorite) of this bimodal igneous intrusion. The Late Diabase dikes have major element compositions that are olivine and nepheline-normative, and trace element abundances indicate affinities transitional between tholeiite and alkaline magmas, with a distinct "within plate" signature (Gilbert and Hughes, 1986; Cameron *et al.*, 1986). They can exhibit positive Eu anomalies which have been attributed to assimilation of plagioclase xenocrysts derived from anorthositic layers associated with a mid-crustal (15-20 km) mafic complex (Gilbert and Hughes, 1986).

Mafic dike swarms are commonly associated both with AMCG complexes and with large layered mafic intrusions. Representative analyses of major element compositions of mafic dikes from both occurrences are compared with those of the Late Diabase dikes in Table 3. Although not entirely diagnostic, P_2O_5 contents of mafic dikes from AMCG complexes tend to be greater than those from layered mafic intrusions. The Late Diabase dike suite exhibits some compositional similarities with mafic dikes from AMCG complexes in having typically high Fe, Ti, as well as P contents. However, the Al_2O_3 content of the Late Diabase dikes is noticeably lower than dikes associated with either AMCG complexes or layered intrusions. However, for some AMCG complexes such "late" diabase dikes are known to be much younger than the complexes they intrude (*e.g.*, the Harp dikes are nearly 200 Ma younger than the Harp Lake Complex, see Cadman *et al.*, 1993). Thus, any petrogenetic connection between these igneous rocks, that is based solely on their close spatial association, may be tenuous at best due to the possibility of potentially large hiatuses in magmatic activity separating these events.

High Fe-Ti-P_2O_5 contents are a characteristic signature of jotunites, ferrogabbros, ferrodiorites, ferromonzonite, and oxide-rich gabbro, all of which are common to AMCG complexes. The major element composition of the Late Diabase dikes bears a close resemblance to the average composition of four chilled mafic pillows from the Tigalak intrusion, one of many ferrodiorite intrusions present in the Nain Complex. These pillows are interpreted to be representative of the liquids that gave rise to the ferrodiorite suite (Wiebe, 1992). The major element composition of the Late Diabase dikes is also remarkably similar to that of ferrodiorite dikes, and distinct from those of the High-Al biotite gabbro dikes, from the Laramie Anorthosite Complex (Fig. 7). Mitchell et al., (1996) interpreted the ferrodiorite dikes to be representative of residual liquids after the crystallization of anorthosite. Gilbert and Hughes (1986) suggested the Late Diabase dikes were derived from a mid-crustal (15-20 km depth) mafic complex inferred to underly the SOA on the basis of geophysical and petrologic arguments (see Coffman *et al.*, 1986). Roosevelt Gabbros and Late Diabase dikes have been previously linked to a common source on the basis of geochemical similarities (Gilbert and Hughes, 1986; Cameron *et al.*, 1986). However, the presence of early primary hydrous silicates (*e.g.*, biotite and amphibole) in Roosevelt Gabbros and the anhydrous mineral assemblage of the Late Diabase dikes is an important and fundamental difference that is mirrored by the correspondingly distinct mafic liquids associated with AMCG

Table 3. Whole Rock Compositions of Late Diabase dikes from the Southern Oklahoma Aulacogen and selected basalt dikes from Layered Mafic Intrusions, and basalt dikes and ferrodiorites from Anorthosite Massifs.

	SOA	Massif Anorthosites								Layered Mafic Intrusions				
	Late Diabase	Harp Lake	Nain Complex					Mealy Swarm	Laramie	Bushveld		Duluth		Still-water
	1	2	3	4	5	6	7	8	9	10	11	12	13	14
SiO_2	47.21	46.81	48.47	49.07	47.93	44.42	44.70	46.87	47.45	49.94	51.51	47.5	50.07	50.30
TiO_2	3.76	1.93	2.80	2.81	3.36	2.44	3.34	2.63	3.18	0.68	0.40	2.56	3.45	3.40
Al_2O_3	13.62	15.47	14.90	15.46	13.27	16.34	15.97	16.3	14.51	16.21	16.32	15.29	13.46	15.70
Fe_2O_3	14.92	3.35	3.10	1.66	4.22	3.38	2.90	1.88	15.55			2.9	2.76	1.31
FeO		9.82	11.97	13.08	13.24	11.31	12.42	11.13		11.96	9.01	10.53	11.29	14.30
MnO	0.25	0.20	0.23	0.20	0.26	0.20	0.20	0.19	0.21	0.20	0.16	0.33	0.19	0.23
MgO	5.69	7.21	3.77	2.14	4.11	6.19	5.52	5.9	5.69	6.95	8.37	5.43	4.27	4.07
CaO	9.40	8.02	8.77	7.71	8.09	8.87	7.93	8.99	9.58	11.61	11.64	8.74	7.41	6.45
Na_2O	2.54	3.42	3.43	3.58	3.22	3.14	3.41	2.76	2.55	2.15	2.35	2.54	2.96	2.41
K_2O	0.79	0.76	0.63	1.42	0.90	0.70	1.32	1.05	0.60	0.15	0.20	0.93	1.34	0.22
P_2O_5	0.60	0.41	1.10	1.66	0.77	0.36	1.19	0.84	0.80	0.14	0.03	0.39	0.49	0.48
LOI	1.24	2.73	0.66		1.12	2.42	1.49	0.81	0.30					1.06
Total	100.02	101.13	99.83	98.77	100.50	99.77	100.39	99.32	100.34	99.99	99.99	97.76	98.19	99.93

1. Average of 10 basalt dikes from the Southern Oklahoma Aulacogen (Aquilar, 1988).
2. Average of 15 olivine diabase dikes from the Harp lake Complex, Labrador (Meyers and Emslie, 1977).
3. Average of 3 ferrodiorites from the Nain Complex, Labrador (Emslie, et al., 1994).
4. Average of 4 jotunites from the Nain Complex, Labrador (de Waard and Wheeler, 1971).
5. Average of 4 chilled mafic (diorite) pillows from the Nain Complex, Labrador (Wiebe, 1992).
6. Average of 12 basalt dikes of the low phosphorus group from the Nain anorthosite complex, Labrador (Wiebe, 1985).
7. Average of 11 basalt dikes of the high phosphorus group from the Nain anorthosite complex, Labrador (Wiebe, 1985).
8. Average of 15 olivine diabase dikes from the Mealy Dyke Swarm, Labrador (Emslie et al., 1984).
9. Average of 16 ferrodiorite dikes from the Laramie Anorthosite Complex, Wyoming (Mitchell et al., 1996).
10. Average composition of marginal rocks and tholeiitic sills, presumed parental B2 magma Bushveld Complex, (Harmer and Sharpe, 1985).
11. Average composition of tholeiitic sills, presumed parental B3 magma,Bushveld Complex (Harmer and Sharpe, 1985).
12. Average of 13 dykes from the Duluth Dyke swarm, Lake Superior Region (Green et al., 1987)
13. Average of 16 dykes from the Carlton County Dyke swarm, Lake Superior Region (Green et al., 1987).
14. High-Ti norite dike from the Stillwater Complex, Montana (Helz, 1985).

complexes (*i.e.*, high-Al biotite gabbros and ferrodiorite dikes). This suggests, that in the SOA, these mafic liquids also have unique sources and petrogenetic histories.

4. FELSIC ROCKS

4.1. CARLTON RHYOLITE GROUP

The Carlton Rhyolite Group consists of a thick sequence (up to 1.4 km thick) of voluminous (44,000 km^2) subaerial flows, minor ignimbrites, non-marine air-fall tuffs, agglomerates, and rare basalt flows (Ham *et al.*, 1964; Hanson, 1977; Hanson and Al-Shaieb, 1980). Although extensive in the subsurface, outcrops of Carlton Rhyolite are of limited extent in the Wichita Mountains (Fig. 2). An age of 525±25 Ma was established for Carlton Rhyolite exposed at Bally Mountain by U-Pb dating of zircon (Tilton *et al.*, 1962). A U-Pb age of 525±25 Ma on zircon from the Quanah Granite (Tilton *et al.*, 1962) permits a close temporal association of granite and rhyolite as suggested from field relationships. Results from recent geochronologic investigations substantiates this and indicates that many of the granites as well as the rhyolite crystallized within a relatively short time interval between 530 and 533 Ma (Wright *et. al.*, 1996).

Carlton Rhyolite shares many characteristics with other extensive high-temperature silicic lavas and may have a similar origin as a flood-rhyolite (*e.g.*, Henry and Wolf, 1992). The results of Zr-geothermometry suggest crystallization temperatures of ≈950°C for Carlton Rhyolite magmas (Hogan *et al.*, 1995). Other evidence for a high temperature origin include initial precipitation of vug-quartz from magmatic vapors as the high-temperature silica polymorphs β-tridymite and β-cristobalite (Bigger and Hanson, 1992). However, critical features used to distinguish flood-rhyolites from rheomorphic tuffs, such as basal contact characteristics, have not been observed due to the limited exposure. Nonetheless, the presence of single large flow-banded rhyolite flows (*e.g.*, Bigger and Hanson, 1992) and the paucity of welded tuffs (Ham *et al.*, 1964) argue against an ash-fall origin as a means of explaining the widespread areal extent of Carlton Rhyolite.

Carlton Rhyolite is typically porphyritic with phenocrysts of alkali-feldspar, lesser plagioclase, oxides, and variable amounts of partially resorbed quartz, which can locally be absent from the phenocryst assemblage, and pseudomorphs of a mafic silicate, presumably pyroxene (Ham *et al.*, 1964). Zircon and apatite occur as accessory minerals. The groundmass is comprised of feldspar, quartz, and oxides and is variably recrystallized. The development of devitrification textures (*e.g.*, spherulitic intergrowths) in the Carlton Rhyolite has been discussed in detail by Ham *et al.*, (1964) and by Bigger and Hanson (1992).

The Carlton Rhyolite exhibits many compositional features typical of A-type rhyolites. It is characterized by low CaO and high Fe/Fe+Mg (Table 4), has elevated

Table 4. Whole Rock Compositions of Granites from the Southern Oklahoma Aulacogen, AMCG Complexes, and Layered Mafic Intrusions.

	Southern Oklahoma Aulacogen					Massif Anorthosites						Layered Mafic Intrusions			
						Nain Complex			Laramie Complex			Bushveld			Sept Is.
	1	2	3	4	5	6	7	8	9	10	11	12	13	14	15
SiO_2	76.12	73.56	74.65	76.81	75.38	72.20	70.74	74.46	70.13	70.90	74.20	68.56	72.97	75.51	72.56
TiO_2	0.29	0.45	0.18	0.15	0.25	0.52	0.48	0.4	0.39	0.27	0.37	0.53	0.27	0.10	0.44
Al_2O_3	12.30	12.59	11.75	12.66	12.57	12.68	12.99	12.3	15.28	14.28	13.63	11.70	11.91	11.54	12.27
Fe_2O_3	3.11	3.82	2.22	1.46	2.37	0.86	1.2	0.42	3.73	2.57					2.04
FeO						2.96	3.1	2.46			1.41	6.63	3.69	2.18	2.01
MnO	0.04	0.08	0.03	0.03	0.05	0.04	0.05	0.04	0.1	0.04	0.03	0.16	0.07	0.03	
MgO	0.22	0.34	0.06	0.21	0.36	0.38	0.32	0.36	0.78	0.41	0.28	0.41	0.02	0.01	0.54
CaO	0.35	1.17	0.23	0.52	0.50	1.54	1.63	1.22	1.89	1.24	1.06	2.31	1.08	0.57	0.85
Na_2O	3.21	3.73	4.30	3.67	4.01	2.80	2.91	3.32	4.08	3.48	3.26	1.70	3.71	3.60	4.08
K_2O	4.49	4.30	4.69	4.79	4.91	5.07	5.38	4.38	5.27	6.38	5.37	4.22	5.01	5.11	5.10
P_2O_5	0.03	0.08	0.20	0.02	0.03	0.11	0.1	0.07	0.04	0.05	0.05	0.14	0.03	0.01	0.06
LOI						0.72	0.78	0.52	0.67	0.52		2.79	0.43	0.75	
Total	100.16	100.12	98.31	100.32	100.43	99.88	99.68	99.85	101.36	100.15	99.46	99.15	99.38	99.61	99.95

1. Average of 9 rhyolites from the Carlton Rhyolite,Oklahoma (Hogan and Gilbert, unpubl. data).
2. Average of 6 medium- to fine-grained, amphibole-biotite granites from the Mount Scott Granite, Oklahoma (Price et al., 1996).
3. Average of 2 coarse-grained biotite granites from the Quanah Granite, Oklahoma (Myers et al., 1981).
4. Average of 5 fine-grained, variably granophyric, biotite granites of the Headquarters Granite, Oklahoma (Hogan and Gilbert, unpubl. data).
5. Average of 10 coarse-grained, hornblende-biotite granites of the Reformatory Granite, Oklahoma (Hogan and Gilbert, unpubl. data).
6. Average of 11 biotite-hornblende granites, Umiakovik batholith, Nain Complex, Labrador (Emslie and Stirling, 1993).
7. Average of 8 biotite-hornblende granites, Makhavinekh pluton, Nain Complex, Labrador (Emslie and Stirling, 1993).
8. Average of 5 biotite granites, Voisey Bay - Zoar pluton, Nain Complex, Labrador (Emslie and Stirling, 1993).
9. Welded tuff, Laramie Anorthosite Complex, Wyoming (Geist et al., 1989).
10. Average of 3 granites from the Sherman Granite, Laramie Anorthosite Complex, Wyoming (Geist et al., 1989).
11. Average of 4 granites from the Maloin Ranch pluton, Laramie Anorthosite Complex, Wyoming (Kolker and Lindsley, 1989).
12. Average of 182 Low-Mg felsites of the Rooiberg Group, Bushveld Igneous Province, South Africa (Twist and Harmer, 1987).
13. Average of 12 coarse-grained, hornblende-biotite granites of the Nebo Granite, Bushveld Igneous Province (Kleemann and Twist, 1989).
14. Average of 9 typically fine-grained,biotite granites of the Klipkloof Granite, Bushveld Igneous Province (Kleemann and Twist, 1989).
15. Average of 7 granites from the Sept Iles Complex, Quebec, (Higgins and Doig, 1986).

abundances of high field strength elements (*e.g.*, Zr ≈ 600-750 ppm), and distinctly "within-plate" trace element characteristics (Weaver and Gilbert, 1986). Previously, the rhyolites and granites have been interpreted to be comagmatic (Ham *et al.*, 1964; Gilbert, 1982), but differences in trace element abundances, particularly Zr, have been used to suggest that Carlton Rhyolite is not the direct extrusive equivalent of Wichita Granites (Weaver and Gilbert, 1986).

4.2. WICHITA GRANITE GROUP

Members of the Wichita Granite Group form extensive subhorizontal granite sheets that appear to be preferentially localized along the unconformable contact between the underlying Glen Mountains Layered Complex and the overlying Carlton Rhyolite Group (Ham *et al.*, 1964; Hogan and Gilbert, 1997). Intrusive relationships of the Wichita Granite Group with these two units are unequivocal: 1) Wichita Granites exhibit sharp cross-cutting contacts, with well defined chilled-zones, against Carlton Rhyolite Group rocks, 2) dikes of Wichita Granite cross-cut the Glen Mountains Layered Complex at several locations, 3) gabbroic xenoliths are present in the basal contact zones of some granites, 4) rhyolite xenoliths are commonly observed in Wichita Granites, 5) partially resorbed anorthite-rich xenocrysts are observed within granite that is adjacent to the Glen Mountains Layered Complex, and 6) the Glen Mountains Layered Complex is extensively altered adjacent to the contact with Wichita Granite (*e.g.*, Stockton, 1984).

Contact relationships between Wichita Granite and Roosevelt Gabbros are more enigmatic and remain the source of some debate (*e.g.*, Gilbert and Myers, 1986; Price *et al.*, this volume). The Mount Scott Granite sheet, the largest recognized lithodemic unit, becomes considerably more heterogeneous, and more mafic, as contacts with the Raggedy Mountain Gabbro Group are approached. A highly variable population of mafic, and less commonly felsic, enclaves can be locally abundant in Mount Scott Granite adjacent to Roosevelt Gabbro. Hybrid rock types, some of which have been described by Huang (1955) and Stockton (1984) can be spatially associated with these contacts.

Members of the Wichita Granite Group are typically hypersolvus leucocratic alkali feldspar granites (Myers *et al.*, 1981; Gilbert and Myers, 1986). However, minor amounts of primary plagioclase crystallized in some granites (*e.g.*, Mount Scott Granite, Headquarters Granite). Porphyritic textures are common, although most granites are seriate, and rarely equigranular. They are typically medium (1-5 mm) to fine-grained (<1 mm) and variably granophyric (Hogan and Gilbert, 1997). Distinctly coarse-grained (1-2 cm) granites are present but less abundant. Coarser-grained granites invariably intrude finer-grained granites. Quartz and feldspar commonly exhibit textural evidence for multiple periods of growth separated by resorption (Hogan and Gilbert, 1991). Early crystallizing antiperthitic ternary anorthoclase, with reintegrated compositions of $Ab_{63-76}Or_{15-33}An_{4-12}$, have been identified in the Mount Scott Granite sheet (Price *et al.*, 1996a). The Mount Scott Granite sheet also exhibits

rapakivi textures, including facies with mantled (*i.e.*, wiborgite) and unmantled (*i.e.*, pyterlite) ovoid phenocrysts. Amphibole, biotite, and Fe-Ti oxides are common as minor phases. The amphiboles are ferro-edenitic hornblende and are characterized by low Al contents, high Fe^{2+}/Fe^{3+}, high Fe/Fe+Mg (.67-.77) and high F contents (Hogan and Gilbert, 1995). Biotites are also characterized by low Al, high Fe/Fe+Mg, and high F contents (Hogan, unpublished data). Accessory minerals include zircon, apatite, titanite, fluorite, ±allanite, and carbonate. Although zircon can be common, recent geochronologic investigations have failed to identified the presence of inherited zircon in plutons studied thus far (Wright *et al.*, 1996). Thus, temperatures of ≈900-950°C recorded by the Zr and P_2O_5 chemical geothermometers may represent minimum liquidus temperatures for these magmas (Hogan *et al.*, 1995).

Major element abundances of rhyolite and granite from AMCG complexes, from layered mafic complexes, and from the Carlton Rhyolite Group and Wichita Granite Group, are presented for comparison in Table 4. As expected, the major element compositions of these granites are all broadly similar: a reflection of many petrologic processes ultimately resulting in melt compositions that coincide with thermal minima in the haplogranite system (Tuttle and Bowen, 1958). The subtle differences that do exist from one complex to another (*e.g.*, Na_2O) do not appear to be diagnostic of a particular origin. For example, felsic rocks from the Bushveld Complex are noticeably lower in Al_2O_3, and those associated with the Laramie AMCG complex noticeably higher in Al_2O_3. However, there is little difference between Al_2O_3 of granites from the Nain Complex and those from the Sept Isles Complex. At low SiO_2 contents (50-65 wt%) the compositional trends for AMCG granite suites diverge from those of other mid-Proterozoic A-type granites: AMCG A-type granites typically exhibit consistently higher total alkali content, Fe/Fe+Mg, CaO, TiO_2, Sr, and lower Rb abundances (Emslie, 1991). This comparison is hindered by the fact low silica "granitoids" are essentially restricted in occurrence to AMCG complexes. However, the high Fe/Fe+Mg (>0.8%) values of AMCG granites persist at high SiO_2 contents whereas other mid-Proterozoic A-Type granites display a considerably broader range (see Emslie, 1991 Fig. 2A). The Fe/Fe+Mg of both Carlton Rhyolite and Wichita Granites remains high (>0.8%) at high SiO_2 contents as well and displays considerable overlap with the field defined by AMCG granites (Fig. 8). This ratio is also very high for the Bushveld Granites due to their *distinctively* low MgO abundances (Table 4).

5. DISCUSSION

Igneous rocks of the SOA and those of Mid-Proterozoic AMCG complexes exhibit many broad similarities that suggest a commonality in their petrogenesis. These similarities, as well as important differences, will be compared in the following sections.

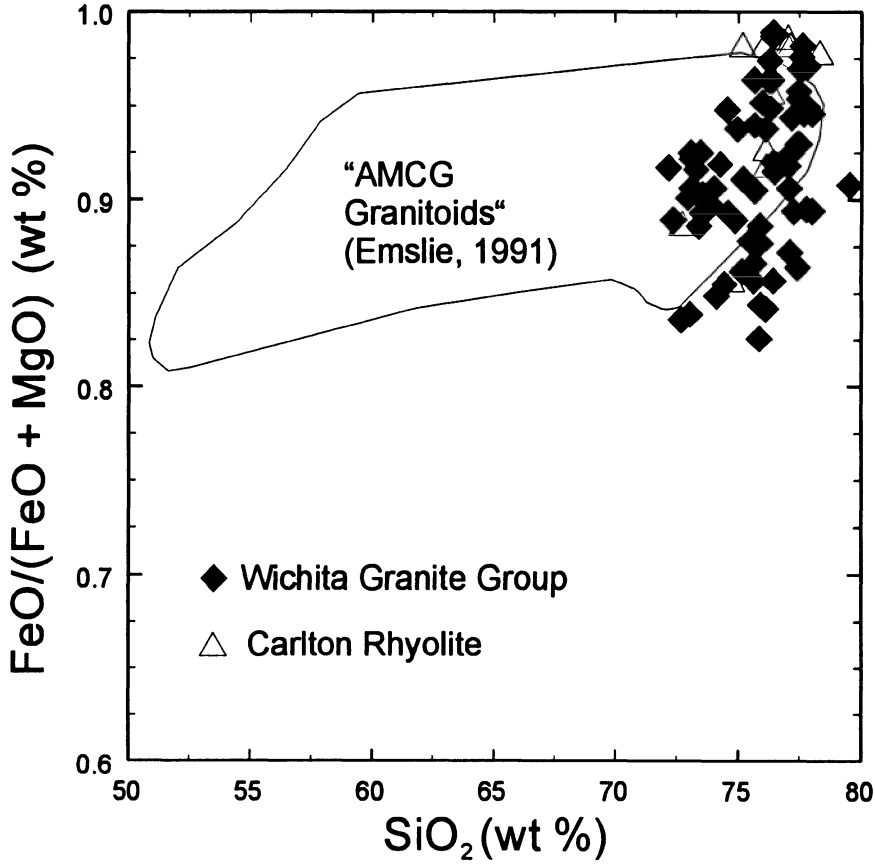

Figure 8. "FeO#" vs SiO_2 for whole rock samples of granite from the Wichita Granite Group and of rhyolite from the Carlton Rhyolite formation, Wichita Mountains, OK.

5.1. PRINCIPAL ROCK TYPES

AMCG complexes are best known for the close temporal and spatial association of three distinctive rock types: massif anorthosites, rapakivi granite, and the volumetrically minor, "jotunite" or ferrodiorites. Comparison of these rock types with potential counterparts in the SOA is discussed below.

5.1.1. Massif-type anorthosites

The absence of coarse-grained massif-type anorthosite plutons in the SOA represents a prominent void in the characteristic igneous assemblage of AMCG complexes. Ashwal (1993) previously considered the Glen Mountains Layered Complex transitional between massif-type anorthosites and anorthosites associated with layered

mafic complexes. However, the presence of calcic plagioclase, well defined macro-cyclic units, modal layering, cryptic layering, and distinctive "pothole" structures indicates the Glen Mountains Layered Complex is best considered as a typical layered mafic complex (*e.g.*, Bushveld Complex). A similar conclusion was previously reached by Powell and Phelps (1977) on the basis of mineral compositional variations. This is further substantiated by the similarity in whole rock composition of anorthosite from the Glen Mountains Layered Complex with anorthosite from other typical layered mafic complexes (Table 1).

More importantly, the distinctive high-Al orthopyroxene megacrysts, a hallmark of AMCG massif-type anorthosites, have yet to be reported from the Glen Mountains Layered Complex. In fact, orthopyroxene is typically a minor constituent of rocks of the Glen Mountains Layered Complex, occurring mainly as a post-cumulus reaction rim on olivine phenocrysts (Powell *et al.*, 1980b). The abundance of clinopyroxene, lack of orthopyroxene, and plagioclase compositions typical for layered mafic intrusions in the Glen Mountains Layered Complex suggests limited contamination of the magma by aluminous crustal sediments (see Bowen 1928). Values for oxygen ($\delta^{18}O$ 5.7-7.2 per mil) and sulfur ($\delta^{34}S$ 0.0-+3 per mil) isotopes from unaltered whole rock samples also eliminate the possibility that parent magmas assimilated *substantial* amounts of mature continental crust (Cooper, 1991). This would suggest that εNd_{528} values of 3.63 to 5.35 reported for this complex by Lambert *et al.*, (1988) are an intrinsic feature of their mantle source rather than the result of crustal contamination.

The role of crustal contamination in the formation of massif-anorthosites is clearly a complex one. Emslie (1985) noted that orthopyroxene-bearing anorthosite massifs exhibit consistently higher initial Sr and lower εNd in comparison to olivine-bearing anorthosites, a feature he attributed to assimilation of felsic material. Anderson and Morrison (1992), pointed out that the majority of mafic plutonic rocks associated with the mid-Proterozoic AMCG complexes exhibit initial εNd values that are significantly less than that of depleted mantle, and suggested derivation of these magmas from subcontinental mantle that was slightly enriched to chondritic in composition, but they did not rule out the possibility of some crustal contamination. Scoates and Frost (1996) were able to demonstrate an important role for assimilation in formation of the Laramie Anorthosite Complex that increasingly diminished in successively younger batches of magma. They suggested that the magma conduit that fed this mid-crustal complex must have become increasingly more insulated from crustal contamination with time. Thus, the apparently limited role for crustal contamination in the formation of the Glen Mountains Layered Complex suggest the magmas that formed this body traversed the crust along "preconditioned" conduits, thereby inhibiting crustal contamination and heat loss, and facilitating a relatively rapid ascent to shallow crustal levels.

Although absent from the AMCG acronym, layered mafic complexes are a common feature of many AMCG complexes. The Kiglapait (Morse, 1969), Newark Island (Wiebe, 1988), and Reid Brook (Ryan *et al.*, 1995) are just a few of the better known layered mafic intrusions temporally and spatially associated with the Nain

Plutonic Suite. The Bjerkreim-Sokndal is a prominent layered mafic intrusion associated with the Rogaland AMCG complex in Norway (Duchesne *et al.*, 1989). Detailed mapping of massif-type anorthosite plutons of the Laramie Anorthosite Complex (*e.g.*, Poe Mountain anorthosite) has revealed internal structure, compositional layering, and cryptic variations that are akin to those observed in much more typical mafic layered complexes (Frost et al., 1996). Morse (1968) considered massif anorthosites and layered mafic intrusions to be very closely related, postulating flotation of plagioclase during crystallization of a high-alumina basalt (i.e, a reasonable parent magma for many layered mafic intrusions) as a plausible mechanism for generating massif anorthosites. Thus, the Glen Mountains Layered Complex, although not a massif-type anorthosite body, is considered by us to be an important link in the similarity of igneous activity associated with the SOA and that of AMCG complexes.

5.1.2. Ferrodiorite suite

For AMCG complexes, intermediate rock types are represented by the distinctive, but volumetrically minor, ferrodiorite or "jotunite" suite (*e.g.*, McLelland and Whitney, 1990; Wiebe, 1992; Owens *et al.*, 1993). These intrusions are referred to as ferrodiorites due to the characteristically high Fe/Fe+Mg content of the mafic silicates and the presence of andesine (*e.g.* Emslie, 1978). However, they are commonly comprised of olivine gabbro, olivine monzogabbro, monzonorite and monzonite, as well as olivine-ilmenite rocks, and were originally classified as "intermediate" because of their temporal and compositional relationship *relative* to the anorthositic and granitic plutons (Ryan and Emslie, 1996). In this sense, the Roosevelt Gabbros exhibit many of these characteristic rock types, including olivine-ilmenite rocks (*e.g.*, Powell, 1986) and thus bear a strong similarity to the ferrodiorite plutons of AMCG complexes. Roosevelt Gabbros also exhibit the relatively high TiO_2 and P_2O_5 contents that are a hallmark of the AMCG ferrodiorite suites (Table 2). However, Mitchell et al., (1995; 1996) have recognized two distinct mafic liquids in the Laramie Anorthosite Complex that have unique petrogenetic histories: 1) Ferrodiorite melts interpreted to be residual liquids derived from crystallization of anorthosite massifs, and 2) High-Al biotite gabbro melts interpreted to be primary liquids to the anorthosite massifs. An important distinction between rock types that are representative of these two liquids is the anhydrous nature of the ferrodiorite suite and the hydrous nature (*e.g.*, early biotite) of the high-Al gabbroic suite. Examples of these two distinct liquids are also present in the SOA. The intrinsically "hydrous" Roosevelt Gabbros exhibit mineralogical and compostional similarities to the high-Al biotite-bearing gabbros of the Laramie Anorthosite Complex (see Table 2). The anhydrous Late Diabase dikes are more mineralogically and compositionally similar to ferrodiorite from AMCG complexes (see Table 3). This fundamental similarity suggest a commonality in the petrogenetic evolution of the SOA and Mid-Proterozoic AMCG complexes.

In AMCG complexes, as well as in the SOA, "intermediate" plutons typically occur along the contact between underlying anorthositic plutons and overlying granite plutons. Intrusive relationships with the anorthositic rocks indicate the ferrodiorite

plutons are younger (*e.g.*, Ryan and Emslie, 1996), however contacts with granite are more complex and the presence of hybrid and mingled rock types suggest intrusion of coeval felsic and mafic magmas (*e.g.*, Wiebe, 1990). Similarly styled contacts are observed for Roosevelt Gabbro plutons, which exhibit clear intrusive relationships with anorthositic gabbro of the Glen Mountains Layered Complex but complex enigmatic hybrid contacts with the Wichita Granite Group (*e.g.*, Gilbert and Myers, 1986) and appear to be emplaced near the contact between the Glen Mountains Layered Complex and the overlying granite sheets (see Price *et. al.*, this volume). Recent geochronologic investigations have determined crystallization ages of 539±2 Ma from $^{40}Ar/^{39}Ar$ laser investigation of primary amphibole, and an age of 533±2 Ma from a U-Pb age of zircon, for the Mount Scott Granite sheet (Hogan *et al.*, 1996). These ages permit a close temporal association of Mount Scott Granite and the adjacent Mount Sheridan Gabbro (see previous discussion) and indicate that magmatism associated with formation of the SOA may be better characterized by penecontemporaneous mafic and felsic magmatism rather than two compositionally distinct magmatic events as previously thought.

5.1.3. Granites

Although Cambrian in age, granites of the Wichita Granite Group share many characteristics of A-type granites of the Proterozoic AMCG complexes (see Emslie, 1991 for a recent summary of AMCG granite characteristics). Close temporal and spatial association with anorthositic rocks is considered a distinguishing characteristic of AMCG granite suites. In this sense the Wichita Granite Group has affinities for AMCG granites because of their association with anorthositic gabbros of the Glen Mountains Layered Complex. AMCG granite suites are dominantly metaluminous in composition, peraluminous granites are considerably less abundant and perakaline granites are rare, and of small volume, as is also the case for the Wichita Granite Group (Gilbert and Myers, 1986). In both suites alkali feldspar, plagioclase, and quartz commonly exhibit evidence for multiple episodes of growth, and resorption, and rapakivi textures are common, although not universal. Hypersolvus ternary feldspars are reported from some AMCG granites as well as some Wichita Granites (*e.g.*, Price *et al.*, 1996a), attesting to the relatively high temperature and low fH_2O for these magmas. In AMCG complexes, hornblende and biotite, with Fe/Fe+Mg >0.8, are typical minor phases in high level intrusions, whereas Fe-rich pyroxene and fayalite can occur locally, but are more common in deeper level mangerites and charnockites. Ferroedenitic hornblende and annitic biotite are typical of the high-level Wichita Granites whereas Fe-rich pyroxene and Fe-rich olivine are rare (*e.g.*, Hogan and Gilbert, 1995). Common accessory minerals in both suites include Fe-Ti oxides, zircon, apatite, ±allanite, and fluorite. Although zircon is commonly an abundant accessory mineral, the presence of old inherited zircon in AMCG granites is rare and suggestive of initially high temperatures for these dominantly metaluminous magmas (Emslie, 1991). Zircon from the Wichita Granites exhibit evidence for multiple periods of growth but U-Pb dating of these minerals has yet to reveal substantial amounts of inheritance (Wright *et al.*, 1996). Titanite, monazite, carbonate, and sulphides are rare

to absent in AMCG granites, whereas all but monazite occur as primary and secondary accessory minerals in Wichita Granites.

AMCG granites appear to have crystallized under consistently reduced fO_2 in comparison to other A-type granites (Emslie, 1991). This is in contrast to the Wichita Granites which commonly contain primary titanite, suggesting crystallization under slightly higher fO_2 conditions (*e.g.*, Wones, 1989). The scarcity of miraolitic cavities, pegmatites, and aplites, and the late crystallization of hydrous silicates is used to infer crystallization under low-fH_2O (*i.e.*, fluid-undersatured conditions) for the bulk of granites from AMCG complexes and from the Wichita Granite Group. The presence of primary fluorite, and high F contents of mafic silicates suggests F has played an important role in the petrogenesis of some Wichita Granites (Price *et al.*, 1996; Hogan and Gilbert, 1997). However, the role of F and CO_2 in the petrogenesis of AMCG granites remains a source of debate (Emslie, 1991; Frost and Touret, 1989).

5.2. TECTONIC SETTING

Igneous activity associated with the SOA and with AMCG complexes is anorogenic. AMCG complexes typically straddle prominent tectonic boundaries between older crustal blocks (*e.g.* Laramie Complex, Geist *et al.*, 1989; the Nain Plutonic Suite, Ryan and Emslie, 1996) having formed within 100 Ma (or less) to 600 Ma after the collisional event (Emslie, 1991). The Cambrian rifting event that formed the SOA postdates the ≈1.1 Ga Grenvillian Orogeny by several 100's of Ma. The resulting aulacogen transects an older tectonic boundary between distinct crustal blocks (Fig. 1). In addition, the orientation of rift-related faults coincides with the structural grain of the underlying 1.3-1.4 Ga basement making a strong case for structural inheritance (Ham *et al.*, 1964; Denison, 1995).

AMCG magmatism is thought to have been triggered by mantle plumes, or hot spots, and presumably may reflect magmatism associated with aborted continental rifting (*e.g.*, Emslie, 1978, Emslie *et al.*, 1994). Roosevelt Gabbros and Late Diabase dikes exhibit trace element characteristics typical of "within-plate" magmatism and suggest the involvement of a mantle-plume component in their petrogenesis (Cameron *et al.*, 1986). The Carlton Rhyolite and Wichita Granites are definitive examples of A-type felsic magmas associated with a intracontinental rift environment with trace element characteristics similar to those of Ocean Island Basalts (Hogan *et al.*, 1995). In addition to the Late Diabase dikes, rare "rhyolite" dikes cross-cut members of the Wichita Granite Group (Ham *et al.*, 1964). Their presence demonstrates that felsic-magmas continued to rise and presumably breached the surface after emplacement and cooling of granite, but more importantly they signify that tectonism, resulting in uplift and erosion, accompanied younger magmatic events (Gilbert and Myers, 1986). McConnell and Gilbert (1990) present a convincing case that fault block rotation, along listric normal faults related to extension, accompanied magmatism during formation of the SOA. However, unlike the SOA, direct evidence for rifting during emplacement of massif anorthosites has not been established (Wiebe, 1992).

5.3. INTRUSIVE STYLE

AMCG complexes are built up from sequences of closely spaced igneous events that result in multiple intrusions, commonly in the form of tabular sills and sheets. Gravity studies suggest that most of the massif anorthosite bodies are relatively tabular sheet-like plutons (Wiebe, 1992). In the Nain Plutonic Suite, many of the granites (Wheeler, 1968; Ryan, 1991), as well as the ferrodiorites (Wiebe, 1992; Ryan and Emslie, 1996), also have sheet forms, with flat floors underlain by anorthosite plutons and the adjacent gneissic country rock. The ferrodiorites are typically sandwiched between the underlying anorthosite and overlying granite and commonly exhibit hybridized contacts with the granite (Wiebe, 1992).

A similar history and intrusive style is beginning to emerge for igneous activity in the SOA. Gravity modeling indicates the aulacogen is floored by the Glen Mountains Layered Complex a large tabular shaped intrusion approximately 3-4 km thick (Coffman *et al.*, 1986). Overlying this intrusion is a very thin veneer (≈1-2 km thick) of granite and rhyolite. Hogan and Gilbert (1997) have documented the sheet-form for many of the Wichita Granite plutons. Recent geochronological investigations indicate that these granites and the overlying rhyolite cover were extruded and intruded in a narrow time interval, potentially less than 5 Ma (Wright *et al.*, 1996). The Fe-Ti-P-rich Roosevelt Gabbros are also spatially associated along the contact between underlying anorthositic gabbro and overlying granite sheet. Some Roosevelt Gabbro plutons may have begun to spread out along this contact and developed immature sheet-like morphologies for portions of the intrusions (Price *et al.*, this volume). Hybridized rocks are common along the gabbro-granite contacts. Recent age determinations indicate that some of these intrusives may be slightly younger than or coeval with spatially associated granite sheets (Hogan *et al.*, 1996).

5.4. DEPTH OF EMPLACEMENT

AMCG complexes appear to have been emplaced at mid- to shallow-crustal levels. Thermobarometric studies suggest final emplacement at depths ranging from 6 to 16 km (Fuhrman *et al.*, 1988; Jansen *et al.*, 1985; Berg, 1979). Many of the magmas of these complexes are likely to have undergone a period of high pressure (6-11 kb) crystallization before reaching the emplacement level (*e.g.*, Emslie *et al.*, 1994). However, there is scant evidence for deeper levels of emplacement at depths of 25 km or more (Emslie, 1981; Anderson, 1980). The presence of rare volcanics (Emslie, 1991) and rhyolite dikes (*e.g.*, Ryan and Emslie, 1996) associated with younger intrusions in these complexes suggest a substantial amount of uplift, accompanied by erosion, must have occurred during the course of the igneous activity. Such uplift can be attributed to doming and lithospheric thinning as a result of invasion of the crust by large volumes of high temperature magmas (Hill and Miller, 1990).

In contrast to the mid-crustal AMCG complexes, the preponderance of rhyolite and intrusive relationships of sheet-granites with the coeval rhyolite cover demonstrates a

subvolcanic emplacement for felsic plutonic rocks of the SOA. If the Roosevelt Gabbros are indeed penecontemporaneous with the intrusion of the granites (see previous discussion), stratigraphic constraints would indicate a shallow level of emplacement for these magmas as well. As previously discussed, prior to extrusion of the Carlton Rhyolite the older Glen Mountains Layered Complex was presumably uplifted and 1-4 km of layered section eroded, possibly exposing the middle of the intrusion (Powell and Phelps, 1977). Although the original depth of emplacement for the Glen Mountains Layered Complex is unknown, the fine-grained nature of this intrusion and the presence of orthopyroxene reaction rims on olivine at very low fH_2O implies crystallization at low pressures. The absence of any significant sedimentary rift-fill suggests the aulacogen must have been part of a large area of positive topographic relief, presumably due to the high heat flow associated with the rift. Powell and Phelps (1977) questioned if uplift due to crustal doming would be sufficient to expose the intrusion at its mid-section in a reasonable amount of time. However, McConnell and Gilbert (1990) suggest rapid uplift and erosion of the Glen Mountains Layered Complex is likely to have been accentuated by block faulting and tilting during lithospheric extension. The late intrusion of "rhyolite" dikes also indicates contemporaneous igneous and tectonic activity (*i.e.*, uplift) throughout the duration of the rifting event (see earlier discussions).

Geophysical and petrologic arguments suggest near surface to extrusive igneous activity in the SOA was accompanied by intrusion of a substantial amount of magma at mid-crustal depths. Gravitational modeling, and petrologic arguments, require a second more substantial layered mafic complex to reside at mid-crustal levels (≈15-21 km depth) to account for the significant gravitational anomaly centered over the aulacogen (Coffman *et al.*, 1986). Gilbert and Hughes (1986) postulated this buried mafic complex as the source for the Late Diabase dike suite. McConnell and Gilbert (1990) used the normative compositions of the granites to suggest felsic liquids were initially derived at pressure of 4 kb or approximately 12-15 km depth. They further postulated that the mid-crustal mafic complex may have supplied the necessary heat to produce the Wichita Granites. One of the these granites, the Mount Scott Granite sheet is interpreted to have undergone partial crystallization at approximately 2 kb prior to emplacement beneath the volcanic cover, suggesting the possible development of temporary magma chambers as this magma migrated up towards its ultimate emplacement level (Hogan and Gilbert, 1995; Price *et al.*, 1996). The ponding of magmas at several levels in the crust raises the possibility for a connection between the typical AMCG complexes that developed at mid-crustal levels during extension and complexes similar to the SOA that formed at the surface. The numerous dikes that cut AMCG complexes, such as the the Laramie complex, may represent conduits that were feeding near surface complexes such as the SOA as suggested by the compositional similarities in rock types exhibited by these two provinces. Such near-surface expressions of magmatism related to Mid-Proterozoic AMCG complexes are rare as most are likely to have been removed by erosion. Conversely, we speculate that if the inferred mid-crustal mafic complex beneath the SOA were to be exposed it would look like a typical Mid-Proterozoic AMCG complex (Fig. 9).

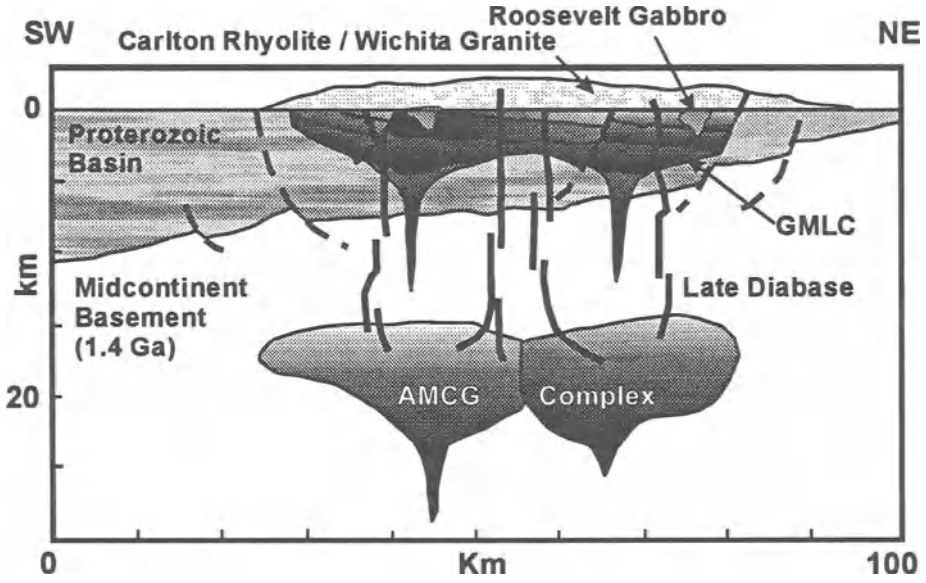

Figure 9. Schematic cross-section of the crust across the Southern Oklahoma Aulacogen during Cambrian time. The presence of a large mid-crustal AMCG complex is inferred on the basis of petrologic and geophysical data (see Coffman et al., 1986; McConnell and Gilbert, 1990; and this paper). The brittle-ductile transition, and temporary storage chambers for felsic magmas, at approximately 8 km depth (see Hogan and Gilbert, 1995) have been omitted for clarity.

5.5. PETROGENESIS

5.5.1. AMCG Complexes

The petrogenesis of AMCG complexes has attracted considerable interest (see Weibe, 1992 for a review). Proposed models include derivation by fractionation of high alumina basaltic magma (*e.g.*, Fram and Longhi, 1992), accompanied by crustal assimilation (*e.g.*, Emslie *et al.*, 1994), to coeval crystallization of distinct magmas from unique sources (*e.g.*, McLelland and Whitney, 1990) as well as variants of these models. As summarized from Weibe (1992) and Emslie *et al.*, (1994) basaltic magma trapped at the base of a thick, tectonically stable, craton would undergo a period of extended high pressure fractionation. The heat released from this basaltic underplate triggers crustal anatexis and the formation of granitoid magma. Extraction of these felsic magmas leaves behind an aluminous plagioclase-pyroxene granulite restite that is assimilated by the basaltic underplate. Isotopic studies of AMCG complexes have identified the signature of older crust in some of these mafic intrusions (Geist *et al.*, 1990; Emslie *et al.*, 1994; Scoates and Frost, 1996). During crystallization of this magma, gravitational separation of plagioclase crystals from more dense ultramafic cumulates results in enrichment of the magma in the upper levels of the chamber in plagioclase and plagioclase components. With continued fractionation the denser

magma approaches compositions which may represent parental magmas for the ferrodiorite suite. Recharge of the chamber with new hot basaltic liquid results in resorption of some plagioclase crystals and the formation of hyperfeldspathic liquids. Such a process may be enhanced due to relatively slow rates of heat loss from deep crustal magma chambers. Once formed, these low density magmas, laden with plagioclase crystals, are gravitationally unstable and may rise as diapirs to mid-crustal levels to form the massif anorthosite complexes (Longhi and Ashwal, 1985). Subsequent basaltic liquids may rise to this same level filling mid-crustal magma chambers capable of convection, which then crystallized insitu as layered mafic complexes. The "intermediate" ferrodiorites have been interpreted as crystallizing from magma consanguineous with those that formed the massif anorthosites and may represent residual liquids that were squeezed out by filter pressing (Owens *et al.*, 1993; Emslie *et al.*, 1994; Mitchell *et al.*, 1996). Alternatively, McLelland and Whitney (1990) suggest massif anorthosites, ferrodiorites, and granites all crystallized from unrelated magmas with distinct sources. The more enriched isotopic signature of granites associated with AMCG complexes suggest their derivation primarily from anatexis of older continental crust with supplements from materials with shorter crustal residence times (Emslie *et al.*, 1994).

5.5.2. The Southern Oklahoma Aulacogen

The temporal and spatial relationships of major igneous events in the SOA resembles that of the AMCG complexes. An early formed, extensive anorthositic gabbro (*i.e.*, Glen Mountains Layered Complex) forms the substrate to overlying younger A-type sheet granites (*i.e.*, Wichita Granite Group), and in the case of the SOA, their associated rhyolite cover (*i.e.*, Carlton Rhyolite Group). In the SOA, rocks of the ferrodiorite suite of AMCG complexes have the closest compositional match with the Fe-rich and Ti-rich Late Diabase dikes, whereas the Roosevelt Gabbros are most similar to the high-Al biotite gabbro dikes. However, Roosevelt Gabbros form plutons, as well as dikes, which have spatial and temporal relationships in the SOA that are similar to those of the ferrodiorite plutons in AMCG complexes (*e.g.*, the Nain Complex, see Wiebe, 1992). The Roosevelt Gabbros commonly share contacts with both the Glen Mountains Layered Complex and the Wichita Granite Group. Although clearly intrusive into the layered complex, contact relationships with the granites are more enigmatic and commonly delineated by the presence of hybridized rock types. Previously considered to be older than the granites (*e.g.*, McConnell and Gilbert, 1990), new geochronologic information indicates the possibility that some Roosevelt Gabbro magmas may have been penecontemporaneous with the granite liquids. Powell (1986) argued convincingly for derivation of the Glen Mountains Layered Complex and Roosevelt Gabbros from distinct mantle derived magmas. If the SOA is a younger analog for AMCG complexes, this raises the possibility that some ferrodiorite plutons crystallized from magma independent of that which gave rise to the massif anorthosites (*e.g.*, Duchesne *et al.*, 1989; McLelland and Whitney, 1990; Vander Auwera and Longhi, 1994)

Formation of the SOA involved contemporaneous lithospheric extension and extensive bimodal igneous activity (McConnell and Gilbert, 1990). Although the tectonic setting of SOA is well constrained (Gilbert, 1983), petrogenesis of the associated igneous rocks, particularly the rhyolites and granites, is not well known. Early on, Hamilton (1956) suggested the granites and rhyolites were derived from extensive fractionation of the underlying layered mafic complex. However, Ham *et al.*, (1964) recognized the older layered mafic complex and younger felsic igneous rocks to be separated by an unconformity and concluded the Carlton Rhyolite and Wichita Granites were not differentiates of the parent gabbroic magma which created the GMLC. Subsequent workers have predominantly proposed derivation of the felsic magmas by partial melting of older continental crust as a result of intraplating of mafic magmas during crustal extension (*e.g.*, McConnell and Gilbert, 1990). However, recent Nd isotopic studies of the Carlton Rhyolite, Wichita Granites, and the Late Diabase dikes show strong isotopic similarities, which preclude direct derivation of the felsic magmas by anatexis of ancient crust (Hogan *et al.*, 1995).

The limited role for assimilation of older continental crust in the petrogenesis of both mafic and felsic igneous rocks in the SOA, as indicated by their primitive isotopic signatures, is in contrast with isotopic results from AMCG complexes (see previous discussions). A lack of isotopic contrast between the intruding magma and the crustal contaminant, for example as a result of relatively small differences in the formation ages of the two rock types, can mask the importance of assimilation in the petrogenesis of some plutons associated with AMCG complexes (*e.g.*, see Frost *et al.*, 1996). However, in the case of the SOA, a significant isotopic contrast is expected between potential crustal contaminants, the 1.4-1.3 Ga mid-continent Granite-Rhyolite terrane with T_{DM} ages of 1.7-2.0 Ga (see Fig. 1), and the $\approx$0.535 Ga mantle derived igneous rocks associated with the aulacogen because of the large difference in their formation ages. Thus, the primitive isotopic composition of mafic rocks from the SOA suggests that assimilation of old continental crust was of minor importance in their petrogenesis. For the SOA, this distinction may be a consequence of the rapid transport of magma from deep source regions to surface and subvolcanic conditions of emplacement. Here magma transport is likely to have been facilitated by the presence of large-scale crustal fractures associated with the rifting event (Hogan and Gilbert, 1997). Rapid ascent of theses magmas through the crust, and quick cooling at the emplacement level, would inhibit wall rock assimilation. In addition, the crust may be preconditioned by the repeated passage of earlier magmas such that the potential for crustal contamination is significantly reduced for younger magma batches (Scoates and Frost, 1996). The presence of mafic igneous rocks, inferred to underlie the SOA, may have contributed in a similar fashion to limiting crustal contamination, as well as heat loss, thus enabling some magma batches to rise to the surface, and near-surface, relatively pristine.

The substantial mid-crustal mafic complex that is inferred to reside beneath the SOA may have been emplaced at a depth more favorable for development of a typical AMCG complex. The experimental studies of Fram and Longhi (1992) demonstrate plagioclase-melt partitioning in high-alumina basalts is highly dependent on pressure.

Crystallization at pressures of 10-11.5 kb yield liquidus plagioclase crystals with compositions of An_{60}-An_{54} that are well within the range of plagioclase compositions typical for massif anorthosites. Crystallization at low pressure produces more anorthitic plagioclase (*e.g.*, An_{76} at 1 bar). Thus, at substantially higher pressures, the high alumina basalt which formed the epizonal Glen Mountains Layered Complex would be an appropriate parent magma for massif anorthosites. The positive Eu anomalies exhibited by several Late Diabase dikes indicate derivation from hyperfeldspathic liquids, possibly as a result of plagioclase assimilation (Gilbert and Hughes, 1986). If derived from the inferred mid-crustal mafic complex, these dikes lend support to the possibility that this deep level intrusion may more closely resemble a typical AMCG complex. Conversely, the SOA may be considered an analog for upper crustal igneous and tectonic processes concomitant with emplacement of the deeper level AMCG complexes (Fig. 9).

6. CONCLUSIONS

Igneous rocks of the SOA and those of the mid-Proterozoic AMCG complexes bear many similarities that suggest a commonality in the petrogenesis. Counterparts in AMCG complexes can be found for most igneous rock units in the SOA. In particular the Fe-Ti-P-rich biotite gabbros of the Roosevelt Gabbros and Late Diabase dikes bear strong compositional and mineralogical similarities to high-Al biotite gabbros (*e.g.*, Mitchell et al., 1995) and to the well known "intermediate" ferrodiorite suites respectively, that are so characteristic of the Mid-Proterozoic AMCG complexes.

A rift-related origin for igneous rocks of the SOA is well documented whereas direct evidence for extension during emplacement of AMCG complexes may be obscured presumably due to their development at considerably greater depths in the crust. Both provinces exhibit evidence for continued uplift during igneous activity. Nonetheless, significant differences between these igneous provinces, such as the absence of massif-type anorthosites in the SOA, may therefore be more of a function of differences in crystallization conditions, which are related to the level of emplacement in the crust, rather than tectonic setting. Although of minor importance to the petrogenesis of mafic and felsic igneous rocks in the SOA, assimilation of continental crust plays a significant role in the petrogenesis of igneous rocks, particularly granites, in AMCG complexes. This difference may reflect quick transport and crystallization of magmas emplaced into cold brittle crust at subvolcanic levels in the SOA. In contrast, assimilation should be more efficient for large magma chambers developed at mid-crustal levels where the adjacent crust has been warmed by the passage of previous magmas and the high heat flow from melts ponded at the base of the crust. Thus, we suggest the mid-crustal layered mafic complex underlying the SOA (see McConnell and Gilbert, 1990), if exposed may closely resemble a more typical Mid-Proterozoic AMCG complex. Conversely, the SOA may represent a good analog of what igneous and tectonic activity in the crust above AMCG complexes may have been like before subsequent removal by erosion.

7. ACKNOWLEDGMENTS

This manuscript benefited from comments by Sören Fröjdö on an early draft, and from thoughtful reviews by Carol Frost and Ron Emslie on a later version. We would also like to thank Jonathan D. Price for his help in drafting some of the figures. This work was supported in part by NSF grant #EAR-9316144 to J.P. Hogan and M.C.Gilbert and by Eberly Chair Funds available to M.C. Gilbert.

8. REFERENCES

Anderson, J.L. (1983) Proterozoic anorogenic granite plutonism of North America, *Geological Society of America Memoir* **161**, 133-154.

Anderson, J.L. (1980) Mineral equilibria and crystallization conditions in the late Precambrian Wolf River rapakivi massif, Wisconsin, *American Journal of Science* **280**, 289-332.

Anderson, J.L., and Cullers, R.L. (1978) Geochemistry and evolution of the Wolf River Batholith, a Late Precambrian rapakivi massif in north Wisconsin, U.S.A., *Precambrian Research* **7**, 287-324.

Anderson J.L., and Morrison J. (1992) The role of anorogenic granites in the Proterozoic crustal development of North America, *in* K.C. Condie (ed.), *Proterozoic Crustal Evolution,* Elsevier, Amsterdam, pp. 263-299.

Aquilar, J. (1988) *Geochemistry of mafic rock units of the southern Oklahoma aulacogen, southwestern Oklahoma*, unpublished M.S. thesis University of Oklahoma, 167 p.

Ashwal, L.D. (1993) *Anorthosites*, Springer-Verlag, Heidleberg, 422 p.

Berg, J.H. (1979) Physical constraints and tectonic setting of the Nain complex: Geological Association of Canada Abstracts, **4**, 39.

Berg, J.H., and Wheeler, E.P. (1976) Osumilite of deep-seated origin in the contact aureole of the anorthosite Nain complex, Labrador, *American Mineraolgist* **61** 29-37.

Bigger S., and Hanson, R.E. (1992) Devitrification textures and related features in the Carlton Rhyolite in the Blue Creek Canyon area, Wichita Mountains, southwestern Oklahoma, *Oklahoma Geology Notes* **52**, 124-142.

Bowen, N.L. (1928) *The evolution of the igneous rocks*, Dover, New York, 332 pp.

Bowring, S.A., and Hoppe, W.J. (1982) U/Pb Zircon ages from the Mount Sheridan Gabbro, Wichita Mountains: *in* M.C. Gilbert and R.N. Donovan (eds.), *Geology of the eastern Wichita Mountains, southwestern Oklahoma* Oklahoma Geological Survey Guidebook **21**, pp. 54-59.

Cadman, A.C., Heaman, L., Tarney, J., Wardle, R.J., and Krogh, T.E. (1993) U - Pb geochronology and geochemical variation within two Proterozoic mafic dyke swarms, Labrador, *Canadian Journal of Earth Sciences* **30**, 1490-1504.

Cadman, A.C., Tarney, J., and Baragar, W.R.A. (1995) Nature of mantle source contributions and the role of contamination and *in situ* crystallization in the petrogenesis of Proterozoic mafic dykes and flood basalts Labrador, *Contributions to Mineralogy and Petrology* **122**, 213-229.

Cameron, M. Weaver, B.L., Diez de Medina, D. (1986) A preliminary report on the trace element geochemistry of mafic igneous rocks of the Southern Oklahoma Aulacogen: *in* M.C. Gilbert (ed.), *Petrology of the Cambrian Wichita Mountains Igneous Suite,* Oklahoma Geological Survey Guidebook **23** pp. 80-85.

Coffman, J.D., Gilbert, M.C., and McConnell, D.A. (1986) An interpretation of the crustal structure of the Southern Oklahoma Aulacogen satisfying gravity data: *in* M.C. Gilbert (ed.), *Petrology of the Cambrian Wichita Mountains Igneous Suite,* Oklahoma Geological survey Guidebook **23** pp. 1-10.

Cooper, R.W. (1991) Geology, geochemistry, and Platinum-Group-Element mineralization of the Cambrian Glen Mountains Layered Complex and associated rocks, southwestern Oklahoma: *Oklahoma Geological Survey Circular* **92** 98-108.

Czamanske, G.K., and Scheidle, D.A. (1985) Characteristics of the Banded-series anorthosites: *in* G.K., Czamanske and M.L., Zientek (eds.), *The Stillwater complex Montana: Geology and Guide,* Montana Bureau of Mines and Geology Special Publication **92**, pp. 334-345.

Denison, R.E. (1995) Significance of air-photograph linears in the basement rocks of the Arbuckle Mountains, *Oklahoma Geologic Survey Circular* **97** 119-131.

Diez de Medina, D. (1988) *Geochemistry of the Sandy Creek Gabbro, Wichita Mountains, Oklahoma,* unpublished M.S. thesis University of Oklahoma, 163 p.

Duchesne, J. (1984) Massif anorthosites: Another partisan review: *in* W.L. Brown (ed.), *Feldspars and Feldspathoids,* D. Reidel Publishing Company, pp. 411-433.

Duchesne, J., Denoiseux, B., and Hertogen, J. (1987) The norite-mangerite relationships in the Bjerkreim-Sokndal layered lopolith (southwest Norway). *Lithos,* **20**, p. 1-17.

Duschene, J., Wilmart, E., Demaiffe, D. and Hertogen, J. (1989) Monzonorites from Rogaland (southwest Norway): a series of rocks coeval but not comagmatic with massif-type anorthosites, *Precambrian Research* **45**, 111-128.

Eales, H.V., Marsh, J.S., Mitchell, A.A., De Klerk, W.J., Kruger, F.J., and Field, M. (1986) Some geochemical constraints upon models for the crystallization of the upper critical zone-main zone interval, northwestern Bushveld complex, *Mineralogical Magazine* **50**, 567-582.

Emslie, R.F. (1978) Anorthosite massifs, rapakivi granites, and Late Proterozoic rifting of North America, *Precambrian Research* **7**, 61-98.

Emslie, R.F. (1980) Geology and Petrology of the Harp Lake Complex, central Labrador: An example of Elsonian magmatism, *Geological Survey of Canada Bulletin* **293**, 136p.

Emslie, R.F. (1981) Exceptionally high grade metapelitic gneisses in the Red Wine Mountains, southern Labrador, *Geological Association of Canada Abstract* **6**, A-17.

Emslie, R.F. (1985) Proterozoic anorthosite massifs: *in* A. Tobi and J.L.R. Touret (eds.), *The Deep Proterozoic Crust in the North Atlantic Provinces,* Reidel, Dordrecht, pp. 39-60.

Emslie, R.F. (1991) Granitoids of rapakivi granite-anorthosite and related associations, *Precambrian Research* **51**, 173-192.

Emslie, R.F., and Hegner, E. (1993) Reconnaissance isotopic geochemistry of anorthosite-mangerite-charnockite-granite (AMCG) complexes, Grenville Province, Canada, *Chemical Geology* **106**, 279-298.

Emslie, R.F., and Hunt, P. A. (1990) Ages and petrogenetic significance of igneous mangerite-charnockite suites associated with massif anorthosites, Grenville Province, *Journal of Geology* **98**, 213-231.

Emslie, R.F. and Loveridge, W.D. (1992) Fluorite-bearing Early and Middle Proterozoic granites, Okak Bay area, Labrador: Geochronology, geochemistry and petrogenesis, *Lithos* **28**, 87-109.

Emslie R.F., and Stirling, J.A.R. (1993) Rapakivi and related granitoids of the Nain plutonic suite: geochemistry, mineral assemblages and fluid equilibria, *Canadian Mineralogist* **31**, 821-847.

Emslie, R.F., Loverridge, W.D., and Stevens, R.D. (1984) The Mealy dykes, Labrador: petrology, age, and tectonic significance, *Canadian Journal of Earth Sciences* **21**, 437-446.

Emslie, R.F., Hamilton, M.A., and Theriault (1994) Petrogenesis of a Mid-Proterozoic Anorthosite-Mangerite-Charnockite-Granite (AMCG) Complex: Isotopic and chemical evidence from the Nain Plutonic Suite, *Journal of Geology* **102**, 539-558.

Farquhar, J., (1986) The Western Platinium Mine: *in* Anhaeusser, C.R., and Maske, S., (eds.), *Mineral deposits of Southern Africa* **II**, Geological Society of South Africa, Johannesburg, pp.1135-1142.

Fountain, J.C. Hodge, D.S., Hills, F.A. (1981) Geochemistry and petrogenesis of the Laramie anorthosite complex, Wyoming, *Lithos* **14**, 113-132.

Fram, M.S., and Longhi, J. (1992) Phase equilibria of dikes associated with Proterozoic anorthosite complexes, *American Mineralogist* 77, 605-616.

Frost, B.R., and Touret, J.L.R. (1989) Magmatic CO_2 and saline melts from the Sybille monzosyenite, Laramie anorthosite complex, Wyoming: *Contributions to Mineralogy and Petrology* v. 103, 178-186.

Frost, B.R., Frost, C.D., Chamberlain, K.R., Scoates, J.S., and Lindsley, D.H. (1996) A field guide to the Proterozoic anorthositic, monzonitic, and granitic plutons, Laramie Range, southeastern Wyoming: *in* R.A. Thompson, M.R. Hudson, and C.L. Pillmore (eds.), *Geologic excursions to the Rocky Mountains and beyond, Field Trip Guidebook for the 1996 Geological Society of America Annual Meeting*: Colorado Geological Survey Special Publication **44**. Field Trip #6.

Fuhrman, M.L., Frost, B.R., and Lindsley, D.H. (1988) Crystallization conditions of the Sybille Monzosyenite, Laramie Anorthosite Complex, Wyoming, *Journal of Petrology* **29** 699-729.

Geist, D.J., Frost, C.D., Kolker, A., and Frost, R.B. (1989) A geochemical study of magmatism across a major terrane boundary: Sr and Nd isotopes in Proterozoic granitoids of the southern Laramie Range, Wyoming, *Journal of Geology* **97**, 331-342.

Gilbert, M.C. (1982) Geologic setting of the eastern Wichita Mountains, with a brief discussion of unresolved problems: *in* M.C. Gilbert and R.N. Donovan (eds.), *Geology of the eastern Wichita Mountains, southwestern Oklahoma*, Oklahoma Geological Survey Guidebook **21**, pp. 1-30.

Gilbert, M.C. (1983) Timing and chemistry of igneous events associated with the Southern Oklahoma Aulacogen, *Tectonophysics* **94**, 439-455.

Gilbert, M.C. (1992) Speculations on the origin of the Anadarko Basin: *in* R. Mason (ed.), *Proceedings of the 7th International Conference on Basement Tectonics, Kingston Ontario*, Kluwer Academic, pp. 195-208.

Gilbert, M.C., and Hughes, S.S. (1986) Partial chemical characterization of Cambrian basaltic liquids of the Southern Oklahoma Aulacogen: *in* M.C. Gilbert (ed.), *Petrology of the Cambrian Wichita Mountains Igneous Suite,* Oklahoma Geological Survey Guidebook **23**, pp. 73-79.

Gilbert, M.C., and Myers, J.D. (1986) Overview of the Wichita Granite Group: *in* M.C. Gilbert (ed.), *Petrology of the Cambrian Wichita Mountains Igneous Suite,* Oklahoma Geological Survey Guidebook **23**, pp. 73-79.

Granath, J.W. (1989) Structural evolution of the Ardmore basin, Oklahoma: progressive deformation in the foreland of the Ouachita collision, *Tectonics* **8**, 1015-1036.

Green, J.C., Bornhorst, T.J., Chandler, V.W., Mudrey, M.G. Jr., Myers, P.E., Pesonen, L.J., and Wilband, J.T. (1987) Keweenawan dykes of the Lake Superior region: evidence for evolution of the Middle Proterozoic Midcontinent Rift of North America: *in* H.C. Hall and W.F. Fahrig (eds.), *Mafic dyke swarms*, Geological Association of Canada Special Paper **34**, pp. 289-302.

Ham, W.E., Denison, R.E., and Merritt, C.A. (1964) *Basement rocks and structural evolution of southern Oklahoma,* Oklahoma Geological Survey Bulletin, **95**, 302 p.

Hames. W.E., Hogan, J.P., and Gilbert, M.C. (1995) Revised granite-gabbro age relationships, Southern Oklahoma Aulacogen U.S.A., *12th International Conference on Basement Tectonics*, Norman, OK, p. 44.

Hamilton, W.B. (1956) Precambrian rocks of the Wichita and Arbuckle Mountains, Oklahoma, *Geological Society of America Bulletin*, **67**, 1319-1330.

Hanson, R.E. (1977) *Petrology and geochemistry of the Carlton Rhyolite, southern Oklahoma*: unpublished M.S. thesis, Oklahoma State University, 161p.

Hanson, R.E., Al-Shaieb, Z. (1980) Voluminous subalkaline silicic magmas related to intracontinental rifting in the southern Oklahoma aulacogen, *Geology*, **8**, 180-184.

Harmer, R.E., and Sharpe, M.R. (1985) Field relations and strontium isotope systematics of the marginal rocks of the eastern Bushveld Complex, *Economic Geology*, **80**, 813-837.

Henry, C.D., and Wolff, J.A. (1992) Distinguishing strongly rheomorphic tuffs from extensive silicic lavas, *Bulletin of Volcanology*, **54**, 171-186.

Helz, R.T. (1985) Composition of fine-grained mafic rocks from sills and dikes associated with the Stillwater Complex: *in* G.K., Czamanske and M.L., Zientek (eds.), *The Stillwater complex Montana: Geology and Guide,* Montana Bureau of Mines and Geology Special Publication **92**, pp. 97-117.

Higgins, M.D., and Doig, R. (1981) The Sept Isles anorthosite complex: field relationships, geochronology, and petrology, *Canadian Journal of Earth Sciences* **18**, 561-573.

Higgins, M.D., and Doig, R. (1986) Geochemical constraints on the differentiation processes that were active in the Sept Isles complex, *Canadian Journal of Earth Sciences* **23**, 670-681.

Hill, J.D., and Miller, R.R. (1990) A review of Middle Proterozoic epigenic felsic magmatism in Labrador: *in* Gower, C.F., Rivers, T., and Ryan, B., (eds.), *Mid-Proterozoic Laurentia-Baltica*, Geological Association of Canada, Special Paper **38**, pp. 417-431.

Hoffman, P., Dewey, J.F., and Burke, K. (1974) Aulacogens and their genetic relationship to geosynclines, with a Proterozoic example from the Great Slave Lake, Canada: *in* Dott, R.J. Jr., and Shaver, R.H. (eds.), *Modern and ancient geosynclinal sedimentation*, Society of Economic Paleontologists and Economic Mineralogists Special Publication **19**, pp. 38-55.

Hogan, J.P., and Gilbert, M.C. (1991) Contrasting crystallization styles of sheet granites from the Wichita magmatic province: Implications for source region heterogeneity, *Geological Society of America, Abstracts with Programs* **23**, 33.

Hogan, J.P., and Gilbert, M.C. (1995) The A-type Mount Scott Granite sheet: Importance of crustal magma traps, *Journal of Geophysical Research* **100**, No. B8, 15,779-15,792.

Hogan, J.P., and Gilbert, M.C. (1997) Intrusive style of A-type sheet granites in a rift environment: The Southern Oklahoma Aulacogen: *in* R.W. Ojakangas, A.B. Dickas, and J.C. Green (eds.), *Middle Proterozoic to Cambrian Rifting, Central North America*, Geological Society of America Special Paper **312-19**, pp. 299-311.

Hogan, J.P., Gilbert, M.C., Price, J.D., and Wright, J.E. (1995) Petrogenesis of A-type sheet granites from an ancient rift: *in* M. Brown and P.M. Piccoli (eds.), *The Origin of Granites and Related Rocks, Third Hutton Symposium Abstracts*, U.S. Geological Survey Circular **1129**, pp. 68-69.

Hogan, J.P., Gilbert, M.C., Price, J.D., Wright, J.E., Deggller, M., and Hames, W.E. (1996) Magmatic evolution of the Southern Oklahoma Aulacogen: *Geological Society of America Abstracts with Programs* **28**, no. 1, 19.

Huang, W.T. (1955) Occurrences of leucogranogabbro and associated igneous rocks in the Wichita Mountains, Oklahoma, *American Journal of Science* **253**, 341-357.

Irvine, T.N. (1987) Glossary of terms for layered intrusions: *in* I. Parsons (ed.), *Origin of Igneous Layering*, NATO ASI Ser C, 196, Reidel, Dordrecht, pp. 641-647.

Jansen, B., Blok, A., and Scheelings, M. (1985) Geothermometry and geobarometry in Rogaland and preliminary results from the Bamble area, south Norway: *In* Tobi, A., and Touret, J., (eds.), *The deep Proterozoic crust in the North Atlantic Provinces*, Reidel, Dordrecht, pp. 499-518.

Kleeman, G.J., and Twist, D. (1989) The compositionally-zoned sheet-like granite pluton of the Bushveld Complex: Evidence bearing on the nature of A-type magmatism, *Journal of Petrology* **30**, 1383-1414.

Kolker, A., and Lindsley, D.H. (1989) Geochemical evolution of the Maloin Ranch pluton, Laramie Anorthosite Complex: Petrology and mixing relations, *American Mineralogist 74*, 307-324.

Kolker, A., Lindsley, D.H., and Hanson, G.N. (1990) Geochemical evolution of the Maloin Ranch pluton, Laramie Anorthosite Complex: Trace element and petrogenetic models, *American Mineralogist 75*, 572-588.

Kolker, A., Frost, C.D., Hanson, G.N., and Geist, D.J. (1991) Neodymium, strontium, and lead isotopes in the Maloin Ranch Pluton, Wyoming: Implications for the origin of evolved rocks at anorthosite margins, *Geochimica et Cosmochimica Acta*, **55**, 2285-2297.

Lambert, D.D., Unruh, D.M., and Gilbert, M.C. (1988) Rb-Sr and Sm-Nd isotopic study of the Glen Mountains Layered Complex: Initiation of rifting within the Southern Oklahoma Aulacogen, *Geology* **16**, 13-17.

Longhi, J., and Ashwal, L.D. (1985) Two-stage models for lunar and terrestrial anorthosites: Petrogenesis without a magma ocean. Proceedings of the 15th Lunar Planetary Science Conference, Part II, *Journal of Geophysical Research 90*, C571-C584.

McConnell, D.A., and Gilbert, M.C., 1990, Cambrian extensional tectonics and magmatism within the Southern Oklahoma Aulacogen, *Tectonophysics 174*, 147-157.

McLelland, J., and Whitney, P. (1990) Anorogenic, bimodal emplacement of anorthositic, charnockitic, and related rocks in the Adirondack Mountains, New York, *in* Stein, H.J., and Hannah, J.L., (eds.), Ore-bearing granite systems; Petrogenesis and mineralizing processes: *Geological Society of America Special Paper* **246**, pp. 301-315.

Meyers, R.E., and Emslie, R.F. (1977) The Harp dikes and their relationship to Helikian geological record in central Labrador, *Canadian Journal of Earth Science* **14**, 2683-2696.

Miller, J.D., Jr., and Weiblen, P.W. (1990) Anorthositic rocks of the Duluth Complex: Examples of rocks formed from plagioclase crystal mush, *Journal of Petrology* **31**, 295-339.

Mitchell, J.N., Scoates, J.S., and Frost, C.D. (1995) High-Al gabbros in the Laramie Anorthosite Complex, Wyoming: implications for the composition of melts parental to Proterozoic anorthosite, *Contributions to Mineralogy and Petrology* **119**, 166-180.

Mitchell, J.N., Scoates, J.S., Frost, C.D., and Kolker, A. (1996) The geochemical evolution of anorthosite residual magmas in the Laramie Anorthosite Complex, Wyoming, *Journal of Petrology* **37**, 637-660.

Morse, S.A., 1968, Layered intrusions and anorthosite genesis: *in* Y.W. Isachsen (ed.), *Origin of anorthosite and related rocks*, New York State Museum Science service Memoir **18**, pp. 175-187.

Morse. S.A. (1969) The Kiglapait Layered Intrusion, Labrador, *Geological Society of America Memoir* **112**, 204 p.

Morse, S.A. (1981) Kiglapait geochemistry, IV. The major elements, *Geochimica et Cosmochimica Acta* **45**, 461-479.

Myers, J.D., Gilbert, M.C., Loiselle, M.C. (1981) Geochemistry of the Cambrian Wichita Granite Group and revisions of its lithostratigraphy, *Oklahoma Geology Notes* **41**, 172-195.

Owens, B.E., Rockow, M.W., and Dymek, R.F. (1993) Jotunites from the Grenville Province, Quebec: petrological characteristics and implications for massif anorthosite petrogenesis, *Lithos* **30**, 57-80.

Papezik, V.S. (1965) Geochemistry of some Canadian anorthosites, *Geochimica et Cosmochimica Acta* **29** 673-709.

Perry, W.J. Jr. (1989) Tectonic evolution of the Anadarko basin region, Oklahoma: *United States Geological Survey Bulletin* **1866A**, 19 pp.

Powell, B.N. (1986) The Raggedy Mountains Gabbro Group: *in* M.C. Gilbert (ed.), *Petrology of the Cambrian Wichita Mountains Igneous Suite*, Oklahoma Geological Survey Guidebook **23**, pp. 21-52.

Powell, B.N., and Gilbert, M.C. (1982) Relationships among Glen Mountains Layered Complex, Glen Creek Gabbro, Cold Springs Breccia, and Late Diabase. Sec13-14, T. 4 N., R. 17 W., Kiowa County, Oklahoma: *in* M.C. Gilbert and R.N. Donovan (eds.), *Geology of the eastern Wichita Mountains, southwestern Oklahoma*, Oklahoma Geological Survey Guidebook **21**, pp. 79-96.

Powell, B.N., and Phelps, D.W. (1977) Igneous cumulates of the Wichita province and their tectonic implications, *Geology* **5**, 52-56.

Powell, B.N., Gilbert, M.C., Fischer, J.F. (1980a) Lithostratigraphic classification of basement rocks of the Wichita Province, Oklahoma: Summary, *Geological Society of America Bulletin Part I* **91**, 509-514.

Powell, B.N., Gilbert, M.C., Fischer, J.F. (1980b) Lithostratigraphic classification of basement rocks of the Wichita Province, Oklahoma, *Geological Society of America Bulletin Part II* **91**, 1875-1994.

Pratt, T.L., Hauser, E.C., and Nelson, K.D. (1992) Widespread buried Precambrian layered sequences in the U.S. Mid-continent: Evidence for large Proterozoic depositional basins, *Bulletin of the American Association of Petroleum Geologists*, **76**, # 9, 1384-1401.

Price, J.D., Hogan, J.P., and Gilbert, M.C. *in press*, Surface and near-surface geometry of the Sandy Creek Gabbro pluton, Hale Spring Area, Wichita Mountains, Oklahoma: *this volume.*

Price, J.D., Hogan, J.P., and Gilbert, M.C. (1996a) Rapakivi texture in the Mount Scott Granite, Wichita Mountains, Oklahoma, *European Journal of Mineralogy* **8**, 435-451.

Price, J.D., Hogan, J.P., and Gilbert, M.C. (1996b) Investigation of Late Diabase dikes at Lake Elmer Thomas Dam, Wichita Mountains, Oklahoma, *Geological Society of America Abstracts with Programs* **28**, no. 1, 59.

Ryan, B.A. (1991) Makhavinekh Lake pluton, Labrador, Canada: geologic setting, subdivisions, mode of emplacement, and a comparison with Finnish rapakivi granites, *Precambrian Research* **51**, 193-225.

Ryan. B.A., and Emslie, R.F. (1996) Field excursion to examine the metamorphic and plutonic rocks of the Nain Area: Pre-conference field excursion, *Proterozoic Evolution in the North Atlantic Realm, COPENA-ECSOOT-IBTA conference*, Goose Bay, Labrador, July 29-August 2, 1996, Field Excursion Guide **2**, 60 p.

Ryan, B.A., Wardle, R.J., Gower, C.F., and Nunn, G.A.G. (1995) Nickel-Copper sulphide mineralization in Labrador: the Voisey Bay discovery and its exploration implications, *Current Research*. Newfoundland Department of Natural Resources, Geological Survey, Report **95-1**, 177-204.

Scofield, N. (1968) *Vertical variation in the layered series, Raggedy Mountains Gabbro Group, Kiowa County, Oklahoma,* unpublished M.S. thesis University of Oklahoma, 155 p.

Scoates, J.S., and Chamberlain, K.R. *in press*, Orogenic to post-orogenic origin for the 1.76 Ga Horse Creek Anorthosite Complex, Wyoming, USA, *Journal of Geology*.

Scoates, J.S., and Frost, C.D., 1996, A strontium and neodymium isotopic investigation of the Laramie anorthosites, Wyoming, USA: Implications for magma chamber processes and the evolution of magma conduits in Proterozoic anorthosites, *Geochimica et Cosmochimica Acta* **60**, 95-107.

Stockton, M.M. (1984) *Geology of the gabbroic rocks in southern Cooperton Quadrangle and northern Odetta Quadrangle, Oklahoma*, unpublished M.S. thesis University of Texas, Arlington, 83 p.

Taylor, R.J. (1978) *Petrography of the layered series, Saddle Mountain Quadrangle, eastern Wichita Mountains, Oklahoma*, unpublished M.S. thesis University of Texas, Arlington, 66 p.

Thornton, E.C. (1975) *Anorthosite-gabbro-granophyre relationships, Mount Sheridan area, Oklahoma,* Rice University unpublished M.S. thesis, 65p.

Tilton, G.R., Wetherill, G.W., and Davis, G.L. (1962) Mineral ages from the Wichita and Arbuckle Mountains, Oklahoma, and the St. Francois Mountains, Missouri: *Journal of Geophysical Research* **67**, 4011-4019.

Tuttle, O.F., and Bowen, N.L. (1958) Origin of granite in the light of experimental studies in the system $NaAlSi_3O_8$-$KAlSi_3O_8$-Si_2O_4-H_2O, *Geological society of America Memoir* **74**, 153 pp.

Twist, D., and Harmer, R.E.J. (1987) Geochemistry of contrasting siliceous magmatic suites in the Bushveld Complex: Genetic aspects and implications for tectonic discrimination diagrams, *Journal of Volcanology and Geothermal Research* **32**, 83-98.

Vander Auwera, J., and Longhi, J. (1994) Experimental study of a jotunite (hypersthene monzodiorite): constraints on the parent magma composition and crystallization conditions (P, T, fO_2) of the Bjerkreim-Sokndal layered intrusion (Norway), *Contributions to Mineralogy and Petrology* **118**, 60-78.

Vidrine, D.M., and Fernandez, L.A. (1986) Geochemistry and petrology of the Cold Springs Igneous Breccia, Wichita Mountains, Oklahoma: *in* M.C. Gilbert (ed.), *Petrology of the Cambrian Wichita Mountains Igneous Suite*, Oklahoma Geological Survey Guidebook **23**, 86-106.

de Waard, D., and Wheeler, E.P. (1971) Chemical and petrologic trends in anorthositic rocks and associated rocks of the Nain massif, Labrador, *Lithos* **4**, 367-380.

Weaver, B.L., and Gilbert, M.C. (1986) Reconnaissance geochemistry of silicic igneous rocks of the Wichita Mountains, Oklahoma: *in* M.C. Gilbert (ed.) *Petrology of the Cambrian Wichita Mountains Igneous Suite,* Oklahoma Geological Survey Guidebook **23**, pp. 117-125.

Wheeler, E.P. (1968) Minor intrusives associated with the Nain anorthosite: *in* I.W. Isachsen, (ed.), *Origin of Anorthosites and Related Rocks*, New York State Museum of Science Memoir **18**, pp. 189-206.

Wiebe, R.A. (1978) Anorthosite and related plutons, southern Nain complex, Labrador, *Canadian Journal of Earth Sciences* **15**, 1326-1340.

Wiebe, R.A. (1985) Proterozoic basalt dikes in the Nain anorthosite complex, Labrador, *Canadian Journal of Earth Sciences* **22**, 1149-1157.

Wiebe, R.A. (1988) Structural and magmatic evolution of a magma chamber: The Newark Island layered intrusion, Nain, Labrador, *Journal of Petrology* **29**, 383-411.

Wiebe, R.A. (1990) Dioritic rocks in the Nain Complex, Labrador: *Schweizerische Mineralogische und Petrographische Mitteilungen* **70**, 199-208.

Wiebe, R.A. (1992) Proterozoic anorthosite complexes: *in* K.C. Condie (ed.), *Proterozoic Crustal Evolution*, Elsevier, Amsterdam, pp. 215-261.

Wones, D.R. (1989) Significance of the assemblage titanite + magnetite + quartz in granitic rocks, *American Mineralogist* **74**, 744-749.

Wright, J.E., Hogan, J.P., and Gilbert, M.C. (1996) The Southern Oklahoma Aulacogen: Not just another B.L.I.P., *EOS Transactions of the American Geophysical Union* 77, #46, F845.

SURFACE AND NEAR-SURFACE INVESTIGATION OF THE ALTERATION OF THE MOUNT SCOTT GRANITE AND GEOMETRY OF THE SANDY CREEK GABBRO PLUTON, HALE SPRING AREA, WICHITA MOUNTAINS, OKLAHOMA

JONATHAN D. PRICE, JOHN P. HOGAN,
M. CHARLES GILBERT, AND JAMES D. PAYNE
University of Oklahoma, School of Geology and Geophysics
Norman, OK 73019 USA
email: jon_price@ou.edu

Abstract

Surface and subsurface investigation of the spatial relationships between the Cambrian-age Glen Mountains Layered Complex, Mount Scott Granite, and Sandy Creek Gabbro in the Hale Spring Area of the Wichita Mountains, shows that the upper portion of the Sandy Creek gabbro pluton is largely steep-walled, with a blunt irregular subhorizontal roof capped by Mount Scott Granite. In the subsurface, the near vertical sidewalls of the gabbro are presumed to truncate an older subhorizontal contact of regional extent, between the Glen Mountains Layered Complex substrate and the Mount Scott Granite cap. This subhorizontal contact is interpreted as an angular unconformity that developed on the layered complex and was subsequently buried by volcanic deposits of the Carlton Rhyolite Formation prior to intrusion of the Mount Scott Granite sheet. The Sandy Creek Gabbro does contain xenoliths of Glen Mountains Layered Complex and Meers Quartzite, a metasedimentary unit associated with this unconformity. Locally, a thin ledge of gabbro, with an irregular floor, protrudes more than 0.5 km to the south from the main body of the intrusion presumably exploiting this subhorizontal contact. Thus, the Sandy Creek Gabbro is a stock, capped by the floor of the Mount Scott Granite sheet, and only locally spreads laterally along the older unconformity, the contact between the Mount Scott Granite sheet and the underlying Glen Mountains Layered Complex.

The Mount Scott Granite was cored to a depth of 87.5 m adjacent to the contact at the Ira Smith Quarry (site SQ-1). The core is homogeneous with respect to primary

igneous mineralogy and texture. The only exceptions are the presence of a thin aplitic zone at a depth of 47.1 m and sodic amphibole at a depth of 87 m, both of which can be seen in surface exposures in the adjacent quarry. However, subsequent events have altered the primary igneous mineralogy and texture of Mount Scott Granite, and important variations in fracture density, color, oxide mineralogy, and magnetic susceptibility (χ) occur within the upper 30 m of the core. Macro-fracture densities are 0.6 cm^{-1} at the surface to 0.0 cm^{-1} at 30 m depth. Fracture density, although variable throughout this upper 30 m, generally decreases with depth. Oxide mineralogy varies from hematite + iron hydroxide near the surface, to magnetite + hematite (adjacent to microfractures and grain boundaries) + ilmenite, at depths between 23 and 30 m, to magnetite + ilmenite below 30 m. Color changes from grayish reddish orange (2YR 5/6) near the surface to moderate grayish red (8R 4/6) below 30 m due to alteration of sub-microscopic hematite flakes structurally trapped within the abundant alkali feldspar grains, to iron hydroxide. Magnetic susceptibility varies from 2×10^{-4} at the top, to $\sim 9 \times 10^{-3}$ (SI mass) below 30 m. The order of magnitude change in susceptibility values reflects oxidation of the primary igneous mineral assemblage (principally titanomagnetite) to hematite and hemoilmentite, and hydration of secondary hematite to iron-hydroxide, and is likely to be a result of interaction with meteoric fluids. This significant change in magnetic susceptibility in the upper 30 m of Mount Scott Granite was incorporated in geomagnetic modeling of the subsurface. Changes in color, magnetic susceptibility, and oxide mineralogy are directly correlated to changes in fracture density. Thus, brittle fractures provided conduits for fluid-flow and subsequent alteration of the crystalline basement. The extent of alteration reflects the fluid/rock ratio which, in part, is a function of fracture density and connectivity. The timing of the fracturing and the composition of fluid(s) is largely unconstrained, but is likely to be groundwater in equilibrium with atmospheric conditions. As evidenced by the alteration within the core, circulation of these fluids has been restricted to depths less than 30 m below the present erosional surface. Thus, opening of these fractures is likely to be directly related to unroofing of this basement. The timing of alteration may be a relatively recent phenomenon. However, because the Wichita Mountains were previously exposed to atmospheric conditions in the Permian, the possibility for multiple alteration events cannot be excluded.

1. Introduction

Spatial and temporal relationships between the Sandy Creek Gabbro, Mount Scott Granite sheet, and Glen Mountains Layered Complex, in the Hale Spring Area of the Wichita Mountains, Oklahoma, were investigated through surface mapping, core drilling, and magnetic surveying. Although the subhorizontal contact between the underlying gabbro and overlying granite sheet is regionally well exposed, details of this contact are typically obscured by talus, vegitation, and extensive alteration. Thus, a drilling investigation was designed with two primary goals: 1) retrieve a continuous core across the contact between Mount Scott Granite and Sandy Creek Gabbro for

direct observation of the contact relationships between these two units and 2) obtain "fresh" samples of these units in the vicinity of the contact for petrologic investigation. The Ira Smith Quarry location was selected with these goals in mind, particularly with the intent of transecting the contact at a relatively shallow depth, within 20 m of the surface, based on the local spatial distribution of Sandy Creek Gabbro and Mount Scott Granite. The initial result, 87.5 m of continuous core of Mount Scott Granite, was surprising, and became the impetus for initiating a magnetic survey designed to determine the subsurface morphology of the Sandy Creek Gabbro pluton and the nature of its contact with Mount Scott Granite. The results of this study require important revisions to earlier models of the temporal and spatial evolution of magmatism in the province as a whole. The subsurface spatial relationships between these units are more compatible with the Sandy Creek Gabbro being younger than the Mount Scott Granite rather than *vice versa* as previously thought (*e.g.*, Powell *et al.*, 1982).

1.1. REGIONAL GEOLOGY

The geology of the Wichita Mountains is summarized here from Ham *et al.* (1964), Powell *et al.* (1980), Gilbert (1982), and Hogan and Gilbert (*1997*) and references therein. The Wichita Mountains are a series of rounded hills and rocky promontories located in southwestern Oklahoma, extending northwest from the city of Lawton, past the town of Granite. They are the fault-bounded geomorphic expression of the Wichita Igneous Province, a northwest-southeast trending zone of Cambrian bimodal igneous activity. This igneous activity is believed to be related to crustal extension and formation of the Southern Oklahoma Aulacogen during the breakup of the Laurentian supercontinent (see Hogan and Gilbert, this volume).

The mountains result from a complex tectonic history. Subsequent to the rifting event, the province underwent extensive thermal subsidence and was buried by clastic and carbonate sediments from the early Paleozoic to the Mississippian. This was followed by uplift and exhumation of the igneous rocks as a result of the Wichita Orogeny (Ham and Wilson, 1967) in the Pennsylvanian. The resulting mountain range had a similar form to the currently exposed Wichita Mountains. Permian clastics, largely sediments shed from the Ouachita Mountains to the east, but also locally derived sediments (*e.g.*, Post Oak Conglomerate) buried these early mountains. Re-exhumation of the mountains began in the Tertiary and continues today: All that covers these ancient mountains is a veneer of westward thickening Permian clastics.

Exposed igneous units in the eastern Wichita Mountains (east of Oklahoma Hwy. 54, Fig. 1), are compositionally stratified: mafic units are overlain by silicic units. In near vertical exposures, the larger mafic bodies (GMLC and Roosevelt Gabbros) crop out below the sheet granites, which in turn typically crop out beneath Carlton Rhyolite. The major mafic bodies (GMLC and Roosevelt Gabbros) were previously interpreted to have been uplifted and eroded, covered by rhyolite, prior to intrusion of the granite

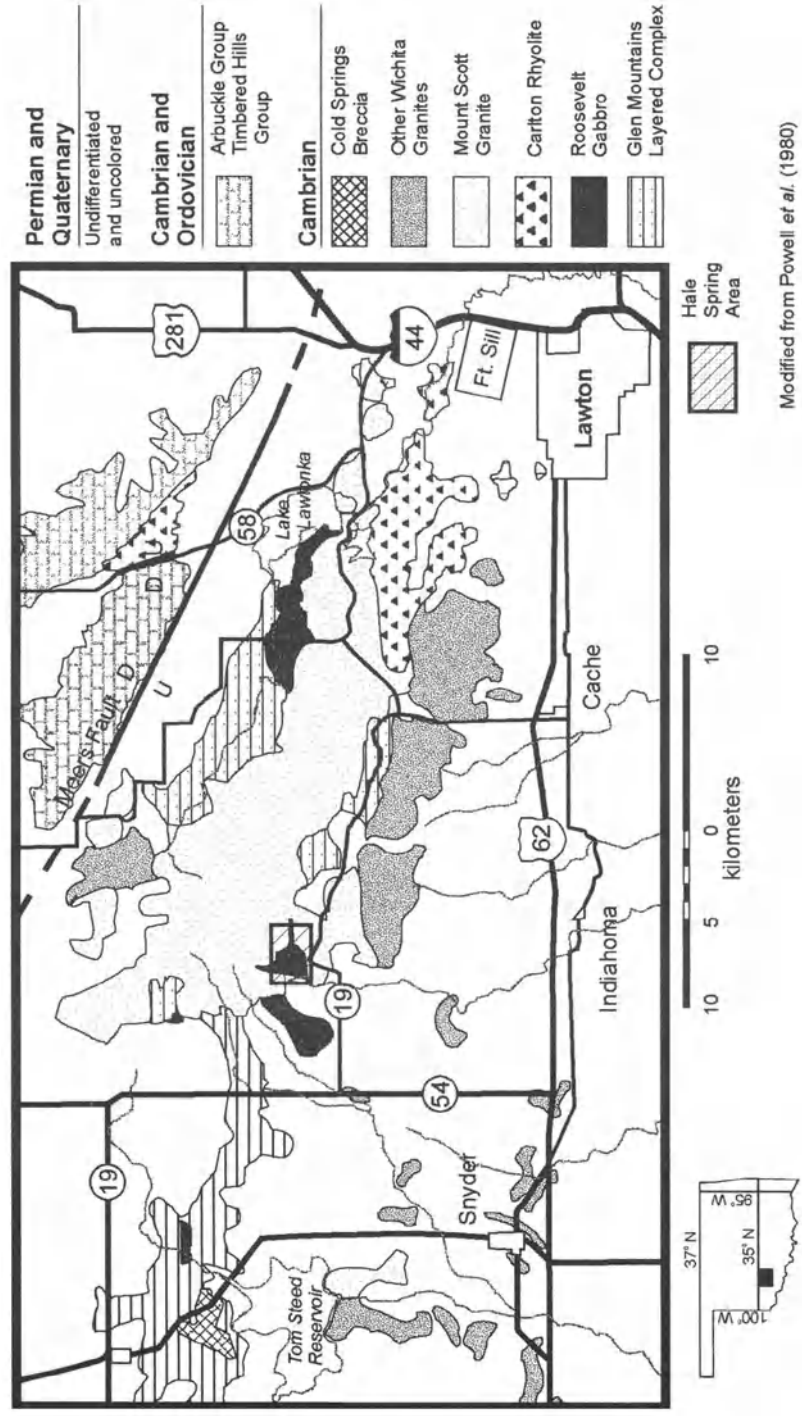

Figure 1. Generalized geologic map of the eastern Wichita Mountains, Oklahoma. Hale Spring Area, within the box, is enlarged in figure 3.

(Ham *et al.*, 1964; Hogan and Gilbert, 1995). Then granite magmas spread out laterally along the rhyolite-gabbro contact resulting in sheet-like plutons (Hogan and Gilbert, 1997). These units are crosscut by later dikes of diabase (Late Diabase), locally abundant pegmatite (*e.g.*, Hale Spring Pegmatite), aplite, and rhyolite (Fig. 2).

Recent geochronologic investigations suggest that some members of the Roosevelt Gabbros may not have been part of the eroded mafic substrate, but rather intruded the GMLC after early silicic magmatism, thus requiring modification of earlier models for the rift. Laser $^{40}Ar/^{39}Ar$ dating of amphibole and biotite from the Mount Sheridan Gabbro, a member of the Roosevelt Gabbros, places its age at 533 ± 2 Ma, whereas amphibole from the Mount Scott Granite yields an age of 539 ± 2 Ma (Hogan *et al.*, 1996). If these hydrous gabbro plutons are indeed younger than the silicic rocks, then the magmas that gave rise to these gabbros were possibly stopped and trapped beneath the silicic cover. Thus, resolving contact relationships between the Mount Scott Granite sheet and the underlying Roosevelt Gabbro plutons is critical to determining the temporal and spatial evolution of magmatism during formation of the Southern Oklahoma Aulacogen. The Hale Spring Area (Fig. 1), a region on the western edge of the large, continuous eastern exposure of the Mount Scott Granite (Cooperton 7.5 minute U.S.G.S. quadrangle, Oklahoma Coordinates T.3N. R.15W. Sec. 2-4, 9-11, 98° 45-46.5' West Longitude, 34° 45-46' N Latitude), provides an area where these units crop out and can be readily investigated.

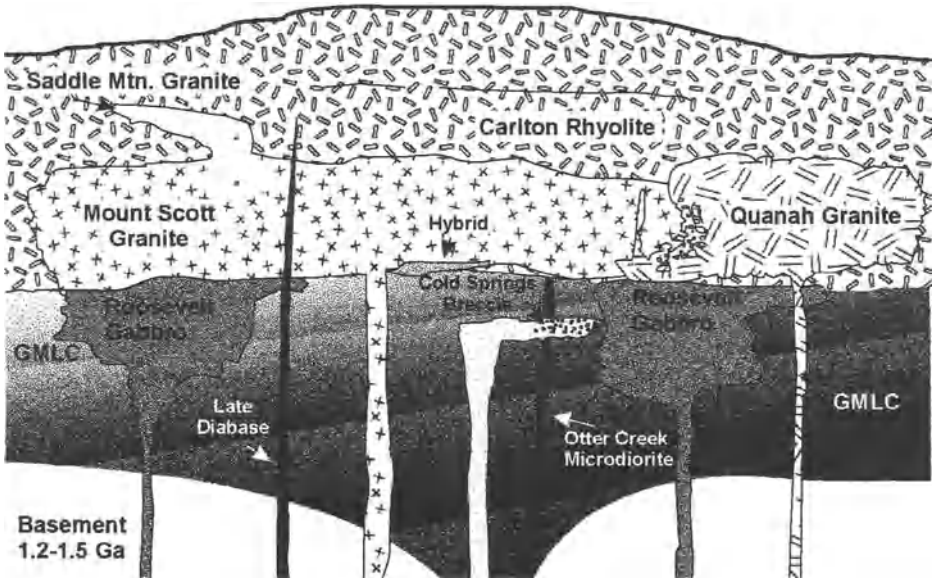

Figure 2. Schematic stratigraphic cross-section through the eastern Wichita Igneous Province illustrating the Cambrian contact relationships between the observed units. No erosion or faulting shown. This study examines the relationship between the Sandy Creek Gabbro, one of the Roosevelt Gabbros and the Mount Scott Granite.

1.2. GEOLOGY OF THE HALE SPRING AREA

Many lithologies are exposed within the Hale Spring Area. These include the Meers Quartzite (age uncertain), the Cambrian Glen Mountains Layered Complex (GMLC), Mount Scott Granite, Sandy Creek Gabbro, Hale Spring Pegmatite, a hybrid rock unit, Permian Post Oak Formation (granite conglomerate), and Quaternary alluvial sediments. The following geologic description is summarized from Johnson (1955), Gilbert (1982), Powell *et al.* (1982), Stockton and Giddens (1982), Stockton (1984), Diez de Medina (1988), and references therein. Figure 3 is a "bedrock" (Permian and Quaternary sediments removed) geologic map of the area.

The Sandy Creek Gabbro, of the Roosevelt Gabbro Group, crops out in the lower elevations (< 600 m), mostly on the valley floor and adjacent to the stream cuts of the Hale Spring Area. The rock is hard and dense. Weathered surfaces are dark-reddish black and scalloped; however, weathering does not appear to penetrate the rock more than two or three centimeters. The gabbro is largely composed of plagioclase, with variable amounts of olivine, typically exhibiting pyroxene coronas. Olivine-rich exposures are laminated; lamination of plagioclase in the southern portion of the area dips ESE 20-30°. Primary interstitial pink-brown amphibole and red-brown mica are common. Exposures to the north of Big Four Mountain also contain quartz and alkali feldspar. Work by Powell *et al.* (1982) and Diez de Medina (1988) found that the samples in the south are compositionally more primitive than those collected from Hollis Canyon, north of Big Four Mountain. Within the central portion of the area, exposures include altered gabbro containing sericite and calcite replaced plagioclase crystals, and chlorite, epidote-zoisite, calcite and fibrous or acicular amphibole replacing mafic grains (Powell *et al.*, 1982).

The Mount Scott Granite crops out in the higher elevations (>500 m). On the surface, the rock is variably fractured, and weathers to an orange-red color. Weathered exposures commonly contained spheroidal boulders that are substantially altered to their cores, the result of weathering below the groundwater table along fractures in the granite (Gilbert, 1982). The rock texture is porphyritic, with gray ovoid anorthoclase phenocrysts, many with rapakivi-texture albitic rims of plagioclase, set in a matrix largely of alkali feldspar and quartz (Price *et al.*, 1996). Although many localities contain abundant granophyre, here matrix quartz and feldspar are seriate (Merritt, 1965). Minor and accessory minerals comprise less than 5 modal percent. Typically, these minerals, ferroedenitic amphibole, biotite, magnetite, ilmenite, along with titanite, fluorite, zircon, apatite and rare allanite, occur together in clots throughout the matrix. Secondary minerals include hematite, calcite, sericite, titanite, epidote, and clays.

The contact between the Sandy Creek Gabbro and the Mount Scott Granite is not easily observed; the faster weathering rate of the gabbro relative to the granite results in steep granite hill slopes, with granite talus covering much of the contact. However,

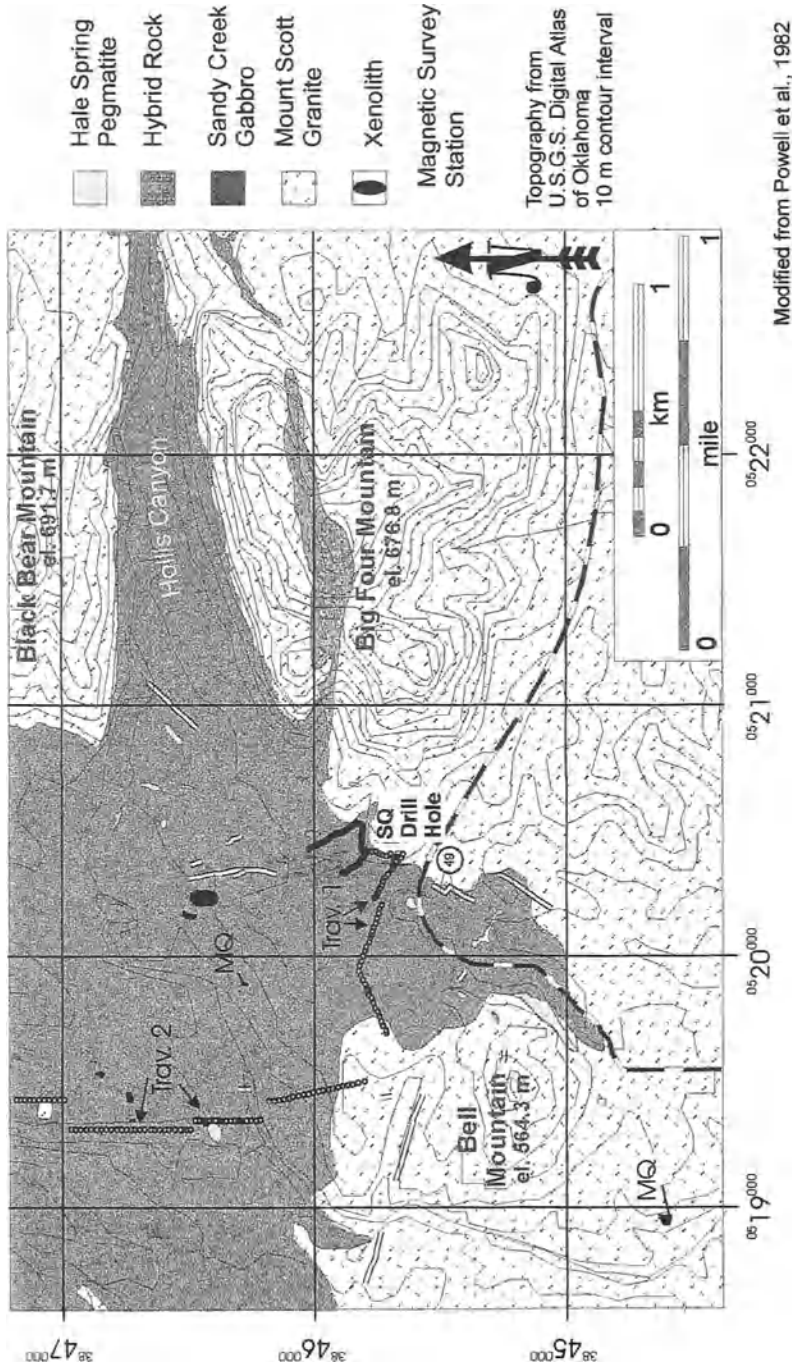

Figure 3. Geologic map of the Hale Spring Area with Permian and Quaternary removed. Surface magnetic traverses are plotted as a series of points that correspond with reading stations. Trav. 1 and Trav. 2 refer to two modeled traverses presented in this paper (Figs. 8 and 9 respectively).

the exposure is typically sufficient enough to allow placement of the contact to within several meters. The regional shape of the contact between the Sandy Creek Gabbro and the Mount Scott Granite sheet can be inferred from elevations of the contact within the area, provided that there has been no significant offset by faulting. Based on the Mount Scott Granite's sheet-like morphology, its exposure on hill tops, and that exposures of Sandy Creek Gabbro are confined to the valleys, Powell *et al.* (1982) concluded that the area is an erosional window, where Sandy Creek is dissecting a subhorizontal granite/gabbro contact, stripping away the overlying granite to expose the gabbro.

Cropping out largely within the Mount Scott Granite, and only locally in contact with the gabbro, is a rock of highly variable appearance called hybrid rock. The outcrop pattern of the hybrid rock trends east-west from Sandy Creek Valley across Big Four Mountain (Fig. 3). The hybrid rock is variable in color index, grading from pink and gray to dark gray. It is medium-grained, with quartz and pink feldspar phenocrysts, and contains xenoliths of biotite gabbro. Similar rocks are found elsewhere in the Wichita Mountains, and workers have attributed their origin to partial melting of the gabbro's weathered erosional surface (*i.e.,* saprolitic regolith) during granite intrusion over and along this surface (Powell *et al.*, 1982). Alternatively, if the gabbro is younger the granite, it is plausible that the hybrid rock originated along the contact between these two units as a partial melt of the granite that may have mingled with the gabbroic magma. The exposure on Big Four Mountain therefore may represent a "dike" of this contaminated partial melt which intruded the overlying granite.

Exposures of Hale Spring Pegmatite crop out over much of the area in the lower elevations (<550 m) as dikes and ~oval shaped bodies that cross cut both Sandy Creek Gabbro and Mount Scott Granite. The Hale Spring pegmatite has aplitic to pegmatitic texture, is largely quartz, albite, and microcline, and contains large crystals of sodic amphibole (arfvedsonite) along with magnetite and acmite (Scofield and Gilbert, 1982). Hale Spring Pegmatite is mineralogically similar to the nearby Quanah Granite and this has lead previous workers to infer their derivation from this granite.

The Glen Mountains Layered Complex crops out as small (1-30 m^2) blocks within the Sandy Creek Gabbro. Powell *et al.* (1982) concluded these are xenoliths, confirming the younger age of the Sandy Creek Gabbro relative to the layered complex. They are composed of anorthositic gabbro, and are similar to nearby exposures of the GMLC to the east and the west of the Hale Springs Area.

Also present as xenoliths within the Sandy Creek Gabbro are several exposures of Meers Quartzite, some of which are spatially associated with xenoliths of GLMC, a relationship which may be preserving an unconformable relationship between these two units. Here, the Meers Quartzite is largely composed of quartz, abundant sillimanite, and lessor muscovite. Xenoliths of Meers Quartzite, entirely within the

Mount Scott Granite, also occur nearby. This quartzite contains only trace sillimanite and muscovite.

Covering much of the valley floor is Post Oak Conglomerate, composed largely of granite clasts in a matrix of calcrete, clay, and ferric oxides (Donovan, 1982). Elsewhere, this unit has been assigned a Permian age based on gradational contacts into Permian clastics (Chase, 1954). Within the Hale Spring area, stream dissection of this unit is extensive in places, and it is difficult to discriminate between this Permian unit, and much younger, reworked fluvial deposits.

This study found scant evidence for faulting wihtin the Hale Spring Area. However, two previous studies have proposed faults. Stockton (1984) placed an east-west fault along the southern base of Black Bear Mountain, although more recent magnetic data argue against its existence (discussed below). McLean and Stearns (1986) placed an east-west trending, left-lateral fault, and a smaller, northeast-southwest trending, left-lateral fault through the southern portion of the Hale Spring area, related to Pennsylvanian uplift. These two faults were based on analysis of regional lineaments and linears and the horizontal offset of local quartz veins. Although these quartz veins are indeed offset, the timing of the offset remains speculative. While a Pensylvanian origin is possible, it is equally likely that the veins record earlier movements within the granite, perhaps even previous to Sandy Creek Gabbro intrusion. Because of the limited amount of evidence regarding timing and nature of the of faulting within the region, the conclusions presented here minimize the role of faulting in developing a spatial model for the units.

2. Procedure

2.1. DRILLING AND CORE RETRIEVAL

The drill site is located on the Snell Ranch adjacent to one of the several pits of the defunct Ira Smith Quarry on the west slope of Big Four Mountain, (Township-range, Oklahoma Coordinates: SE SE SW NW Sec. 4 T.4N. R.15W.; NAD 27 UTM 14 S 0520394 N, 3845679 E). The site was chosen on the basis of regional considerations to intercept the granite-gabbro contact within 20 m or less, the ability to start drilling in bedrock, and the close proximity to an ample supply of fresh water.

The SQ-1 hole was spudded in the Mount Scott Granite, just west of the quarry pit and less than 50 m east from the contact with the gabbro. Drilling began in the Spring of 1993, and concluded in September of that year. The SQ-1 hole was cored to a total depth of 87.5 m by 2 inch (5.08 cm) I.D. diamond drill bit, using a water-cooled rotary rig. The rig is owned and operated by the Oklahoma Geological Survey.

The second hole, SQ-2, was a short hole spudded in soil and fill and completed in Sandy Creek Gabbro to an estimated depth of 10.4 m. Only a little over 1.67 m of core was retrieved using the same drilling equipment as SQ-1. Both cores were initially examined, logged, and oriented by J.P. Hogan at the drill site.

2.2. COLOR

Color was assessed by visual observation of the interior of dry core samples using the Geological Society of America Rock-Color chart (Goddard et al., 1948). All estimates indicate the bulk color of the sample, unless otherwise noted. Estimates are reported using color names defined in the U.S. National Bureau of Standard's Special Publication #440 on color (Kelly and Judd, 1976) and the corresponding identification number in the Munsell color system: **hue value/chroma** (*e.g.*, **10R 7/4**). Visual estimation of Munsell identification numbers have the following errors: hue ±4, value ±1, chroma ±1.

2.3. MAGNETIC SUSCEPTIBILITY (χ)

Magnetic susceptibility readings of the SQ-1 core were taken every 0.5 feet (0.153 m) using an Exploranium™ KT-5, hand-held susceptibility meter. Measurements from the hand-held meter were correlated to selected analyses of the core on a Sapphire Instruments™ SI-2, 5 cm diameter, copper coil susceptibility and anisotropy meter housed in the School of Geology and Geophysics Paleomagnetic Laboratory. The SI-2 meter was calibrated using a known volume and mass of MnO. Readings on the SI-2 were taken in SI mass units. However a limited number of readings in SI volume units were acquired to verify the mass readings.

Magnetic susceptibility readings on the SQ-2 core were done exclusively on the SI-2 susceptibility meter. Most of the core was analyzed in 4 cm increments in SI volume measurements. SI volume values were converted to SI mass values using the measured density of the core. SI mass units were taken on three 4 cm long pieces with known masses, and were used to check against the volume readings for the same interval. All magnetic susceptibility measurements are reported in SI mass units (dimensionless).

2.4. MAGNETIC SURVEYING

The magnetic survey of the area was conducted to constrain the relative subsurface relationships and geometry of the Sandy Creek Gabbro and Mount Scott Granite. Several traverses were made using an EG&G™ proton-procession magnetometer. Observations points were located 25 ft (7.63 m) apart in early traverses and 20 m (65.6 ft) apart in later traverses. However, when significant changes in total field were observed, suveying employed smaller stations interval distances to better characterize the noted change. Direction and distances were

measured using compass and measuring tape, and with a GPS unit. Stations were carefully plotted on the appropriate U.S. Geological Survey 7.5' quadrangle to ascertain the elevation. Five or more readings were taken at each observation station, and these were then averaged to produce a total field reading. Averages with 2σ standard deviation > ±3.00 gammas were discarded from the data set. A base-station was reoccupied to monitor drift (observed drift <10 gammas) every two hours or less. The main field was then subtracted from the total field data. Data were then modeled using *GM* a commercially available MS-DOS software package (Northwest Geophysical Associates) for forward 2-D modeling of gravity and magnetic data.

2.5. FRACTURE DENSITY

Fracture density (fractures/cm of core) data were acquired by counting the number of macro-fractures (visible to the unaided eye) over 0.5 ft (0.153 m) sections of the core. Two types of fractures were observed: 1) *Complete fractures* which transect the entire core, and 2) *Incomplete fractures* which cross-cut only a portion of the core.

2.6. PETROGRAPHIC ANALYSIS

Thin sections of the core were made every ~15 m and at selected additional depths. Observations were made in both transmitted and reflected light. Selected feldspar phases were analyzed by electron microprobe as part of a separate study published in Price *et al.*, 1996.

3. Results

3.1. DRILL CORE INVESTIGATION

Drilling at SQ-1 produced 87.5 m of continuous core, entirely of Mount Scott Granite. The absence of the granite-gabbro contact came as a surprise and prompted a magnetic survey in order to better resolve the subsurface geometry of this contact. The results of this survey are discussed later in the paper. Cursory inspection of the core revealed little if any significant variation with respect to primary igneous texture and mineralogy of the Mount Scott Granite as a function of depth. However, more detailed studies documented systematic variation in oxide mineralogy, fracture density, color, and magnetic susceptibility as a function of depth within the first 30 m of the surface.

The granite of the SQ-1 core is typical of surface exposures of Mount Scott Granite as observed within the Ira Smith Quarry. Although this granite may contain abundant granophyre at other locales (*e.g.*, Mount Scott), here the Mount Scott Granite is porphyritic with a seriate matrix, and granophyre is noticeably absent. Miarolitic cavities were not observed. The granite contains the characteristic gray ovoid rapakivi-textured anorthoclase feldspars phenocrysts discussed by Price et al.,

(1996). These phenocrysts are set in a matrix of red to pink alkali feldspar and quartz, with lessor plagioclase and with glomerocrystic ferroedenitic hornblende + biotite + accessory minerals which include titaniferous oxides, titanite, fluorite, zircon, apatite, ± allanite. The core also contains a substantial amount of mafic enclaves, characteristic of the Mount Scott Granite (Merritt, 1965). Sodic amphibole is present in the very deepest sample from the core (87.5 m) and is observed in surface exposures in vein fillings. A 0.1 m thick aplitic zone is present at 47.05 m depth. The aplite is fine-grained, ~equigranular, and devoid of ovoid feldspars or other phenocrysts. The color index grades from 5% to 0% from 47.05 to 47.11 m depth, and then grades back to 5% over the next 0.04 m.

The primary igneous mineralogy of the Mount Scott Granite is variably altered over the first ~30 m of the SQ-1 core. Largely, it is the titaniferous oxides that are altered, however, many of the silicates are altered to a lesser extent. With increasing depth to 27 m, the proportion of primary titanomagnetite and ilmenite increases and the proportion of secondary hematite decreases. At 20.5 m depth and shallower, oxide grains are largely hematite (Fig. 4d), with a small amount of ilmenite, and have a martite texture. In samples between 20.5 m and 34.7 m depth (Fig. 4b, c), hematite, propagating inward from grain boundaries, fractures, and partings, has encroached upon primary magnetite grains leaving only small domains of the original magnetite. This encroachment decreases as a function of depth and by 34.7 m, (Fig. 4a) and in deeper samples, the oxide assemblage is near-pristine primary titanomagnetite and primary ilmenite. Here magnetite grains typically exhibit only trace amounts of hematite along grain boundaries and partings.

The color of the core changes substantially over the first 30 m of the SQ-1 core (Fig. 5a). Close to the surface, the color is a grayish reddish orange (2YR 5/6). With increasing depth, the color darkens to a moderate grayish red (8R 4/6) (depth of 10 m). The color becomes lighter and more yellow from 10 to 13 m, ending at a grayish reddish orange (2YR 5/6). Over the next 14 m, the color gradually grades darker, and largely remains a moderate grayish red (8R 4/6) at depths below 27 m. This color is observed above and below the aplitic zone at 47.1 m, although the zone itself is a lighter color (8 R 6/3).

Magnetic susceptibility (χ) increases almost two orders of magnitude (Fig. 5b and Appendix 1) in the first 27 m of the SQ-1 core and then remains constant with depth. The lowest susceptibility values, 3×10^{-4} SI, are found at depths less than 2 m. From 2 to 10 m, susceptibility values rise to just below 1×10^{-3} SI, and are ~constant for 2 m. Between 12 m and 19.5 m, susceptibility varies from 3×10^{-4} to 1×10^{-3} SI. From 19.5 m to 27 m, susceptibility values increase to 9×10^{-3} SI. Below 27 m, to a depth of 55 m, values average ~9×10^{-3} SI, with only one notable exception at 47.1 m, where values drop over the corresponding interval of the aplitic-texture zone noted above.

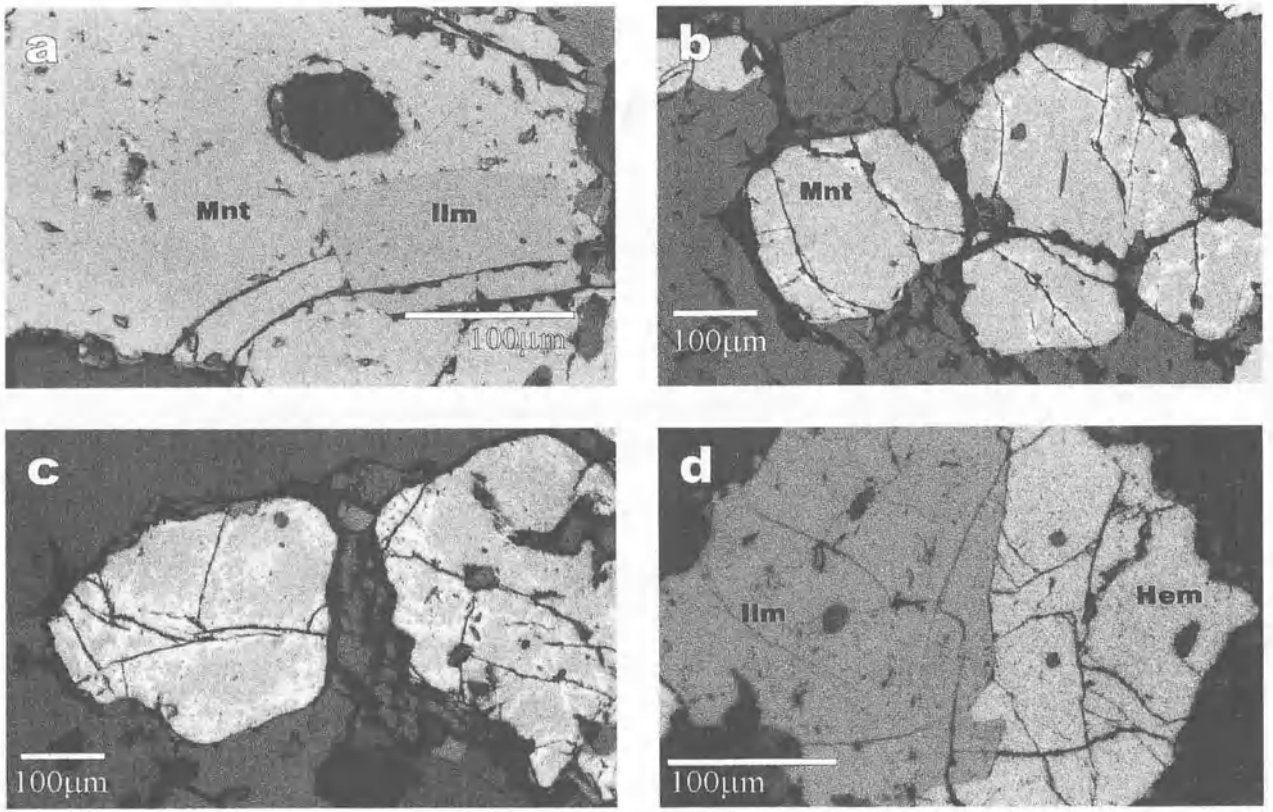

Figure 4. Four photomicrographs of the SQ-1 drill core (reflected light) documenting a change in the oxide mineralogy as a function of depth. a). An example of near-pristine (unaltered) oxides: magnetite (Mnt) and euhedral ilmenite (Ilm) from 34.7 m depth. b). Hematite (highest reflectivity) replacing magnetite grains along fractures at 27.5 m depth. c). Hematite (highest reflectivity) replacing magnetite along fractures and grain boundaries at 23.3 m. Note alteration is more extensive than at 27.5 m. d). Hematite (Hem) (higher reflectivity) after magnetite and ilmenite (Ilm) at 20.5 m.

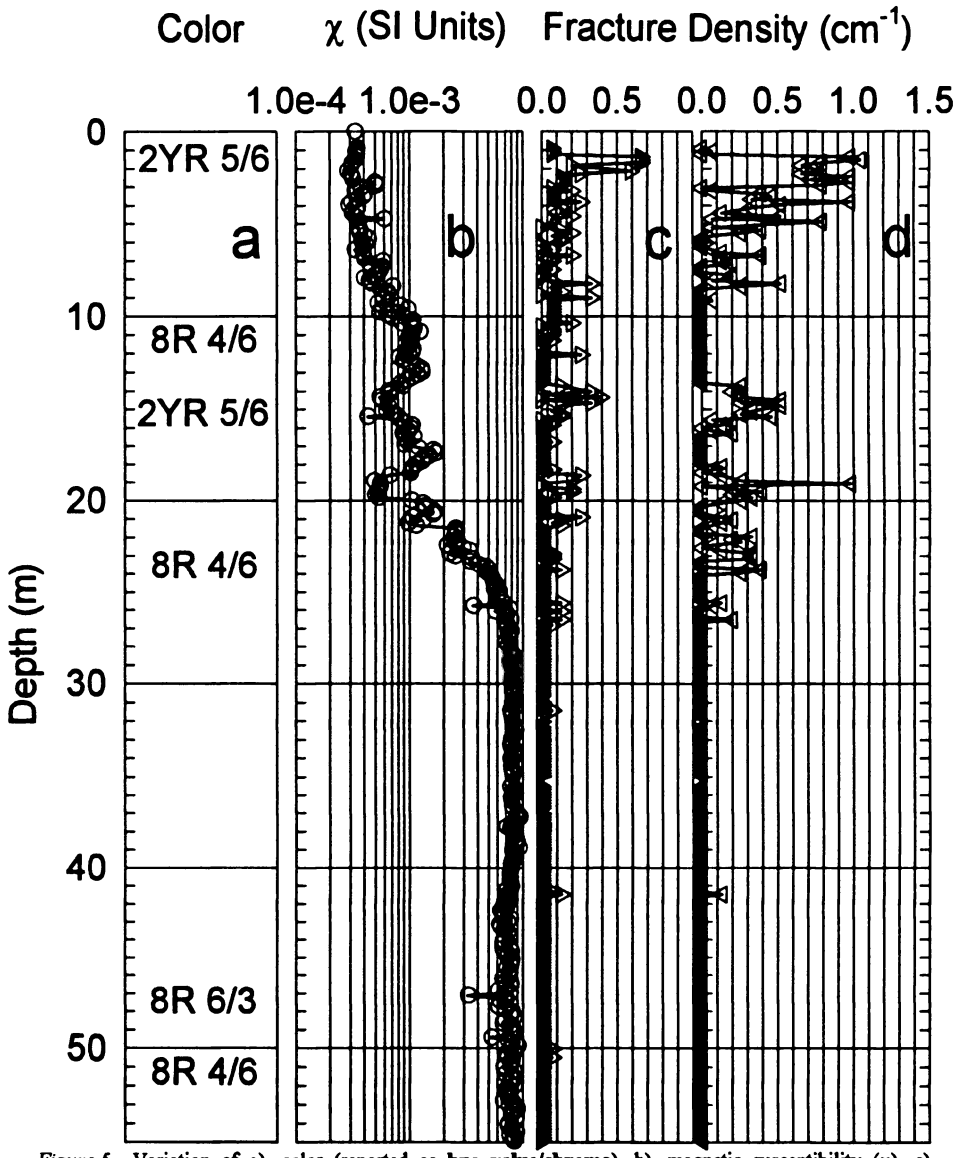

Figure 5. Variation of a). color (reported as **hue value/chroma**), b). magnetic susceptibility (χ), c). complete fracture density, and d). incomplete fracture density with depth. Lowest hue, lowest susceptibility, and highest fractures density values occur near the surface, grading to higher hue, higher susceptibility and lower fracture density values by 27 m depth. Between 0 and 27 m, increases in hue, susceptibility, correspond to increases in fracture density. Below 27 m, all of these measured parameters are largely constant, with the exception of a change in color (increased value, decreased chroma) and a drop in susceptibility at 47.1 m corresponding to aplite in the core. See text for further description

The SQ-1core is variably fractured, and the fracture density decreases with depth to nil in the first ~30 m from the surface (Fig. 5c, d and Appendix 1). Fractures are irregular to planar, exhibit several orientations, and are observed both macroscopically and microscopically. Larger fractures commonly have thin (~1 mm) coatings of secondary minerals (*e.g.*, calcite, pyrite, clays). Fractures contain little evidence of offset but zones of micro-brecciation have been observed. Above 0.9 m depth, the rock is largely incompetent and crumbly as a result of the extremely high number of fractures. Between 0.9 m and 27 m, fracture density varies, but shows an overall decrease with increasing depth. Partial fracture densities between 1 and 3 m are as great as 0.60 cm^{-1}. Complete fracture densities were large in this same interval, with densities above 1.0 cm^{-1}. Complete fracture density dropped to zero from 9.5 m to 14 m, and partial fracture density was low (~0.07 cm^{-1}) for this interval. Fracture densities increase at 14 m, to 0.45 cm^{-1} partial fractures and 0.50 cm^{-1} complete fractures. Below 15 m, fracture densities taper off to 0.0 by 27 m. Below 27 m the core is unfractured, except at 31.5 m, 41.5 m, and 56.5 m.

Color, oxide mineralogy, magnetic susceptibility, and fracture density vary systematically with depth over the first 27 m of SQ-1 core. At depths greater than 27 m the core remains largely homogeneous. In general, from the surface to 27 m, magnetic susceptibility, hue, and modal primary magnetite and ilmenite increase, whereas fracture density and modal secondary hematite decrease. More importantly there is a direct correspondence between these properties and fracture density. For example, at 14.5 m depth and again at 19.5 m depth, magnetic susceptibility decreases drastically, the color lightens, with a corresponding *increase* in fracture density. Conversely, at 11 m depth and again at 18 m depth, magnetic susceptibility increases, the color becomes pinker, with a corresponding *decrease* in fracture density (Fig 5).

In contrast to this, the Sandy Creek Gabbro from the near-surface SQ-2 core, although containing a significantly fractured interval (0.70 cm^{-1} partial fractures) from 9.5 to 10 m, shows no alteration of magnetite to hematite (Fig. 6) and insignificant change in magnetic susceptiblity (Appendix 2). Although the core length is short and perhaps insufficient for documenting trends in mode or suceptibility, it is shallow (<11 m) and one would expect to find magnetite to hematite alteration here if present. However, exsolution of fine ilmenite needles (Fig. 6b) within magnetite grains was the only observed secondary featureof the SQ-2 oxides. Magnetite crystals are otherwise pristine, showning not even the slightest alteration, including along grain boundaries, fractures, and partings.

3.2. MAGNETIC SURVEY

Magnetic susceptibility of the Mount Scott Granite is considerably lower (at any depth) than for the Sandy Creek Gabbro (Bradley and Jones-Cecil, 1991). Thus, as a result of failing to intersect the granite gabbro contact with the drill, a magnetic survey of the area was initiated in order to better resolve the subsurface geometry of the Sandy

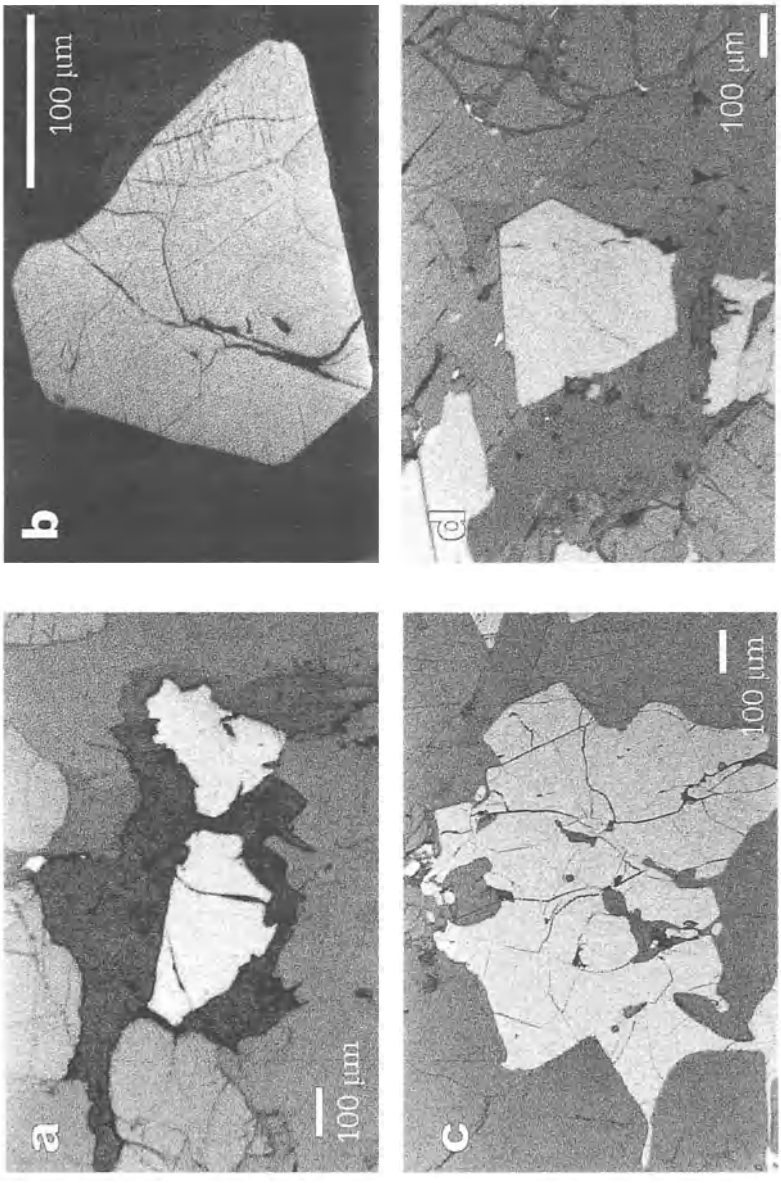

Figure 6. Four photomicrographs of the Sandy Creek Gabbro drill core SQ-2 reflected light from depths less than 11 m. Despite the shallow depth, there is no visible alteration of these oxides. a). A sample from 10.7 m containing near-pristine (unaltered) magnetite. b). Magnetite with ilmenite exsolution needles with no alteration to hematite at 9.7 m depth, perhaps the most fractured interval of the SQ-2 core. c). Another pristine magnetite at 9.7 m depth. d). An exsolved oxide (magnetite with ilmenite) from 9.4 m depth with no hematite.

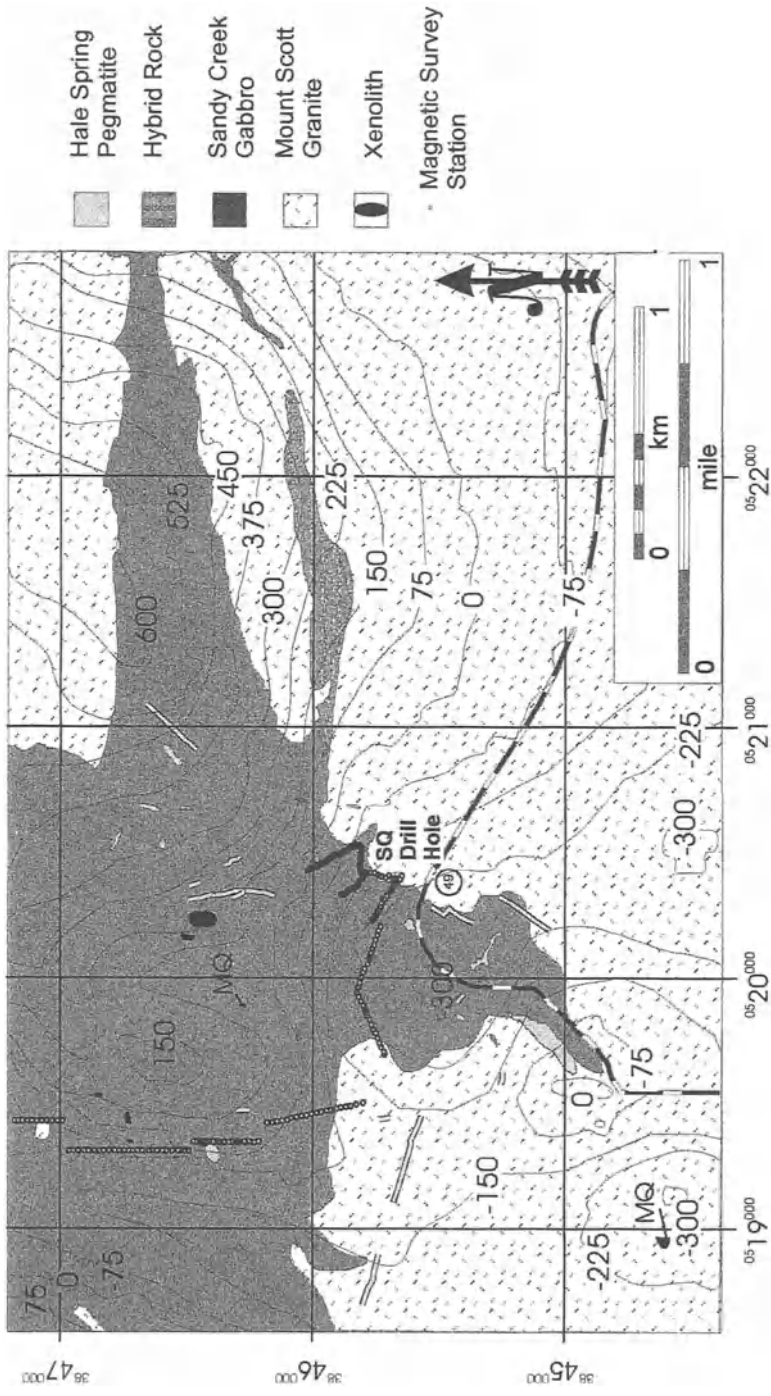

Figure 7. Geomagnetic map superimposed on geologic map (Figure 3). High values indicate near-subsurface domains of higher magnetic susceptibility (e.g. Sandy Creek Gabbro), while low values indicate domains of lower susceptibility (e.g. Mount Scott Granite). Data from Jones-Cecil (1995) reduced to the pole with 75 gamma contour line spacing.

Creek Gabbro and Mount Scott Granite contact. The large contrast in magnetic susceptibility ($\Delta\chi$) between these units greatly facilitates modeling the subsurface spatial geometries of these two bodies from geomagnetic data.

Jones-Cecil (1995) presents the results of a detailed aeromagnetic survey of the Wichita Mountains as with the total-field data from the survey reduced to the pole. Figure 7 places that data over the geology shown in figure 3. Substantial magnetic highs on this map should correspond with relatively shallow and/or large bodies of material with a large $\Delta\chi$ with their surroundings. Although the survey indicates there are substantial changes in magnetism within this area, very few coincide with mapped contacts. For instance, the highest readings in the Hale Spring Area are found beneath Black Bear Mountain, the surface of which is composed entirely of Mount Scott Granite. This is likely to correspond to Sandy Creek Gabbro under a thin veneer of Mount Scott Granite.

Several magnetometry ground traverses resolved local details of the magnetic field (see Fig. 3). Traverses across the contact between the Sandy Creek Gabbro and all of the surrounding and intruding lithologies were always marked by a change in total field. Total field variations were also noted elsewhere along many of the traverse lines, and, in many cases, direct observation of the geology during such variations was obscured by alluvium. Two extensive traverses are presented in this paper (Table 1 and 2), and a permissible subsurface geometry for the units was constructed by 2D forward modeling.

4. Discussion and Conclusions

4.1. VARIATION WITHIN THE GRANITE

Analysis of the SQ-1 drill core indicates little change in the primary magmatic character of Mount Scott Granite over the 87.5 m hole depth. The majority of variations in the core result from fracture-controlled fluid-rock interaction and alteration of the granite (Price *et al.*, 1985).

4.1.1. Magmatic Variation

Magmatic variation refers to changes resulting from igneous processes operating during crystallization of the cooling granite magma. The homogeneous nature of the primary igneous mineralogy and primary texture of the core suggest a largely uniform composition, and a uniform cooling history, for the Mount Scott Granite magma over the interval examined (87.5 m). Detailed investigations of feldspar compositions (Price *et al.*, 1996) and amphibole compositions (Hogan and Gilbert, 1995) from this core revealed little if any compositional variation, indicating rather uniform magma composition and intensive parameters (*e.g.*, T, fO_2) during crystallization of this portion of the granite.

TABLE 1. Position of stations, distance and angle from origin, and anomalous field values for East to West traverse from SQ to Bell Mountain for Trav 1.

NAD 27 UTM		Elevation	Distance	Azimuth	Anomaly
Easting	Northing	(meters)	(meters)	(degrees)	(gammas)
520408	3845673	531	15	115	302
520401	3845676	531	8	115	104
520394	3845679	531	0	318	51
520389	3845685	528	-4	318	140
520384	3845690	527	-8	318	140
520379	3845696	526	-23	318	226
520374	3845702	525	-31	318	219
520367	3845705	525	-38	313	173
520360	3845708	523	-45	310	68
520353	3845711	522	-52	308	114
520346	3845714	521	-60	306	162
520340	3845719	521	-67	306	287
520334	3845724	520	-75	307	415
520328	3845728	520	-83	307	299
520322	3845733	520	-90	307	351
520318	3845739	519	-98	308	402
520313	3845746	519	-105	309	299
520306	3845748	518	-112	308	350
520298	3845750	515	-119	306	348
520291	3845752	514	-126	305	357
520284	3845755	514	-134	305	273
520277	3845757	514	-141	304	248
520269	3845759	515	-148	303	356
520263	3845763	515	-156	303	411
520256	3845766	515	-163	302	338
520249	3845770	515	-171	302	389
520243	3845774	516	-179	302	400
520236	3845778	516	-186	302	503
520230	3845782	515	-194	302	469
520205	3845752	514	-203	302	362
520188	3845762	514	-222	300	807

The one exception to the primary mineralogical and textural homogeneity of the core is the aplitic zone observed at 47.1 m. In general aplite dikes are rarely observed within the Mount Scott Granite. This aplite is finer grained and more felsic than the adjacent granite and is free of ovoid phenocrysts. Although currently compositional information is unavailable on this zone, we interpret it to be a late stage differentiate of the Mount Scott Granite rather than a distinctly separate magma.

4.1.2. Subsolidus Variation (Alteration)

Circulation of presumably meteoric waters through a near-surface fracture network in this crystalline basement has significantly altered the primary mineralogy of the Mount Scott Granite. This alteration has drastically modified both the magnetic susceptibility and color of the Mount Scott Granite.

TABLE 1. Continued

NAD 27 UTM		Elevation	Distance	Azimuth	Anomaly
Easting	Northing	(meters)	(meters)	(degrees)	(gammas)
520168	3845765	514	-242	290	420
520149	3845771	513	-262	288	417
520130	3845776	513	-282	288	376
520112	3845786	513	-302	290	160
520103	3845789	513	-312	290	-23
520098	3845791	513	-317	290	-224
520093	3845792	513	-322	290	-736
520088	3845794	512	-327	290	-123
520084	3845795	513	-332	290	326
520074	3845799	513	-342	290	331
520055	3845804	514	-362	289	401
520036	3845812	514	-382	290	292
520018	3845820	515	-401	290	271
520000	3845829	515	-421	291	182
519981	3845834	516	-441	290	94
519962	3845841	518	-461	290	-16
519943	3845846	518	-481	290	-19
519924	3845838	518	-501	287	132
519906	3845830	518	-521	285	48
519888	3845822	517	-541	282	110
519879	3845817	517	-551	281	281
519861	3845809	517	-571	279	654
519851	3845805	516	-581	279	590
519833	3845797	516	-601	277	301
519815	3845789	516	-621	275	57
519797	3845781	516	-641	274	-34
519778	3845773	515	-661	273	-20
519760	3845765	515	-681	272	-70
519723	3845748	515	-721	270	100
519705	3845740	515	-741	269	407

Fluids altered the primary titanomagnetite grains within the Mount Scott Granite. Samples from depths below 27 m in the core contain primary titanomagnetite, largely free of hematite. With decreasing depth, these grains are increasingly replaced by hematite by the following reaction:

$$2Fe^{2+}Fe_2^{3+}O_4 + \tfrac{1}{2}O_2 \rightarrow 3Fe_2^{3+}O_3 \qquad (1)$$

Hematite growth proceeds from grain boundaries and fractures into the crystals.

Fluids altered the color of Mount Scott Granite through hydration of chromophores in alkali feldspar. Based on cathodoluminescence studies of other samples of Mount Scott Granite (Price, unpublished data), and what is known about feldspar chromophores (Smith, 1974), the color of matrix alkali-feldspars results from submicroscopic hematite flakes as inclusions. If water-rich fluid were to permeate the

TABLE 2. Position of stations, distance and angle from origin, and anomalous field values for East to West traverse from SQ to Bell Mountain for Trav 1.

NAD 27 UTM		Elevation	Distance	Azimuth	Anomaly
Easting	Northing	(meters)	(meters)	(degrees)	(gammas)
519428	3847230	489	-655	0	799
519428	3847210	489	-635	0	482
519428	3847190	488	-615	0	457
519428	3847170	487	-595	0	435
519428	3847150	487	-575	0	440
519428	3847130	486	-555	0	578
519428	3847110	485	-535	0	473
519428	3847090	488	-515	0	478
519428	3847070	488	-495	0	218
519428	3847050	488	-475	0	-615
519428	3847050	488	-455	0	307
519317	3846973	482	-455	0	-412
519317	3846953	482	-435	0	-387
519317	3846933	482	-415	0	-298
519317	3846913	482	-395	0	-503
519317	3846893	482	-375	0	46
519317	3846873	482	-355	0	302
519317	3846853	482	-335	0	340
519317	3846833	482	-315	0	75
519317	3846813	482	-295	0	597
519317	3846793	482	-275	0	103
519317	3846773	482	-255	0	168
519317	3846753	482	-235	0	
519317	3846733	482	-215	0	319
519317	3846713	482	-195	0	953
519317	3846713	482	-195	0	959
519317	3846697	482	-179	0	945
519317	3846657	482	-139	0	236
519317	3846637	482	-119	0	828
519317	3846617	482	-99	0	644
519317	3846597	482	-79	0	913
519317	3846577	483	-59	0	371
519317	3846557	482	-39	0	680
519317	3846537	482	-19	0	482
519349	3846509	501	0	0	1446
519349	3846489	501	20	180	981
519349	3846479	501	30	180	680
519349	3846469	501	40	180	363
519349	3846459	501	50	180	65
519349	3846449	501	60	180	-91

TABLE 2. Continued

NAD 27 UTM		Elevation	Distance	Azimuth	Anomaly
Easting	Northing	(meters)	(meters)	(degrees)	(gammas)
519349	3846439	501	70	180	1005
519349	3846429	500	80	180	994
519349	3846409	499	100	180	1345
519349	3846399	499	110	180	813
519349	3846389	498	120	180	411
519349	3846369	497	140	180	657
519349	3846349	496	160	180	1429
519349	3846339	496	170	180	1282
519349	3846329	496	180	180	559
519349	3846316	495	193	180	-104
519349	3846309	494	200	180	31
519349	3846289	493	220	180	68
519349	3846269	491	240	180	332
519349	3846249	491	260	180	221
519349	3846232	491	277	180	348
519426	3846199	490	310	180	23
519426	3846179	491	330	180	236
519429	3846159	495	350	175	573
519434	3846140	498	370	173	1059
519438	3846120	499	390	171	275
519442	3846101	500	410	171	688
519446	3846081	502	430	170	1295
519450	3846061	503	450	170	1406
519454	3846042	504	470	170	1012
519459	3846022	505	490	170	1235
519463	3846003	506	510	169	957
519467	3845983	507	530	169	538
519471	3845964	509	550	169	445
519475	3845944	510	570	169	13
519479	3845925	512	590	169	51
519484	3845905	513	610	169	-60
519488	3845885	513	630	169	27
519492	3845866	511	650	169	47
519496	3845846	509	670	169	97
519502	3845820	509	696	169	-6

crystals, perhaps along perthite boundaries or cleavage planes, it could react with the inclusions, to produce iron hydroxide (*e.g.*, goethite) at the expense of hematite:

$$Fe_2^{3+}O_3 + H_2O \rightarrow 2(Fe^{3+}O(OH)) \quad (2)$$

Hydration of red hematite flakes to yellow iron hydroxide turns the alkali feldspar grains from pink to orange. Since alkali feldspar comprises over 80 percent of the rock, the entire color of the rock is changed when alteration is thorough.

The oxidation of primary magnetite to hematite and the hydration of hematite to iron hydroxide deminish the magnetic susceptibily of the rock. Magnetic susceptibility is a function of the concentration, size, shape, and type of the ferromagnetic (*s.l.*) minerals (*i.e.* magnetite, hematite, ilmenite) within a rock (Tarling and Hrouda, 1993). Changes in concentration, size, shape are not significant here: the mode of oxides remains unchanged throughout the upper portion of the core, and replacement appears to be largely pseudomorphic. However, the secondary alteration of magnetite to hematite and hematite to iron hydroxide, can readily account for the decrease in the magnetic susceptibility. The mass magnetic susceptibility values of magnetite are ten times those of hematite, and the values for hematite are one hundred times those for the iron hydroxide, goethite (Tarling and Hrouda, 1993).

All of the above alteration features, changes in color, oxide mineralogy, and magnetic susceptibility, correlate with fracture density. The greater alteration occurs closer to the surface, as do the greater numbers of fractures. In highly fractured intervals (*i.e.* near surface) alteration was more pervasive because of enhanced permability and because of the increased surface area for fluid/rock interaction.

The exact origin, timing, or temperature of the fluid(s) that altered the Mount Scott Granite remains unknown. However, because of the decrease in intensity of alteration as a function of depth, and because of the oxidizing nature of the reactions, we suggest that relatively recent circulation of meteoric water through this near surface fracture system is a likely explanation. Since many of the observed fractures within the core and on the surface of the granite are open, it is likely that the oxidation and hydration of the granite are ongoing phenomena. However, because of the previous exposure of the Wichita Mountains to surface conditions in the Permian, we do not rule out the possibility of multiple alteration events. The presence of clay minerals and calcite within some fractures indicate that much of the interaction occurred at low temperature. The presence of rare sulfide mineralization along some fractures indicates interaction with low-fO_2 fluid(s). This suggests more complicated scenarios involving more than one alteration period with fluids of differing composition.

The ultimate origin of the fractures and their distribution is poorly constrained at this time. The region was subjected to several episodes of compression during the late Paleozoic, and faults have been located proximal to the core site (Stockton and Giddens, 1984; McClean and Stearns, 1986). However, the lack of offset and the presence of only minor brecciation argues against a compressional tectonic origin for the fractures observed in the core. Moreover, the decreasing fracture density with depth is more indicative of sheet fracturing developed during overburden unloading

(Holtzhausen, 1989; Turcotte and Schubert, 1982). Because of the early Paleozoic burial level of this region, removal of overburden would have had a pronounced effect on the structural integrity of the Mount Scott Granite. Some 4-5 km of volcanic and sedimentary rocks once covered the Mount Scott Granite, and these were stripped away during the late Paleozoic. Additionally, the region returned to a depth of 1 km during the Mesozoic (Gilbert, 1982), and the current re-exhumation provides a second opportunity for sheet fracture genesis.

Perhaps the most significant conclusion from this portion of the study is the depth to which significant alteration of the granite is observed. To obtain what would be pristine igneous rock, one must penetrate >30 m below the surface. Typically, compositional analyses from granites are performed on near-surface samples. The effect of alteration on major-elements appears to be negligible, based on the lack of mineral mode variation. The possible effect on trace element chemistry is unknown, but may be substantial for elements easily mobilized by the fluids described here.

4.2. THE MOUNT SCOTT GRANITE - SANDY CREEK GABBRO CONTACT

Based on the regional relationships, the granite-gabbro contact was inferred to be subhorizontal and should have been encountered within ~15 m of the surface at the drill site. However, the contact was not encountered with 87 m of drilling through solid Mount Scott Granite. Clearly, within the immediate vicinity of the drill hole the contact is neither subhorizontal nor does it dip shallowly to the east. Thus, we employed forward 2-D modeling of the magnetic survey data to resolve the subsurface geometry of this contact. Modeling provides a calculated profile that fits the observed data. This is largely dependent on the contrast in magnetic susceptibility, the shape of the boundary between the units, and the depth of the units. Although by themselves such models produce non-unique solutions, when augmented by detailed surface mapping, known regional relationships, and, albeit limited, drill hole data, the result is a reasonable geologic model of the subsurface.

As previously discussed, the magnetic susceptibility of the Mount Scott Granite gradually increases through a zone of fracturing and alteration to a depth of 27 m where it remains largely uniform. Thus, the Mount Scott Granite was subdivided into two units: a 27 m thick altered cap, with an average susceptibility of 1.23×10^{-3} SI, and an unaltered subsurface unit with a susceptibility of 7.60×10^{-3} SI. In construction of the models, we assumed the boundary bewteen altered and unaltered granite parallels topography. Although we recognize that a more complicated geometry reflecting fracture intensity and paleo-groundwater circulation is more likely, significant variation to the depth of this contact will not drastically alter the conclusions presented here.

Magnetic susceptibilities for the Sandy Creek Gabbro core (SQ-2) are quite consistent (Appendix 2), and magnetite grains throughout the core appear pristine and

largely unaltered. It appears that the Sandy Creek Gabbro does not share the same alteration profile as the Mount Scott Granite. Two reasons for this: 1.) there are fewer fractures and joints within surface exposures of the Sandy Creek Gabbro relative to the Mount Scott Granite so there is less surface area for fluid interaction. 2.) The diffusion rate of fluid through the rock is much slower than that of the Mount Scott Granite. This is evidenced by the difference in the weathering of the gabbro, as seen on surface outcrops. Whereas exposed Mount Scott Granite weathers completely, producing meter-sized boulders of crumbly rock that are completely altered to their cores, the Sandy Creek Gabbro produces a weathering rind that is cm thick, with pristine-appearing rock below this surface.

Although weathering will have created little to no variation in magnetic susceptibility of the Sandy Creek Gabbro, some variation, including higher values than those observed in the SQ-2 core, should be anticipated as the gabbro exhibits pronounced layered mineralogical variation throughout the body, including apatite-pyroxene-titaniferous oxide cumulates in the central portion of the Hale Spring Area (Powell, 1986; Diez De Medina, 1988). Furthermore, other Roosevelt Gabbro bodies contain appreciable amounts of high magnetic susceptibility rocks: there is a magnetite-ilmenite-olivine body (21-60% modal magnetite, Powell and Gilbert, 1982) exposed within the Glen Creek Gabbro, and some Mount Baker Gabbro float contains magnetite crystals as large as 15 cm in diameter (Stockton and Giddens, 1982). In many parts of the pluton, it is likely that overall susceptibility of the gabbro is much greater than that measured from the core.

Modeling attempted to use the collected susceptibilities (average = 1.64×10^{-2} SI) from the core SQ-2. These were employed for the construction of Trav. 1 (Fig. 8), as the core hole penetrates much of the modeled section, and the susceptibility satisfied the observed magnetic readings. However, we were unable to model the gabbro in Trav. 2 (Fig. 9) with this susceptibility: the calculated magnetic profile falls far below the observed data. It was therefore necessary to increase the susceptibility to produce the observed magnetic anomaly. In comparison to Trav. 1, Trav 2. crosses a more mafic section of the pluton (Diez de Medina, 1988): the mineralogy may differ substantially from that observed in the SQ-2 core. Additionally, if the gabbro extends to great depths (500 m), as has been modeled, more mineralogical (and susceptibility) variation is likely, and should be accounted for within the model. Therefore, in modeling the gabbro in Trav 2, we employed a much greater susceptibility (5.00×10^{-2} SI) for the gabbro, chosen because it produces the intensity of magnetism necessary to fit the profile and because it is a reasonable estimate of a gabbro pluton with small magnetite-dominated layers or zones.

The susceptibility data for the other modeled units was taken from literature sources, where available, or approximated based on rock composition. The magnetic susceptibility value for the GMLC (5.7×10^{-3} SI) was taken from Bradley and Cecil-Jones, (1991). This value does not significantly differ from that of unaltered

Mount Scott Granite. Because of the lack of contrast, the contact between the Mount Scott Granite and GMLC within the subsurface was interpolated from exposures to the north and east of the Hale Spring Area. Its presence in the near subsurface is likely, as xenoliths or possibly roof pendants of GMLC are present within the Sandy Creek Gabbro. No data are available for the Hale Spring Pegmatite. Its felsic mineral composition indicates that its susceptibility is quite low, and was modeled with values similar to the altered Mount Scott Granite. Likewise, there are no available data for the Post Oak Conglomerate or younger alluvium. Altered Mount Scott Granite

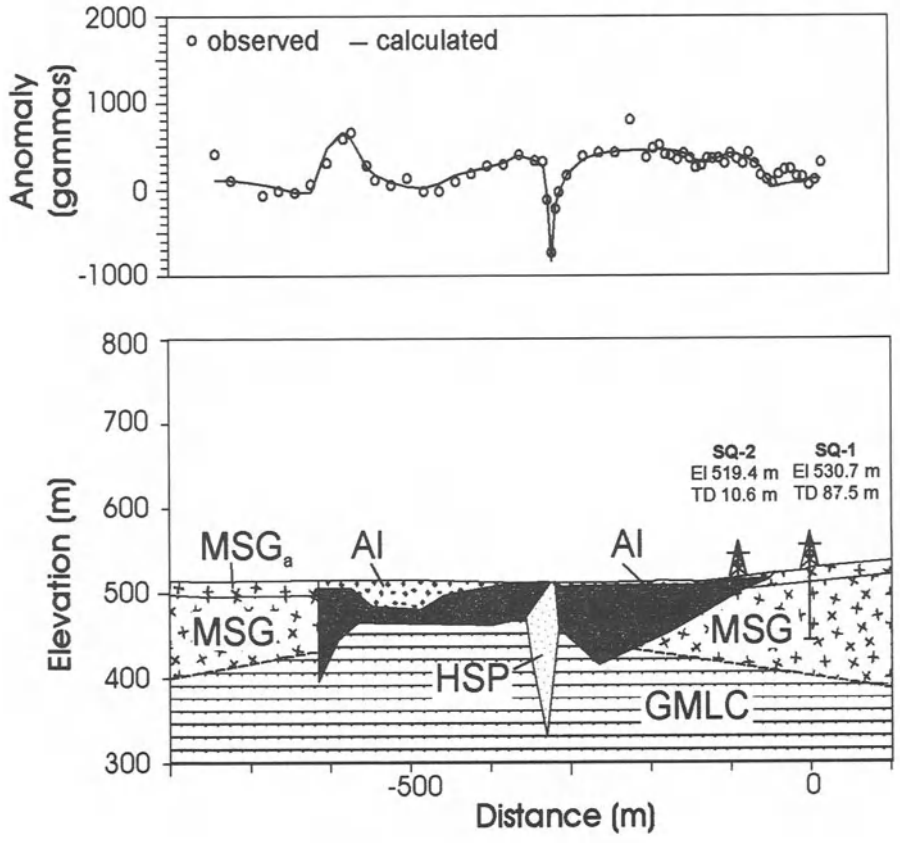

Figure 8. 2D forward magnetic model of Trav. 1, a traverse extending west from the Smith Quarry to the slopes of Bell Mountain. Observed anomaly marked by open circles, modeled profile marked by a line. SQ-1 and SQ-2 drill sites marked, along with total depth of penetration. Modeled lithologies include MSG - Mount Scott Granite, MSG$_a$ - Altered Mount Scott Granite, SCG - Sandy Creek Gabbro, GMLC- Glen Mountains Layered Complex, Al - Alluvium, fill, and soil, and HSP - Hale Spring Pegmatite.

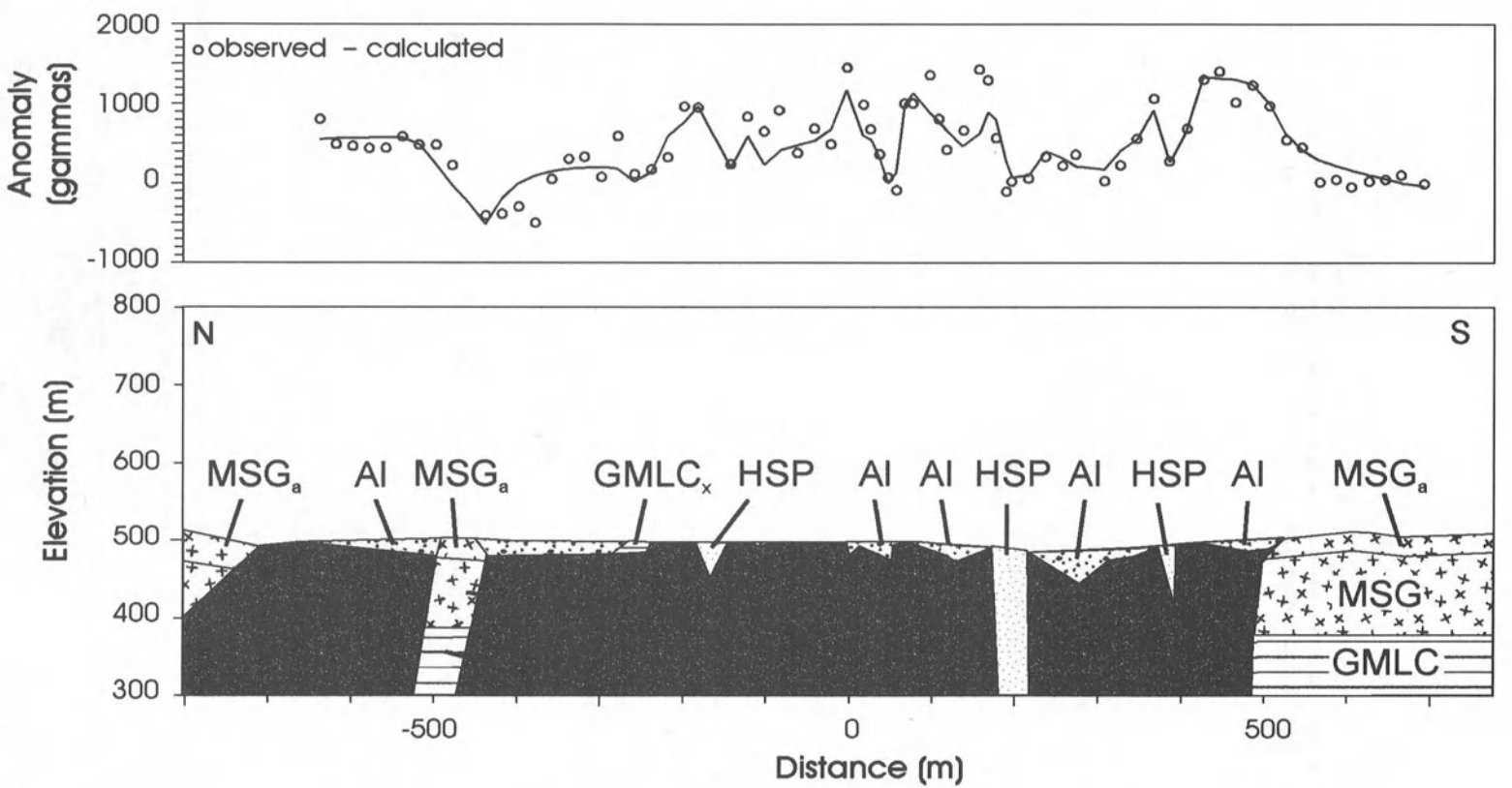

Figure 9. 2D forward magnetic model of Trav. 2, a traverse extending north from Bell Mountain, across Sandy Creek. Observed magnetic anomaly marked by open circles, modeled anomaly by a line. Modeled lithologies include Al - Alluvium, fill, and soil, MSG - Mount Scott Granite, MSG$_a$ - Altered Mount Scott Granite, SCG - Sandy Creek Gabbro, GMLC- Glen Mountains Layered Complex, GMLC$_x$- Xenolith of Glen Mountains Layered Complex, and HSP - Hale

susceptibility values were used for these units, as they are largely comprised of detrital grains and cobbles from the granite.

Figure 8 displays the modeled results for an ~east-west magnetic survey across the southern portion of the Sandy Creek Gabbro (Trav. 1, Fig. 3). The traverse begins 15 m east of the SQ-1 drill hole in Mount Scott Granite, transects the gabbro, and ends 100 m into exposed Mount Scott Granite on the western side of the body. Beneath this traverse, the Sandy Creek Gabbro is relatively thin with an irregular floor. The eastern contact dips shallowly to the west, readily explaining why the granite-gabbro contact was not intersected by the SQ-1 drill hole. The western contact is near vertical. An anomaly of low-susceptibility material is present roughly in the middle of the traverse, and although not exposed at the surface, its location, shape, and low susceptibility are indicative of Hale Spring Pegmatite. The subhorizontal contact between the Mount Scott Granite and the underlying GMLC is interpreted from regional map patterns and appears to be truncated by emplacement of the Sandy Creek Gabbro.

A south-north traverse (Fig. 9) beginning on Mount Scott Granite at Bell Mountain, crosses Sandy Creek Gabbro, and terminates on a small exposure of pegmatite within the gabbro. The Sandy Creek Gabbro displays considerable thickness, and the floor of the pluton is not imaged by this data. The contacts between the Sandy Creek Gabbro and the Mount Scott Granite along this traverse are near vertical, dipping only slightly to the north. The Sandy Creek Gabbro contact is again interpreted to truncate an older contact between the GMLC and Mount Scott Granite in the subsurface. No compelling evidence for faulting was observed in surface exposures of nearby Mount Scott Granite, suggesting that this geometry is the direct result of intrusion of the magma which gave rise to the Sandy Creek Gabbro. Numerous Hale Spring Pegmatite dikes crop out along this traverse, and thus, regions with low magnetic anomalies were modeled as pegmatite.

Magnetic data indicate that shape of the gabbro-granite contact varies. The models show that in the southern portion of the area, the surface contact outlines the furthest extent of the gabbro into the granite. The areomagnetic data (Jones-Cecil, 1995, Fig. 6) indicate the gabbro extends beneath the granite to the northeast. This may indicate that the contact is indeed subhorizontal for a short distances in the less eroded regions of the eastern Hale Spring Area.

4.3. THE SHAPE OF THE SANDY CREEK PLUTON

The subsurface geometry of the Sandy Creek Gabbro and its spatial relationships with adjacent units were evaluated from a series of north-south cross-sections, spaced 1 km apart, constructed on the basis of the results of this study (*i.e.*, surface mapping, drill-hole core data, and magnetic surveys), aeromagnetic data from Jones-Cecil (1995) fig. 7), and the surface geologic data from Powell *et al.* (1982), and Stockton

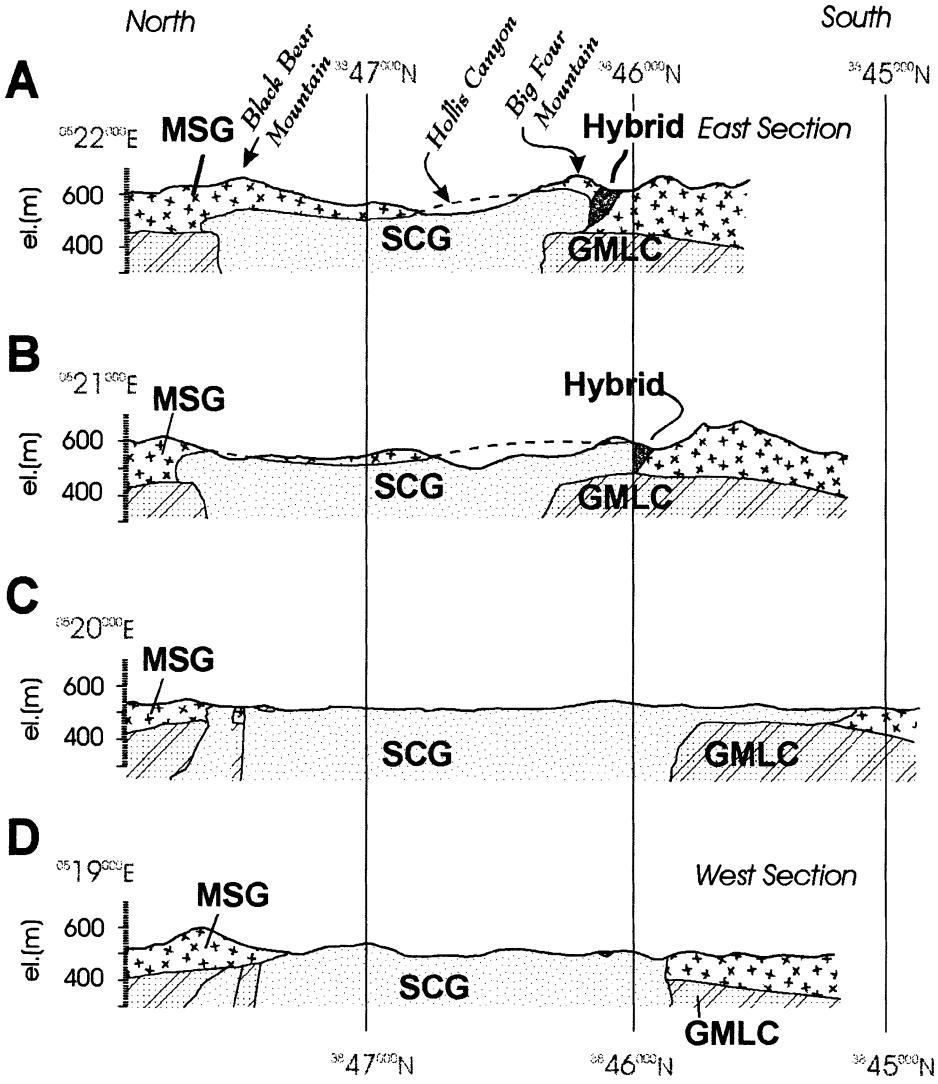

Figure 10. North-south cross sections of the Hale Spring Area. Sections follow UTM coordinates (see fig. 3) and are spaced 1 km apart. See text for description.

(1984) and are shown in figure 10. Additional field data from exposures elsewhere in the Wichita Mountains aided in constraining this geologic model.

Cross sections A and B on figure 10 reveal that the present erosional surface is just beginning to expose the subhorizontal roof of the Sandy Creek Gabbro pluton in the vicinity of Hollis Canyon. The gabbro is interpreted to extend back beneath Black Bear Mountain where it is capped by a relatively thin veneer of Mount Scott Granite on the basis of the large regional magnetic anomaly associated with this mountain (see Fig. 7). The hybrid rock, present along the southern contact of the gabbro, is interpretively depicted here as a dike-like body, generated by partially melting Mount Scott Granite (see Big Four Mountain, Fig. 3). The Sandy Creek Gabbro is also shown to lip over, and, to an extent, exploit the GMLC-Mount Scott Granite contact. This is an interpreted extension of the Sandy Creek Gabbro ledge that protrudes out from the main body to the south seen on magnetic surveys further west (see cross section C).

Section C crosses the most eroded portion of Sandy Creek Valley. The surface geology is mostly Permian and younger sediments, but exposures of gabbro are found throughout the valley. Additionally, small blocks of GMLC and Meers Quartzite crop out: xenoliths, possibly roof pendants, suggesting the level of exposure is proximal to the former unconformity, that is the GMLC-Mount Scott Granite sheet contact. The southern end of section C is perpendicular to the E-W geophysical traverse (Trav. 1, Fig. 8). Here the Sandy Creek Gabbro is relatively thin, with inwardly dipping margins, which we interpret as a protruding subhorizontal ledge of gabbro that exploited the preexisting GMLC-Mount Scott Granite contact. Such lateral spreading occurs when the overlying strata (*e.g.,* Mount Scott Granite and Carlton Rhyolite) are lifted by the driving pressure of the emplaced magma (Hogan and Gilbert, 1995). Although much of the Sandy Creek Gabbro pluton has steep sides, and it probably made room for itself largely through stopping or displacing the crust horizontally, a small amount of magma had sufficient driving pressure to exploit the horizontal discontinuity and form a shallow ledge.

Section D is ~0.3 km west and parallel to the S-N geophysical profile (Trav. 2) in figure 9. The moderately eroded profile has similar geometry to that seen in the other sections. However, geophysical data indicate that the southern contact of the Sandy Creek Gabbro pluton is best modeled as a steep, near-vertical wall that truncates, rather than spreading laterally along, the older contact between the GMLC and the Mount Scott Granite sheet. As previously discussed, evidence of faulting was not observed at the surface. Thus we attribute this geometry to intrusion of a younger gabbroic magma that gave rise to the Sandy Creek Gabbro. Additional support for this conclusion includes a recently determined younger crystallization age for another Roosevelt Gabbro pluton, the Mount Sheridan Gabbro, than that determined for the Mount Scott Granite (Hogan *et al.*, 1996).

The Sandy Creek Gabbro pluton may have made room for itself through a combination of stoping, passive lifting of the overburden, and partial melting of its roof rocks. The pluton is typically a steep walled, >300 m deep ~oval shape, with a short axis ~1.5 km wide, and a long axis excessive of 5 km. However, minor amounts of spreading occurred along the anisotropy created by the GMLC-Mount Scott Granite contact (*i.e.*, the 100 m thick subhorizontal gabbro ledge along the southern margin of the body; see fig. 8).

Work by Diez de Medina (1988) shows the gabbro fractionated after emplacement, producing a general distribution of relatively high MgO, cumulitic gabbro adjacent to highway 49 in the southern portion of the area and moderate, less cumulitic, moderate to low MgO gabbro located to the north in the drainage of Sandy Creek. Her work concluded that the gabbro adjacent to the creek results from and fractional crystallization of the gabbro to the south and assimilation of crustal materials. This is consistent with our model, in that the gabbro to the south, crystallizing within a thin ledge, would cool prior to the rest of the body, and preserve a more primative composition. Addtionally, granite assimilation would occur in the bulk of the body to the north, producing the observed contamination .

Powell *et al.*, (1982) and Powell (1986) concluded that the Sandy Creek Gabbro is tilted to the east with respect to the nearly horizontal Mount Scott Granite on the basis of dipping lamination and compositional differentiation within the gabbro. Such an interpretation is only valid for a scenerio where the Sandy Creek Gabbro is much older than the Mount Scott Granite, and is emplaced and tilted prior to the Carlton unconformity. As mentioned above, the evidence from this study precludes this case. Instead we suggest that these features arise from floor irregularity and assimilation of the granite. Powell *et al.* (1982) report 20-30° ESE dips on plagioclase lamination within the olivine gabbro in the southern portion of the Hale Spring area. However, no additional layering is observed elsewhere in the exposed gabbro, so it is doubtful that laminations continue for any great distance. Furthermore, the observed lamination occurs within the thin ledge of our model, and since lamination is the likely result of crystal settling, probably reflects the irregular floor of the ledge (see fig. 8). In addition to the evolution of the gabbro pluton noted in Diez de Medina (1998), the olivine gabbro grades into quartz gabbro adjacent to the contact with the Mount Scott Granite in Hollis Canyon. Differentiation away from the ledge, as mentioned above, should be expected, so that the gabbro becomes increasingly evolved in the uppermost portions of the main body (*i.e.* the roof). Additionally, although the degree of chemical contamination of the gabbro by the granite remain unconstrained at this time, it is likely that the gabbro will becomes more pronouncedly evolved adjacent to the contact because of interaction with partially melted Mount Scott Granite (hybrid rock).

5. Summary

Combined surface and subsurface methods have been used to image the spatial relationships of the Sandy Creek Gabbro and the Mount Scott Granite. The upper portion of the Sandy Creek Gabbro pluton can be modeled as an oval cylinder with steep-walls and a relatively flat roof. The southern contact, as modeled from magnetic surveying, is best interpreted with the Sandy Creek Body intruding the Mount Scott Granite. Other contacts of the pluton are inferred to truncate in the subsurface a preexisting contact between Mount Scott Granite and Glen Mountains Layered Complex, implying a younger age for the Sandy Creek Gabbro than either of these two units. The presence of xenoliths, or possibly roof pendants, of Glen Mountains Layered Complex and Meers Quartzite within the Sandy Creek Gabbro, and the geometry of the surrounding contacts with Mount Scott Granite, suggest the roof of this pluton is spatially associated with an older regional unconformity that developed on the layered complex. This unconformity and associated sediments (*i.e.*, Meers Quartzite) were subsequently buried by the Carlton Rhyolite Formation prior to intrusion of the Mount Scott Granite along this surface. Limited subhorizontal protrusion of gabbro out from the main body of the pluton along this older contact suggests that locally accommodation of the gabbroic magma was achieved by passive lifting of the overburden.

Alteration of the Mount Scott Granite core, presumably by meteoric fluids, is fractured controlled. Macro-fracture density is variable but, overall decreases with depth, from an intensely fractured surface to unfractured rock at 30 m depth. Interaction with these fluids has changed the rock color and oxidized primary titanomagnetite to hematite and hydrated hematite to iron hydroxide. This change in magnetic mineralogy of the granite resulted in a drastic reduction of the magnetic susceptibility of Mount Scott Granite. This was incorporated into construction of subsurface models from magnetic field data. Changes in color, magnetic susceptibility, and oxide mineralogy are directly correlated to changes in fracture density. Domains of intense fracturing correspondingly exhibit more intense alteration. Thus, brittle fractures provided conduits for fluid-flow and subsequent alteration of the crystalline basement. The extent of alteration reflects the fluid/rock ratio which in part is a function of fracture density and connectivity. The exact timing of the fracturing and the composition of fluid(s) is unconstrained, but fluids likely include groundwater in equilibrium with atmospheric conditions. Circulation of these fluids has been restricted to depths less than 30 m below the present erosional surface. Thus, opening of these fractures is likely to be directly related to unroofing of this basement and the timing of alteration may be a relatively recent phenomenon. However, because the Wichita Mountains were previously exposed to atmospheric conditions in the Permian, the possibility for multiple alteration events is not excluded.

6. Acknowledgments

The authors thank Charles J. Mankin, Director of the Oklahoma Geological Survey, for providing the drilling rig and crew, R. Douglas Elmore, for use of the Paleomagnetism Laboratory, W. Glenn Bixler, for information and guidance on the SI-2 magnetic susceptibility and anisotropy meter, and Judson Ahern, for use of and instruction on the proton procession magnetometer, for use of his IGRF program for main-field data subtraction, as well as advice and guidance on 2-D modeling, and for his comments on this paper. The authors also thank B. N. Powell and R. E. Dennison, whose thoughtful reviews contributed much to this paper, and M. D. Barton for corrections. The authors thank Sam Waldstein and his staff at the Wichita Mountains Wildlife Refuge for land access and sampling permission. And Jim Snell is especially thanked for property access and for permission to drill on his land. This study was partially funded by NSF grant #EAR-9316144 to J. P. Hogan and M. C. Gilbert, by U.S.G.S. National Cooperative Mapping Program Grant #1434-HQ-96-AG-01547 to J. D. Price and M. C. Gilbert, and by Eberly Family Chair funds made available to M. C. Gilbert.

7. References Cited

Bradley, L., and Jones-Cecil, M., 1991, Density and magnetic susceptibility measurements of the rocks in the Wichita uplift and Slick Hills, southwestern Oklahoma: United States Geological Survey Open-File Report 91-269, 31 p.

Chase, G.W., 1954, Permian conglomerate around Wichita Mountains, Oklahoma: Bulletin of the American Association of Petroleum Geologists, v. 38, p. 2028-2035.

Diez de Medina, D.M., 1988, Geochemistry of the Sandy Creek Gabbro, Wichita Mountains, Oklahoma: Unpublished M.S. Thesis, University of Oklahoma, Norman, 163 p.

Donovan, R. N., 1982, Geology of Blue Creek Canyon Wichita Mountains Area: *in* Gilbert, M. C.; and Donovan, R. N. (eds.), Geology of the Eastern Wichita Mountains Southwestern Oklahoma: Oklahoma Geological Survey, Guidebook 21, p. 65-77.

Gilbert, M. C., 1982, Geologic setting of the Eastern Wichita Mountains, with a brief discussion of unresolved problems, *in* Gilbert, M. C.; and Donovan, R. N. (eds.), Geology of the Eastern Wichita Mountains Southwestern Oklahoma: Oklahoma Geological Survey, Guidebook 21, p. 1- 28.

Goddard, E.N., Trask, P.D., De Ford, R.K., Rove, O.N., Singewald, J.T., and Overbeck, R.M., 1948, Rock Color Chart: Geological Society of America, Boulder, Colorado, 16 p..

Ham, W. E.; Denison, R. E.; and Merritt, C. A., 1964, Basement rocks and structural evolution of Southern Oklahoma: Oklahoma Geological Survey, Bulletin 95, 302 p.

Ham, W.E., and Wilson., J.L., 1967, Paleozoic epeirogeny and orogeny in the Central United States: American Journal of Science, 265, 332-407.

Hogan, J.P., and Gilbert, M.C., 1995, The A-type Mount Scott Granite Sheet: Importance of Crustal Magma Traps: Journal of Geophysical Research, 100, B8,

Hogan, J.P., and Gilbert, M.C., 1997, The intrusive style of A-type sheet granites from the Southern Oklahoma Aulacogen: *in* Middle Proterozoic to Cambrian Rifting: Mid-North America, R.W. Ojakangas, A.B. Dickas, and J.C. Green (eds.), Geological Society of America Special Paper, 312, p. 299-311.

Hogna, J.P., and Gilbert, M.C., this volume, The Southern Oklahoma Aulacogen: A Cambrian analog for Mid-Proterozoic AMCG (Anorthosite-Mangerite-Charnockite-Granite) complexes?: Basement Tectonics, 12.

Hogan, J.P., Gilbert, M.C., Price, J.D., Wright, J.E., and Deggeller, M., and Hames, W.E., 1996, Magmatic evolution of the Southern Oklahoma Aulacogen: Geological Society of America, Abstracts with Programs, 28, p. 19.

Holtzhausen, G. R., 1989, Origin of sheet structure, 1. Morphology and boundary conditions, *in*: A.M. Johnson, C.W. Burham, C.R. Allen, And W. Muehlberger (eds.), Richard H. Jahns Memorial Volume: Engineering Geology, 27, 225-278.

Johnson, E. L., 1955, Geology of the pegmatite in the Hale Spring Area, Wichita Mountains, Oklahoma: Unpublished M.S. Thesis, University of Oklahoma, Norman, 87 p.

Jones-Cecil, Meridee, 1995, Total-field Aeromag and Derivative Maps of the Lawton Area, Southwestern Oklahoma: United States Geological Survey, Map GP-998-A, 2 plates, 1:100000.

Kelly, K. L.; and Judd, D. B., 1976, Color, universal language and dictionary of names: National Bureau of Standards, Special Publication 440, 158 p.

Merritt, C.A., 1965, Mt. Scott Granite, Wichita Mountains, Oklahoma: Oklahoma Geology Notes, 25, 263-272.

McLean, T. R.; and Stearns, D. W., 1986, Stop 7: Hale Spring Locality, *in* Gilbert, M.C., (ed.), Petrology of the Cambrian Wichita Mountains Igneous Suite: Oklahoma Geological Survey, Guidebook 23, p. 172-178.

Powell, B.N., 1986, The Raggedy Mountain Gabbro Group: *in* Gilbert, M.C., (ed.), Petrology of the Cambrian Wichita Mountains Igneous Suite: Oklahoma Geological Survey, Guidebook 23, p. 21-52.

Powell, B.N. and Gilbert, M.C., 1982, Stop 1 - Reid's Pit:, *in* Gilbert, M. C.; and Donovan, R. N. (eds.), Geology of the Eastern Wichita Mountains Southwestern Oklahoma: Oklahoma Geological Survey, Guidebook 21, 79-96.

Powell, B. N.; Gilbert, M. C.; and Fischer, J. F., 1980, Lithostratigraphic classification of basement rocks of the Wichita province, Oklahoma: Summary: Geological Society of America Bulletin, Part I, vol. 91, p. 509-514, Part II, v. 91, p. 1875-1994.

Powell, B. N.; Stockton, M. L.; Giddens, J. D., III.; and Gilbert, M. C., 1982, Stop 3 - Hale Spring Locality, *in* Gilbert, M. C.; and Donovan, R. N. (eds.), Geology of the Eastern Wichita Mountains Southwestern Oklahoma: Oklahoma Geological Survey, Guidebook 21, p. 102-117.

Price, J. D.; Hogan, J. P.; Payne, James; and Gilbert, M. C., 1985, Investigation of the Mount Scott Granite Drill Core, Wichita Mountains, Oklahoma, Abstracts from the 12th International Conference on Basement Tectonics '95: International Basement Tectonics Association, Norman, Oklahoma, p. 65.

Price, J. D.; Hogan, J. P.; and Gilbert, M. C., 1996, Rapakivi-texture feldspar within the Mount Scott Granite, Wichita Mountains, Oklahoma: European Journal of Mineralogy, v. 8, p. 435-451.

Scofield, N., and Gilbert, M.C., 1982, Alkali amphiboles of the Wichita Mountains, *in* Gilbert, M. C.; and Donovan, R. N. (eds.), Geology of the Eastern Wichita Mountains Southwestern Oklahoma: Oklahoma Geological Survey, Guidebook 21, p. 60-64.

Smith, J. V., 1974, Feldspar Minerals II: Springer-Verlag, Heidelberg, 627 p.

Stockton, M. L.,1984, Geology of the gabbroic rocks in southern Cooperton Quadrangle and northern Odetta Quadrangle, Oklahoma: University of Texas, Arlington, unpublished M.S. thesis, 83 p.

Stockton, M. L.; and Giddens, J. D., III., 1982, Igneous Geology of Cooperton Quadraqngle, Wichita Mountains, *in* Gilbert, M. C.; and Donovan, R. N. (eds.), Geology of the Eastern Wichita Mountains Southwestern Oklahoma: Oklahoma Geological Survey, Guidebook 21, p. 47-50.

Tarling, D. H.; and Hrouda, F., 1993, The magnetic anisotropy of rocks: Chapman and Hall, New York, 217 p.

Turcotte, D. L.; and Schubert, Gerald, 1982, Geodynamics, Applications of continuum physics to geological problems: John Wiley & Sons, New York, 450 p.

APPENDIX 1. Magnetic susceptibility and fracture density data for the SQ-1 drill hole core.

Depth	Magnetic Susceptibility	Standard Deviation	Fracture Density	
			Complete	Incomp.
(m)	(SI mass)	(SI mass)	(Cm^{-1})	(Cm^{-1})
0.00				
0.15				
0.31				
0.46				
0.61				
0.76				
0.92	1.19E-04	5.16E-06	0.07	0.00
1.07	1.08E-04	1.21E-05	0.07	0.07
1.22	1.16E-04	1.39E-05	0.07	0.00
1.37	1.15E-04	1.23E-05	0.66	0.98
1.53	1.03E-04	8.16E-06	0.66	1.05
1.68	8.52E-05	8.56E-06	0.66	0.79
1.83	8.00E-05	4.47E-06	0.20	0.66
2.14	5.51E-05	1.29E-05	0.59	0.79
2.29	7.36E-05	9.91E-06	0.26	0.66
2.44	8.52E-05	9.31E-06	0.13	0.98
2.59	8.95E-05	6.44E-06	0.13	0.72
2.75	2.68E-04	1.22E-04	0.13	0.98
2.90	2.81E-04	1.10E-04	0.13	0.79
3.05	1.45E-04	4.19E-05	0.07	0.00
3.20	1.05E-04	5.63E-06	0.20	0.07
3.36	1.77E-04	4.06E-05	0.07	0.39
3.51	1.61E-04	2.23E-05	0.07	0.46
3.66	1.20E-04	1.77E-05	0.07	0.33
3.81	8.00E-05	1.48E-05	0.26	0.98
3.97	6.32E-05	7.64E-06	0.07	0.52
4.12	1.24E-04	6.32E-06	0.13	0.33
4.42	8.52E-05	1.29E-05	0.13	0.13
4.58	1.05E-04	3.15E-05	0.20	0.52
4.73	3.75E-04	1.51E-04	0.07	0.07
5.19	1.28E-04	9.22E-06	0.00	0.07
0.00	1.30E-04	1.18E-05	0.07	0.79
5.34	1.39E-04	8.16E-06	0.13	0.39
5.49	1.38E-04	6.71E-06	0.20	0.26
5.64	1.72E-04	1.48E-05	0.07	0.07
5.80	2.09E-04	5.08E-05	0.13	0.00
5.95	1.50E-04	1.46E-05	0.13	0.00
6.10	1.85E-04	8.78E-06	0.00	0.00
6.25	1.62E-04	2.32E-05	0.00	0.00
6.41	1.03E-04	1.21E-05	0.07	0.07
6.56	1.61E-04	4.45E-05	0.00	0.13
6.71	1.66E-04	1.88E-05	0.20	0.39
6.86	1.70E-04	2.22E-05	0.07	0.13
7.02	3.59E-04	8.10E-05	0.07	0.13
7.17	2.18E-04	1.38E-05	0.00	0.20
7.32	3.42E-04	6.51E-05	0.00	0.00
7.47	3.32E-04	1.18E-05	0.07	0.00
7.63	3.08E-04	4.74E-05	0.00	0.00

APPENDIX 1. Continued

Depth	Magnetic Susceptibility	Standard Deviation	Fracture Density	
			Complete	Incomp.
(m)	(SI mass)	(SI mass)	(Cm^{-1})	(Cm^{-1})
7.78	2.67E-04	5.86E-05	0.00	0.20
7.93	1.72E-04	1.57E-05	0.00	0.20
8.08	2.14E-04	1.60E-04	0.07	0.07
8.24	2.39E-04	1.70E-05	0.33	0.52
8.39	4.81E-04	5.93E-05	0.07	0.26
8.54	3.28E-04	3.28E-05	0.07	0.00
8.69	4.13E-04	6.90E-05	0.13	0.00
8.85	4.17E-04	1.34E-05	0.00	0.00
9.00	3.64E-04	1.65E-05	0.33	0.00
9.15	3.56E-04	3.94E-05	0.07	0.07
9.30	2.97E-04	1.16E-04	0.07	0.00
9.46	6.14E-04	3.25E-05	0.07	0.00
9.61	7.40E-04	6.55E-05	0.07	0.00
9.76	3.16E-04	4.75E-05	0.07	0.00
9.91	4.08E-04	2.63E-05	0.07	0.00
10.07	4.80E-04	4.49E-05	0.07	0.00
10.22	8.46E-04	1.28E-04	0.07	0.00
10.37	6.33E-04	3.77E-05	0.20	0.00
10.52	8.46E-04	2.80E-05	0.00	0.00
10.68	8.77E-04	6.20E-05	0.07	0.00
10.83	1.01E-03	1.30E-04	0.07	0.00
10.98	8.35E-04	4.86E-05	0.07	0.00
11.13	7.52E-04	7.12E-05	0.00	0.00
11.29	8.16E-04	4.58E-05	0.07	0.00
11.44	7.07E-04	8.11E-05	0.00	0.00
11.59	7.63E-04	8.16E-05	0.00	0.00
11.74	8.57E-04	1.26E-04	0.00	0.00
11.90	8.35E-04	7.13E-05	0.00	0.00
12.05	7.63E-04	3.71E-05	0.26	0.00
12.20	5.82E-04	5.82E-05	0.00	0.00
12.35	6.50E-04	5.32E-05	0.00	0.00
12.51	8.04E-04	3.76E-05	0.00	0.00
12.66	9.29E-04	3.80E-05	0.00	0.00
12.81	1.05E-03	1.32E-05	0.00	0.00
12.96	1.06E-03	9.52E-05	0.00	0.00
13.12	9.58E-04	1.06E-04	0.00	0.00
13.27	8.25E-04	8.63E-05	0.00	0.00
13.42	7.23E-04	7.72E-05	0.00	0.00
13.57	6.11E-04	3.19E-05	0.00	0.00
13.73	6.47E-04	1.20E-04	0.13	0.26
14.03	4.27E-04	8.16E-05	0.33	0.20
14.18	4.35E-04	8.77E-05	0.00	0.26
14.34	3.20E-04	4.77E-05	0.39	0.26
14.49	3.43E-04	6.25E-05	0.00	0.52
14.64	4.60E-04	2.54E-05	0.33	0.26
14.79	4.18E-04	2.14E-04	0.13	0.52
15.10	4.00E-04	4.63E-05	0.07	0.33
15.25	5.14E-04	8.93E-05	0.13	0.26
15.40	2.04E-04	1.13E-05	0.13	0.46

APPENDIX 1. Continued

Depth	Magnetic Susceptibility	Standard Deviation	Fracture Density	
			Complete	Incomp.
(m)	(SI mass)	(SI mass)	(Cm^{-1})	(Cm^{-1})
15.56	6.04E-04	1.22E-04	0.00	0.07
15.71	6.58E-04	1.06E-05	0.07	0.20
15.86	8.31E-04	3.35E-05	0.07	0.13
16.01	7.90E-04	7.53E-05	0.00	0.00
16.17	7.46E-04	3.35E-05	0.00	0.07
16.32	6.45E-04	3.52E-05	0.00	0.20
16.47	8.68E-04	9.22E-05	0.00	0.00
16.62	6.76E-04	2.99E-05	0.00	0.00
16.78	7.35E-04	4.45E-05	0.07	0.00
16.93	6.74E-04	5.57E-05	0.00	0.00
17.08	9.65E-04	2.77E-05	0.00	0.00
17.23	1.39E-03	5.57E-05	0.00	0.00
17.39	1.46E-03	7.60E-05	0.00	0.00
17.54	1.25E-03	4.02E-05	0.00	0.00
17.69	1.07E-03	4.82E-05	0.00	0.00
17.84	1.06E-03	4.12E-05	0.00	0.00
18.00	9.18E-04	3.33E-05	0.00	0.00
18.15	8.40E-04	2.56E-05	0.00	0.13
18.30	8.12E-04	7.40E-05	0.07	0.07
18.45	7.87E-04	5.85E-05	0.00	0.00
18.61	4.37E-04	7.32E-05	0.26	0.13
18.91	2.59E-04	9.63E-05	0.20	0.26
19.06	3.21E-04	4.28E-06	0.00	0.98
19.22	3.25E-04	3.08E-05	0.00	0.00
19.37	3.08E-04	1.61E-05	0.20	0.20
19.52	2.92E-04	4.47E-06	0.20	0.39
19.67	2.68E-04	1.59E-05	0.07	0.20
19.83	3.03E-04	1.84E-05	0.07	0.33
19.98	8.11E-04	2.38E-05	0.00	0.26
20.13	1.07E-03	3.10E-05	0.00	0.13
20.31	1.15E-03	5.42E-05	0.00	0.00
20.44	1.14E-03	5.98E-05	0.00	0.00
20.59	1.42E-03	1.37E-04	0.00	0.00
20.74	1.37E-03	7.76E-05	0.00	0.00
20.89	8.33E-04	2.46E-05	0.26	0.13
21.05	1.08E-03	1.34E-04	0.13	0.20
21.20	7.48E-04	7.20E-05	0.07	0.13
21.35	9.12E-04	2.19E-05	0.13	0.07
21.50	2.31E-03	7.67E-05	0.00	0.00
21.66	2.39E-03	5.27E-05	0.00	0.00
21.81	2.35E-03	8.81E-05	0.00	0.00
21.96	2.24E-03	1.49E-04	0.20	0.33
22.11	2.39E-03	3.19E-05	0.07	0.20
22.27	2.26E-03	9.75E-05	0.07	0.26
22.42	1.91E-03	7.36E-05	0.00	0.07
22.57	2.72E-03	9.46E-05	0.00	0.00
22.72	3.12E-03	1.77E-04	0.00	0.13
22.88	2.02E-03	1.10E-04	0.07	0.33
23.03	2.29E-03	1.61E-04	0.07	0.33

APPENDIX 1. Continued

Depth	Magnetic Susceptibility	Standard Deviation	Fracture Density	
			Complete	Incomp.
(m)	(SI mass)	(SI mass)	(Cm^{-1})	(Cm^{-1})
23.18	3.33E-03	1.20E-04	0.07	0.33
23.33	3.18E-03	1.19E-04	0.00	0.00
23.49	3.83E-03	3.25E-04	0.00	0.00
23.64	4.56E-03	5.08E-04	0.00	0.00
23.79	4.78E-03	5.56E-04	0.13	0.39
23.94	4.63E-03	5.76E-04	0.00	0.26
24.10	4.99E-03	2.16E-04	0.00	0.00
24.25	5.15E-03	1.07E-04	0.00	0.00
24.40	5.20E-03	1.91E-04	0.00	0.00
24.55	5.52E-03	2.54E-04	0.00	0.00
24.71	5.68E-03	2.94E-04	0.00	0.00
24.86	5.32E-03	1.15E-04	0.00	0.00
25.01	6.05E-03	1.84E-04	0.00	0.00
25.16	5.89E-03	7.64E-05	0.00	0.00
25.32	5.74E-03	7.64E-05	0.00	0.00
25.47	6.26E-03	2.14E-04	0.00	0.00
25.62	6.51E-03	1.93E-04	0.13	0.13
25.77	3.42E-03	7.77E-04	0.00	0.07
25.93	7.43E-03	1.48E-04	0.00	0.00
26.08	5.50E-03	3.91E-04	0.13	0.00
26.23	7.00E-03	2.57E-04	0.00	0.00
26.38	6.92E-03	2.49E-04	0.00	0.00
26.54	7.67E-03	4.42E-04	0.13	0.20
26.69	6.93E-03	1.73E-04	0.00	0.00
26.84	7.06E-03	3.68E-04	0.07	0.00
26.99	7.07E-03	2.44E-04	0.00	0.00
27.15	7.69E-03	2.35E-04	0.00	0.00
27.30	7.16E-03	2.20E-04	0.00	0.00
27.45	7.45E-03		0.00	0.00
27.60	7.41E-03	1.34E-04	0.00	0.00
27.76	6.84E-03	5.23E-04	0.00	0.00
27.91	7.17E-03	3.07E-04	0.00	0.00
28.21	7.47E-03	5.20E-04	0.00	0.00
28.37	7.76E-03	2.49E-04	0.00	0.00
28.52	8.16E-03	1.64E-04	0.00	0.00
28.67	8.02E-03	8.04E-05	0.00	0.00
28.82	7.38E-03	2.64E-04	0.00	0.00
28.98	7.51E-03	4.07E-04	0.00	0.00
29.13	8.19E-03	3.43E-04	0.00	0.00
29.28	7.81E-03	2.46E-04	0.00	0.00
29.43	7.99E-03	2.23E-04	0.00	0.00
29.59	7.94E-03	2.49E-04	0.00	0.00
29.74	7.71E-03	2.20E-04	0.00	0.00
29.89	7.69E-03	1.52E-04	0.00	0.00
30.04	8.11E-03	1.38E-04	0.00	0.00
30.20	7.85E-03	1.10E-04	0.00	0.00
30.35	7.75E-03	2.42E-04	0.00	0.00
30.50	8.00E-03	0.00E+00	0.00	0.00

APPENDIX 1. Continued

Depth	Magnetic Susceptibility	Standard Deviation	Fracture Density	
			Complete	Incomp.
(m)	(SI mass)	(SI mass)	(Cm^{-1})	(Cm^{-1})
30.65	7.94E-03	2.49E-04	0.00	0.00
30.96	8.26E-03	4.29E-04	0.00	0.00
31.11	7.72E-03	1.65E-04	0.00	0.00
31.26	8.31E-03	1.69E-04	0.00	0.00
31.42	7.50E-03	1.10E-04	0.07	0.00
31.57	7.76E-03	2.20E-04	0.00	0.00
31.72	7.70E-03	3.97E-04	0.00	0.00
32.03	7.91E-03	1.69E-04	0.00	0.00
32.33	8.26E-03	1.18E-04	0.00	0.00
32.48	8.46E-03	2.26E-04	0.00	0.00
32.64	7.91E-03	8.14E-04	0.00	0.00
32.79	8.01E-03	1.18E-04	0.00	0.00
32.94	7.65E-03	1.59E-04	0.00	0.00
33.09	7.79E-03	2.72E-04	0.00	0.00
33.25	7.50E-03	2.71E-04	0.00	0.00
33.40	7.58E-03	3.06E-04	0.00	0.00
33.55	8.20E-03	2.26E-04	0.00	0.00
33.70	8.10E-03	3.60E-04	0.00	0.00
33.86	8.13E-03	3.70E-04	0.00	0.00
34.01	7.53E-03	2.77E-04	0.00	0.00
34.16	7.66E-03	2.62E-04	0.00	0.00
34.31	8.27E-03	4.46E-04	0.00	0.00
34.47	7.64E-03	2.20E-04	0.00	0.00
34.62	7.70E-03	3.67E-04	0.00	0.00
34.77	7.91E-03	4.10E-04	0.00	0.00
34.92	7.91E-03	2.05E-04	0.00	0.00
35.53	7.50E-03	6.52E-04	0.00	0.00
35.69	8.27E-03	3.34E-04	0.00	0.00
35.84	8.31E-03	1.94E-04	0.00	0.00
35.99	8.06E-03	2.61E-04	0.00	0.00
36.14	7.61E-03	2.62E-04	0.00	0.00
36.30	7.69E-03	2.54E-04	0.00	0.00
36.45	8.36E-03	1.73E-04	0.00	0.00
36.60	7.79E-03	3.06E-04	0.00	0.00
36.75	8.04E-03	3.49E-04	0.00	0.00
37.06	8.78E-03	2.14E-04	0.00	0.00
37.21	9.24E-03	4.59E-04	0.00	0.00
37.36	8.82E-03	2.59E-04	0.00	0.00
37.52	8.43E-03	2.84E-04	0.00	0.00
37.59	7.64E-03	8.23E-04	0.00	0.00
37.67	7.79E-03	3.77E-04	0.00	0.00
37.74	6.96E-03	9.85E-04	0.00	0.00
37.82	7.45E-03	6.92E-04	0.00	0.00
37.90	7.76E-03	1.10E-03	0.00	0.00
37.97	8.15E-03	1.01E-03	0.00	0.00
38.13	8.18E-03	4.77E-04	0.00	0.00
38.28	8.09E-03	3.00E-04	0.00	0.00

APPENDIX 1. Continued

Depth	Magnetic Susceptibility	Standard Deviation	Fracture Density	
			Complete	Incomp.
(m)	(SI mass)	(SI mass)	(Cm^{-1})	(Cm^{-1})
38.43	8.58E-03	1.48E-04	0.00	0.00
38.58	8.72E-03	3.11E-04	0.00	0.00
38.74	8.31E-03	3.29E-04	0.00	0.00
38.89	9.09E-03	2.57E-04	0.00	0.00
39.04	7.77E-03	3.97E-04	0.00	0.00
39.19	8.26E-03	4.75E-04	0.00	0.00
39.35	8.15E-03	1.83E-04	0.00	0.00
39.50	8.40E-03	8.16E-05	0.00	0.00
39.65	7.73E-03	3.73E-04	0.00	0.00
39.80	7.56E-03	4.22E-04	0.00	0.00
39.96	7.67E-03	4.23E-04	0.00	0.00
40.11	7.62E-03	6.60E-04	0.00	0.00
40.26	7.43E-03	4.02E-04	0.00	0.00
40.41	7.37E-03	6.54E-04	0.00	0.00
40.57	7.53E-03	5.32E-04	0.00	0.00
40.72	7.37E-03	2.44E-04	0.00	0.00
40.87	7.62E-03	3.51E-04	0.00	0.00
41.02	7.71E-03	2.86E-04	0.00	0.00
41.18	7.02E-03	1.09E-03	0.00	0.00
41.33	6.71E-03	1.20E-03	0.07	0.00
41.48	7.12E-03	9.47E-04	0.13	0.13
41.63	7.11E-03	1.45E-03	0.00	0.00
41.79	7.50E-03	6.20E-04	0.00	0.00
41.94	7.17E-03	1.67E-03	0.00	0.00
42.09	6.51E-03	1.35E-03	0.00	0.00
42.24	6.95E-03	1.62E-03	0.00	0.00
42.40	6.09E-03	2.05E-03	0.00	0.00
42.55	6.35E-03	1.63E-03	0.00	0.00
42.70	6.60E-03	1.57E-03	0.00	0.00
42.85	7.55E-03	4.64E-04	0.00	0.00
43.01	7.11E-03	1.53E-03	0.00	0.00
43.16	6.00E-03	2.17E-03	0.00	0.00
43.31	6.13E-03	1.90E-03	0.00	0.00
43.46	6.54E-03	9.59E-04	0.00	0.00
43.62	7.15E-03	1.47E-03	0.00	0.00
43.77	7.48E-03	7.91E-04	0.00	0.00
43.92	7.44E-03	8.43E-04	0.00	0.00
44.07	6.46E-03	1.18E-03	0.00	0.00
44.23	6.38E-03	1.40E-03	0.00	0.00
44.38	7.45E-03	7.30E-04	0.00	0.00
44.53	6.41E-03	9.49E-04	0.00	0.00
44.68	7.69E-03	9.18E-04	0.00	0.00
44.84	7.18E-03	3.85E-04	0.00	0.00
44.99	7.07E-03	6.33E-04	0.00	0.00
45.14	7.80E-03	6.01E-04	0.00	0.00
45.29	7.55E-03	3.81E-04	0.00	0.00
45.45	7.60E-03	3.48E-04	0.00	0.00

APPENDIX 1. Continued

Depth	Magnetic Susceptibility	Standard Deviation	Fracture Density	
			Complete	Incomp.
(m)	(SI mass)	(SI mass)	(Cm^{-1})	(Cm^{-1})
45.60	6.97E-03	5.56E-04	0.00	0.00
45.75	7.41E-03	3.99E-04	0.00	0.00
45.90	7.50E-03	7.39E-04	0.00	0.00
46.06	7.37E-03	5.37E-04	0.00	0.00
46.21	6.40E-03	1.30E-03	0.00	0.00
46.36	6.80E-03	9.24E-04	0.00	0.00
46.51	7.67E-03	9.13E-04	0.00	0.00
46.67	6.87E-03	9.46E-04	0.00	0.00
46.82	5.88E-03	1.18E-03	0.00	0.00
46.97	7.53E-03	6.99E-04	0.00	0.00
47.12	3.06E-03	3.75E-04	0.00	0.00
47.28	6.94E-03	5.93E-04	0.00	0.00
47.43	6.07E-03	1.38E-03	0.00	0.00
47.58	7.51E-03	6.33E-04	0.00	0.00
47.73	5.85E-03	1.38E-03	0.00	0.00
47.89	6.82E-03	8.13E-04	0.00	0.00
48.04	7.87E-03	8.36E-04	0.00	0.00
48.19	7.49E-03	9.43E-04	0.00	0.00
48.34	8.14E-03	4.18E-04	0.00	0.00
48.50	6.75E-03	1.09E-03	0.00	0.00
48.65	6.42E-03	1.19E-03	0.00	0.00
48.80	7.49E-03	8.95E-04	0.00	0.00
48.95	7.96E-03	2.04E-04	0.00	0.00
49.11	7.51E-03	7.98E-04	0.00	0.00
49.26	8.05E-03	4.27E-04	0.00	0.00
49.41	5.09E-03	3.68E-04	0.00	0.00
0.00	7.16E-03	6.24E-04	0.00	0.00
49.72	7.81E-03	6.71E-05	0.00	0.00
49.87	8.89E-03	2.14E-04	0.00	0.00
50.02	7.55E-03	5.29E-04	0.07	0.00
50.17	8.10E-03	2.94E-04	0.00	0.00
50.33	6.84E-03	1.59E-04	0.00	0.00
50.48	7.12E-03	6.84E-04	0.07	0.00
50.63	7.85E-03	4.50E-04	0.00	0.00
50.78	7.51E-03	2.93E-04	0.00	0.00
50.94	6.58E-03	1.13E-03	0.00	0.00
51.09	6.58E-03	8.72E-04	0.00	0.00
51.24	8.17E-03	3.29E-04	0.00	0.00
51.39	6.75E-03	7.05E-04	0.00	0.00
51.55	8.00E-03	5.94E-04	0.00	0.00
51.70	7.89E-03	2.08E-04	0.00	0.00
51.85	7.39E-03	2.49E-04	0.00	0.00
52.00	8.25E-03	1.75E-04	0.00	0.00
52.16	7.06E-03	4.62E-04	0.00	0.00
52.31	6.93E-03	5.83E-04	0.00	0.00
52.46	7.17E-03	4.65E-04	0.00	0.00
52.61	7.16E-03	5.36E-04	0.00	0.00

APPENDIX 1. Continued

Depth	Magnetic Susceptibility	Standard Deviation	Fracture Density	
			Complete	Incomp.
(m)	(SI mass)	(SI mass)	(Cm^{-1})	(Cm^{-1})
52.77	6.50E-03	6.00E-04	0.00	0.00
52.92	7.97E-03	2.27E-04	0.00	0.00
53.07	7.33E-03	3.35E-04	0.00	0.00
53.22	8.74E-03	2.20E-04	0.00	0.00
53.38	8.13E-03	2.21E-04	0.00	0.00
53.53	7.69E-03	3.49E-04	0.00	0.00
53.68	8.54E-03	2.97E-04	0.00	0.00
53.83	8.45E-03	2.85E-04	0.00	0.00
53.99	7.21E-03	4.75E-04	0.00	0.00
54.14	7.17E-03	7.58E-04	0.00	0.00
54.29	7.76E-03	4.02E-04	0.00	0.00
54.44	8.57E-03	4.40E-04	0.00	0.00
54.60	7.36E-03	6.05E-04	0.00	0.00
54.75	8.24E-03	3.43E-04	0.00	0.00
54.90	8.15E-03	7.31E-04	0.00	0.00

Appendix 2. Magnetic susceptibility of the Sandy Creek Gabbro.

The SQ-2 hole encountered the Sandy Creek Gabbro at an estimated depth of 9 m. Retrieved core covers a ~continuous 167 cm interval.

Core SQ-2, Sandy Creek Gabbro

Depth (m)	Magnetic Susceptibility (SI mass)	Standard Deviation (SI mass)
9.04	1.50E-02	2.62E-05
9.12	1.19E-02	1.85E-04
9.16	1.11E-02	3.04E-05
9.25	1.70E-02	7.70E-06
9.29	1.78E-02	3.44E-06
9.33	1.77E-02	4.87E-06
9.37	1.82E-02	4.97E-06
9.41	1.66E-02	3.44E-06
9.68	1.78E-02	1.29E-05
10.09	1.29E-02	2.23E-05
10.13	1.20E-02	6.88E-06
10.38	1.52E-02	2.03E-05

MULTIPLE REACTIVATIONS OF RIGID BASEMENT BLOCK MARGINS: EXAMPLES IN THE NORTHERN READING PRONG, USA

A.E. GATES and R.E. COSTA
Department of Geology
Rutgers University
Newark, NJ 07102 USA

Abstract

Fundamental zones of crustal weakness that were established in the northern Reading Prong, central Appalachians during Grenvillian orogenesis were reactivated multiple times during subsequent tectonic events. The rocks in these fault zones contain complexly overprinted mylonites, cataclasites, and breccias with distinct kinematics and mineralizations. By studying the similarities and differences of rocks from three different fault zones across the Reading Prong of eastern Pennsylvania, New Jersey and the southeastern New York, the tectonic succession and a relative chronology can be determined. As many as seven phases of reactivation can be identified within the major Ramapo, Reservoir, and Morgan Hill fault zones. These weak zones between the rigid crystalline basement blocks exhibit these multiple and intense deformational episodes because they absorbed the majority of the strain that was transmitted through the basement rocks during the subsequent intense tectonic events. The cover sequence was also heavily deformed during these events. The crystalline blocks between the major faults, on the other hand, show relatively little post peak-Grenville deformation. The only evidence of these events are minor faulting and several phases of jointing. The rigid crystalline blocks simply adjusted to the renewed stresses by movement along their boundaries. Depending upon stress and metamorphic conditions, the previously formed mylonites and cataclasites were either sheared in ductile or semi-brittle deformation or fragmented into physically separated blocks.

1. Introduction

Multiple reactivation of major faults and fault systems is common in the Appalachians (Ratcliffe, 1971; Swanson, 1986; Bobyarchick and Glover, 1979; Goldstein, 1989; Gates, 1996). Fundamental zones of crustal weakness were established after consolidation of the crystalline basement predominantly during the Precambrian and then reactivated during every successive orogenic event (Goldstein, 1989; Gates, 1996). Where the metamorphic grade never exceeded the brittle-ductile transition as in the Reading Prong and most other Precambrian crystalline massifs, these zones were especially prone to reactivation because there were no stitching plutons or substantial mineral growth that might hinder or prevent movement on the system. Instead during phases of cyclical (Wilson, 1966) and non-cyclical tectonism, these faults were reactivated while the crystalline blocks between them reacted in a passive manner. These zones of weakness are even active today when stress levels are relatively low (Aggerwal and Yang, 1978). In this paper, several major zones of crustal weakness are examined to illustrate multiple reactivation of crystalline fault block margins during tectonism in the Reading Prong of New Jersey, Pennsylvania and New York.

1.1 REGIONAL GEOLOGY

The northern Reading Prong comprises the Hudson Highlands in southeastern New York, the New Jersey Highlands and their extension into eastern Pennsylvania

(Fig. 1). The Reading Prong is composed of Grenville aged crystalline rocks that have largely been metamorphosed to granulite facies (see Drake, 1984 for review). The Reading Prong is bounded to the west by deformed Paleozoic sedimentary rocks of the Valley and Ridge Province and to the east by the Piedmont Province which consists of Mesozoic rift basin rocks and the Appalachian mobile core. The northern Reading Prong is roughly divided into three blocks separated by major faults, the western, central, and eastern highlands (Ratcliffe, 1980; Hull *et al.*, 1986). The Ramapo fault zone is the boundary between the eastern and central highlands and the Reservoir fault marks the boundary between the central and western highlands. Other major faults cross the crystalline highlands including the Morgan Hill fault (Drake, 1967) but none have been proposed to be fundamental boundaries.

Middle Proterozoic rocks of the central and western Hudson and New Jersey Highlands (Fig. 1) consist of predominantly light colored sodic-rich gneisses and lesser amphibolite (Drake, 1984) of sedimentary, volcanic, and plutonic origin (Dallmeyer, 1974). These rocks were metamorphosed to upper amphibolite through hornblende granulite facies (Dallmeyer, 1974; Young and Cuthbertson, 1994). The rocks are roughly divided into the Lossee Metamorphic Suite and the Byram Intrusive Suite (Drake, 1984). The Lossee Metamorphic Suite is a complex of oligoclase-quartz gneiss with varying amounts of hornblende, biotite, and pyroxene. The Byram Intrusive Suite consists of microperthite- or microcline-bearing hornblende granite, alaskite, biotite granite, hornblende-quartz syenite and pegmatite. Other Proterozoic rocks include marble, pyroxene gneiss, epidote-scapolite-quartz gneiss, sillimanite-cordierite gneiss, pyroxenite, and magnetite deposits.

The basement rocks of the eastern Hudson Highlands are predominantly middle Proterozoic biotite-granitic gneiss, amphibolite, biotite-hornblende quartzo-feldspathic gneiss and minor hornblende granite gneiss (Hall *et al.*, 1975). These rocks are intruded by the Canopus and related intermediate to mafic plutons (Ratcliffe, 1971) and by a series of granitic plutons (Helenek and Mose, 1984). The Precambrian rocks are overlain by Cambrian-Ordovician metasedimentary rocks including the Poughquag and Lowerre quartzites, the Inwood marble, the Manhattan schist, and the Walloomsac Formation (Fisher *et al.*, 1970). These rocks and the underlying basement were regionally metamorphosed to greenschist through upper amphibolite facies conditions during the Ordovician Taconian orogeny (Ratcliffe *et al.*, 1982). A 60-km long belt of east-west- to northwest-striking Silurian alkalic dikes and lamprophyres extends from the igneous Cortlandt Complex, New York westward to the Beemerville Complex, New Jersey (Ratcliffe, 1981; Maxey, 1976). An earlier unrelated suite of northeast-southwest-trending mafic dikes intrude the Reading Prong and Hudson Highlands and may be related to Late Proterozoic rifting at approximately 650-600 Ma (Puffer *et al.*, 1991; Ratcliffe, 1983; 1987).

The approximate 10,000 meter thick sequence of Triassic-Jurassic sedimentary and igneous rocks (Olsen, 1980) of the Newark basin (Fig. 1) rest unconformably on Paleozoic and Precambrian basement rocks. These Mesozoic rocks dip 5° - 25° northwest and into the Ramapo fault.

2. Ramapo Fault

The northeast-trending Ramapo fault system (Figs. 1 and 2) in northern New Jersey and southeastern New York juxtaposes Middle Proterozoic crystalline rocks of the Reading Prong with Triassic and Jurassic sedimentary and igneous rocks of the Newark Basin along most of its length. In southeastern New York, north of the Newark Basin, the many splays of the Ramapo fault include the Thiells, Mott Farm Road, Timp Pass and Canopus faults, known collectively as the Canopus fault zone (Ratcliffe, 1980). The Canopus fault zone separates the rocks of the central Hudson Highlands from the eastern Hudson Highlands. To the south, there is a probable connection of the

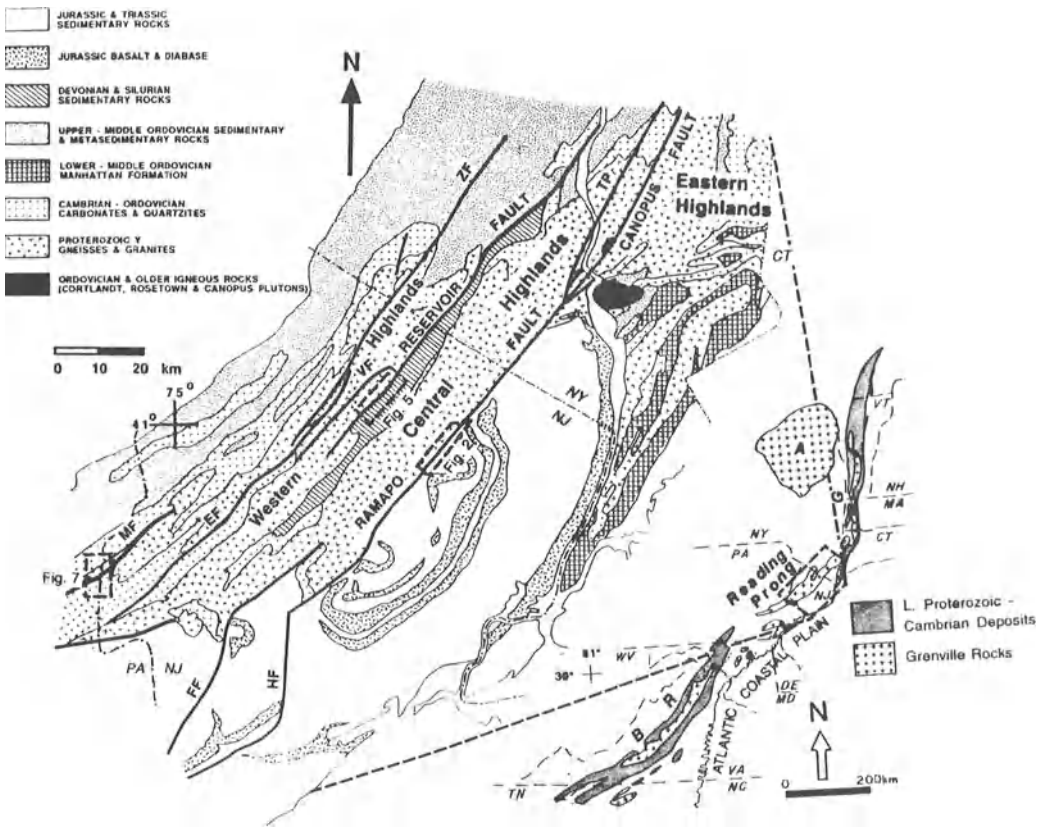

Figure 1. Geologic map of the northern Reading Prong, NY, NJ, and PA with boxed areas showing locations of detailed maps for Figures 2 (Ramapo Fault), 5 (Reservoir Fault), and 7 (Easton area, PA) (after Ratcliffe, 1980). ZF = Zero fault, VF = Vernon fault, EF = East fault, MH = Morgan Hill - Chestnut Hill Faults, TP = Timp Pass Fault, FF = Flemington Fault, HF = Hopewell fault. Inset: location of Reading Prong within the Appalachian orogen. A = Adirondacks, G = Green Mountains, BR = Blue Ridge Province.

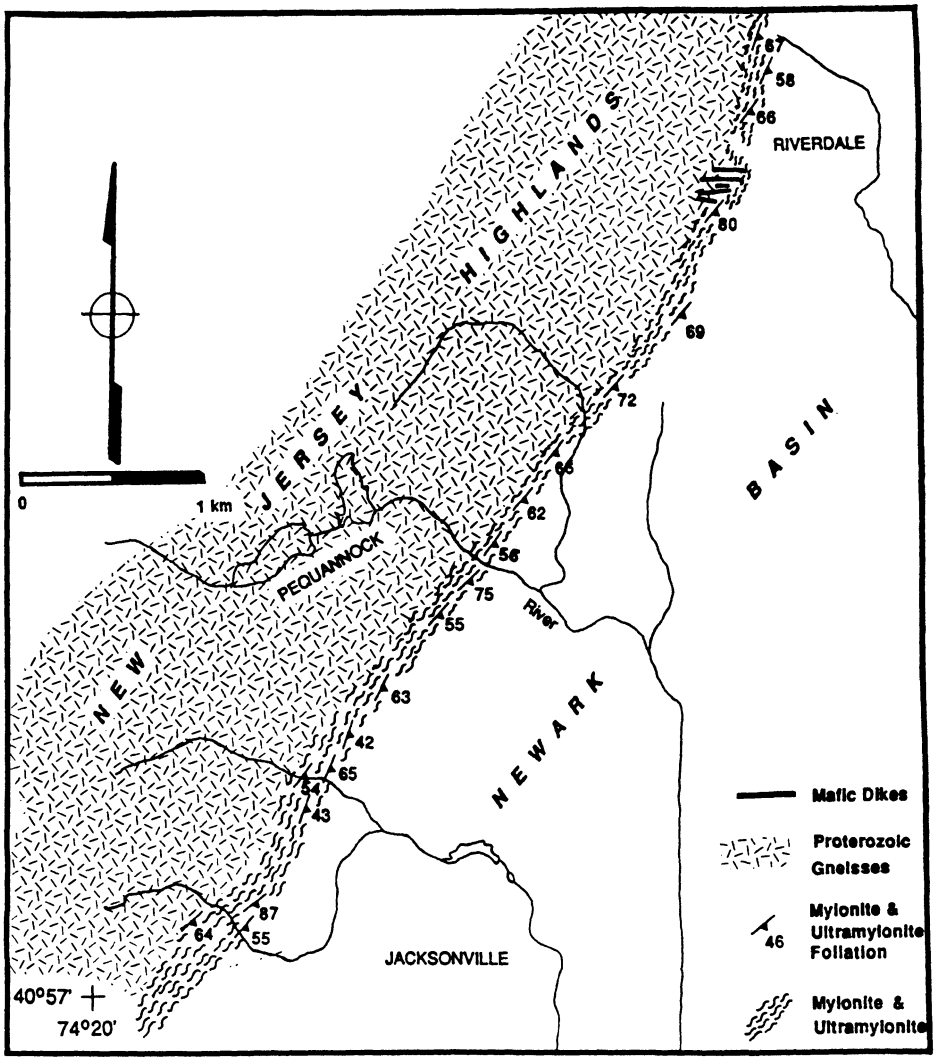

Figure 2. Geologic map of the study area along the Ramapo fault (see Fig. 1 for location).

Hopewell and Flemington-Furlong with the Ramapo fault faults (Ratcliffe, 1980). The Hopewell and Flemington-Furlong faults are moderately southeast-dipping intrabasinal normal faults developed late in the history of the Newark basin (Schlische and Olsen, 1988).

The Ramapo fault system varies in thickness from approximately 5 km to 10 km along strike (Ratcliffe, 1980). It consists of many parallel to subparallel zones of well foliated and poorly to moderately lineated type II S-C mylonite (Lister and Snoke, 1984) and ultramylonite in Grenville gneisses (Fig. 3a). Moderate to steeply southeast-dipping retrograde shear zones, up to 25m thick, developed in granitic and calc-silicate gneisses and exhibit a mesoscopic S-C fabric. C planes typically dip 40° - 50° towards the southeast. The average angle between S and C planes is 20°, but varies from 6° to 40°. C' planes, where present, are spaced from 1.0 mm to 1.0 cm and oriented approximately 20° - 30° shallower than the C plane. Lineations of quartz, amphibole, and chlorite are consistently down dip.

Primary kinematic indicators from the mylonites along the Ramapo fault system in northern New Jersey consistently indicate reverse shearing. Both σ–type and δ–type quartz porphyroclasts (Fig. 3b) (Passchier and Simpson, 1986) are present within the mylonites and confirm the reverse sense of shear. Cores of the porphyroclasts define the southeast-dipping S plane and have tails of dynamically recrystallized quartz. Type B2a and type B2b quartz ribbons (Boullier and Bouchez, 1978) and dynamically recrystallized tails on porphyroclasts (Passchier and Simpson, 1986) define the C plane. The C' plane, where present, is defined by asymmetric boudinage of quartz ribbons.

Potassium feldspar and plagioclase also form σ–type and δ–type porphyroclasts (Fig. 3b) (Passchier and Simpson, 1986) with tails of recrystallized feldspar, quartz, muscovite and chlorite. Cores of these porphyroclasts define the southeast-dipping S plane. The C plane is defined by the porphyroclast tails. Edges of feldspar porphyroclasts are commonly dynamically recrystallized. Plagioclase porphyroclasts have deformed twin lamellae. Feldspar porphyroclasts, less commonly, show pull-apart textures (Stauffer, 1970) that show antithetic shearing along cleavage planes.

Hornblende commonly underwent a brittle response. Pull-apart (Stauffer, 1970) hornblende porphyroclasts underwent reaction-enhanced ductility (White, *et al.*, 1980) in which crude σ–type porphyroclasts evolved from antithetically sheared fragments. In these retrograded grains, metamorphic reactions generated chlorite, tremolite-actinolite, biotite, and muscovite as fillings within conjugate shear planes and as tails on porphyroclasts.

Chlorite and muscovite "fish" (Eisbacher, 1970; Lister and Snoke; 1984) and aligned muscovite, tremolite and biotite define the southeast-dipping S-C fabric. Biotite commonly underwent reaction enhanced ductility (White, *et al.*, 1980). C' planes commonly developed within the chlorite-rich zones.

The ductile behavior exhibited by the feldspar porphyroclasts, indicates that temperatures of this phase of deformation were in excess of 450 ± 50° C (Sibson, 1977; 1983; Tullis and Yund, 1977). This mineral response is consistent with deformation at middle- to upper greenschist facies conditions (Simpson, 1985).

Within these mylonite zones of unequivocal reverse movement, there is evidence for an earlier phase of normal movement at approximately the same metamorphic grade. Several features such as intrafolial rootless isoclines and relict foliations (Fig. 3c), composite porphyroclasts, and V-shaped fractures with two syntaxial overgrowths (Fig. 3d) support this interpretation. The intrafolial folds and relict foliations occur primarily within quartz ribbons but also within the fine-grained mylonitic matrix. Some porphyroclasts and brittle pull apart grains exhibit evidence for two periods and directions of movement. The tails on some of the quartz porphyroclasts are pulled under or over the grain in a direction opposite to that indicated by the porphyroclast. Some of the brittle hornblende grains show pull-apart textures with a

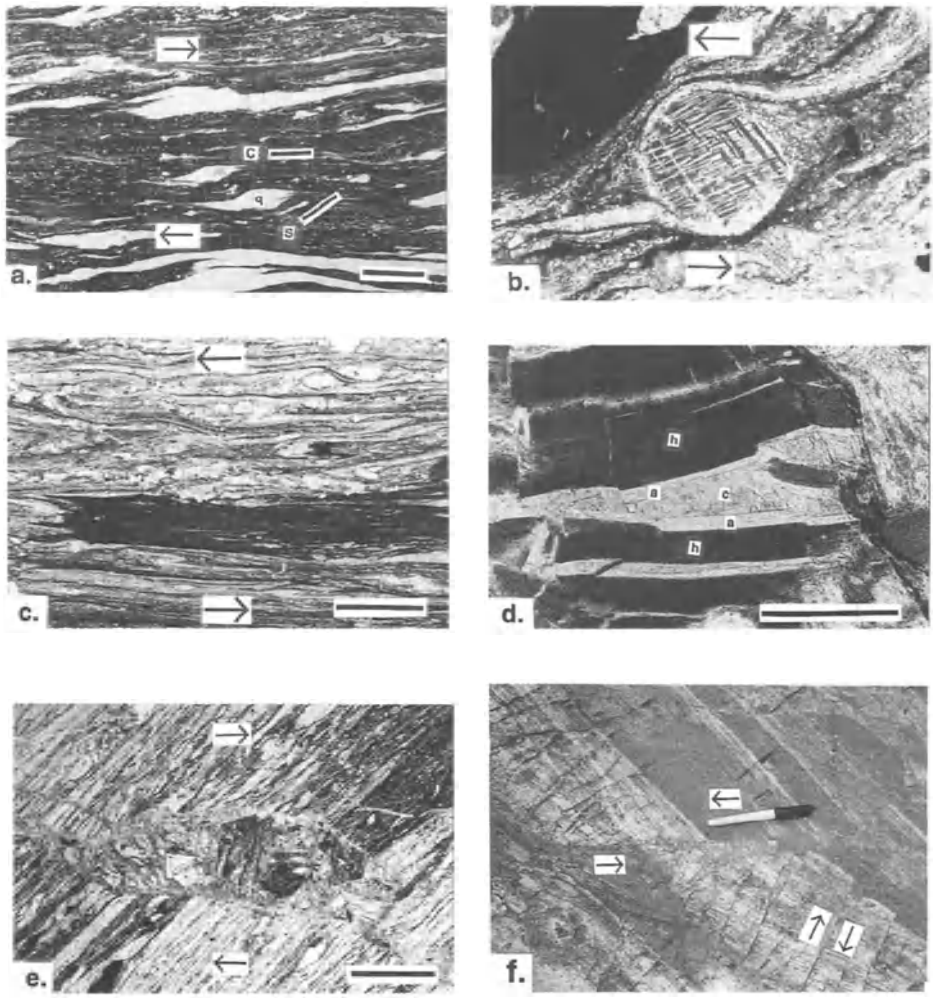

Figure 3. Photographs and photomicrographs of rocks from the Ramapo fault. a) Photomicrograph of S-C mylonite showing mylonitic fabric, quartz ribbons, and rotated quartz porphyroclasts (q). Arrows show shear sense; scale bar = 5mm. b) Photomicrograph of rotated δ-, σ-type porphyroclast (Passchier and Simpson, 1986) of microcline. Arrows show shear sense; scale bar = 2mm. c) Photomicrograph of mylonitic fabric showing intrafolial folds and relict foliations. Arrows show shear sense; scale bar = 5 mm. d) Photomicrograph of V-shaped fracture in a pull-apart texture (Stauffer, 1970) hornblende porphyroclast (h). Composite filling pattern shows early amphibole (a) parallel to the fracture walls and late chlorite-sericite-quartz intergrowth (c) in a V-shaped filling. Scale bar = 2 mm. e) Photomicrograph of seam of microbreccia crossing myloitic foliation. Arrows show shear sense; scale bar = 5 mm. f) Field photograph of Alleghanian conjugate strike-slip brittle faults crossing and offsetting Taconian mylonitic foliation. Arrows show offset direction; pen for scale.

shear sense opposite to that of the mylonitic matrix. Within some of these hornblende grains, the fractures formed during extension and fragmentation of the grain are V-shaped and are syntaxially filled first by amphibole and then by a chlorite-muscovite-quartz intergrowth. The amphibole is parallel to the fracture walls and indicates no rotation whereas the second growth indicates substantial rotation. Hippert (1993) proposed that V-textures could be used as kinematic indicators in single deformations but the textures described here are clearly composite and indicate a complex history.

Cataclastic textures (Sibson, 1977) that overprint the early ductile and brittle-ductile fabrics indicate brittle strike-slip (Figs. 3e and 3f) and normal reactivation of the southeast-dipping faults. Cataclastic seams (0.5 mm to 1.5 cm thick) offset grains and early fabrics and are themselves offset by later faults (Fig 3f). Southeast-dipping foliated greenish-gray to black gouge zones approximately 4.0 cm to 5.0 cm thick are commonly enriched in calcite and sheared antithetically. In addition, there are two generations of type I (Beach, 1975) quartz, calcite and chlorite filled tension gashes and two generations of primary and secondary (Harding, 1974) planar, curvi-planar and listric brittle fault arrays with slickenlines.

Slickenside coated fault surfaces most commonly contain fibrous or stepped slickenlines of fine grained chlorite, tremolite-actinolite, limonite and calcite with lesser amounts of quartz and epidote. Two generations are evident by overprinting relations on single fault surfaces. Each generation of brittle faults includes four sets of moderate to steeply-dipping faults. The early generation of steeply-dipping brittle faults includes east-southeast- and west-northwest-dipping reverse faults, northeast- and southwest-dipping normal faults and a conjugate set of north-northwest- and south-southeast-dipping right-lateral strike-slip and east- and west-dipping left-lateral strike-slip faults (Fig. 4A). The later set of brittle faults includes south-southwest- and north-northwest-dipping reverse faults, southeast- and northwest-dipping normal faults, and a conjugate pair of northeast- and southwest-dipping right-lateral strike-slip and southeast-dipping left-lateral strike-slip faults (Fig. 4B). An additional set of northwest- and southeast-dipping right-lateral strike-slip faults is present. Fault planes also developed P and T criteria kinematic indicators (Petit, 1987) and tension gashes filled with calcite, tremolite-actinolite, chlorite, and quartz.

2.1 TIMING OF DEFORMATION

In addition to its development as a Grenvillian reverse fault (Ratcliffe, 1980), the Ramapo fault system has a long and complex reactivation history which includes up to five periods of fault movement. The dominant reverse ductile deformation which resulted in the development of the southeast dipping type II S-C mylonite (Lister and Snoke, 1984) and ultramylonite zones is post-Grenvillian in age. The mineralogy and texture which are present are indicative of a lower grade deformation than those reached during the Grenville orogeny. Based on the deformation features and metamorphic grade of deformation (Simpson, 1985), the reverse mylonites and ultramylonites within the study area formed at mid- to upper greenschist metamorphic facies. Ratcliffe (1980; 1981) and Ratcliffe *et al.* (1982) assigned a Taconian age reverse ductile movement to the Ramapo fault zone of southeastern New York based on radiometric dates of plutonic and dike rocks of the Rosetown pluton and Cortlandt Complex which are shown to postdate or be partly synchronous with faulting. This event occurred approximately 450 - 460 Ma based on Rb/Sr analysis of biotite and whole rock samples, K-Ar analysis of biotite, hornblende and whole rock samples and $^{40}Ar/^{39}Ar$ analysis of hornblende and biotite from within the fault zone (Ratcliffe *et al.*, 1982).

The mafic dikes can be used to constrain fault movement along the Ramapo fault in New Jersey. Although the dikes that cross the mylonites have not been radiometrically dated they are most likely Late Ordovician in age based on similarities

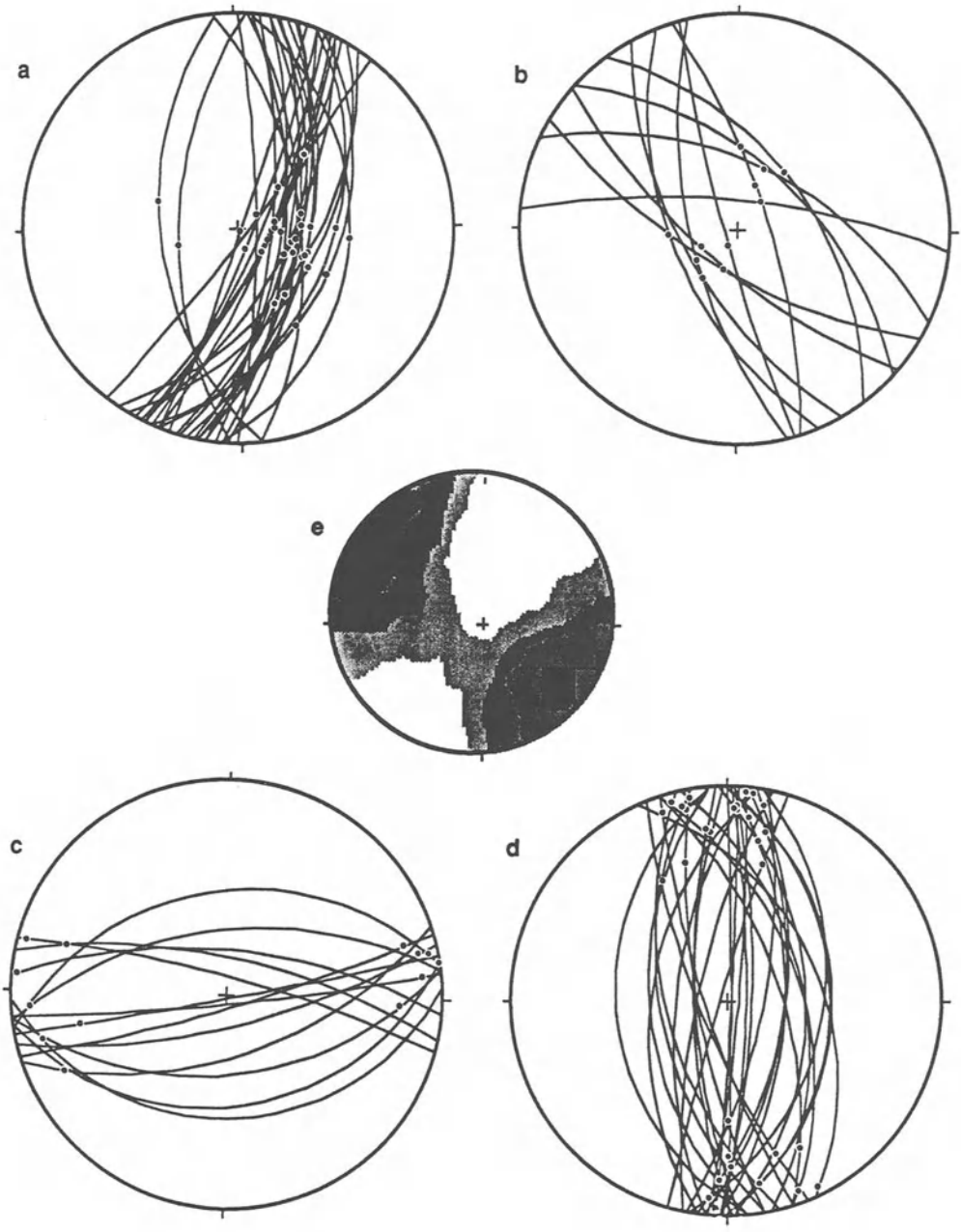

Figure 4. A) Equal area nets of poles to brittle faults for early activity (Costa, 1991): a) Reverse faults and slickenlines, n=30; b) normal faults and slickenlines, n=11; c) dextral faults and slickenlines, n=13; d) Kamb contour of early compressional P-axis, n=27.

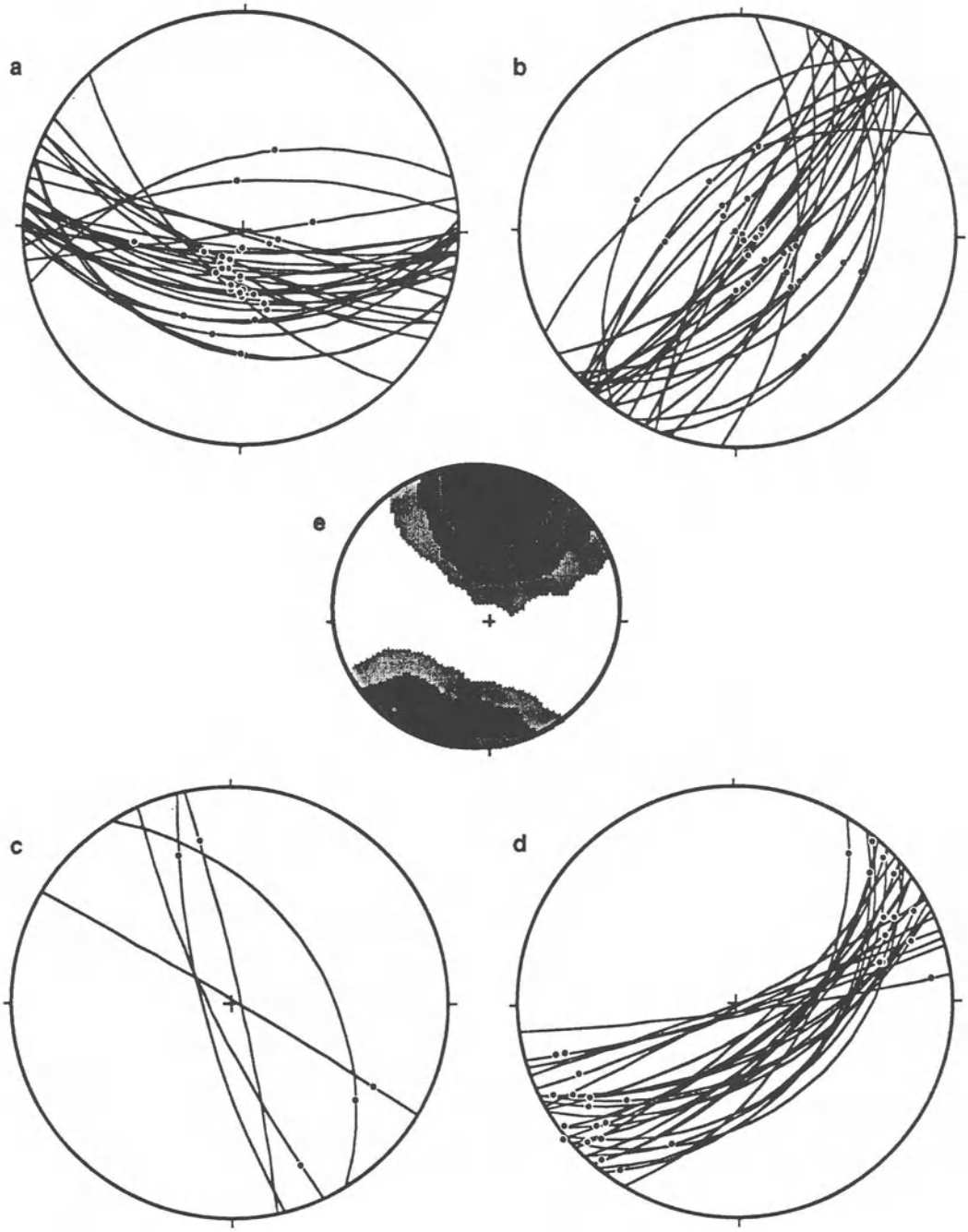

Figure 4 continued. B) Equal area nets of poles to brittle faults for late activity (Costa, 1991): a) Reverse faults and slickenlines, n=30; b) normal faults and slickenlines, n=27; c)) dextral faults and slickenlines, n=5; d) Kamb contour of late compressional P-axis, n=27.

with dated dikes in the area. The chemistry of the altered basaltic dikes (Costa, 1991) does not match the chemistry of Late Proterozoic metagabbros (Ratcliffe, 1983; 1987; Puffer *et al.*, 1991), but instead appear to be part of the Cortlandt-Beemerville dike swarms (Ratcliffe, 1981). The orientation of the basaltic dikes is consistent with the approximate east-west trend of Cortlandt-Beemerville dikes. Because the dikes do not record any reverse shearing, they provide a minimum age for reverse movement.

The dominant ductile reverse mylonite fabric overprints a previously developed normal mylonite fabric. We interpret this activity to be the result of Iapetan rifting. It clearly predates Taconian deformation and postdates Grenville deformation. The presence of late Proterozoic rift related mafic dikes in the area and documented Late Proterozoic normal movement on the Morgan Hill fault support this conclusion.

During post-Ordovician and pre-Mesozoic activity mesoscopic synchronous primary and secondary brittle faults (Harding, 1974) and associated tension gashes (Costa, 1991) developed within the Ramapo fault system. This reactivation shows both reverse and strike-slip motion. Ratcliffe (1971) documents several kilometers of Acadian dextral offset in the area of the Canopus fault. In this study, the strike-slip and reverse motion were found to be of the same generation and interpreted as Alleghanian based on regional relations (Costa and Gates, 1993). This problem of timing has not been resolved.

Overprinting slickenlines on a single fault plane allow the determination of a younger generation of brittle faults superimposed over the interpreted Alleghanian generation. This brittle phase of deformation is corresponds with the southeast dipping normal faults which created the Newark basin. The Mesozoic sediments (Olsen, 1980) within the basin constrain the time of faulting. During Mesozoic rifting primary and secondary brittle faults (Harding, 1974) and associated tension gashes also developed. The generation of overprinting cataclastic textures and fault gouge (Sibson, 1977) indicate faulting was under low temperature (i.e. <250°C) and shallow conditions (i.e. <10 km). An approximate north-northeast-trending maximum compression direction (Fig. 8e) is indicated by the complex fault array and tension gashes. This direction requires that the formation of the Newark basin had a transtensional component.

3. Reservoir Fault

The Reservoir fault is a multiply activated zone of weakness that forms the western boundary of the Silurian-Devonian Green Pond outlier (Figs. 1 and 5). The vertical to steeply northwest- and southeast-dipping shear zone extends from the Hudson Highlands, New York into the central New Jersey Highlands. Cataclasites and mylonites are best developed around Newfoundland, New Jersey within Grenville paragneisses that have been interpreted as being of metasedimentary origin (Lewis and Kummel, 1912; Hague *et al.*, 1956; Drake, 1984; Volkert, 1993). These rocks are dominantly layered amphibole, biotite, and pyroxene quartzo-feldspathic gneisses and minor amphibolite gneiss. The quartzo-feldspathic gneiss is interpreted as being derived from layered volcaniclastic and calcsilicate rocks (Drake, 1984; Gundersen, 1986) and contains scapolite, pyroxene, and garnet assemblages or plagioclase-pyroxene-amphibole-garnet assemblages (Malizzi and Gates, 1989). The gneisses were intruded by uraniferous pegmatite dikes along the Reservoir fault subsequent to or during granulite facies metamorphism (Malizzi and Gates, 1989).

East of the Reservoir Fault, the Green Pond outlier is composed of Late Ordovician - Silurian to early Middle Devonian rocks as well as several isolated occurrences of Cambrian rocks (Darton, 1894; Kummel and Weller, 1902; Herman and Mitchell, 1991). The Ordovician Martinsburg Formation is exposed against the Reservoir fault in one location. The conglomeratic Green Pond Formation of Silurian age rests unconformably on basement rocks in most of the area. The overlying Silurian Longwood Shale and Poxono Island Formation (limestone) are thin and rare. Devonian

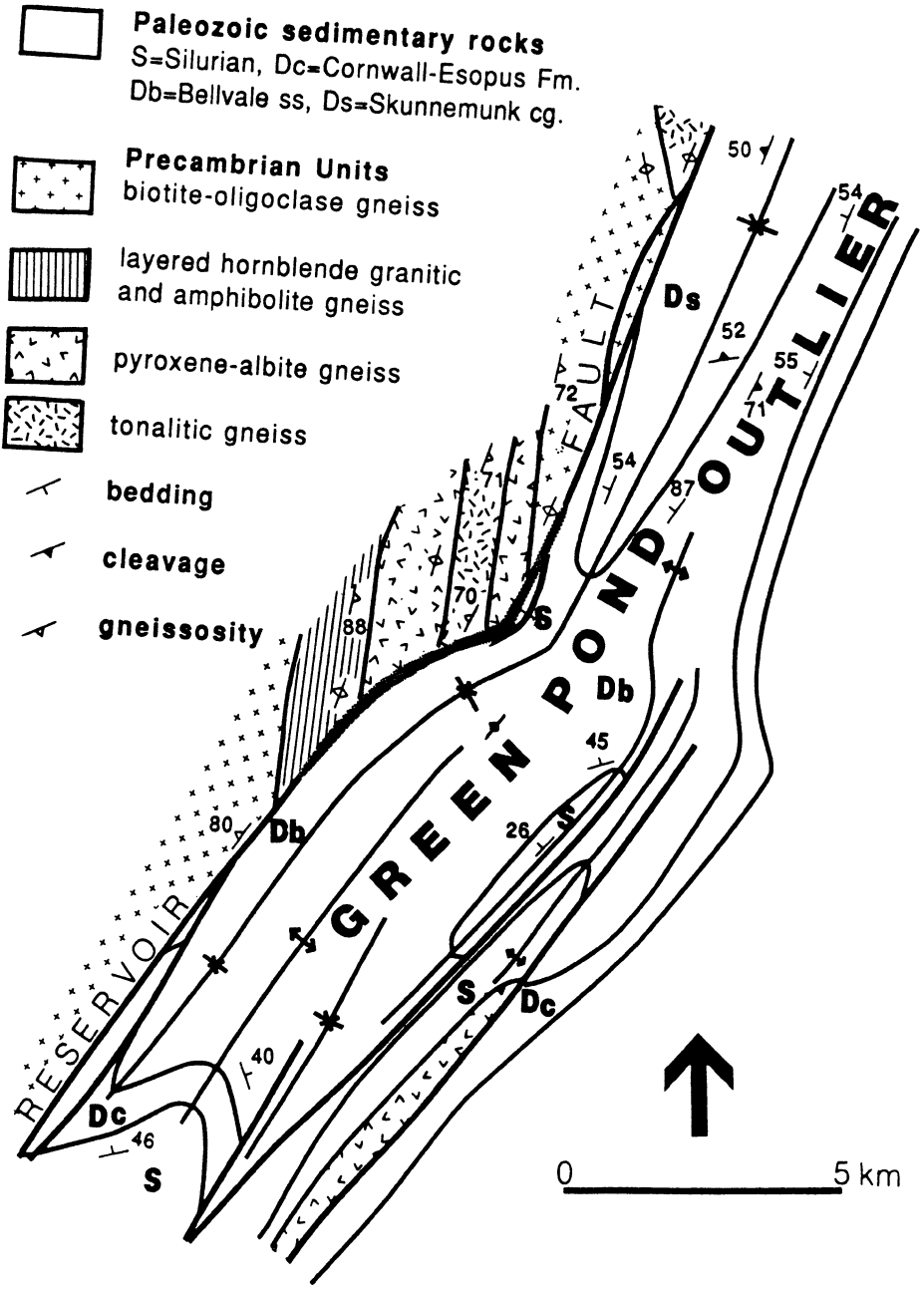

Figure 5. Geologic map of the Reservoir fault zone and Green Pond outlier in the central New Jersey Highlands (from Gates, 1995).

units are the lower Cornwall Shale, Bellvale Sandstone, and Skunnemunk Conglomerate which caps the sequence.

Protoliths of the Reservoir fault rocks are preserved along the western margin of the fault and as xenoclasts and xenocrysts within the fault zone. The protolith is primarily a granitic to tonalitic paragneiss with antiperthite, varietal edenite to hornblende, and/or diopside and minor ilmenite, and apatite with a granoblastic to gneissic texture. Locally these rocks preserve early mylonititc textures (Fig. 6a). The amphibole in this rock is F-rich (1.5-2.0 wt. %) and Cl-bearing (up to 0.5 wt. %). Feldspar is albite with exsolution lamellae of K-spar. There are also minor amounts of pyroxene -bearing amphibolite. In the fractured gneisses adjacent to the main fault zone, plagioclase, edenite-hornblende and, locally diopside are replaced by F-magnesiohastingsite along fractures and cleavage planes. Typically, the most complete replacement occurs closest to the fracture but, in many cases, the new minerals permeate the entire grain (Fig. 6a). Ilmenite has overgrowths of titanite.

Brittle deformation of the granitic-tonalitic gneiss ranges from veining and fracturing in rocks adjacent to the fault to extensive fault breccia and cataclasite within the fault zone. Feldspars are fractured or granulated and commonly offset along microfaults that exploit mineral cleavage planes. The fractures are filled with amphibole, epidote, calcite, chlorite, and hematite. Quartz shows extreme lattice misorientation, much of which likely reflects submicroscopic cataclasis (see Tullis and Yund, 1987) with minimal plastic deformation. Quartz also exhibits extensive fractures that are filled with essentially the same minerals as feldspar. Other minerals are offset along fractures and show extensive reaction textures.

In the mylonitic part of the shear zone, xenoclasts, xenocrysts and coarse grained neomineralized amphibole cores exhibit brittle deformation whereas fine grained amphibole and chlorite display marginal plastic deformation. A well developed S-C mylonitic fabric is formed in the amphibole-rich matrix including late C' planes (terminology of Simpson and Schmid, 1983) (Fig. 6b). S planes are composed exclusively of fine-grained magnesiohastingsite and the cores of magnesiohastingsite porphyroclasts whereas C and C' planes are fine-grained ferro-actinolite and actinolite with variable amounts of chlorite. Larger grains of F-magnesiohastingsite including porphyroclast cores commonly exhibit varying amounts of brittle fracturing primarily as microfaulting along cleavage planes and subsequent bending of the microfault blocks with Cl-magnesiohastingsite and chlorite filling the fractures. These large grains also commonly exhibit mantles and asymmetric tails of fine-grained and aligned Cl-magnesiohastingsite, ferro-actinolite and actinolite and form rotated σ-type. SEM images of the seemingly solid cores of these F-magnesiohastingsite porphyroclasts show that most of their rims and even inner cores, in some cases, are granulated and overgrown by epitaxial Cl-magnesiohastingsite with 1.0 to as much as 2.4 wt. % Cl but with little to no F (Fig. 6c). The outer edge of the porphyroclast in turn is rimmed by ferro-actinolite and actinolite. The S-C fabric, rotated porphyroclasts, and offset brittle grains including pull-aparts consistently show a dextral transcurrent sense of shear.

Overgrowths and fracture fillings on Cl-magnesiohastingsite are optically continuous ferro-actinolite and actinolite and subsequently actinolite + chlorite. Commonly, the transition between the different amphiboles can only be observed in SEM. Unlike the magnesiohastingsite assemblages, the ferro-actinolite is more commonly intergrown with other minerals. Assemblages include fine-grained epidote, albite, titanite, apatite, pyrite, and locally muscovite and biotite but they are still dominated by amphibole. These minerals occur in shear bands and in veins that parallel foliation. Biotite also shows a transition from F-rich to Cl-rich compositions within ferro-actinolite and actinolite-bearing assemblages.

Small pockets within the main fault zone contain extensive breccia and cataclasite that lack foliation. The matrix of these rocks is primarily actinolite. In the well developed cataclasite parts of the shear zone, rounded xenoclasts of both protolith

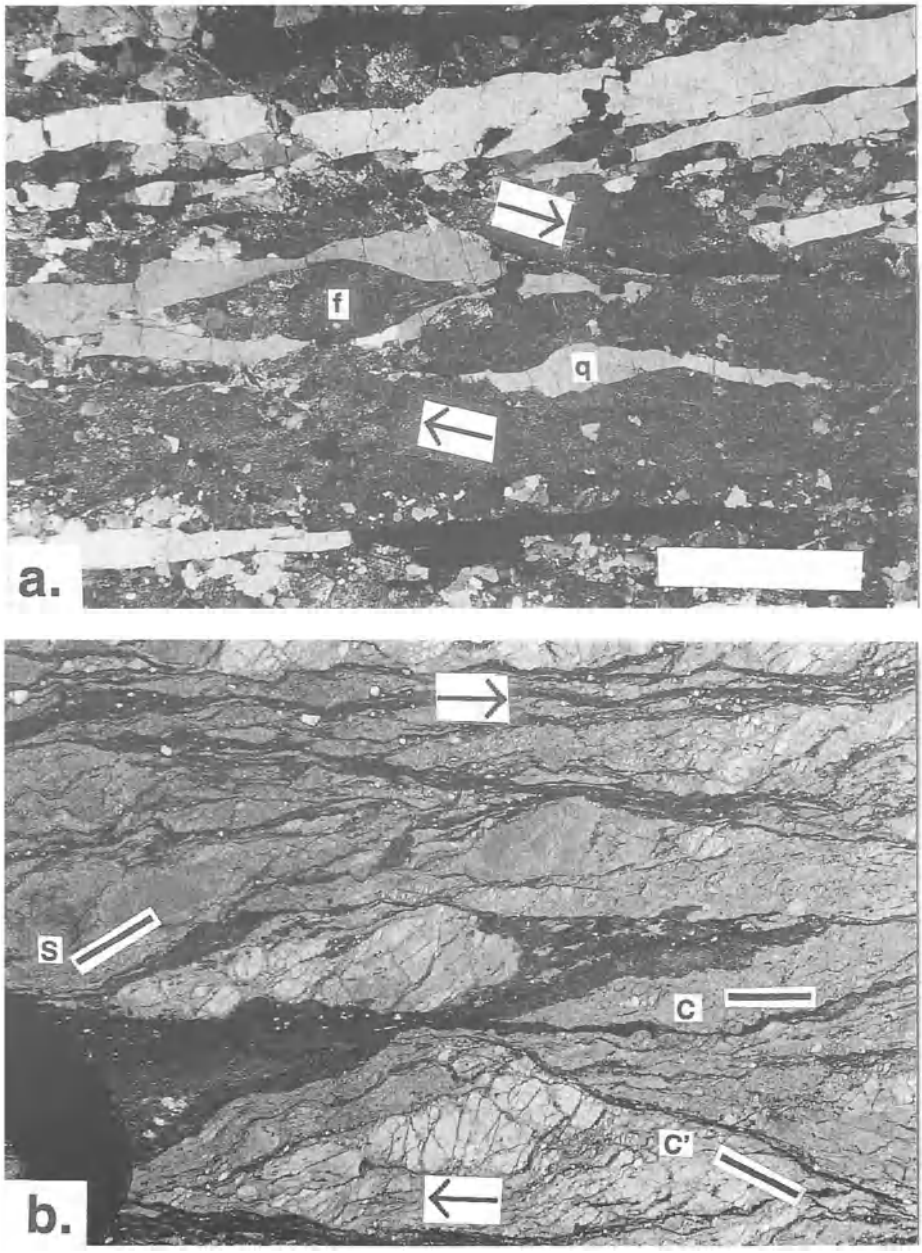

Figure 6. Photomicrographs and SEM image of fault rocks from the Reservoir fault: a) Photomicrograph of relict Grenville mylonite showing recovered quartz ribbons and σ - type rotated quartz (q) and pseudomorphs of feldspar (f) recording early high temperature reverse motion. All feldspar and mafic grains have been replaced by magnesio-hastingsite. Arrows show early shear sense; scale bar = 1 cm. b) Photomicrograph of S-C mylonite in amphibole-rich fault rock. Porphyroclasts are dominantly magnesio-hastingsite and preserve S - planes (s). C planes (c) are ferro-actinolite, and actinolite, and C' planes (c') are actinolite. Shear sense is shown by arrows; scale bar = 8 mm.

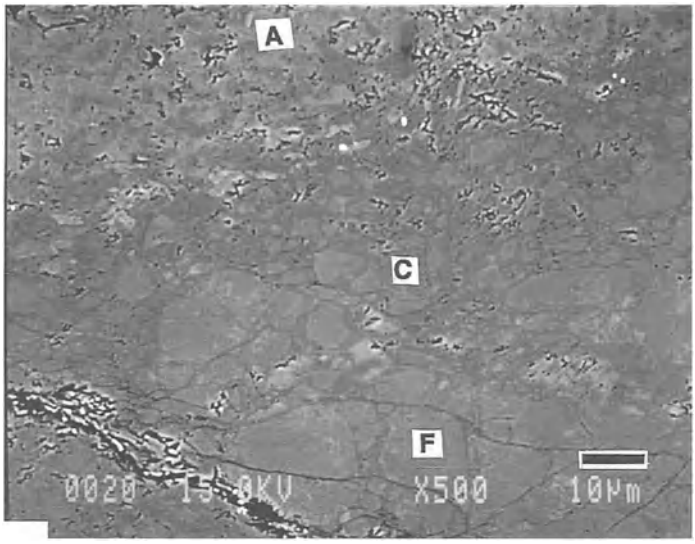

c.

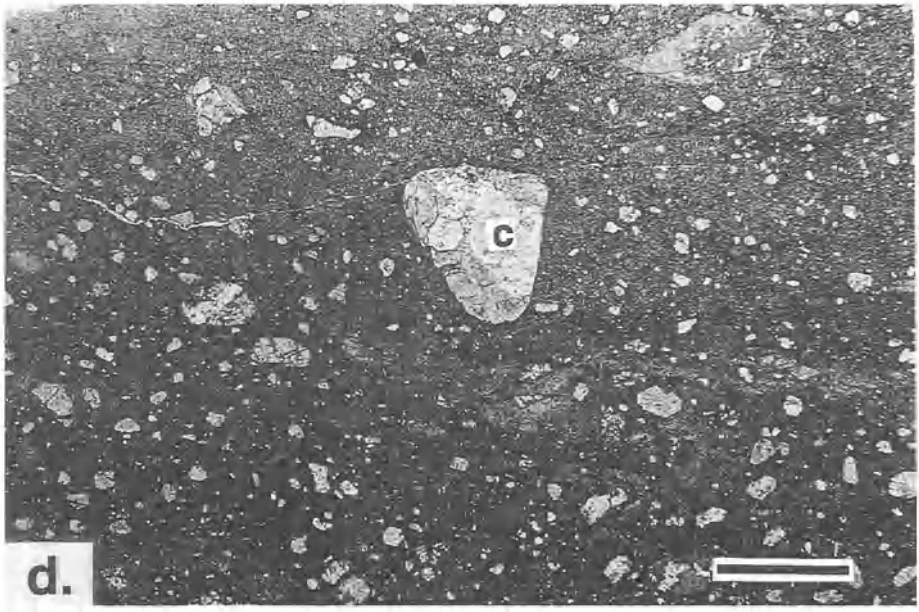

d.

Figure 6 continued. Photomicrographs and SEM image of fault rocks from the Reservoir fault c) SEM backscattered image of an amphibole porphyroclast from Figure 3b. The oldest amphibole is fluoro-magnesio-hastingsite (F) and is fragmented and epitaxially overgrown by chloro-magnesio-hastingsite (C) (dark) which is in turn fragmented and overgrown by ferro-actinolite and actinolite (A) (light). Scale bar = 20 µm. d) Photomicrograph of cataclasite of an actinolite + chlorite + plagioclase matrix enclosing xenoclasts of granitic gneiss (c) and early formed amphibole-rich fault rock in various states of alteration. Scale bar = 5 mm.

and cataclastic fault rock range up to 0.5 m but most relict components are 0.5 - 1.0 mm xenocrysts of quartz and feldspar (Figs. 6d). The xenoclasts and xenocrysts float in a matrix of randomly oriented 0.1 - 0.5 mm actinolite with minor chlorite, biotite, albite, apatite, epidote and rare pyrite.

The retrograde metamorphism that accompanied shearing is reflected in mineralogical changes. The observed protolith assemblages in granitic-tonalitic gneiss are: diopside + low-Ca feldspar (antiperthite) + quartz + ilmenite, or edenite-hornblende + low-Ca feldspar (antiperthite) + ilmenite $\pm$ scapolite $\pm$ garnet. These assemblages were produced during peak granulite facies metamorphism. The first retrograde assemblage is magnesiohastingsite which is locally potassian and consistently a fluoro-amphibole + titanite $\pm$ albite $\pm$ pyrite(?). Amphibole makes up about 90 to 95% of this assemblage. The early magnesiohastingsite is F-rich but subsequent magnesiohastingsite became progressively more Cl-rich. Amphibole analyses with equal parts of F and Cl (~1%) are common. The latest magnesiohastingsite observed is Cl-rich and contains no F. These data indicate that metamorphic fluids underwent a transition from F-rich to Cl-rich compositions that was synchronous with movement on the Reservoir fault.

Ferro-actinolite-rich assemblages succeeded the magnesiohastingsite assemblages and include albite, epidote, titanite, apatite, biotite(?), and chlorite(?).The final retrograde amphibole is actinolite and it is virtually always associated with chlorite in varying proportions. Other common associations include epidote, apatite, albite, titanite, and biotite(?). These later assemblages are most common in cataclasites with random grain orientations.

3.1 TIMING OF DEFORMATION

The Reservoir fault zone has a history of multiple periods of activity. Previous workers have suggested that it underwent Alleghanian movement (Hull *et al.*, 1986; Mitchell and Forsythe, 1988), and that it is currently active, producing regular low magnitude earthquakes (Ratcliffe, 1980). It has been proposed to have had Mesozoic (Lewis and Kummel, 1912), Acadian (Finks, 1990), Taconian (Ratcliffe, 1980), and some form of Precambrian movement (Hull *et al.*, 1986), but these phases of motion are not as easily documented.

Based on overprinting relations, the mechanical response of the minerals and the chlorite-bearing assemblages of the fault rocks, shearing postdated peak granulite facies metamorphism associated with Grenvillian orogenesis. Because quartz appears to straddle the brittle-ductile transition, the temperature of deformation of this strike-slip event appears to have been approximately 300 $\pm$ 50° C (Tullis and Yund, 1977) or less, which is consistent with the chlorite + actinolite + albite assemblages. On the other hand, the presence of early F-rich fluids and halogen-rich fluids in general indicates that it is related to Proterozoic metamorphism. The edenite and hornblende in the protolith of the Reservoir fault rocks have similar F contents to the F-magnesiohastingsite within the fault rocks. Such high F contents and halogen contents in general are common in amphiboles and biotites within rocks that underwent Grenvillian metamorphism in the Reading Prong (Gundersen, pers. comm., 1994). Such concentrations of halogen-rich amphibole within fault zones or otherwise do not occur within the Paleozoic sedimentary rocks of the Green Pond outlier. Other occurrences of amphibole mineralization within the New Jersey Highlands are also restricted to late fault zones within crystalline rocks (Gates, unpublished data) though Paleozoic sedimentary rocks are common in the area. Based on occurrence and composition, the movement accompanying amphibole mineralization on the Reservoir fault is late Middle to Late Proterozoic in age.

Because the movement sense is unequivocally dextral, it is likely late Middle Proterozoic. Costa and Gates (1993) have identified normal movement on the nearby

and parallel Ramapo fault. They propose that this movement is Late Proterozoic to earliest Cambrian and related to the opening of the Iapetus. These results are consistent with the interpretation of Iapetan rift deposits by Drake (1984) in the western Reading Prong. Based on orientation, inferred orientation of the maximum compression direction, and regional relations, the dextral strike-slip faulting on the Reservoir fault is more consistent with the earlier movement on the Ramapo fault (Ratcliffe *et al.*, 1972) than Iapetan rifting although oblique extension cannot be ruled out.

The timing of the multiple movement periods on the Reservoir Fault is poorly constrained by both geochronology and the stratigraphy of the area. Clearly the dominant deformation in the Green Pond outlier is Late Paleozoic Alleghanian and compressional in nature (Hull *et al.*, 1986, Mitchell and Forsythe, 1988, Herman and Mitchell, 1991) and the Reservoir fault was certainly active during this event. Malizzi and Gates (1989) proposed that this movement may have been dextral transpressional rather than simply compressional. Hull *et al.* (1986) and Malizzi and Gates (1989) speculated on Grenvillian movement on the fault, possibly recorded by gneissic foliation and aligned uraniferous pegmatites. The Reservoir fault was active several times during the Paleozoic and Mesozoic(?). Ratcliffe (1980), Mitchell and Forsythe (1988) and Malizzi and Gates (1989) documented two post-depositional phases of movement, one of which preserved the Green Pond outlier through west-side-up movement. Lewis and Kummel (1912) and Ratcliffe (1980) considered the entire Green Pond outlier to be preserved in a Mesozoic graben, the Reservoir fault having had normal movement. Finks (1990) proposed that the thick, high energy Devonian sedimentary rocks were deposited in a restricted dextral transtensional pull-apart basin, accounting for it's separation from the Catskill depocenter to the west. Ratcliffe (1980) proposed Taconian movement on the zone as well as neotectonism, marked by low intensity earthquakes.

4. Morgan Hill Shear Zone

The geology around Easton, PA is characterized by a complex series of blocks of Grenville gneiss within complexly deformed Early Paleozoic sedimentary rocks (Figs. 1 and 7). The sedimentary rocks include the Cambrian Hardyston Formation, a sporadic basal sandstone-conglomerate of interpreted fluvial origin. The overlying carbonates are Cambrian to Ordovician in age and include the Leithsville, Allentown, and Jacksonburg Formations and the Beekmantown Group and include limestone, cherty limestone, lime mudstone, and dolomite (Drake, 1967). There are also sporadic occurrences of lower Martinsburg Formation. The Grenville gneiss includes layered calc-silicates, marble, granitic to tonalitic gneiss with varietal biotite, hornblende, and/or pyroxene, alaskite, amphibolite, and pyroxene-hornblende gneiss (Drake, 1967). Interpretations on the origins of the Grenville package are controversial and range from a rift zone to a back-arc basin sequence. Late Paleozoic thrust faulting has shuffled these two contrasting sequences to produce the current geometry.

Faults of all ages abound in the Easton area. The two major fault complexes are the Morgan Hill shear zone (Drake, 1967) and the Chestnut Hill shear zone (Fig. 7). They are herein referred to as fault complexes because they are complexly reactivated zones of multiple faults with a wide range of orientations, kinematics, and ages. Subsequent faulting overprints, fragments, and block rotates previously formed fault rocks. At least four to five fault generations can be identified in these complexes.

4.1 PEAK GRENVILLIAN SHEARING

During peak Grenvillian tectonism, the Morgan Hill and Chestnut Hill fault complexes underwent reverse movement. Moderately southeast dipping high temperature mylonites are well foliated, contained within most rock types, and defined by peak

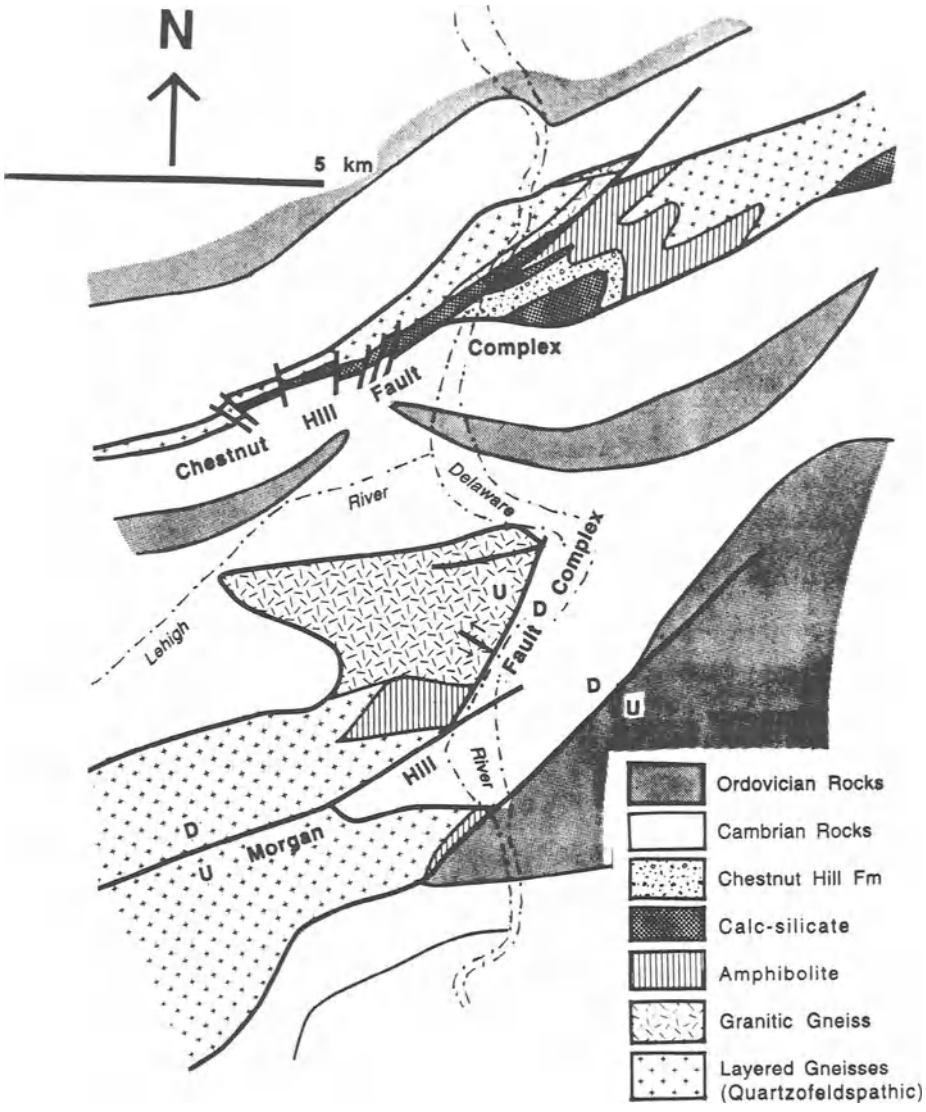

Figure 7. Geologic map of the Easton area, PA-NJ (after Drake, 1967)

metamorphic minerals. Granitic-tonalitic and mafic gneisses contain rotated porphyroclasts, rotated and sheared veins, and local cryptic S-C structures with consistent reverse shear sense. The minerals contained in the mesoscopic kinematic indicators all show static recovery textures. Sheared marble, calc-silicate, serpentinite, and talc schist form a chain in the Chestnut Hill fault complex. They also record this early reverse movement although it has largely been overprinted by later shearing. The well foliated mylonites form an anastomosing pattern within the calc-silicate-marble bodies. They exhibit some S-C development but shear sense is more readily determined by drag of amphibole and mica grains at the fault block-mylonite interfaces.

4.2 LATE- POST-GRENVILLE STRIKE-SLIP SHEARING

Sinistral strike-slip shear zones cross the Grenville reverse shear zones within the Morgan Hill shear zone. These later shear zones are thin (5-20 m), steeply southwest-dipping bands of mylonite that anastomose across the area. The mylonites are well foliated and contain highly strained marginally ductile quartz but brittle feldspar and magnetite. The feldspar and large magnetite grains within quartz-magnetite rocks show brittle pull apart textures with antithetic microfaults (Fig 8a). Quartz forms type A ribbons and rotated porphyroclasts. These kinematic indicators show consistent sinistral strike-slip offset. No significant strike-slip faulting has been identified in the Chestnut Hill fault complex.

4.3 IAPETAN EXTENSIONAL SHEARING

Significant normal movement has been identified in both the Morgan Hill and Chestnut Hill fault complexes. Steeply southeast-dipping mylonites cut off and fragment both the Grenville reverse shear zones and post-Grenville strike-slip zones in the Morgan Hill complex. Well developed S-C mylonites to ultramylonites occur within granitic rocks along the southeast margin of the Morgan Hill block (Fig. 8b). The highly foliated matrix is composed of highly recrystallized quartz, chlorite, muscovite, and feldspar, and defines the C planes. Relict feldspar grains form the cores of rotated porphyroclasts and commonly show brittle pull apart textures. Late spaced C' planes offset the C planes. All kinematic indicators show a consistent and purely normal sense of shear.

The shear zones within the calcsilicate-marble pods were strongly reactivated during this event. The anastomosing shear zones contain well developed fibrous slickensides of both asbestiform serpentine and amphibole as well as talc schist. The lensoidal fault slivers between the anastomosing shears show reaction enhanced ductility along their margins to form the highly foliated mylonites (Fig. 8c). These slivers are fragmented in a complex sequence of fractures. On the microscopic scale, S-C fabrics are evident as well as rotated xenoclasts and porphyroclasts. All kinematic indicators yield an unequivocal normal sense of shear.

There is a near vertical northwest striking zone of megabreccia within the Morgan Hill complex. Clasts ranging from 2m to microscopic are randomly oriented within a chloritic matrix. The edges of the unit are sheared and minor shear zones permeate it. It appears to be a fault zone. However, enclosed within the zone is a folded and rootless layer of sedimentary rock. The layer contains a 6 cm thick graded bed from coarse sand to shale and several 1 to 2 cm thick graded silt to shale beds with laminations (Fig. 8d). The framework grains in the sandstone are predominantly K-feldspar with subordinate amounts of quartz, plagioclase, and rock fragments. These deposits are interpreted as turbidites from their composition and geometry. The problem is that no unit in the overlying sequence matches this unit. The only possible equivalent is the Chestnut Hill Formation of Drake (1984) which is proposed to be an Iapetan rift deposit. Where we have observed the Chestnut Hill Formation, it contains 2 to 3 cm

Table 1. Timing and Kinematics of Fault Activity in the Northern Reading Prong.

EVENT	AGE	RAMAPO FAULT	RESERVOIR FAULT	MORGAN HILL FAULT
Grenville	1.2 -1.0 Ga	reverse, ductile	reverse, ductile (?)	reverse, ductile
Post-Grenville	1.0-0.9 Ga (?)	dextral, ductile	dextral, brittle-ductile	sinistral (NW) ductile
Iapetan(?)	1.0-0.9 Ga-Cambrian	normal, ductile	(?)	normal, brittle-ductile
Taconian	Middle Ordovician	reverse, ductile	(?)	(?)
Acadian	Devonian	dextral*	dextral*	(?)
Alleghanian	Carboniferous Permian	reverse, ductile	reverse/dextral brittle	reverse, brittle
Atlantic	Mesozoic	normal, brittle	sinistral(?), brittle	(?)
Current		yes	Yes	No

* = proposed in other studies but no evidence found here.
(?) = none identified.
NW = northwest-striking, all others are northeast-striking

The first reactivation after Grenville compression was the dextral strike-slip event recorded in both the Ramapo and Reservoir zones and as conjugate sinistral zones in the Morgan Hill complex (Fig. 9b). Ratcliffe (1971) reports that the dextral shearing on the Canopus segment of the Ramapo fault lasted from at least 1,062 Ma to about 900 Ma. Gates (1995) reported that dextral shearing was pre-Iapetan but occurred after 1,000 Ma on the Reservoir fault. The sinistral faults in Morgan Hill similarly are post-Grenville but pre-Iapetan. Helenek (1987) proposed a regional Proterozoic strike-slip event in the Reading Prong. Gates (1995) proposed that this event is orogen-wide and reflects escape tectonism during the later stages of the Grenville orogeny. The Grenville orogeny is proposed to represent a Himalayan-type event (Windley, 1986). Therefore, just as in the Himalayas, late strike-slip deformation related to tectonic escape is consistent (Burke and Sengor, 1986). Only with more data can the magnitude of this event be judged.

The Iapetus Ocean formed as the result of extension normal to the Appalachian orogen beginning in the late Proterozoic and lasting until approximately 570 Ma (Fig. 9c) (Rankin, 1975; Rankin *et al.*, 1993). Southeast-dipping mylonites and cataclasites developed under greenschist and lower amphibolite facies conditions during crustal extension (Bailey and Simpson, 1993; Simpson and Kalaghan, 1989). This extension was accompanied by severe hydration of basement rocks (Evans, 1991) and intrusion of Proterozoic plutons (see Rankin *et al.*, 1993). Evidence for this Late Proterozoic rifting episode in the northern Reading Prong is provided by the presence of northeast-striking mafic alkalic dikes in the New Jersey Highlands (Puffer *et al.*, 1991) and probable rift generated northeast-striking metadiabase dikes in the Hudson and New Jersey Highlands (Ratcliffe, 1987). Additionally, Drake (1984) identified Iapetan rift deposits in the Easton, PA area. The normal faulting, excessive hydration of the country rock

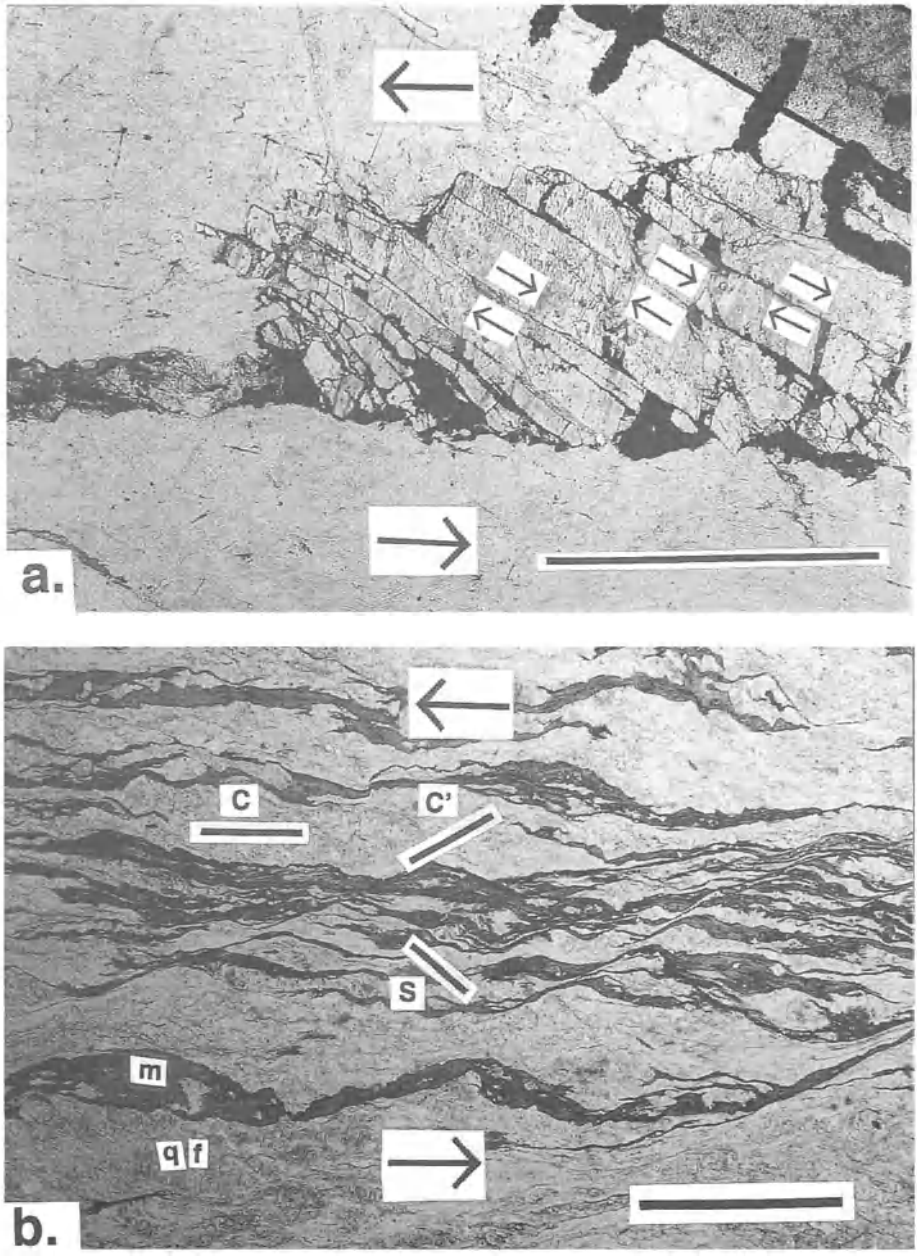

Figure 8. Photomicrographs of rocks from and near fault zones in the Easton area. a) Rare brittle pull-apart orthoclase grain within a quartz-magnetite matrix from conjugate sinistral strike-slip zone in the Morgan Hill fault complex. Large arrows show overall shear sense of mylonite, small arrows show antithetic movement along cleavage planes in feldspar. Scale bar = 8 mm. b) S-C mylonite from an Iapetan normal fault from the Morgan Hill complex. Light bands are dominated by quartz and feldspar (qf) and preserve S planes (S). Dark bands are mica-rich (m) and define C planes (C). Both dark and light bands are cut by C' planes (C'). Arrows indicate shear sense; scale bar = 1 cm.

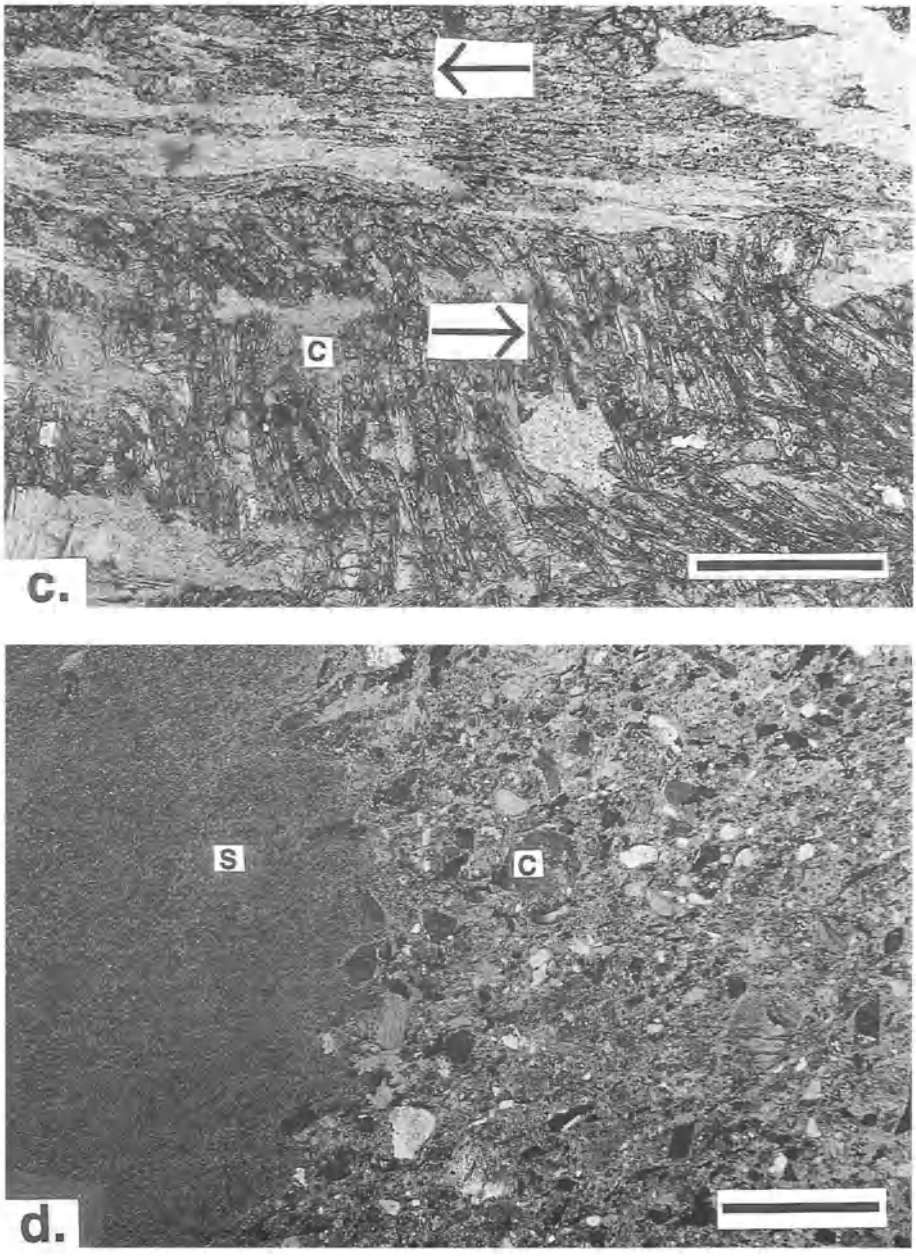

Figure 8 continued. Photomicrographs of rocks from and near fault zones in the Easton area. c) Relict lens of calcsilicate (C) being dragged into a talc-rich shear zone from the Chestnut Hill shear zone. Arrows indicate shear sense; scale bar = 5 mm. d) Sedimentary contact between coarse-sandstone to granule conglomerate (C) and siltstone (S) from the Morgan Hill shear zone. Clasts in the sandstone-conglomerate are primarily feldspar with lesser amounts of quartz. All layers show normal grading. Scale bar = 4 mm.

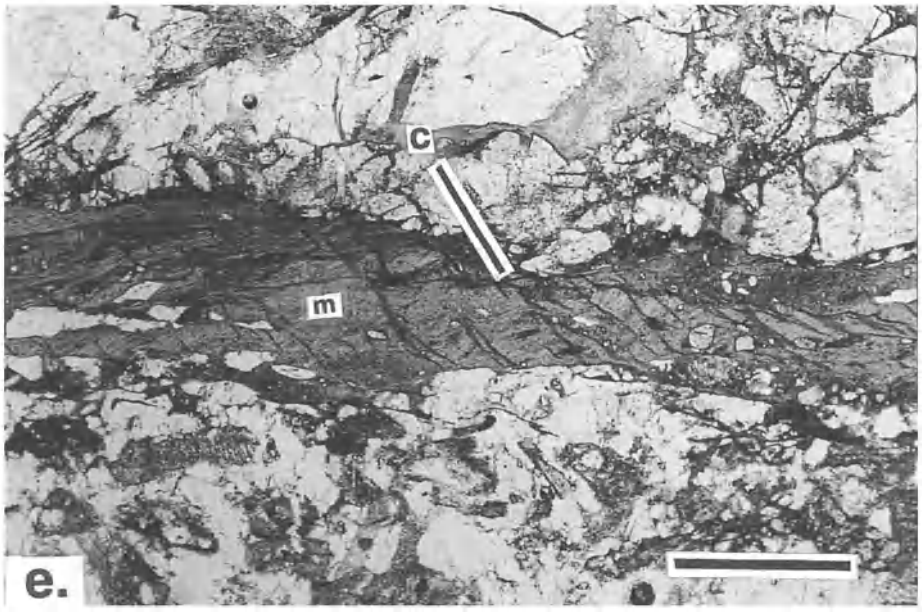

Figure 8 continued. Photomicrographs of rocks from and near fault zones in the Easton area. e) Mica-rich band of mylonite from the Iapetan normal faults in the Morgan Hill fault complex showing superimposed spaced crenulation cleavage interpreted as the result of Taconian or Alleghanian compression. Scale bar = 3 mm.

garnets and is ubiquitously sheared. Along strike it merges into a chloritized breccia. Therefore the sedimentary rock is likely part of the Iapetan rift sequence and either a unit that has subsequently been removed by erosion and not represented in the cover sequence or else it is a less deformed and metamorphosed version of the Chestnut Hill Formation.

In the vicinity of the normal faults, the crystalline rocks have undergone severe hydrothermal alteration. Most of the feldspars and varietal mafic minerals have been replaced by intergrowths of chlorite, sericite, and hematite. Even in fresh samples, the feldspars appear corroded and pseudomorphed. Adjacent to the Chestnut Hill Formation, hematite was commercially mined. In all other instances in the northern Reading Prong, only magnetite is mined for iron. These textures and mineralogy indicate excessive alteration relative to the other rocks in the area.

4.4 PALEOZOIC THRUST/REVERSE FAULTING

There is extensive post Middle Ordovician deformation recorded in the cover sequence in the Easton area. Folding, thrust faulting, pervasive cleavage formation, veining, and emergence of the basement blocks are all products of this deformation. The crystalline rocks contain thin chloritized fault zones that are well developed in segments along the basement block margins. These faults further fragment and segment the preexisting faults. Thrust faults also occur less commonly within the basement blocks where they appear as fine grained well foliated layers of chlorite and muscovite. Shear sense appears consistently reverse as indicated by fibrous slickensides and S-C fabric within the zone. The mylonitic part of the fault is clearly the result of reaction enhanced ductility (White and Knipe, 1978). There is also crenulation cleavage developed on the Iapetan mylonites during this event (Fig. 8e).

There are also several north-northeast and north-northwest striking and near vertical strike-slip faults that are especially prevalent in the Chestnut Hill block. The faults are identified on map scale by offsets of contacts on the order of 10s to at most 100s of meters and in the field by horizontal polished slickensides. These faults could be features that were produced late in Paleozoic compressional activity or else as the result of Mesozoic extension.

5. Fault Reactivation and Tectonics

Ratcliffe (1980), Drake (1984), and Hull *et al.* (1986) proposed the development of several major fault systems in the northern Reading Prong during high grade metamorphic conditions and compressional tectonics of the Grenville Orogeny (Table 1, Fig. 9a). The timing of this event is controversial because some workers argue that there were two peak events between 1.2 Ga and 1.0 Ga (Mose, 1982; Helenek and Mose, 1984; Helenek, pers. comm., 1994) whereas others argue for a single protracted event (Rankin *et al.*, 1993). Although the fault systems are marked by rocks that record high strains, virtually all rocks in the Reading Prong underwent significant deformation at this time. Several of the fault systems continued to be active until well after the peak of the Grenville orogeny and developed into major zones of crustal weakness. The crystalline blocks between these zones exhibit largely only minor and sporadic deformation after this consolidation event. These deformations are manifested in minor faulting, and jointing, and rigid block translations and rotations. Virtually all of the stress imposed upon this area subsequent to the Grenville orogeny was absorbed by several fundamental zones of crustal weakness while the crustal blocks between them remained rigid and passive.

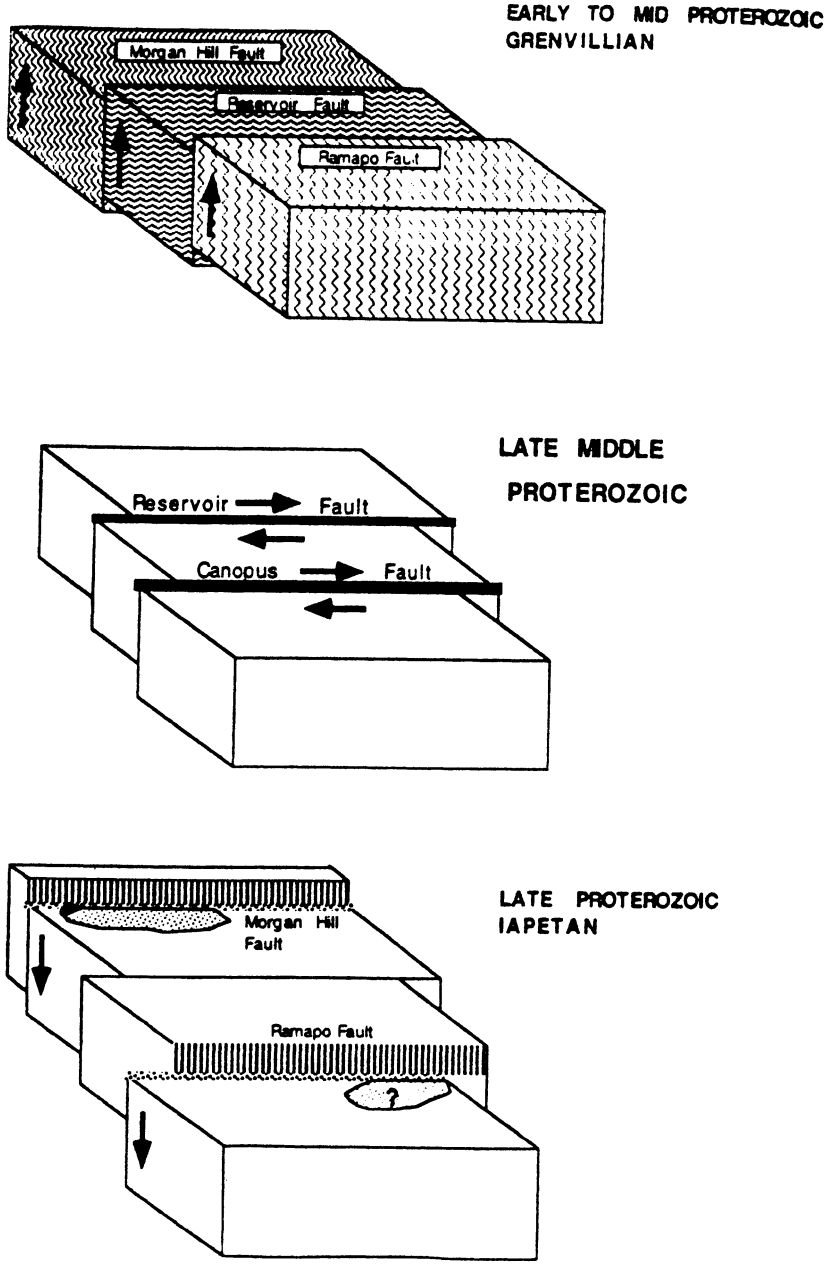

Figure 9. Tectonic model for the formation and reactivation of the major faults in the northern Reading Prong: a) Middle Proterozoic Grenville compression, reverse movement on Ramapo, Reservoir, and Morgan Hill shear zones, and penetrative internal deformation of crystalline fault blocks as indicated by patterns, b) Late Middle Proterozoic dextral strike-slip reactivation of the Ramapo (Canopus), and Reservoir shear zones and conjugate sinistral movement on the Morgan Hill shear zone, c) Late Proterozoic normal reactivation of the Morgan Hill and Ramapo shear zones, hydration of Grenville gneiss, and fault controlled deposition of rift sediments.

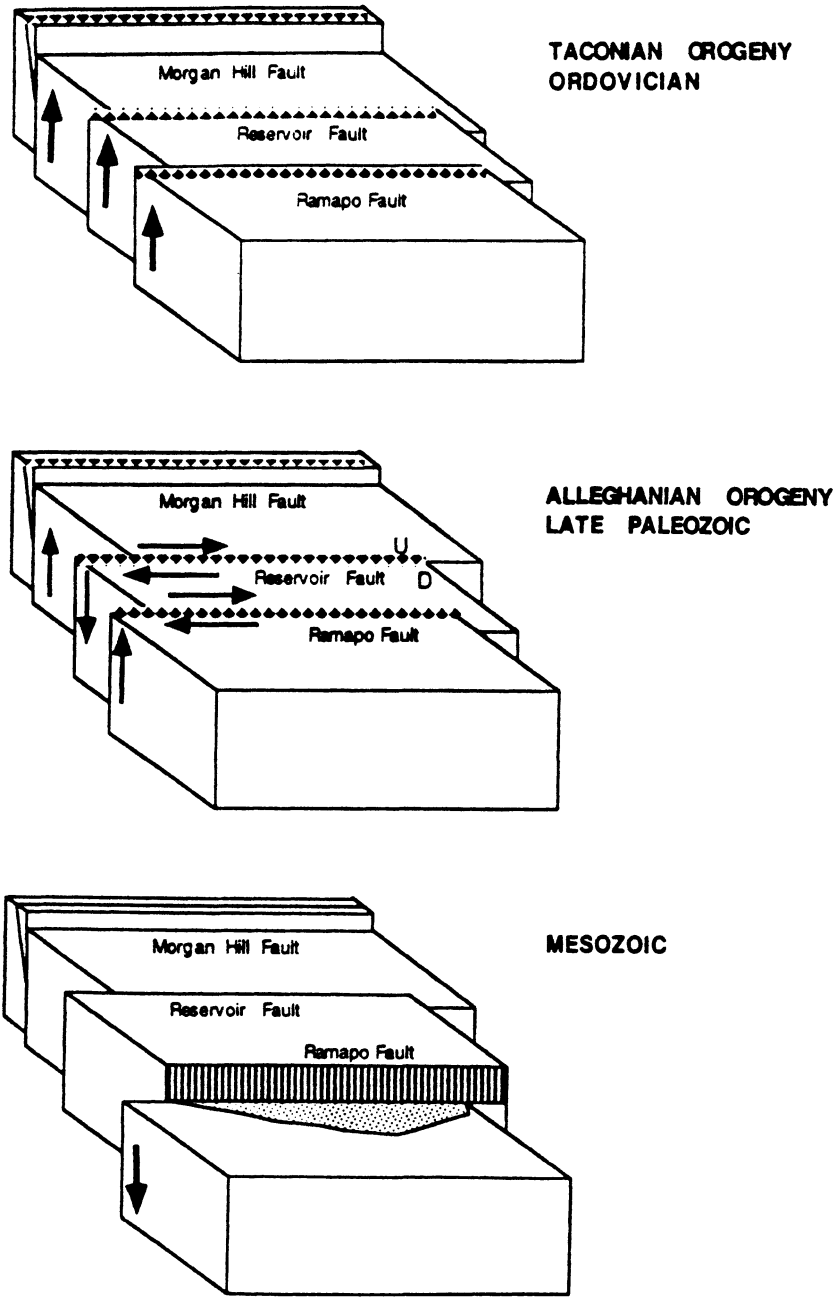

Figure 9 continued. Tectonic model for the formation and reactivation of the major faults in the northern Reading Prong: d) Taconian (Middle Ordovician) reverse reactivation of the Ramapo, and likely the Reservoir and Morgan Hill shear zones, e) Alleghanian (Late Paleozoic)reverse and dextral strike-slip reactivation of the Ramapo, Reservoir, and Morgan Hill shear zones, f) Mesozoic normal reactivation of the Ramapo fault and deposition.

associated with these faults, and the sedimentary rock found within the Morgan Hill shear zone are consistent with Late Proterozoic extension. Brock (1989) correlated late Precambrian to early Cambrian rift-to-drift metasedimentary and metavolcanic rocks of southeast New York and eastern Connecticut to the break-up of the Proterozoic supercontinent. Late Proterozoic rifting along the Ramapo fault system, although not previously identified, is consistent with the continental extension elsewhere along the east coast of North America.

Ratcliffe (1971; 1980) suggests that the Ramapo fault system was reactivated as a reverse fault during the Ordovician Taconian orogeny (Fig. 9d). The dominant southeast-dipping ductile foliation in the Ramapo fault system was formed during this event. Late Ordovician mafic dikes cross the fault and provide a minimum age for the timing of faulting. Taconian deformation has been proposed for both the Reservoir fault (Ratcliffe, 1980; Hull *et al.*, 1986) and the Morgan Hill fault complex (Drake, 1984) but direct age constraints are lacking. Both areas contain deformed pre-Taconian sedimentary rock and exhibit the classic Taconian unconformity but direct evidence of fault movement is lacking. It is, however, likely that both faults were active at that time.

All of the fault systems had demonstrable post-Ordovician reactivation (Fig. 9e). Two complex systems of brittle faults overprint the Taconian mylonite in the Ramapo fault. Relative dating of the two different ages is demonstrated by overprinting relations. The first episode is the result of a west-northwest maximum compression direction and offsets Late Ordovician dikes. Faulting includes both reverse and strike-slip components. Ratcliffe (1971) demonstrated Acadian dextral strike-slip movement on the Canopus segment of the Ramapo fault as well, but it is in uncertain relation to that shown in the New Jersey segment. Alleghanian deformation including both compression (Mitchell and Forsythe, 1988) and dextral strike-slip (Malizzi and Gates, 1989) is well documented along the Reservoir fault. Faulting as well as folding and cleavage development are evident in the Skunnemunk conglomerate and all of the older formations in the Green Pond outlier. The middle Devonian Skunnemunk conglomerate is the easternmost exposure of Catskill facies deposition which resulted from the building of the Acadian highlands. Deformation of this rock must have postdated the Acadian orogeny and therefore is Alleghanian. The Morgan Hill and Chestnut Hill fault complexes were also strongly reactivated during the Alleghanian. The thrusting of the basement rocks over the Early Paleozoic cover sequence that forms the alternating sequences across the Easton area is Alleghanian (Drake, 1984). Both the cover and basement are riddled with thrust faults of all sizes. The cover rocks exhibit well developed Alleghanian folds and cleavage as well (Drake, 1984).

The second episode of brittle faulting in the Ramapo fault is the result of an approximately north-south maximum compression direction. Malizzi and Gates (1989) attributed a late brittle overprint on the Reservoir fault to a Triassic maximum compression based on correlation with structures in the Newark basin which indicate a maximum compression direction of 020° (Lucas *et al.*, 1988). Geiser and Engelder (1983) reported a similar trend for maximum compression which deformed middle Carboniferous strata in the Appalachian Plateau of eastern Pennsylvania. Mitchell and Forsythe (1988) analyzed structures which developed in Silurian and Devonian rocks of the Green Pond outlier and attributed them to an approximate north-south trending maximum compression direction. Geiser and Engelder (1983) and Mitchell and Forsythe (1988) both consider the late phase brittle deformation to be the second phase of a non-coaxial Alleghanian deformation. None of the studies, including this one, provides any direct evidence which can be used to determine whether this late stage brittle deformational event is Late Paleozoic or Triassic in age. The brittle mineral responses of the latest movement are consistent with those proposed by Ratcliffe (1980) for Triassic reactivation of the Ramapo fault. This Mesozoic reactivation of the Ramapo fault formed the northwestern margin of the large Newark rift basin (Fig. 9f).

A population of southeast- and northwest-dipping right-lateral strike-slip faults have corresponding maximum compression directions uncommon to Alleghanian and Triassic deformation. These brittle faults are difficult to constrain. The east-north-east- and west-south-west-trending maximum compression directions may represent continued post-Triassic clockwise rotation of compression. This third maximum compression trend is similar to proposed Jurassic maximum compression (Ratcliffe and Burton, 1985). The normal reactivation of Ordovician dikes and the northeast trend of Jurassic Watchung basalt flows are also consistent with this Jurassic paleostress direction.

6. Conclusions

Fundamental zones of crustal weakness in the Reading Prong of Pennsylvania, New Jersey and New York were established during Grenvillian orogensis. Three of these zones, the Ramapo, Reservoir and Morgan Hill shear zones, were reactivated multiple times thereafter and contain evidence of the major orogenic and extensional events of the central Appalachians. The crystalline rocks between these shear zones appear to have experienced relatively little deformation during the reactivations. The tectonics of the area appears to have reflected passive movement of rigid crystalline blocks with the great majority of the strain taken up at their margins which comprise the shear zones studied.

Acknowledgments: Funding for research on this project was provided by the Pennsylvania Geological Survey, the New York State Geological Survey, and through U.S. Department of Energy grant 05-88-ER60665. Mineral chemistry of nine samples fault rocks from the Reservoir fault were determined using the JEOL JXA-8600 Superprobe at Rutgers University, New Brunswick with help from J. Delaney. Thanks to G. Herman for suggesting field locations and for useful discussions. The manuscript was improved through reviews by D. West and J. P. Hogan.

7. References

Aggerwal, Y. P. & Yang, J. (1978) Earthquake risk provinces in northeastern North America, *Earthquake Notes* **49**, 8-9.

Bailey, C.M. and Simpson, C. (1993) Extensional and contractional deformation in the Blue Ridge Province, Virginia: *Geol. Soc. Amer. Bull.* **105**, 411-422.

Beach, A. (1975) The geometry of en-echelon vein arrays, *Tectonophysics* **28**, 245-263.

Bobyarchick, A. R. and Glover, L., III (1979) Deformation and metamorphism in the Hylas zone and adjacent parts of the eastern Piedmont in Virginia, *Geol. Soc. Amer. Bull.* 90, 739-752.

Boullier, A. M. and Bouchez, J. -L. (1978) Le quartz en rubans dans les mylonites, *Bull. Soc. Geol. Fr.* **20**, 253-262.

Brock, P. C. (1989) Stratigraphy of the northeastern Manhattan Prong, Peach Lake quadrangle, New York-Connecticut, in D. Weiss (ed.) Field Trip Guidebook, Middletown, New York, New York State Geologic Association, **61**, 1-28.

Burke, K., and Sengor, C. (1986) Tectonic escape in the evolution of the continental crust, in (Barazangi, M., and Brown, L., eds.) *Reflection Seismology: The Continental Crust*, Am. Geophys. Union Geodyn. Ser., Washington, D.C., **14**, 41-53.

Burton, W. C. and Ratcliffe, N. M. (1985) Compressional structures associated with right-oblique normal faulting of Triassic-Jurassic strata of the Newark Basin near Flemington, New Jersey, *Geol. Soc. Amer. Abst. Prog.* **17**, 9.

Costa, R.E. (1991) Structural Evolution and neotectonics of the Ramapo fault system, northern New Jersey, Dept of Geological Sciences, Rutgers University, Newark, unpublished Master's thesis, 83 p.

Costa, R., and Gates, A.E. (1993) Multiple episodes of movement on the Ramapo fault system, northern New Jersey, in (Puffer, J.H., ed.) *Geologic Traverse across the Precambrian Rocks of the New Jersey Highlands*; Geol. Assoc. New Jersey Field Guide and Proc., **10**, 168-195.

Dallmeyer, R. D. (1974) Metamorphic history of the northeastern Reading Prong, New York and Northern New Jersey, *Jour. of Petrology,* **15**, 325-359.

Darton, N.H. (1894) Geologic relations from Green Pond, New Jersey to Schunemunk Mountain, New York. *Geol. Soc. Am. Bull.*, **5**, 367-394.

Drake, A.A., Jr. (1967) Geologic map of the Easton quadrangle New Jersey - Pennsylvania, U.S. Geological Survey Map GQ-594.

Drake, A.A., Jr. (1984) The Reading Prong of New Jersey and eastern Pennsylvania; An appraisal of rock relations and chemistry of a major Proterozoic terrane in the Appalachians, in (Bartholomew, M.J., ed.) *The Grenville Event in the Appalachians and Related Topics*, Geol. Soc. Am. Spec. Pap. **194**, 75-109.

Eisbacher, G. H. (1970) Deformation mechanisms of mylonite rocks and fractured granulites in Cobequid Mountains, Nova Scotia, Canada, *Geol. Soc. Amer. Bull.:* **81**, 2009-2020.

Evans, N. H. (1991) Latest Precambrian to Ordovician metamorphism in the Virginia Blue Ridge: Origin of the contrasting Lovingston and Pedlar basement terranes, *Amer. J. Sci.* **291**, 425-452.

Finks, R.M. (1990) The Green Pond outlier as a Silurian right-lateral transpressional basin, *Geol. Soc. Am. Abst. Programs*, **22**, 15.

Fisher, D. W., Isachsen, Y. W. and Rickard, L. V. (1970) Geologic Map of New York; Lower Hudson sheet, New York State Museum and Science Service, Map and Chart series, 15.

Gates, A.E. (1995) Middle Proterozoic dextral strike-slip event in the central Appalachians: Evidence from the Reservoir fault, NJ, *J. Geodynamics,* **19**, 195-212.

Gates, A.E. (1996) Multiple activations of accreted terrane boundaries: An example from the Carolina terrane, Brookneal, Virginia, in (Glover, L., III, and Gates, A.E., eds.) *Central and Southern Appalachian Sutures: Results of the EDGE Project and Related Studies,* Geol. Soc. Am. Spec. Pap., in press.

Geiser, P. and Engelder, T. (1983) The distribution of layer parallel shortening fabrics in the Appalachian foreland of New York and Pennsylvania: Evidence for two non-coaxial phases of the Alleghanian orogeny, in (Robert Hatcher, H. Williams and I. Zietz, eds)., *Geol. Soc. Am. Mem.* **158**, 161-176.

Goldstein, A.G. (1989) Tectonic significance of multiple motions on terrane-bounding faults in the northern Appalachians, *Bull. Geol. Soc. Am.,* **101**, 927-938.

Gundersen, L.C. (1986) Geology and geochemistry of the Precambrian rocks of the Reading Prong, New York and New Jersey - Implications for the genesis of iron-uranium-rare earth deposits, in (Carter, L.M.H., ed.) *USGS Research on Energy Resources - 1986 Programs and Abstracts*, U.S. Geol. Surv. Circular **974**, 19.

Hague, J.M., Baum, J.L., Hermann, L.A., and Pickering, R.J. (1956) Geology and structure of the Franklin-Sterling area, New Jersey, *Geol. Soc. Am. Bull.*, **68**, 435-473.

Hall, L. M., Helenek, H. C., Jackson, R. A., Caldwell, K. G., Mose, D., and Murray, D. P. (1975) Some basement rocks from Bear Mountain to the Housatonic Highlands, New England Intercollegiate Geological Congress , **67**, 1-29.

Harding, T. P., 1974, Petroleum traps associated with wrench faults: Amer. Assoc. Petrol. Geol. Bull.: v. 58, p. 1290-1304.

Helenek, H.L. (1987) Possible Late Proterozoic wrench tectonic in the Reading Prong, New York - New Jersey - Pennsylvania, *Northeastern Geology,* **9**, 211-222.

Helenek, H.L., and Mose, D.G. (1984) Geology and geochronology of Canada Hill Granite and its bearing on the timing of Grenvillian events in the Hudson Highlands, New York, in (Bartholomew, M.J., ed.)*Grenville Events and Related Topics in the Appalachians*, Geol. Soc. Am. Spec. Pap., **194**, 57-73.

Herman, G.C., and Mitchell, J.P. (1991) Bedrock geologic map of the Green Pond Mountain region from Dover to Greenwood Lake, New Jersey. New Jersey Geol. Surv., Geol. Map Ser. **91-2**.

Hippert, J.F.M. (1993) 'V'-pull-apart microstructures: a new shear-sense indicator. *J. Struct. Geol.* **15**, 1393-1403.

Hull, J., Koto, R., and Bizub, R. (1986) Deformation zones in the Highlands of New Jersey, in (Husch, J.M., and Goldstein, F.R., eds.) *Geology of the New Jersey Highlands and Radon in New Jersey*, Geol. Assoc. New Jersey Field Guide, **3**, 19-67.

Kummel, H.B., and Weller, S. (1902) The rocks of the Green Pond mountain region, *Annual Report of the State Geologist 1901*, N.J. Geol. Surv., 1-51.

Lewis, J.V., and Kummel, H.B. (1912) Geologic map of New Jersey (1910-1912), New Jersey Dept. of Conservation and Economic Development, Atlas Sheet 20.

Lister, G. S. and Snoke, A. W. (1984) S-C mylonites: *Jour. Struct. Geol.,* **6,** 17-38.

Lucas, M., Hull, J. and Manspeizer, W. (1988) A foreland-type fold and related structures in the Newark rift basin, in (W. Manspeizer, ed.)*Triassic-Jurassic rifting: Continental breakup and the origin of the Atlantic ocean and passive margins*, Elsevier, N.Y., 307-332.

Maxey, L. R. (1976) Petrology and geochemistry of the Beemerville carbonatite-alkalic rock complex, New Jersey, *Geol. Soc. Amer. Bull.* **87**, 1551-1559.

Malizzi, L. D. and Gates, A. E. (1989) Late Paleozoic deformation in the Reservoir Fault zone and Green Pond Outlier, New York State Geol. Assoc. Field Trip Guidebook, **61**, 75-93.

Mitchell, J.P., and Forsythe, R. (1988) Late Paleozoic non-coaxial deformation in the Green Pond Outlier, New Jersey Highlands. *Geol. Soc. Am. Bull.*, **100**, 45-59.

Mose, D.G. (1982) 1,300-million-year-old rocks in the Appalachians. *Geol. Soc. Am. Bull.*, **93**, 391-399.

Olsen, P. E. (1980) Triassic and Jurassic formations of the Newark basin: in (W. Manspeizer, ed.) Field studies of New Jersey Geology and Guide to Field Trips, *New York State Geol. Assoc.*, **52**, 1-39.

Passchier, C.W., and Simpson, C. (1986) Porphyroclast systems as kinematic indicators. *J. Struct. Geol.*, **8**, 831-843.

Petit, J.P. (1987) Criteria for the sense of movement on fault surfaces in brittle rocks, *J. Struct. Geol.,* **9**, 597-608.

Puffer, J. H., Volkert, R. A. and Hoszik, M. J. (1991) Probable late Proterozoic mafic dikes in the New Jersey highlands, *Geol. Soc. Amer. Abst. Prog.* **23**, 118.

Rankin, D. W. (1975) The continental margin of eastern North America in the southern Appalachians: The opening and closing of the Proto-Atlantic ocean, *Amer. J. Sci.:* **275-A**, 298-336.

Rankin, D.W., Drake, A.A., Jr., and Ratcliffe, N.M. (1993) Proterozoic North American (Laurentian) rocks of the Appalachian orogen. in (J.C. Reed ed.) *Precambrian Conterminous U.S.*: Geology of North America Series, v. C2, Geol. Soc. Am., Boulder, Colorado, 378-403.

Ratcliffe, N.M. (1971) The Ramapo fault system in New York and adjacent New Jersey: A case of tectonic heredity. *Geol. Soc. Am. Bull.*, **82**, 125-142.

Ratcliffe, N.M. (1980) Brittle faults (Ramapo, fault) and phyllonitic ductile basement rocks of the Ramapo seismic zones, New York and New Jersey, and their relationship to current seismicity, in (Manspeizer, W., ed.) *Field Studies of New Jersey Geology*, New York State Geol. Assoc. Guidebook, **52**, 278-311.

Ratcliffe, N. M. (1981) Cortlandt-Beemerville magmatic belt: a probable late Taconian alkalic cross trend in the central Appalachians, *Geology,* **9**, 329-335.

Ratcliffe, N. M. (1983) Possible Catoctin age diabase dikes in the Hudson highlands of New York and New Jersey: Geochemistry and tectonic significance, *Geol. Soc. Amer. Abst. Prog.* **15**, 172.

Ratcliffe, N. M. (1987) High TiO_2 metadiabase dikes of the Hudson Highlands, New York and New Jersey: possible late Proterozoic rift rocks in the New York recess, *Amer. J. Sci.* **287**, 817-850.

Ratcliffe, N.M., Armstrong, R.L., Chai, B.H., and Senechal, R.G. (1972) K-Ar and Rb-Sr geochronology of the Canopus pluton, Hudson Highlands, New York. *Geol. Soc. Am. Bull.*, **83**, 523-530.

Ratcliffe, N.M., Armstrong, R.L., Mose, D.G., Seneschel, R., Williams, N., and Baiamonte, M.J. (1982) Emplacement history and tectonic significance of the Cortlandt Complex, related plutons, and dike swarms in the Taconide zone of southeastern New York based on K-Ar and Rb-Sr investigations, *Am. J. Sci.* **282**, 358-390.

Ratcliffe, N. M. and Burton, W. M. (1985) Fault reactivation models for the origin of the Newark basin and studies related to eastern U.S. seismicity, in (G.R. Robinson Jr. and A. J. Froelich eds.) Proceedings of the Second U.S. Geological Survey Workshop on the Early Mesozoic Basins of the Eastern United States, U.S. Geological Survey Circular 0946, 36-45.

Schlische, R. W. and Olsen, P. E., 1988, Structural evolution of the Newark basin: in J. Husch and M. Hozick eds., Geology of the Central Newark Basin, 5th annual meeting of GANJ, p. 43-65.

Sibson, R. H. (1977) Fault rocks and fault mechanisms: *J. Geol. Soc. Lon.* **123**, 191-213.

Sibson, R. H. (1983) Continental fault structure and the shallow earthquake source, *J. Geol. Soc. London* **140**, 741-767.

Simpson, C. (1985) Deformation of granitic rocks across the brittle-ductile transition, *J. Struct. Geol.* **7**, 503-511.

Simpson, C. and Kalaghan, T. (1989) Late Precambrian crustal extension preserved in Fries fault zone mylonites, southern Appalachians, *Geology* **17**, 148-151.

Simpson, C. and Schmid, S.M. (1983) An evaluation of criteria to deduce the sense of movement in sheared rocks. *Geol. Soc. Am. Bull.*, **94**, 1281-1293.

Stauffer, M. R. (1970) Deformation textures in tectonites: *Can. J. Earth Sci.* **7** 498-511.

Swanson, M. T. (1986) Preexisting fault control of Mesozoic basin formation in eastern North America. *Geology*: **14**, 419-422.

Tullis, J. A., and Yund, R.A. (1977) Experimental deformation of dry Westerly granite. J. Geophys. Res., **82**, 5705-5718.

Tullis, J. A., and Yund, R.A. (1987) Transition from cataclastic flow to dislocation creep of feldspar: Mechanisms and microstructures. *Geol.*, **15**, 591-595.

Volkert, R.A. (1993) Geology of the Middle Proterozoic rocks of the New Jersey Highlands, in (Puffer, J.H., ed.)*Geologic Traverse across the Precambrian Rocks of the New Jersey Highlands* , Geol. Assoc. New Jersey Field Guide and Proc., **10**, 23-55.

White, S. H., Burrows, S. E., Carreras, J., Shaw, N. D. and Humphreys, F. J. (1980) On mylonites in ductile shear zones, *J. Struct. Geol.* **2**, 175-187.

White, S.H., and Knipe, R.J. (1978) Transformation- and reaction-enhanced ductility in rocks. *J. Geol. Soc. London*, **135**, 513-516.

Wilson, J.T. (1966) Did the Atlantic close and then reopen?, *Nature* **211**, 676-681.

Windley, B.F. (1986) Comparative tectonics of the western Grenville and the western Himalaya, in (J.M. Moore, A. Davidson and A.J. Baer, eds.) *The Grenville Province*, Geol. Assoc. Can. Spec. Pap., **31**, 341-348.

Young, D.A., and Cuthbertson, J. (1994) A new ferrosilite and Fe-pigeonite occurrence in the Reading Prong, New Jersey, USA. *Lithos*, **31**, 163-176.

THE VARISCAN GEODYNAMIC CYCLE IN THE SARDINIAN-CORSICAN MASSIF, ACCORDING TO THE MOST RECENT DATA

N. MINZONI
Dipartimento Scienze Geologiche - Paleontologiche Universita
Corso Ercole D'Este 32, 44100 Ferrara
ITALY

Abstract

The most recent data indicate that, in the Sardinian-Corsican Massif, the Variscan ocean was formed in northern Sardinia during middle Ordovician times by transtension tectonics. The quasi-contemporaneous development of the" Sardinian Phase" transpression folding suggests that the oceanic area was opened as a transtension pull-apart basin, along a mega-shear zone.The middle Ordovician magmatic rocks outcropping in central Sardinia do not represent (as proposed by Carmignani *et al.*, 1992) an arc related to subduction processes, but they are connected to transtension tectonics marking the break-up of the continental crust and the subsequent opening of the oceanic area. In agreement with Pin and Marini (1993), middle Ordovician magmatism in the Sardinian-Corsican Massif can be related, as in the Central Europe Variscan chain, to ensialic extension causing crustal thinning and initiating rifting.

Introduction

The most recent studies (Carmignani *et al.*, 1979; 1981; 1992, with references; Minzoni, 1988; 1992) suggest that the Sardinian-Corsican Massif (SCM) was formed, as the European Variscan chain, by the collision of two passive margins. In the SCM, the collision is documented by the "Asinara-Posada Oceanic Suture" (APOS) in northern Sardinia (Figs.1,2,4D). The oceanic nature of this line is indicated by the occurrence of mafic rocks displaying a composition similar to modern evolved oceanic tholeiites (Cappelli *et al.*, 1991-92). Although these rocks were retrograded in the amphibolite facies during late Variscan metamorphism, they still

contain granulite and eclogite relics (Ghezzo *et al.*, 1980), which may be related to subduction processes.

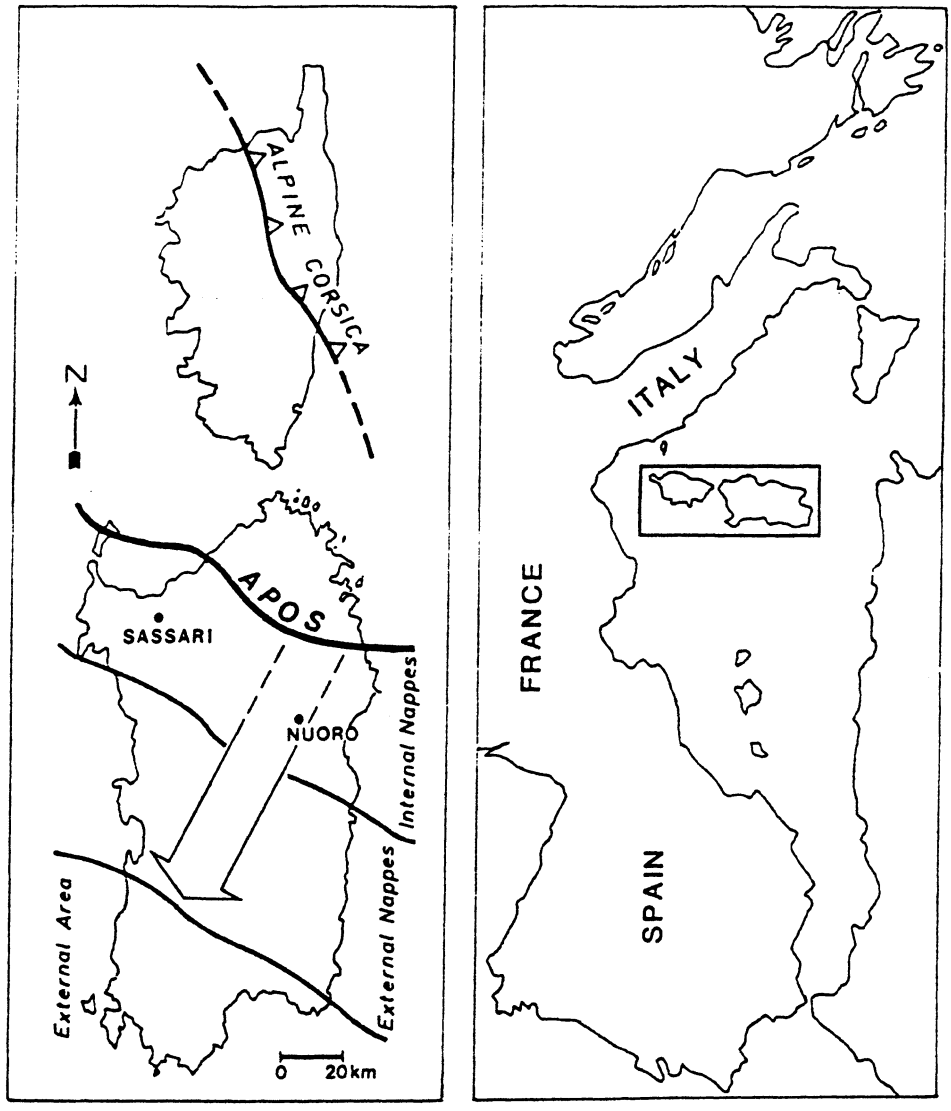

Figure 1. Main structural elements of the Sardinian-Corsican Variscan Massif. Arrow indicates tectonic transport of nappes outcropping in central-northern Sardinia. Middle-late Ordovician magmatic complexes occur in the nappe zone. APOS: Asinara-Posada Oceanic Suture. NE Corsica is characterized by the occurrence of Mesozoic-Cenozoic Alpine chain. See text for further explanations.

A strong magnetic anomaly along the APOS (Cassano *et al.*, 1979) is probably connected to important buried mafic bodies, (Fig. 2), thus suggesting a crustal-scale structure formed by the convergence and collision of two ancient passive margins. Consequently, the mafic rocks exposed at the surface and inferred from geophisics to be buried at depth are presumed to represent fragments of oceanic crust, emplaced along the contact between the two margins.

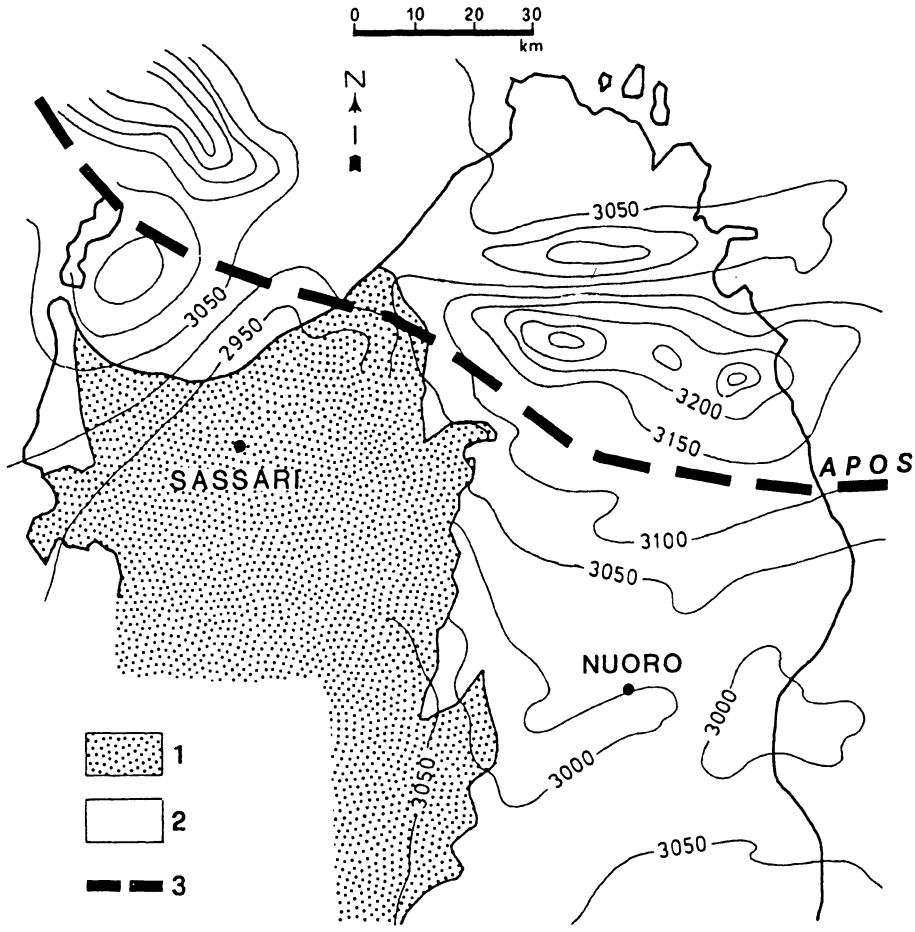

The area south of the APOS represents the southern paleomargin, overthrust by the northern one. In fact, this area is characterized by the occurrence of a wide nappe zone (NZ) in which the allocthon units show a tectonic transport toward a southern external zone (Fig. 1), and a low to medium-grade Barrovian metamorphism developed during Variscan times (Carmignani *et al.*, 1981; Del Moro *et al.*, 1991).
The northern margin, represented by northern Sardinia and Variscan Corsica, is composed of Variscan metamorphic rocks (radiometric dating: Beccaluva *et al.*, 1985). However, in NW Corsica a pre-Cambrian migmatite complex (Carmignani *et al., 1992)* is unconformably overlain by an early Paleozoic succession (Baudélot *et al.*, 1977) affected by very low-grade Variscan metamorphism (Fig. 3).

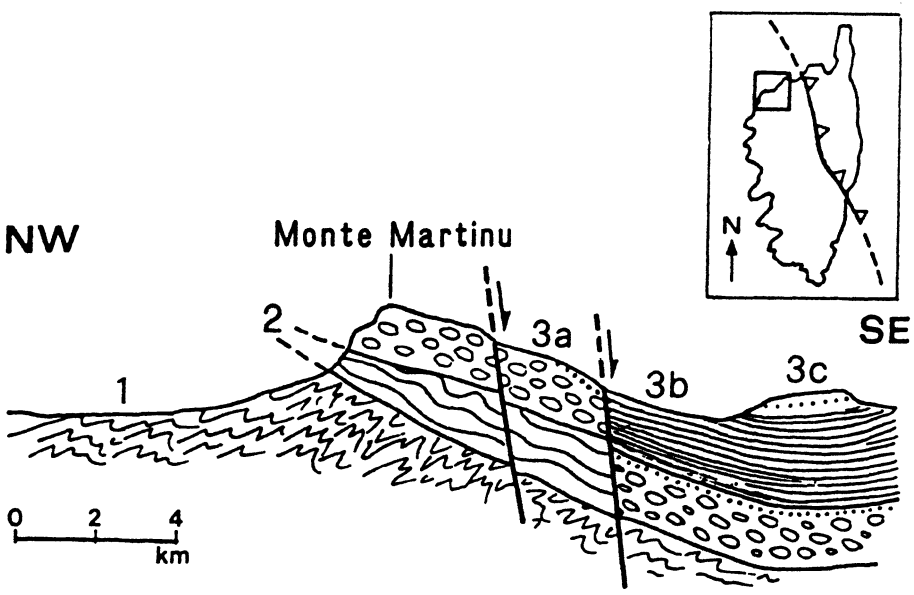

Figure 3. Geological setting of NW Corsica, after Baudélot *et al.*, 1977, simplified. 1: basement of pre-Cambrian age; 2: middle Cambrian-early Ordovician siltite and sandstone. 3: late Ordovician-Silurian deposits (3a: conglomerate; 3b: siltite and shale; 3c: sandstone). Middle Ordovician compression tectonics are suggested by folding in middle-Cambrian-early Ordovician sequences and by occurrence, in overlying middle-late Ordovician sediments, of basal conglomerate and, in 3b, of early Ordovician reworked microfossils.

A Sm/Nd whole rock isochron on an amphibolite from the APOS yields an age of 960 ± 93 Ma for the protolith (Cappelli *et al.*, 1991-92).

The middle Ordovician magmatic rocks of central Sardinia (Fig. 7) are represeted by subaerial and submarine volcanics, ranging from rhyolite to sub-alkaline basalt (Memmi *et al.*, 1982). The late Ordovician volcanics, outcropping in central-northern Sardinia, are represented by alkali basalt. Using these data, Carmignani *et al.*, (1992) proposed a geodynamic cycle implying opening of an oceanic area, along the present APOS, during pre-Cambrian times and B-type subduction processes, accompanied by the formation of a magmatic arc in central Sardinia, during the middle Ordovician.

This proposed cycle conflicts with several data resulting from recent studies. The aim of this paper is to propose a geodynamic cycle consistent with all available data.

1. The Variscan cycle

1.1. EARLY-MIDDLE CAMBRIAN

The oldest deposits outcrop in southern Sardinia (Fig.4 A). In this area, an early Cambrian succession, consisting of terrigenous sequences which grade upward into Archeocyat and Trilobite-bearing carbonate sequences (*a* in Fig. 4 A), covers a pre-Cambrian crystalline basement. The middle Cambrian is represented by a carbonate platform (*b* , in Fig. 4A).

All of these sediments were deposited in a continental shelf environment characterized by delta systems evolving in oolite lagoonal and arid tidal-flat areas (Boni and Cocozza, 1978; Boni and Gandin, 1980; Cocozza, 1980; Gandin, 1987). This indicates that southern Sardinia was affected, during this long period, by a very slow subsidence.

1.2. MIDDLE CAMBRIAN-EARLY ORDOVICIAN

During this time, extension tectonics affected the whole SCM. Contemporaneous with extension are intrusion of alkaline granitoids (Délaperrière and Lancélot, 1989) and sedimentation of epicontinental terrigenous deposits (Albani *et al.*, 1985; Martini *et al.*, 1991; Minzoni, 1988; 1992) showing different thickness in adjoining areas (*c*, in Fig. 4 A).

This indicates that sedimentation was governed by normal growth faults forming, throughout the SCM, a horst-graben structure.

This paleogeographic setting conflicts with the occurrence of an oceanic area along the APOS before early-middle Ordovician times.

1.3. MIDDLE - LATE ORDOVICIAN

The middle Ordovician is characterized by a sudden, strong tectonic activity, intense magmatism, and sedimentation (Fig. 4). Compression and extension tectonics developed contemporaneously throughout SCM. The compression tectonics are mainly expressed by the "Sardinian Phase" folding in southern Sardinia (Fig 4B). According to Baudélot *et al.*,

(1977), similar deformation occurs in northern Corsica (Fig. 3 and 4B). The extension tectonics are documented by the effusion in central Sardinia (Memmi *et al.*, 1982) of abundant acidic, intermediate and basic volcanics (Fig.7), showing calc-alkaline characteristics, and especially by the deposition (Minzoni, 1988; 1992) of a thick turbidite trough-filling succession in central- northern areas of the island (Fig. 4B). On the contrary, central-southern Sardinia and northern Corsica (Fig. 4B) was characterized by deposition of epicontinental terrigenous-carbonate sediments (Carmignani *et al.*, 1992).

The late Ordovician is characterized by sedimentation of epicontinental deposits in central-southern Sardinia and northern Corsica, while central-northern Sardinia was still receiving turbidite sedimentation (Fig. 4B). The magmatism is represented by alkali basalt (Fig.7) in several areas of central-northern Sardinia (Memmi *et al.*, 1982).

These data indicate that extension tectonics are the most important aspect of middle-late Ordovician geodynamics and that they developed with increasing intensity from central Sardinia northward. This suggests that the APOS represents maximum extension of the geodynamic system and the oceanic area opened from middle Ordovician times (Fig. 4B).

1.4. SILURIAN-EARLY DEVONIAN

During this time, the SCM was characterized, (Carmignani *et al.*, 1981), by deposition of Graptolith-bearing black-shale and Tentaculite-bearing carbonate sequences (Fig. 4C).

1.5. MIDDLE DEVONIAN-EARLY CARBONIFEROUS

This time period is characterized by convergence and collision of the passive margins formed from middle Ordovician onwards (Fig. 4C, D). These processes are documented by two tectonic-metamorphic events.

An early event, related to subduction, is indicated by the occurrence of eclogitic relicts in the amphibolites scattered along the APOS (Carmigani *et al.*, 1992). In Sardinia, this metamorphism has not been dated; however, it occurs in several European Variscan oceanic sutures, where radiometric dating yields ages between 430 and 380 Ma (Peucat and Cogné, 1977; Peucat *et al.*, 1982; Ducrot *et al.*, 1983; Peucat, 1986; Paquette *et al.*, 1985; Quadt and Gebauer, 1988); the eclogitic metamorphism has been interpreted as related to subduction stage (Matte, 1986; Bodinier *et al.*, 1986; Bouchardon *et al.*, 1989; Pin, 1990; Pin and Marini, 1993).

A subsequent event, connected to collision, is documented by the Barrovian metamorphism dated at about 350 Ma in central Sardinia (Del Moro *et al.*, 1991).This metamorphism, of low to medium grade, increases downward and especially northward (from NZ to APOS) from greenschist to amphibolite facies. It was sincronous with deformation that is characterized by formation of isoclinal south-facing recumbent folds, affected by pervasive schistosity and strong stretching lineations, and by emplacement of nappes. During the thrusting of the northern margin over the southern

one, relics of eclogitic oceanic crust were trapped along the APOS. The collision caused crust-mantle detachments, crustal stacking, migration of deformation, metamorphism from northern Sardinia southward and emplacement of allocthon units in the NZ (Fig. 4D).

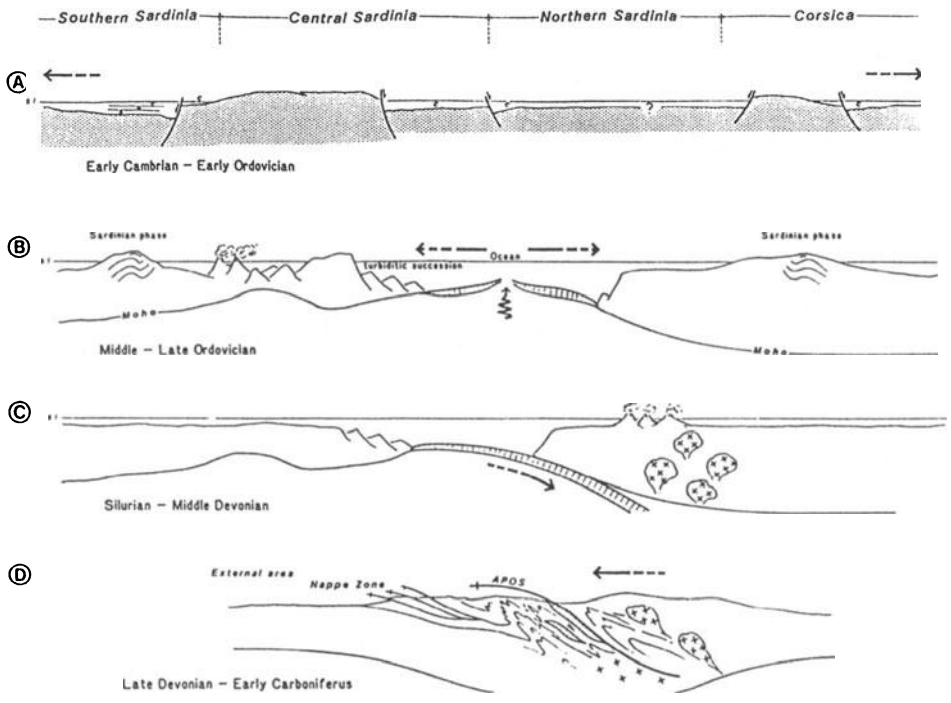

Figure 4. Proposed geodynamic cycle in Sardinian-Corsican Massif. APOS: Asinara-Posada Oceanic Suture. Compression tectonics, indicated by folding of the"Sardinian phase", developed contemporaneously with extension tectonics, documented by effusion of volcanics in central Sardinia and by sedimentation of turbidite succession in central-northern Sardinia. See text for further explanation.

On the basis of their litho-stratigraphic characteristics, the nappes may be divided into internal and external, both indicating different paleogeographic domains developed along the southern paleomargin. The internal nappes mainly consist of middle-late Ordovician turbidite sequences deposited in the internal basinal area, formed south of the APOS. On the contrary, the external nappes are composed of middle Cambrian-early Ordovician terrigenous succession grading upward into middle-late Ordovician epicontinental sequences deposited in external domains. Therefore, the nappe emplacement is the result of inversion tectonics, which was realized by exploiting of middle Cambrian-early Ordovician (external nappes) or middle-late Ordovician normal faults (internal nappes).

The external area, in southern Sardinia, is a fold-thrust belt characterized (Carmignani *et al.*, 1981; Minzoni, 1992) by medium to steeply-dipping axial plane cleavage. The Variscan metamorphism is of low grade and increases downward. The lowermost structural levels are characterized by sub-horizontal schistosity, greenschist facies metamorphism, tight isoclinal recumbent folds and detachment of the Paleozoic successions from the pre-Cambrian crystalline basement.

1.6. MIDDLE-LATE CARBONIFEROUS

During the middle-late Carboniferous, the sediments eroding from the front of the developing mountain chain and accumulaing in the foreland, were strongly deformed and overthrust by the southward advancing nappes (Culm-type flysch). The latest stage of the Variscan cycle is represented by the emplacement of abundant granitoids. The plutonism ended about 275 Ma ago; it probably took place during post-orogenic crust extension at least partially concomitant with the development of the late Carboniferous-early Permian molasse basins (Carmignani *et al.*, 1992).

2. Discussion and conclusions

The data presented here indicate that the oceanic area along the present APOS began to form from middle Ordovician times. In fact, only from the middle Ordovician did a basin area form in northern Sardinia. In this framework, the radiometric age of the APOS amphibolite protolith (960 ± 93 Ma) is probably due (as suggested by Pin and Marini, 1993, for other areas of the European Variscan chain) to crustal contamination.

The formation of the basinal area in northern Sardinia (and therefore the opening of the ocean along the APOS) was quasi-contemporaneous with the "Sardinian Phase" compression structure in southern Sardinia. This is consistent with deformation along a mega-shear zone. The oceanic area of the APOS may be considered as a pull-apart basin formed by transtension while the "Sardinian Phase" folding is probably the result of transpression.

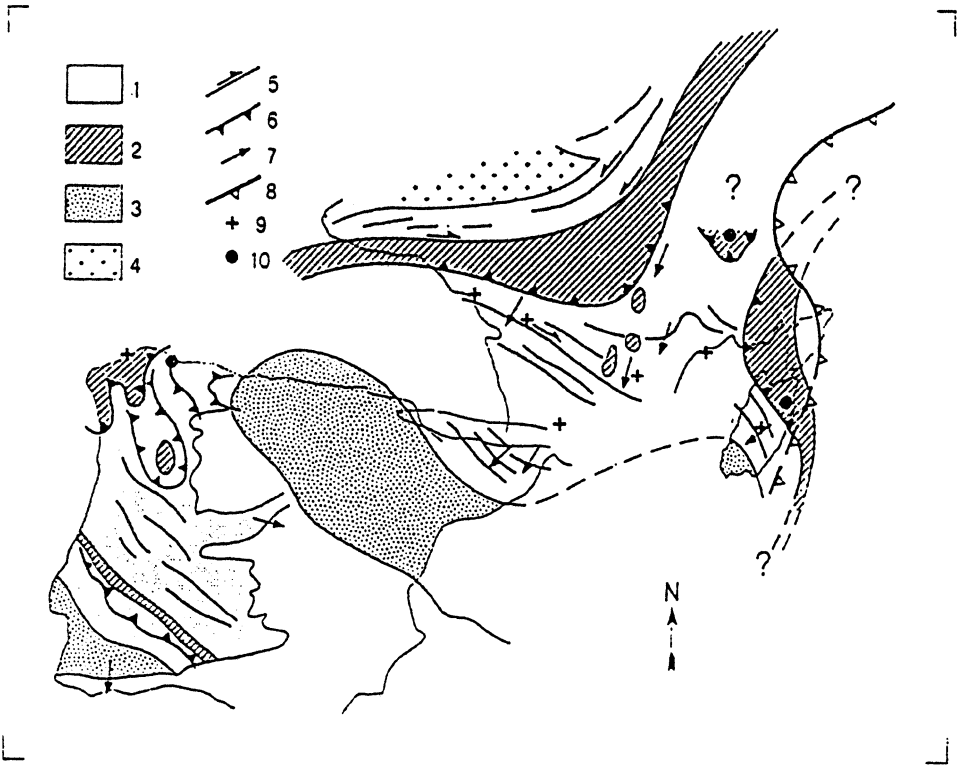

Figure 5. Central-Southern Europe Variscan Chain (modified and simplified from Matte 1986, Franke 1989,Pin and Marini, 1993).1 : nappe and external zone. 2: innermost nappe zone, with ophiolitic remnants. 3: outher foredeep basin. 4: crystalline basement. 5: strike-slip faults. 6: main overthrust. 7: nappe tectonic transport. 8: Alpine chain. 9: early-middle Ordovician "bimodal" magmatics. 10: ophiolitic suites.

In this framework, the middle Ordovician magmatic rocks outcropping in central Sardinia (Fig. 7) cannot represent, in spite of their calc-alkaline characteristics, an arc related (as proposed by Carmignani *et al.*, 1992), to subduction processes; in fact, they are closely connected to the transtension tectonics leading to opening of the oceanic area. In this way, the middle Ordovician magmatic rocks of cental-northern Sardinia can be related, as the "bimodal" magmatics of the European Variscan Chain (Pin and Lancélot, 1982; Pin and Marini (1993), to extension tectonics marking the

break-up of continental crust and the subsequent opening of oceanic areas (Fig. 5).
The production of alkali basalt during the late Ordovician in central-northern Sardinia (Fig. 7) can be connected to crustal thinning and initiating rifting in an ensialic extension setting.

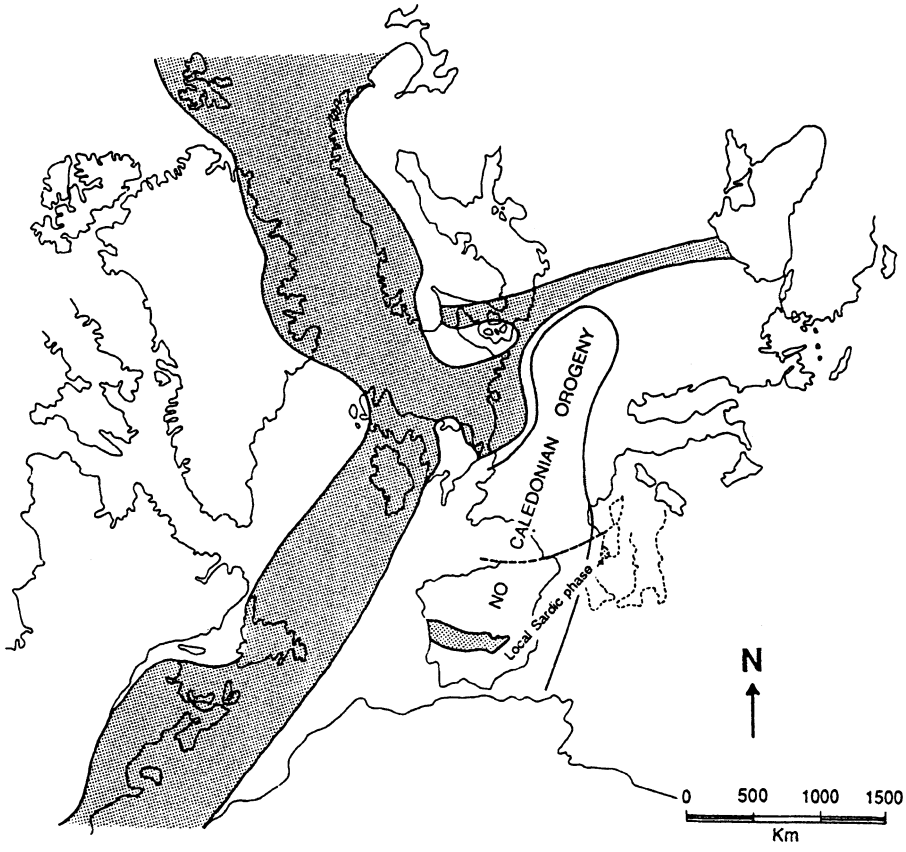

Figure 6. Area affected by Caledonian orogenesis and "Sardinian Phase" (after Zwart and Dornsiepen 1980).

Like the European Variscan sutures, the APOS is characterized by a scarcity of oceanic remnants. This may be due to dynamics that led to the opening of several transtension pull-apart oceanic areas, along a mega-shear zone (Vai, 1991), formed in connection with the Caledonian orogeny (Fig. 6). This may also explain the extraordinary geometrical complexity of

the European Variscan belt, its unusual width and its space-time development; indeed, the oceanic areas in the Variscan Europe were opened during early Ordovician times (Pin and Marini, 1993, with references), while the present APOS was opened starting from the middle Ordovician.

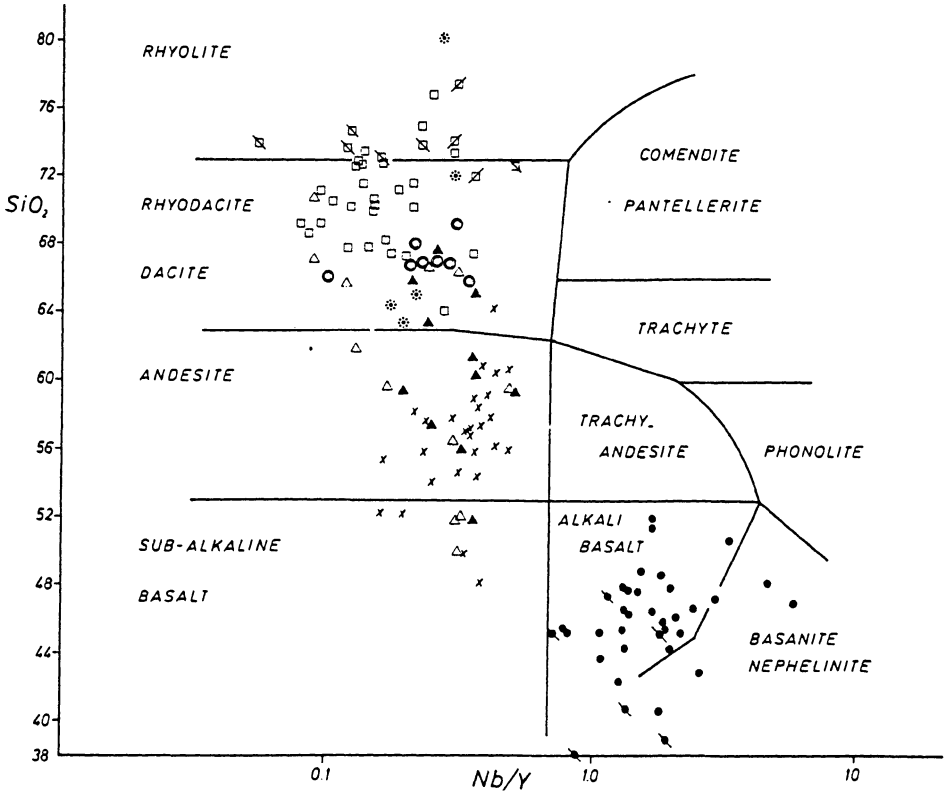

Figure 7. SiO2-Nb/Y diagram for middle-late Ordovician magmatics of central-northern Sardinia. The middle Ordovician is characterized by effusion in central Sardinia of volcanics ranging from rhyolite to sub-alkaline basalt. The late Ordovician is characterized by effusion in central-northern Sardinia of alkali basalt. Symbols indicate samples from different areas of central-northern Sardinia.

Acknowledgements

This research was founded by grants from the italian M.U.R.S.T.
I thank my son Marcello for useful discussions and the unknown reviewers for critical yet constructive comments

References

Albani, R., Di Milia, A., Minzoni, N. and Tongiorgi M. (1985) Nuovi dati palinologici e considerazioni geologiche sull'età delle Arenarie di Solanas (Cambro-Ordoviciano; Sardegna centrale), *Atti Soc.Tosc. Sc. Nat. Mem.* **91**, 1-20.

Baudelot, S., Doubinger, J., Durand-Delga, M. and Vellutini P.(1977) Caractéristiques et age des cinq cycles palézoiques du Nord-Ouest de la Corse, *Bull. Soc. Géol. France* **18**, 1221-1228.

Beccaluva, L., Civetta, L., Macciotta, G. and Ricci, C. A. (1985) Geocronology in Sardinia: results and problems, *Rend. Soc. It.Miner. Petr.* **40**, 57-72.

Bodinier, J. L.,Giraud, A., Dupuy, C., Leyreloup, A. and Dostal, J. (1986) Caractérisation géochimique des métabasites associées à la suture hercynienne . Massif céntral française et Chamrouse (Alpes), *Bull.Soc. Geol. France* **1**, 115-123.

Boni, M. and Cocozza, T. (1978) Depositi mineralizzati di canale di marea nella Formazione di Gonnesa del Cambrico inferiore della Sardegna, *Giornale di Geologia* **43**, 1-20.

Boni, M., and Gandin, A. (1980) Analisi sedimentologica e giacimentologica del passaggio Formazione di Gonnesa-Formazione di Cabitza del Cambriano sardo, *Mem.Soc.Geol.It.* **20**, 453-459.

Bouchardon, J.L., Santallier D., Briand B., Menot R. and Piboule M. (1989) Eclogites in the French Paleozoic Orogen: geodynamic significance, *Tectonophisics* **169**, 317-322.

Cappelli, B., Carmignani, L., Castorina, F., Di Pisa, A., Oggiano,G. and Petrini, R. (1991-1992) A Hercynian suture in Sardinia: geological and geochemical evidence, *Geodynamica acta* **5**, 101-118.

Carmignani, L., Cocozza,T., Minzoni,N., Pertusati, P.C.and Ricci C.A (1979) E' la Corsica il retropaese della catena ercinica in Sardegna?, *Mem. Soc. Geol. It.* **20**, 47-75.

Carmignani, L., Cocozza, T., Minzoni, N. and Pertusati P.C. (1981) Structural and paleogeographic lineaments of the Variscan cycle in Sardinia, *Geologie en Miynbown* **60**, 171-181.

Carmignani, L., Barca, S.,Cappelli, B., Di Pisa, A., Gattiglio, M., Oggiano, G. and Pertusati,P., C. (1992) A tentative geodynamic model for the Hercynian basement of Sardinia. Contribution to geology of Italy, IGCP 276, *Newsletter* **5**, 61-82.

Cassano, E., Marcello A., Nannini, R., Pretti, S., Ranieri, G., Salvadori R. and Salvadori, I.,(1979) Rilievo aereomagnetico della Sardegna e del mare circostante, *Ente Minerario Sardo* **3-4**,7-30.

Cocozza, T. (1980) The Cambrian of Sardinia, *Mem.Soc.Geol.It.*. **20**, 163-187.

Délaperrière, E. and Lancélot J. (1989) Datation U-Pb sur zircons de l'Orthogneiss du Capo Spartivento (Sardaigne, Italie), nouveau témoin d'un magmatisme alcalin Ordovicien dans le Sud de l'Europe, *C.R.Acad.Sci.Paris* **309**, 2, 835-842.

Del Moro, A., Di Pisa, A., Oggiano, O. and Villa I.M. (1991) Isotopic ages of two cotrasting tectono-metamorphic episodes in the Variscan chain in northern Sardinia (1991), Abstract, Geologia del Basamento Italiano, Siena 21-22 marzo 1991.

Ducrot, J., Lancélot, J.R. and Marchand J. (1983) Datation U-Pb sur zircons de l'éclogite anté-hércynienne de l'Europe occidentale, *Earth Planet. Sc. Lett.* **62**, 385-394

Franke, W. (1989) Variscan plate tectonics in central Europe-current ideas and open questions,*Tectonophisics* **169**, 221-228.

Gandin, A. (1987) Depositional andpaleogeographic evolution of Cambrian in S-W Sardinia: IGCP 5, *Newsletter* **7**,151-166.385-394.

Ghezzo, C., Memmi,I.and Ricci,C.A. (1980) Unevento granulitico nella Sardegna nord-orientale, *Mem. Soc. Geol. It.* **20**, 23-38.

Martini, I.P.,Tongiorgi, M., Oggiano, G. and Cocozza, T. (1991) Ordovician alluvial fan to marine shelf transition in SW Sardinia, Western Mediterranean sea: tectonically ("Sardic phase") influenced clastc sedimentation, *Sedimentary Geology* **72**, 97-115.

Matte, P. (1986) La chaîne varisique parmi les chaînes paléozoiqes périatlantiques, modèle d'évolution et position des blocs continentau au Permo-Carbonifère, *Bull.Soc.Geol.France* **8**, 9-24.

Memmi, I., Barca, S., Carmignani, L.,Cocozza, T., Elter, F., Franceschelli, M., Gattiglio, M., Ghezzo, C., Minzoni, N., Naud, G., Pertusati, P.C. and Ricci C.A. (1982) Further geochemical data on the pre-Hercynian igneous activities of Sardinia and their geodynamic significance. IGCP 5, *Newsletter* **5**, 87-91.

Minzoni, N. (1988) Geologia strutturale della zona di Gadoni-Funtana Raminosa (Sardegna centrale), *Mem. Sc. Geol. Padova* **40**, 195-201.

Minzoni, N. (1992) The geodynamic evolution of the Sardinian-Corsican and Calabrian-Peloritan Hercynian Massifs. *Basement tectonics* **10**, Kluwer Academic Publishers Dordrecth, pp. 333-343.

Paquette, J.L., Peucat, J.J., Bernard-Griffiths, J. and Marchand, J. (1985) Evidence for old Precambrian relics shown by U-Pb zircon dating of eclogites and associated rocks in the Hercynian belt of South Brittany, France, *Chem. Geol.* **52**, 203-216.

Peucat, J.J. (1986) Rb-Sr and U-Pb dating of the blueschist of the Ile the Groix, *Geol.Soc.Am.Mem.* **164**, 229-238.

Peucat, J. and Cogné J. (1977) Geocronology of some blueschists from Ile de Groix (France), *Nature* **28**, 131-132.

Peucat, J., Vidal, P., Godard, G. and Postaire, B. (1982) Precambrian U-Pb zircon ages of eclogites and garnet pyroxenites from Brittany (France): an old oceanic crust in the W European Hercynian Belt, *Earth Plan. Sc. Lett.* **60**, 70-78.

Pin, C. (1990) Variscan oceans: ages, origins and geodynamic implications inferred from geochemical and radiometric data, *Tectonophysics* **177**, 215-227.

Pin, C. and Lancélot, J. (1982) U-Pb dating of an early Paleozoic bimodal magmatism in the French Massif Central and its further metamorphic evolution, *Contr. Miner. Petrolog.* **79**, 1-12.

Pin, C.and Marini, F. (1993) Early Ordovician continental break-up in Variscan Europe: Nd-Sr isotope and trace element evidence from bimodal igneous associoations of the southern Massif Central, France, *Lithos* **29**, 177-196.

Quadt, A. and Gebauer, D. (1988) Sm/Nd, U/Pb and Rb/Sr dating of high-pressure ultramafic to felsic rocks from the Moldanubian area of NE Bavaria (FRG) and the Saxonian Granulite massif (GDR). Abstract, Conf. Bohemian Massif (Prague), 71.

Vai, G.B. (1991) Paleozoic strike-slip rift pulses and paleogeography in the circum-Mediterranean Tethian realm, *Paleogeography, Paleoclimatology , Paleoecology,* **87**, 232-252.

Zwart, H. J. and Dornsiepen, U. F. (1980) The Variscan and pre-Variscan tectonic evolution of central and western Europe; a tentative model. Société Géologique du Nord,Colloque C6, 26 CGI, 227-232.

GEOLOGICAL AND GEOPHYSICAL EXPLORATION FOR URANIUM MINERALIZATION IN THE EL-EREDIYA PROSPECT AREA, CENTRAL EASTERN DESERT, EGYPT.

SAID I. RABIE, AHMED A. ABDEL-MEGUID
AND ASSRAN S. ASSRAN
Nuclear Materials Authority, P. O. Box 530 Maadi, Cairo, Egypt.

Abstract

Ground geologic, structural, radiometric, magnetic, and horizontal-loop electromagnetic data (surface and mining) have been applied to follow the surface and downward extension of the uranium mineralization showings of El-Erediya prospect area, located in the Central Eastern Desert, Egypt.

El-Erediya uranium mineralization is associated with jasperoid silica veins hosted in the El-Erediya granite which is one of the later phase plutons of the Egyptian granitoids (550-590 Ma). The silica veins fill tensional fractures related to ENE normal faulting and to its feather fractures. Geologic and structural investigation of the area indicate a supergene origin for silica veins and uranium mineralization. Firstly, a silica rich solution altered the granite and leached its uranium later and precipitated it in open ENE fractures along with iron sulfides. A second phase of uranium mobilization and concentration was accompanied by tectonic rejuvenation of ENE fractures. During this phase uranium becomes more concentrated in a second jasperoid silica solution which cements the brecciated early silica veins and the host granite at contacts. A third remobilization process is indicated by surface leaching and alteration of the early formed pitchblende and iron sulfides and redistribution of secondary uranium mineralization and hematitization along different fractures and alteration zones.

Integration of magnetic data with bedrock geology led to the construction of a basement tectonic map which aided in identifying mineralization for the area under consideration. The interpretation of the horizontal-loop electromagnetic data of the surface profile (00 NS) and the mining profiles indicate the presence of conductive zones. These zones are mainly associated with the jasperoid veins, shear zones, and fault zones. The conductive parameters such as location, width, dip, depth, and conductivity thickness were estimated for each conductive zone, as averaged from the utilized four frequencies.

The present study suggests a supergene origin for El-Erediya U-mineralization which should be considered in future development of this occurrence.

1. Introduction

El-Erediya prospect area (Fig. 1) is located at about 30 Km south of Qena-Safaga road at El-Faroukiya station (Km 85 from Qena), and forms the southwestern part of Gabal (G) El-Erediya granitic mass along Wadi (W) El-Erediya.

Radioactive anomalies and uranium mineralization have been discovered in the area by airborne radiometric survey (Ammar, 1973) and by ground survey (El-Kassas, 1974). These studies revealed that the recorded radioactive anomalies in the prospect area are caused by secondary uranium mineralization associated with jasperoid veins. They also demonstrated that important radioactive showings are associated with a set of parallel NE-SW trending fractures which cut across the southwestern part of the granitic mass.

An exploratory mine was excavated at the Wadi level to follow the mineralization (Fig.2). Detailed geologic mapping of the mine (El-Tahir, 1985) revealed a relative increase in U- mineralization represented mainly by secondary uranium minerals and by some sulfide minerals in highly fractured granitic and/or jasperoid veins. He suggested that a significant mineral deposits may be reached in the reduction zone.

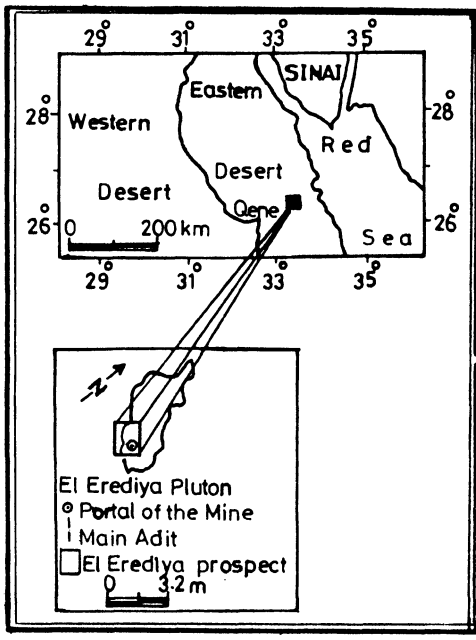

Figure 1. Location map of G. El-Erediya prospect area, Central Eastern Desert, Egypt.

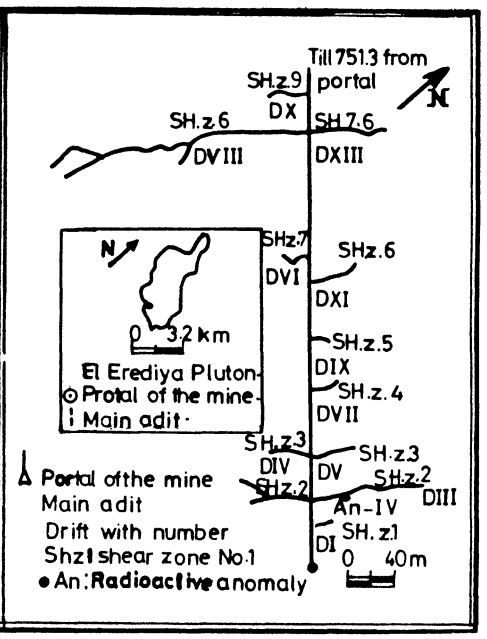

Figure 2. Plan of the executed exploratory mining works in El-Erediya prospect area (After El-Tahir, 1985).

Subsequent ground geophysical investigations are currently being executed in the area,(Rabie et al.,1992) where early results recommended further surface and mining geophysical activities. The present work reports detailed geological and structural

mapping of the prospect area, ground radiometric, magnetic and horizontal-loop electromagnetic surveys. These investigations were conducted to explore any radioactive anomalies and any subsurface extensions of the mineralization below the mine level and to closely investigate the relations between the discovered mineralization, and the geological and structural features of the area. All these studies have been carried out on a base topographic (Fig.3) and tachometric maps with a fixed ground grid 20 X 50 ms prepared for this study.

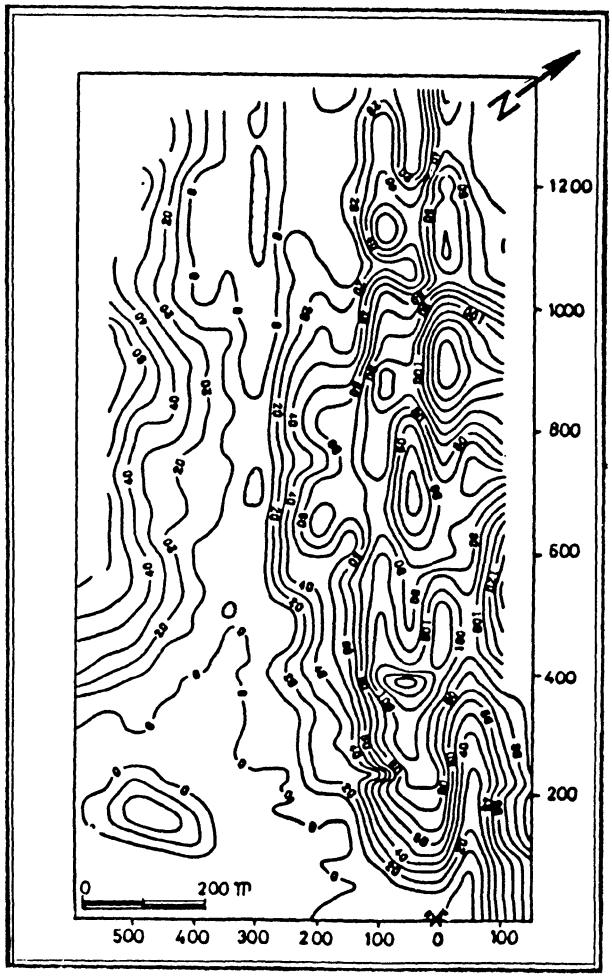

Figure 3. Topographic map of El-Erediya prospect area, Egypt; contours in meters above wadi level, contour interval =10 m.

2. Geological Investigations

2.1. GEOLOGY OF THE AREA

El-Erediya granite mountain is part of a large younger granitic batholith extending northwards and belongs to the Egyptian younger granitoids which intruded between 550-590 Ma (El-Shazly et al., 1980). These granites, especially their late-more siliceous- phases, are characterized by high radioactivity (Hussein and El-Kassas, 1979; Abdel Meguid, 1986). El-Erediya granitic mass has an oval shape extending NW with length of about 6.5 km and width of about 2.5 km. It intruded metavolcanics which have been thermally metamorphosed to hornfelsic amphibolites at the contacts and in the remnant roof pendant. The pluton was subsequently altered mainly by kaolinitization, silicification, and ferrugination, especially along fractures and shear zones. Structurally the granitic mass is bounded by two parallel NW trending regional faults. The granite mass is also cut by minor faults trending NE, NNE, N-S, and NNW in addition to local fractures, joints, and shear zones with the same trends. Topography and uranium mineralization in the prospect area are mainly governed by the NW fractures and its feathers (Figs. 3 & 4).

Several pegmatite and aplite dikes which are related to the granitic magma cut through the pluton and through the country rocks. The granite is also cut by basic and lamprophyric dikes. Several jasperoid silica veins fill fractures in the shear zones. Uranium mineralization is associated with these veins. The following is a brief description of these rocks beginning with the oldest.

2.1.1. *Hornfelsic Amphibolite*

These rocks occupy the southwestern and central parts of the area (Fig.4). They are essentially comprised of hornblende and plagioclase feldspar with subordinate chlorite and orthoclase. Minor constituents include actinolitic hornblende and tremolite shreds, bent biotite flakes altered to chlorite, iron oxides, and epidote. Accessory minerals include sphene, ilmenite, and magnetite.

2.1.2. *Pink Granite*

They are composed of (in decreasing order) potash feldspar (orthoclase, orthoclase microperthite, microcline, and microcline microperthite), quartz (subhedral, sieved by zircon, and exhibite bohemae laminae of fluid and solid inclusions), plagioclase (sodic oligoclase and albite and secondary albite), and minor biotite. The accessory minerals are zircon, magnetite, sphene, and ilmenite.

2.1.3. *Pegmatite*

They are of minor abundance and composed of intergrowth of orthoclase with quartz and microcline. Some pegmatite bodies are traced on the geologic map (Fig. 4), while others are so small to be traced at the present map scale.

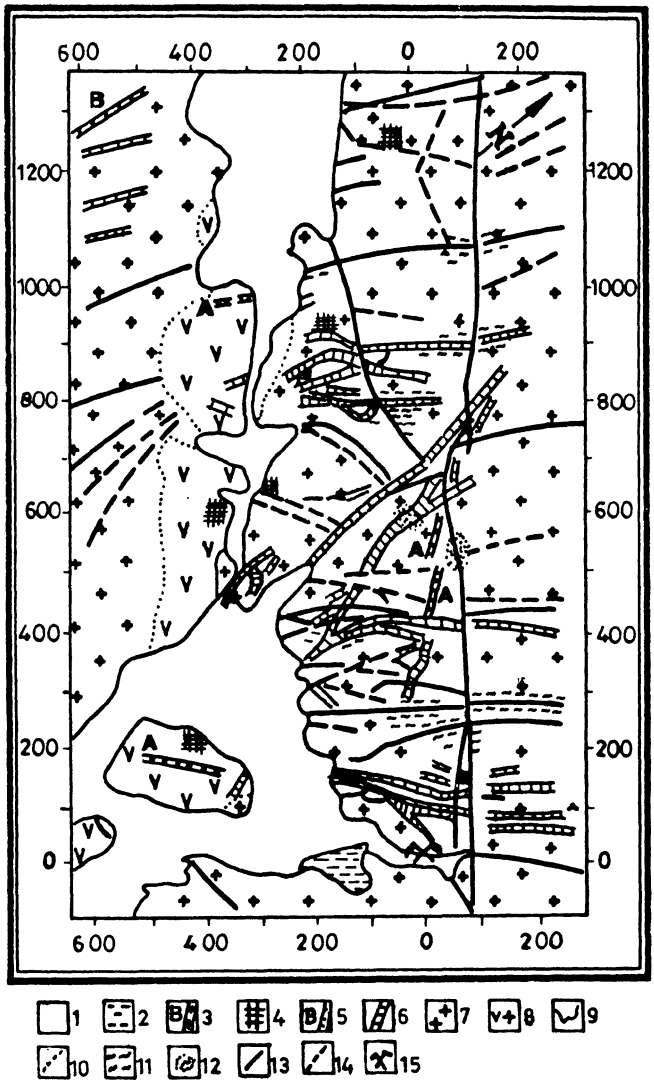

Figure 4. Detailed geological and structural map of El-Erediya prospect area, Egypt; Symbols are: 1. Wadi deposits, 2. Alluvial terraces, 3. Aplite veins, 4. Pigmatite body, 5. Basic dike, 6. Jasperoid vein, 7. Pink granite, 8. Amphibolite, 9. Geologic boundary, 10. Gradational contact, 11. Shear zone, 12. Alteration zone, 13. Fault, 14. Fracture, and 15. Exploratory mine.

2.1.4. *Aplite dikes and veins*

They are more abundant than pegmatites. They can be up to 2 m thick and more than 300 m. long, and trend in both NE and NW directions. Compositionally they are microgranites composed of anhedral quartz, orthoclase, with minor plagioclase and green biotite. Zircon and iron oxides are common accessories in these dikes.

2.1.5. *Basic dikes*

They are rare in the prospect area and composed of basalts and lamprophyres. They are similar to the basic dikes associated with the Mid-Tertiary volcanic activity (El Ramly, 1972). The rocks are composed of equal amounts of plagioclase and amphibole with some biotite, iron oxides and subordinate to rare alkali feldspare and quartz.

2.1.6. *Jasperoid silica veins*

They are the most important rock in the prospect area where the uranium mineralization and mineralized alteration zones are typically related to them. They have a general NE trend (Fig. 5) and branched in other minor trends. Their thickness varies from few centimeters to more than five meters (at the branching zones). Their length can vary from a few meters to more than 500 meters. They are hard , white to deep red -colored silica. At some parts of their contacts, the granite suffered intensive alteration. The jasper and the altered granite are brecciated, fragmented, and cemented with later jasperoid silica solutions that contain iron oxides, black shreds, and sometimes uranium mineralization. Some of the black shreds are formed of carbons (Mohamed, 1989). Generally, these jasperoid silica veins are composed of cryptocrystalline quartz with some scattered relics of anhedral corroded quartz and illite . Anhedral relics of orthoclase and microcline were also described by Mohamed (1989).

2.2. STRUCTURE

Structural analysis of the area was conducted through detailed field mapping of the nature and distribution of faults, fractures, and different types of fracture fillings such as veins and dikes. Special emphasis was placed on their chronological relations and on their relation to the U-mineralization. Figure (5) shows the directional frequency distribution of the measured structures. The most pronounced major structures in the area are the NW faults. These faults control the emplacement of the whole granitic body (Fig. 4). Two movements are traced on this trend. The oldest one, which possibly took place before the emplacement of the granite, is right-lateral and can be correlated to the Najd shear zone in the sense described by Stern (1985) as a single transform shear. After emplacement of the granite, these faults were rejuvenated as normal faults with tension fractures in which the post granitic aplite dikes intruded. The first movement suggest a NNW-SSE compression while the second movement suggest a N30°E-S30°W tension and vertical compression. The presence of the same dikes in the N30°E indicate that the release of the tension σ_3 after fracturing caused another perpendicular tension in the N60°W where permutation exist between σ_2 and σ_3 while σ_1 still vertical.

The second episode is related to the jasperoid veins and to the Tertiary basic dikes which trend in a NNW direction. Presumably this is related to the earliest start of the Red Sea tectonics. The NNW to NS normal faults and open fractures, where the basic dikes and the later jasperoid silica veins were emplaced, represent an ENE extnsional event. The release of the tension σ_3 due to rock yielding, caused permutation between σ_2 and σ_3 which changed the driving tension from the ENE to the NNW. This caused

the ENE normal faults and tensional fractures where another jasperoid veins were emplaced. These normal faults are rejuvenated several times and uranium mineralization were remobilized and concentrated along them.

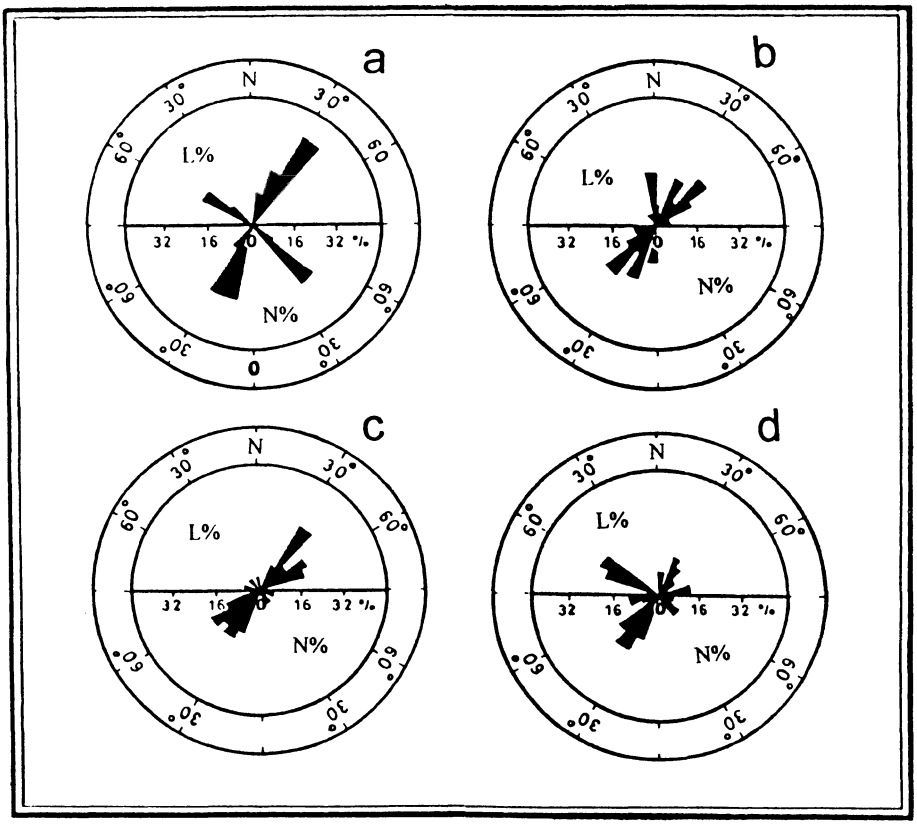

Figure 5. Rose diagrams showing the directions and frequency distribution of lengths and numbers of aplite veins (a), jasperiod veins (b), fractures (c), and faults(d).

2.3. ALTERATION AND U-MINERALIZATION

El-Erediya granitic mass is typically bleached and altered to varying degrees, but most intensive along major fracture zones and contacts with jasperoid veins (Fig.4). Silicification, kaolinitization, and hematitization are the most common alterations along major and minor fractures. Silicification is the earliest and most important. It started with fracture fillings as white silica veins with few pyrite crystals. The granite is bleached along these fractures. The second phase of alteration is indicated by rejuvenation of these fractures as normal faults and by brecciation of the early silica veins and the contact granite. A new uranium-rich red silica solution subsequently cemented the breccia and degraded the early formed pyrites to iron oxides. The contact granites were intensively altered by kaolinitization, sericitization, and hematitization

along parts of early silica veins and fractures. In some zones, the altered granite was intensively silicified and highly radioactive.

Alteration of pitchblende and iron oxides indicates a third alteration event and redistribution process which leached uranium from some of the altered zones, especially the friable unsilicified ones, while the original mineralization is preserved in silicified zones. Most of the high uranium concentrations are associated with the second alteration phase in the cementing red silica of the brecciated contacts, and with the third phase in the alteration zones at the jasperoid veins intersections with the secondary fractures. The U-mineralization in these zones are essentially primary pitchblende associated with pyrite and/or secondary uranophane with some hematitized iron oxides.

The origin of silica veins and uranium mineralization in the El- Erediya area, and in the other similar areas in the Eastern Desert, can be depicted from the previous geological features. The presence of carbon shreds in the second silica phase may indicate organic materials which suggests a supergene origin for the silica veins and associated U-mineralization. Cryptocrystallization of both silica phases, the presence of primary uranium as pitchblende, and the nature of fillings in open fractures, support the supergene origin for the whole process. In the second phase, the supergene circulating meteoric water gained sulfuric acid from oxidizing pyrite, and then leached uranium and precipitated it with some silica in reduction zones along the reactivated fractures. As a result, uranium concentrated during the second phase in the cementing silica. and later on ,through a similar process, became more concentrated during the third alteration phase

3. Geophysical Survey

3.1. GROUND RADIOMETRIC SURVEY

Total radiometric measurements were carried out systematically on each intersection point of the topographic grid (50x20 m). Special emphasis and detailed work was given to the jasperoid veins (3m or less). The instrument used in the present survey is the Gad-6 spectrometer, Scientrex Ltd., Canada, in conjunction with gamma ray sensor (Model GSP-4). The measurements were reduced by subtracting the background from the measured readings, and the data are presented in the form of a ground total-count radiometric map (Fig.6).

3.1.1. *Qualitative Interpretation*

The total-count radiometric map (Fig.6) is characterized by a relatively higher radiometric level in its eastern part than its western one. It is easy to locate the western border of El-Erediya granitic pluton on the radiometric map where it is indicated by a northwest trending belt of high radiometric contours. The surveyed area possesses a wide range of radioactivity varying from about 9.2 to more than 1450 Ur. Some of the high radiometric anomalies are circular in shape reflecting uranium mineralization at the intersection of the NW tectonic trend with the NE and with the ENE trends while

others are elongated and oriented in the NE to ENE trend parallel to the jasperoid veins. The lowest radiometric levels are located in the southwestern part of the area and are associated with the amphibolite rocks.

The radiometric contour lines have shown some interesting structural features and some of the steep radiometric gradients take the NE and ENE directions. The structural elements, as interpreted from the radiometric map, have been correlated with the fault system visible on the detailed geological and structural map of the area (Fig.4).

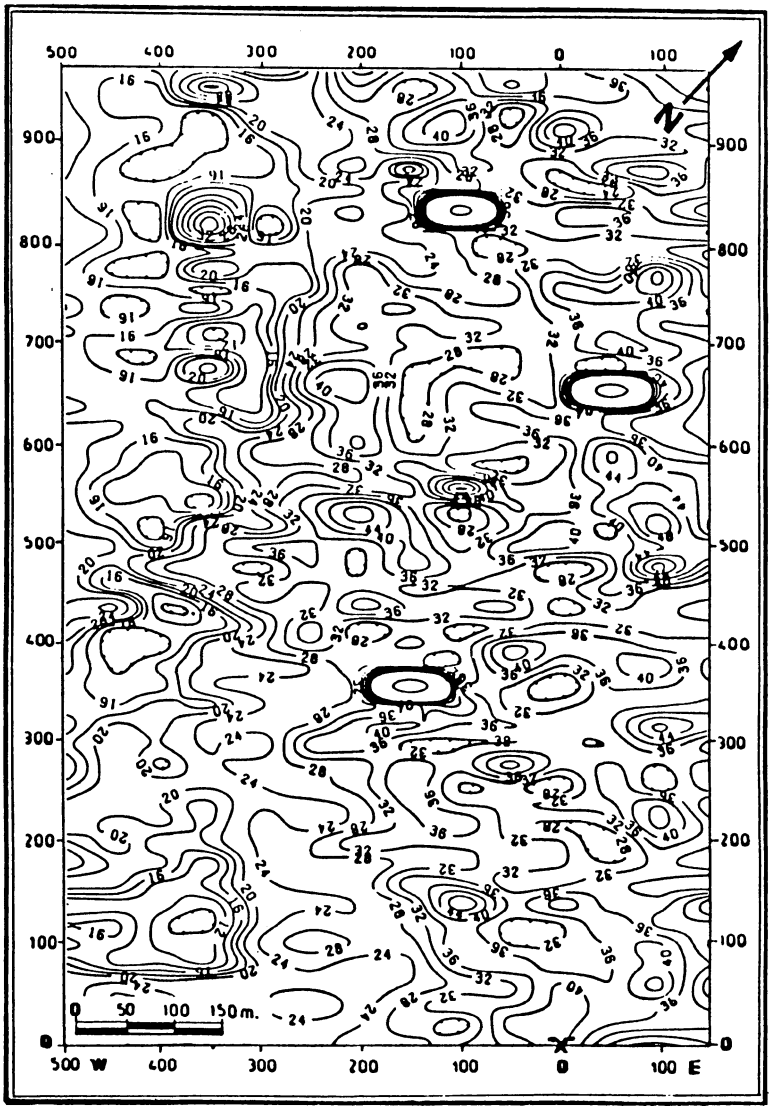

Figure 6. Ground total-count radiometric contour map in Ur units, El-Erediya prospect area Egypt; contour interval = 4 Ur.

3.1.2. *Quantitative Interpretation*

From the study of the total-count radiometric map (Fig.6), three main levels of radioactivity are generally distinguished: 1) less than 20 Ur, 2) 20-30 Ur, and 3) more than 30 Ur. These levels, when compared with the detailed geological and structural map, reflect their association with amphibolite rocks, wadi deposits, and pink granites, respectively. The prepared total-count radioactivity unit map (Fig.7) was the subject of quantitative interpretation, in order to give more accurate definition and identification to the outlined interpreted units though the statistical analysis of the recorded total-count radiometric measurements.

The various rock units in the area under study, have been analyzed statistically and interpreted from the exploration point of view, to assist and enhance the geological interpretation of the different rock units, as well as the radiometric anomalies which might exist in the studied area. Accordingly, the statistical analysis parameters as the minimum value, maximum value, mean (X), standard deviation (S) and coefficient of variation (CV%) were calculated, also the theoretical chi-square test value was calculated and frequency histogram was plotted for each radio-litho unit (Fig.8). Also, to check the normality of each rock unit, the coefficient of variation (CV%) is determined. The coefficient of variability is expressed as (S/X), where S^2 is the population variance and X is the population mean. If CV% of a certain unit is less than 100%, the unit exhibits normal distribution. The computations are, thus, proceeded on the raw data with no need of any type of transformation (Sarma and Koch, 1980). Such analysis has been conducted for the units that have been proved to possess normal distribution of their radioactivity measurements through the application of the Chi-square test. The results of statistical analysis has shown that these interpretative units are normal at the 95% level of significance. Although jasperoid veins display anomalous radioactivity, they do not show normal distribution.

Pink granite shows a wide variation in the total-count radioactivity readings. It ranges between 13.1 Ur to 60.4 Ur. The calculated X value of all registered readings is 32 Ur, with S value about 7.8 Ur and CV% value of 24.38 (less than 100%). Also, the calculated chi-square value is 17.69 while the critical chi-square is 19.68. Therefore, this unit exhibits normal distribution.

Amphibolite shows the least radioactivity among the rock units explored in El-Erediya prospect area. The total-count radioactivity ranges between 9.2 Ur and 31.7Ur. The calculated X value is 16.46 Ur, with S value of about 4.26 Ur and CV% value of about 25.88. The calculated chi-square value is 8.34, while the critical chi-square value is 14.07. Therefore, this unit exhibits normal distribution.

Wadi deposits are represented mainly by the alluvial sediments and gravel terraces, derived mainly from granites and metavolcanics. Accordingly, they show different intensities of radioactivity, reflecting their main constituents of various rock fragments. Their radioactivity ranges from 9.3 Ur to 38.7 Ur, and the calculated X is 21.8 Ur, S is 5.2 Ur and CV% is 23.25. The calculated Chi-square value is 7.17, while the critical Chi-square is 18.31. reflecting normal distribution.

Jasperoid veins show a very wide range of the total-count radioactivity ranging between 25.3 Ur and 1450.5 Ur. Therefore, these jasperoid veins were measured and

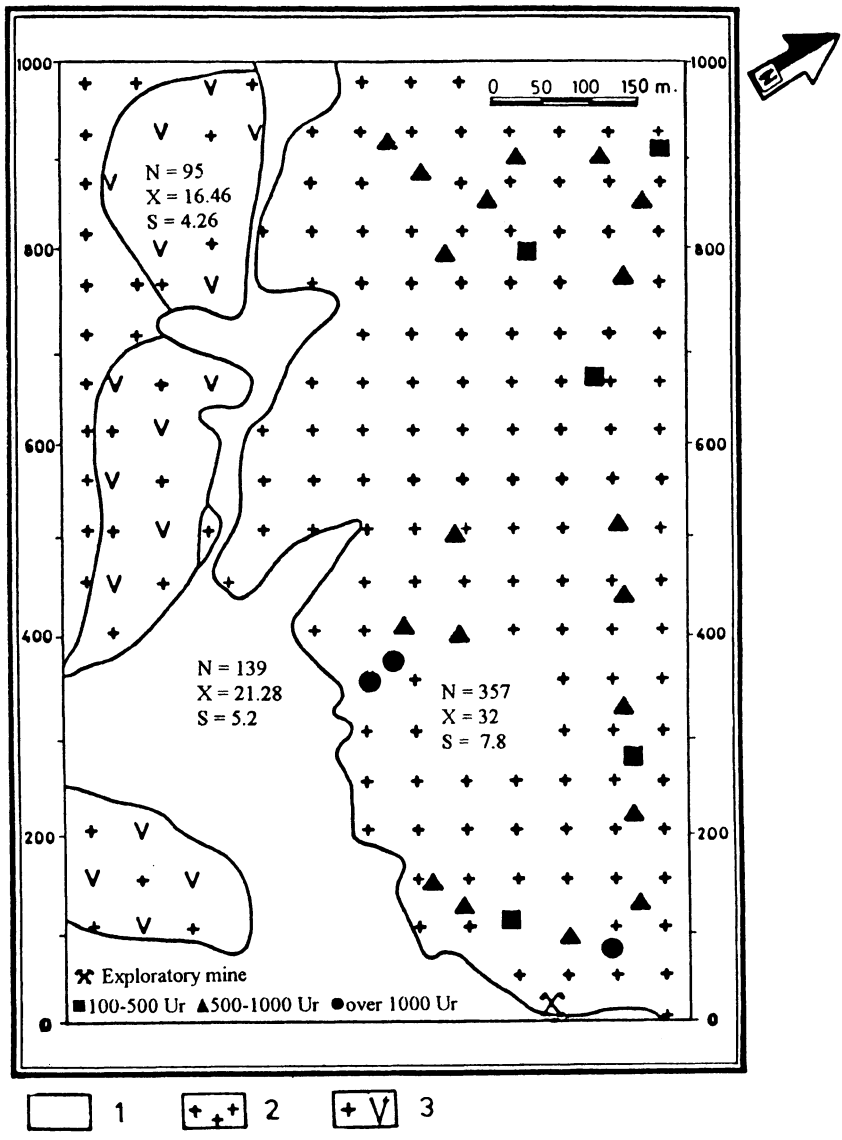

Figure 7. Interpreted radio-litho units map with highest radioactivity anomalies, El-Erediya prospect area Egypt; Symbols are: 1. Wadi deposits, 2. Pink granite, and 3. Amphibolite.

studied separately, in some detail (measuring every 3 meters or less), to delineate the size of the anomalies associated with them. Some of these anomalies are spot anomalies of very limited extent, with few centimeters dimensions, while others comprise several high radioactive spots scattered in zones of up to few meters length and half meter width. Some of the anomalous spots contain visible uranium

mineralization. The intensity of total-count radioactivity increases along the feather joints and at point of the intersection of the main jasperoid veins or their branches. The statistical analysis for the jasperoid veins measurements shows a wide variation in the total-count radioactivity readings. It ranges between 25.3 Ur and 1450.5 Ur, X value of all registered readings is 93.3 Ur, S value about 133.1 Ur. The CV% value is 142.7% which is more than 100%, therefore, this unit does not exhibit normal distribution. The Ur units can be considered as direct uranium concentration in this unit due to the scarcity of both Th and K in the jasperoid veins and the associated anomalies.

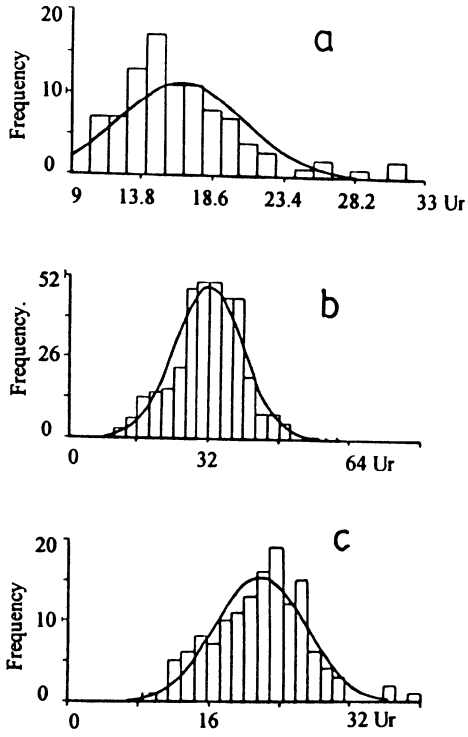

Figure 8. Frequency histograms with fitted normal theoretical curves of total-count radioactivity, El-Erediya prospect area, Egypt.

3.2. GROUND MAGNETIC SURVEY

The main objectives of the ground magnetic interpretation are to assist in solving the problems of regional geologic mapping and structure (Domzalski, 1966). A total magnetic field intensity survey carried out on the previous grid. Two tie lines were used (coded 00 and 500) normal to the profiles to control for the consistency and

reliability of the data. Two digital proton precision magnetometers (model 856) of Geometric Inc. Canada were used: one to collect the survey measurements along the profiles, and the other was established at a selected site as a base instrument. The drift correction of the readings for each station was carried out. Finally, the magnetic observations along each profile were adjusted according to the reference observations at the intersections with the tie lines, the corrected station values, reduced to an arbitrary datum (41000 nT) were plotted and contoured to yield the total magnetic field

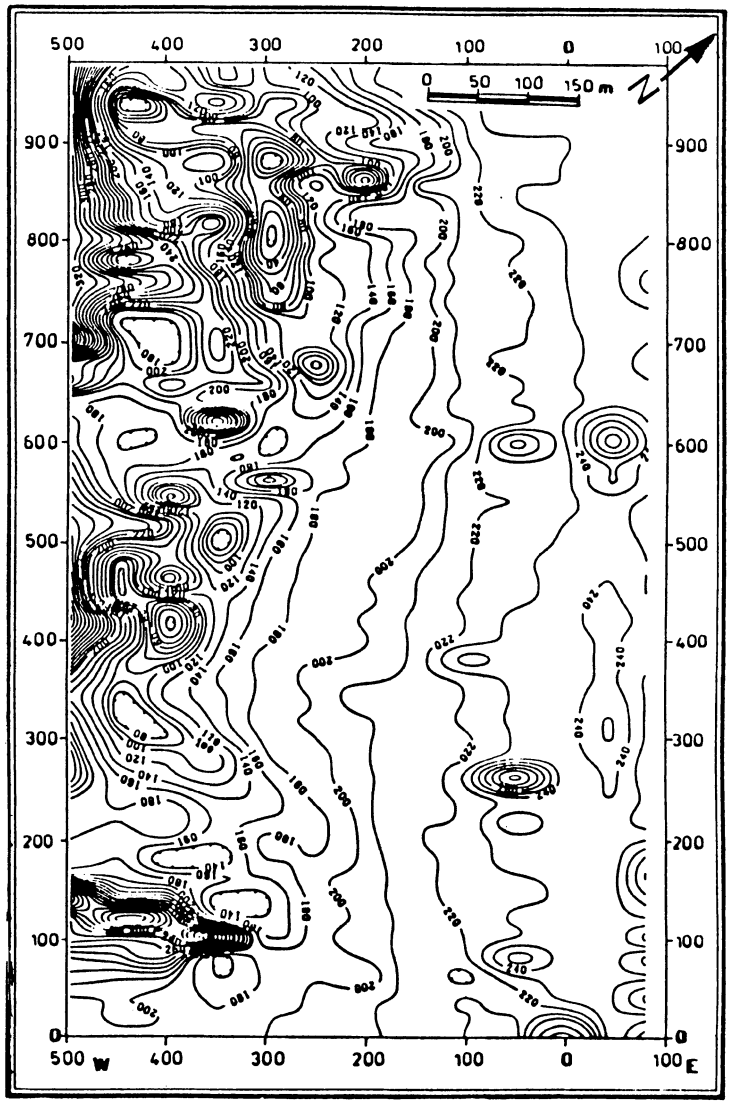

Figure.9. Ground total magnetic intensity map of El Erediya prospect area, Egypt; contour interval = 20 nT.

intensity map. In the present study, the reduced to the pole magnetic map (Fig.9) was produced using FFT GRID software program, available at Nuclear Materials Authority (NMA).

In (Fig.9) it is possible to group the anomalies into three major zones. The first zone (I), which occupies the central part of the area, is characterized by broad magnetic anomalies striking NW parallel to the oldest fault trend in the area and coincides essentially with the main trend of EL-Erediya granitic pluton. It is also characterized by a group of positive high frequency anomalies probably referring to shallow (near-surface) magnetic bodies. The second zone (II) is characterized by steep negative magnetic gradient, extending in a NW direction and occupies the eastern part of the area parallel to zone (I). This zone is interpreted as a major fracture zone trending in the same direction. The third zone (III) is located at the western part of the area, it has a relatively wide aerial extent with alternative groups of positive and negative anomalies striking NW to WNW direction. This zone is mainly associated with the amphibolites constituting the roof pendants within the granites. The observed relative difference in amplitude of the magnetic anomalies recorded over zone(III) may be related to either lateral variation in lithology (intrabasement effect), or in topographic relief (suprabasement effect), or the combined effects of both lithology and topography.

3.1.1. *Basement Tectonic Map*

The integration of the results obtained from the application of interpretation techniques to the magnetic survey data, aided by geological information, led to the construction of a basement tectonic map for the study area (Fig.10), which shows the gross structural framework of the area and displays the following features:

a. A set of faults trending in following directions: NE to ENE, NW and WNW. These faults were defined through the displacement and abrupt termination of magnetic features.

b. Thirteen fracturing and /or vein filling zones cut across the study area in different directions. The fracturing zones (from I to VII) trend in a NE to ENE directions, the fracturing zones (Nos. VIII and IX) trend in approximately WNW to EW directions, and the fracturing zones (Nos. X, XI, XII, and XIII) trend in NW direction. The associated magnetic anomalies may be inferred as signs of the presence of sulfide minerals. The delineated sets of fracturing zones are considered as the most mineral potential controller in the area under investigation. Most of them correlate well with the mapped jasperoid veins in the area.

3.2. HORIZONTAL-LOOP ELECTROMAGNETIC SURVEY

The horizontal-loop method has established its extensive application and utility in mining geophysics, especially in the search for massive sulfides. These are relatively good conductors, in marked contrast to their host rocks, and can thus be detected despite their localization nature and irregular shape (Griffiths and King, 1981).

The horizontal-loop electromagnetic (HLEM) system is manufactured by Scintrex Limited of Canada. The system employs a coplanar TM-2 transmitter and IGS-2/EM-4

receiver coils, which are separated by a fixed distance and connected by a cable. For measurements in rough terrain (such as the zero line in the present study), the IGS-2/EM-4 is equipped with tilt meter feature.

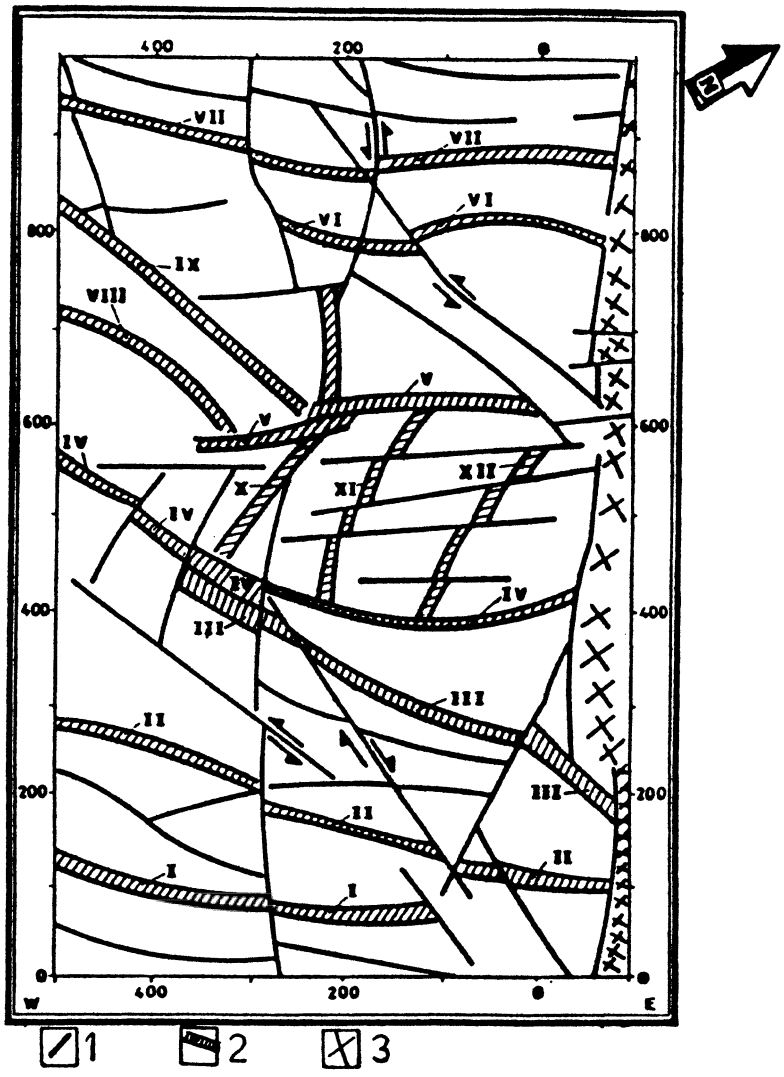

Figure 10. Basement tectonic map of El- Erediya prospect area, Egypt; Symbols are: 1. Fault, 2.Shear zone, and 3. Major fault zone.

The phase reference for each transmitter frequency is then sent over the cable, so that the signals picked up by the receiver coil may be resolved into the in-phase and quadrature (out-of-phase) components of the secondary field, in which such a measurement mode is called "Horizontal-loop". Two frequencies are measured

simultaneously by using this system. In all measurements, four frequencies were used; 112, 337, 1012, and 3037 Hz. The distance a (coil separation) between the transmitting coil and the receiving coil was 100, 70, or 30 m; according to the length of line. During the measurement operation, the combination of transmitting coil and receiving coil was moved by small steps in a horizontal plane, each step was either 20 or 10 m. The measurement of the in-phase and out-of-phase components of the secondary field are reported as percentages of the primary field. By a judicious application of multi-frequency techniques, it is possible to detect weaker conductors (small width) and to derive detailed information about the parameters of the conductors evidenced by anomalies obtained with the HLEM method. The midpoint of the line joining the transmitting and receiving coils is used as the measuring point. The values of the in-phase and out-of-phase (real and imaginary) anomalies measured by the HLEM method are primarily affected by the conductivity and dimensions of the conductor being investigated, its position and the frequency used in the measurements.

Besides just the detection of electromagnetic (EM) anomalies, it is the aim of an EM survey to estimate the parameters of the causative conductor from details of the detected anomalies. The two components measured, in-phase and out-of-phase are plotted, and simple interpretation schemes are used to calculate width, dip, depth and conductance (σ_t). The first step in interpreting the HLEM data is to establish the background in-phase and out-of-phase values away from the anomaly to be interpreted. It is nearly equal to the instrument zero level (in the present work). The peak amplitudes C1, C2, Q, and R (Fig.11) are measured with respect to this background (or zero level).

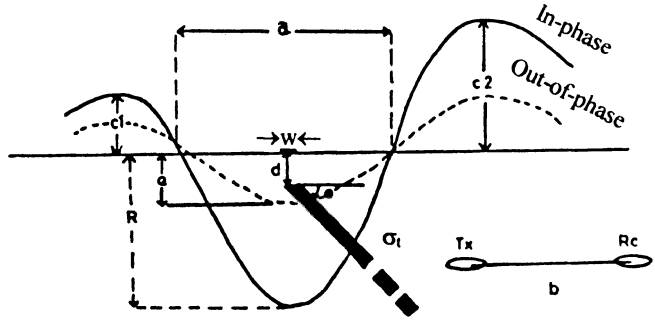

Figure 11. Typical profile over a tilted conducting half-plane showing horizontal loop electromagnetic parameters.

The main targets of the HLEM interpretation are, location, dip, width, depth of burial and conductance these parameters can be estimated by using a family of response diagrams and curves, which designed by Nair et al. (1974). Five HLEM profiles were carried out, one profile on the surface coded OO NS (Fig.3) and four profiles inside the mine coded Main adit, (D II & D III), (D IV & D V), and (D VIII & D XIII) in figure (2). An examination of these profiles led to the following observations.

3.2.1. *Line OO NS*

This profile (Fig.4) is situated over the main adit of the mine and it is approximately normal to the jasperoid veins and shear zones. It was selected to pick up any conductive zone over the two hundreds meters from the portal and also any conductive zone along this line. The measurements were performed with coil separation 100 m and station interval 20 m.

The HLEM data shown on this profile (Fig.12) indicate the presence of one major conductive zone. The negative peaks of in-phase and out-of-phase extend from about station 70 to about station 260 and can be easily identified. This zone is associated with a set of jasperoid veins, as well as shear and fault zones, as shown from the surface geologic map (Fig.4).

The results of the quantitative interpretation, as calculated from all frequencies are; the average width is 86 m, depth to the upper edge is 31 m, dip angle is 58^{0} toward the south, and conductivity thickness reaches about 2.03 Mho/m. The other HLEM responses along the profile "OO NS" are corresponding to the interpreted faults, as well as some minor veins.

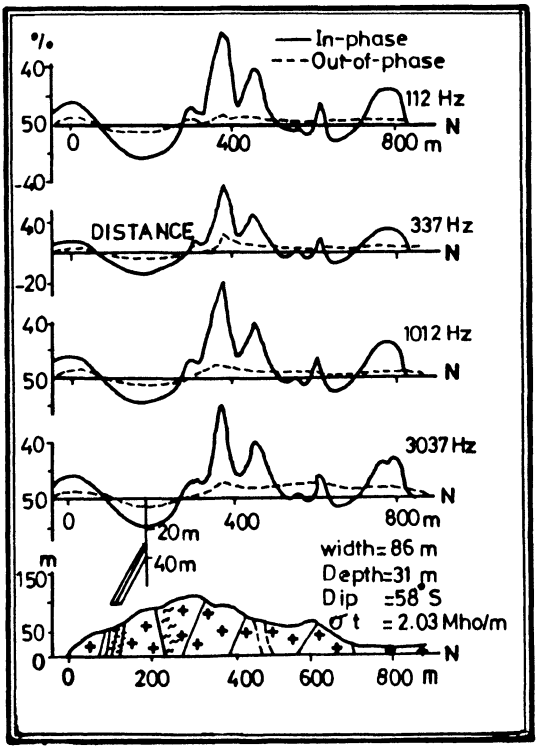

Figure 12. Interpretation of horizontal loop electromagnetic profile (OONS) with the corresponding geologic section, Symbols as in Fig.4.

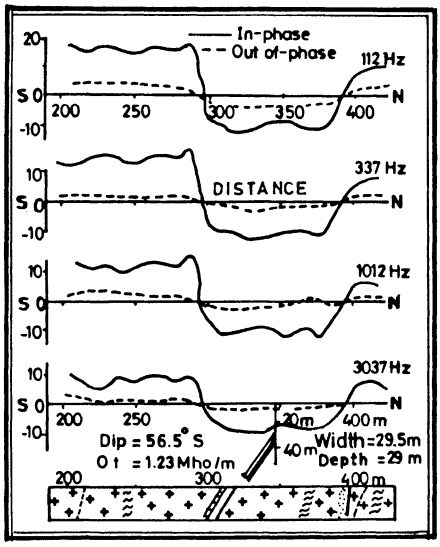

Figure 13. Interpretation of horizontal loop electromagnetic profile (Main Adit) with the corresponding subsurface geology, Symbols as in Fig.4.

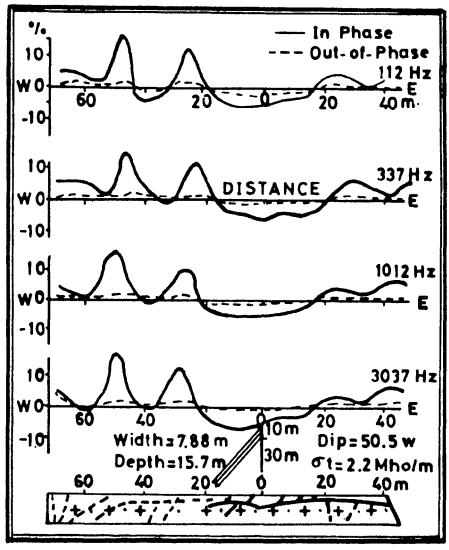

Figure 14. Interpretation of horizontal loop electromagnetic profile(DII&DIII) with the corresponding subsurface geology, Symbols as in Fig.4.

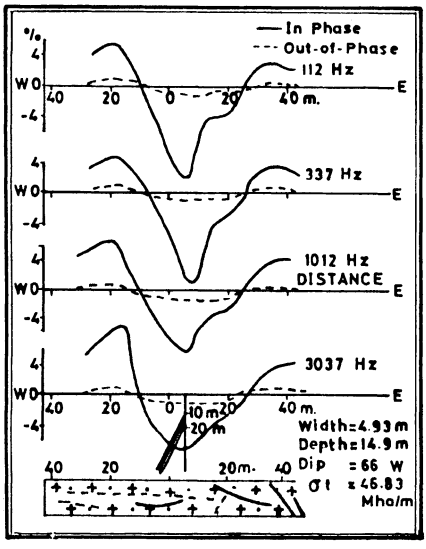

Figure 15. Interpretation of loop electromagnetic profile (DIV&DV) with the corresponding subsurface geology, Symbols as in Fig.4.

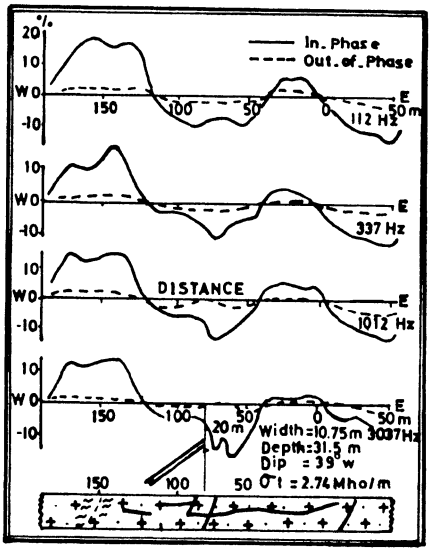

Figure 16. Interpretation of horizontal loop electromagnetic profile (DVIII&DXIII) with the corresponding subsurface geology, Symbols as in Fig.4.

3.2.2. *Main Adit*

The measurements started at station coded 200 from the portal of the mine and carried out with coil separation 70 m and station interval 10 m. Only a broad conductor is indicated by a negative peak extends from about station 296 to about station 394. This zone corresponds with the geologically mapped jasperoid veins and the intersecting fractures. The quantitative interpretation of the HELM data shows that; the average width from all frequencies is 29.5 m, the average depth is 29 m, the average dip angle is 56.5° toward the south, and the conductivity thickness is 1.23 Mho/m (Fig.13). The shape of negative and positive peaks reveals that, the major conductive zone is composed of a series of parallel thin conductors over a width greater than 29.5m of the coil spacing.

3.2.3. *DII & DIII*

This profile was conducted with coil separation 30 m and station interval 10 m. The HLEM data shown on this line (Fig.14) indicates the existence of two EM anomalies. The first is close station 40W, but the width of this anomaly is less than the coil separation. It is due to a thin conductor. The second anomaly has low value of negative peak for in-phase and out-of-phase and extends from about the station coded 20W to about the station coded 18E. The characteristic parameters of this anomaly, as interpreted from the HLEM data, show that the average width is 7.88 m, the depth to the upper edge attains 15.7 m, the approximate dip angle reaches 50.5° to the west and the conductivity thickness is of about 2.2 Mho/m. Moreover, both the two EM anomalies coincide with a set of parallel fractures and faults, as shown in the subsurface geology (Fig.14).

3.2.4. *DIV & DV*

The HLEM profile was conducted with coil separation 30m and station interval 10m. It is characterized by one negative peak and positive shoulders for each in-phase and out-of-phase (Fig.15). The negative peak extends from station 21W to about station 14E and coincides with a set of parallel faults and fractures as shown in the subsurface geology (Fig.15). The quantitative interpretation of the HLEM data shows that the average width reaches 4.93 m, the average depth attains 14.9m, the average dip angle approximates 66° toward the west, and the conductivity thickness reaches 46.38 Mho/m.

It is seen that, there is a slight rotation and attenuation of the anomaly vector with increasing the frequency from 112 to 3037 Hz. This is probably due to the effect of the overburden. A similar result has been obtained for models in a non-conducting host rock under a conducting overburden (Lajoie and West, 1976). In each case, the anomalies are at the low frequency and are relatively unaffected by the conductive weathered layer.

3.2.5. *DVIII & DXIII*

This profile was carried out with coil separation 70m and station interval 10m. The HLEM data indicate the existence of two EM zones. The first has a negative peak for the in-phase and out-of-phase and extends from about the station coded 120 W to about

the station coded 40 W. The other has a negative peak from about the station coded 5 to the eastern end of the line. Both of them coincide with the shear zones and faults as shown in the corresponding subsurface geology (Fig.16).

The characteristic parameters of the first anomaly shows that the average width is about 10.75 m, the average depth to the upper edge attains 31.5m, the dip approximates 39° toward the west, and the average conductivity thickness is about 2.74 Mho/m. The second anomaly is incomplete where one positive peak occurs at the end of the mine (Fig.16). Therefore, its parameters cannot be determined because, the determination requires a negative peak between two positive ones (shoulders). It is recommended to carry out drilling at the eastern end of this line.

The shape of the negative and positive peaks for both anomalies on this line indicates that either two or more thin conductors have come closer or the source body have irregular shape.

4. Conclusion

The interpretation of the geological, structural, and radiometric data proved the association of the radioactive anomalies and uranium mineralization with cryptocrystalline silica veins within NE-SW to N-S tensional fractures which were rejuvenated several times. The nature of mineralization and its association with the jasperoid silica veins points out to its supergene origin in low temperature oxidizing-reducing conditions. In the second stage of the fractures reactivation, uranium was leached out from the granite at fractures walls and it precipitated with a second phase jasperoid silica along the reactivated fractures where they cemented the brecciated early silica veins and granite at the contacts. This proposed supergene origin is supported by the existence of the U-mineralization nearly free of any thorium association, the cryptocrystallization of the associated silica veins, and the presence of black shreds of possible organic origin (Mohamed, 1989). Moreover, their association with tensional fractures of much younger age than the granite (Abdel-Meguid, unpublished work) exclude any granite -related hydrothermal origin for the uranium mineralization in the area. This is also supported by the U-mineralization radiometric ages (160, 120, and 52 Ma) given by Abu Deif (1992) while the granite is about 550 - 590 Ma. The magnetic interpretation demonstrates the gross structural framework of the prospect area and proved that the two main perpendicular fractures (NE to ENE and NW to WNW) may have some considerable depths that permit a reducing conditions for precipitating uranium.

The investigation of the horizontal-loop electromagnetic profiles revealed the occurrence of many conductive zones. These zones are mainly associated with a set of jasperoid veins, fracture zones, and fault zones. The conductive parameters, as averaged from the four frequencies (for surface and mining profiles), revealed widths ranging between 4.93 and 86 m, shallow average depths ranging between 14.9 and 31.5m, dip angles ranging between 40°-70°, and conductivity thickness ranging between 1.23 and 46.38 Mho/m for the mineralized zones.

These shallow depths fluctuations of the expected mineralization reflect the oscillation of meteoric solution level of penetration in the fracture and the fluctuation in the ore precipitating reduction zone. This proposed concept for the origin and depths of the uranium mineralization in El-Eredyia area should be considered in reevaluating the area before any further development.

References

Abdel-Meguid, A.A. (1986) Geologic and radiometric studies of uraniferous granite in Um Ara-Um Shilman area, south Eastern Desert, Egypt, Ph.D. Thesis, Suez Canal Univ., Egypt.

Abou-Deif, A., (1992) The relation between the uranium mineralization and tectonics in some Pan-African granites, west of Safaga, Eastern Desert, Egypt, Ph.D. Thesis, Assiut Univ., Egypt.

Ammar, A.A., (1973) Application of aerial radiometry to the study of the geology of Wadi El Gidami, Eastern Desert, Egypt (with aeromagnetic application), Ph.D. Thesis, Faculty of Science, Cairo University.

Domazalski, W. (1966) Importance of aeromagnitic in evaluation of structural control of mineralization, *Geophysical Prospecting* **14**, 273-291.

El Kassas, I.A., (1974) Radioactivity and geology of Wadi Atalla area, Eastern Desert of Egypt, A.R.E., Ph.D. Thesis, Faculty of Science, Ain Shams University, Cairo Egypt.

El Ramly, M.F., (1972) A new geological map for the basement rocks in the Eastern and the South-Western deserts of Egypt, *Ann. Geol. Surv. Egypt* II. 1-18

El Shazly, E.M., Dixon, T.H., Engel, A.E., Abdel-Meguid, A.A., and Stern, R.J., (1980) Late Precambrian crustal evolution of Afro-Arabia from ocean-arc to craton, *Egypt. Jour. Geol.* **24/1-2**, 101-121.

El Tahir, M.A., (1985) Radioactivity and mineralization of granitic rocks of El-Erediya occurrence and comparison to El Missikat-Rei El Garra occurrence, Eastern Desert, Egypt, Ph.D. Thesis, Faculty of Science, Al Azhar University, Cairo Egypt.

Griffiths, D.M., and King, R.F., (1981) *Applied Geophysics for geologists and engineers, elements of geophysical prospecting*, Pergamon International Library, publisher. Report.

Hussein, H.A. and El-Kassas, I.A., (1979) Some favorable host rock for uranium and thorium mineralization in the Central Eastern Desert, Egypt, The 5th Conference on African Geology, Cairo, Egypt, abstracts

Lajoie, J.J., and West, G.F., (1976) The electromagnetic response of a conductive inhomogeneity in a layered earth, *Geophysics* **41**, 1133-1156.

Mohamed, N.A, (1989) Mineralogical and petrographical characteristics of some alteration product related to U-mineralization in El Misikat -El Erediya areas, Eastern Desert, Egypt, M.Sc. Thesis, Cairo University, Egypt.

Nair, M.R., Biswas, S.K., and Mazumdar, K., (1974) Standard curves for the interpretation of horizontal-loop electromagnetic anomalies, Geol. Surv. of India Miscellaneous publication No. 25.

Rabie, S.I., Sadik, H.S., Abdelhadi, A.S., Mohamed, A.S., and Ibrahim, R.A. (1992) Ground geophysical prospecting for radioactive minerals in El-Erediya prospect, Central Eastern Desert, Egypt, Scientific Internal Report Series (NMA-ED-6/92), Kattamiya, Egypt.

Sarma, D.D., and Koch, Jr., G.S. (1980) A statistical analysis of exploration geochemical data for uranium, *Mathematical Geology* **12/2**, 99-114.

Stern, R.J. (1985) The Najd fault system, Saudi Arabia and Egypt: A late Precambrian rift related transform system, *Tectonics* **4/5**, 497-511.

SEISMIC IMAGING BENEATH THRUST BLOCKS

Z.M. LIU and R.A. YOUNG
School of Geology and Geophysics
University of Oklahoma
Norman, OK 73019, U.S.A

Abstract

In a proof of concept study, conditions under which turning ray fault plane reflections can be applied to imaging sediments beneath an overthrust block are investigated through modeling. In a simplified overthrust model, conventional primary reflections and fault plane reflections are compared as ways of imaging sediments beneath the block. Velocities chosen for basement and sediments in the model correspond broadly to those for igneous rocks, clastics, and carbonates of the Anadarko Basin, Oklahoma. The acquisition geometry required in order to utilize fault plane reflections is considered, and amplitude behaviors associated with vertical velocity gradients of .2, .5, and .7 ft/sec per ft are investigated through ray tracing. In the case of a vertical velocity gradient of .7 ft/sec per ft, the simplified model is modified to include a syncline beneath an overthrust. When the vertical velocity gradient is .7 ft/sec per ft, amplitudes for the fault plane reflection become substantially larger than those for the primary reflection, which suggests that recording the fault plane reflection may be useful in imaging subthrust sediments in some situations. Challenges in the acquisition and processing of actual fault plane reflections are discussed.

1. Difficulties in Conventional Imaging Across an Overthrust

Reliable seismic images of structures beneath basement overthrust blocks are difficult to obtain. Common midpoint (CMP) profiling uses ray paths that are transmitted across the large velocity contrasts at boundaries between crystalline basement and sediments. These contrasts shield subthrust features from illumination by reducing the amplitude of the transmitted wavefield. Severe ray path bending at such a boundary produces non-hyperbolic travel-times so that stacked images are weak. Conventional survey apertures may be too small to record events from more steeply dipping subthrust boundaries. In addition, the extreme lateral velocity variation at such boundaries may render CMP stacking ineffective.

An alternative to stacking primary reflections is to migrate unstacked gathers containing a different reflection ray type. This ray type is a fault plane reflection. This study investigates, by ray trace modeling, what constraints on a thrust model are required in order that a fault plane reflection might be used to image sediments beneath an overlying basement block.

2. Observation of Fault Plane Reflections

Reflections from fault planes have been reported widely in the past for cases of crustal-scale seismic data (e.g., Cook, et al., 1979; Smithson, et al., 1979) and oil industry reflection profiling (Middleton, 1990). A particularly strong reflection from a fault boundary has been observed in Western Australia (Young, et al., 1990) at the edge of the onshore Perth Basin where the Darling Fault separates a Mesozoic sedimentary section in the Perth Basin from the Precambrian basement of the Yilgarn block. The present-day Darling Fault is a normal fault with a 60 deg dip. Structural features of the Perth Basin have been correlated with geophysical data to deduce a long history of normal and reverse movement along this boundary (Iasky and Young, 1990). Despite this reworking of the fault zone, the reflection is sharp, of large amplitude, and continuous on shot records. Ray trace modeling of this reflection on shot records confirms that it is generated by the Darling Fault (Young et al., 1990).

The reflection reported by Young et al. (1990) is recorded on the sediments in the hanging wall of a normal fault. Because the magnitude of the reflection coefficient is independent of illumination direction, a turning ray reflection of equal amplitude might be recorded by a survey in the foot-wall. The same reasoning can be applied to a thrust fault. This leads to the consideration of turning rays in an overthrust situation.

3. Ray Paths in an Overthrust Model

An important geologic situation for hydrocarbon exploration is an overthrust in which basement is placed over sediments bearing hydrocarbons. In this case, there may be a situation in which the fault plane could be used to redirect the energy downwards in order to undershoot the overthrust block and to illuminate a sedimentary target. A generalized overthrust model showing ray paths is shown schematically in Figure 1. The target reflector is the boundary between sediments I and sediments II. The source (labelled S) is located in the footwall. An important issue is where to place the receiver (labelled R) in order to obtain reflection coverage as close as possible to the fault. Figure 1a shows a ray path representing the largest source-receiver separation possible for a conventional primary reflection if the fault is not crossed by the ray. The dark black line along the reflector represents coverage for smaller separations. The reflection coverage is not ideal because it ends a long way from the fault. Raypaths crossing the fault, on the

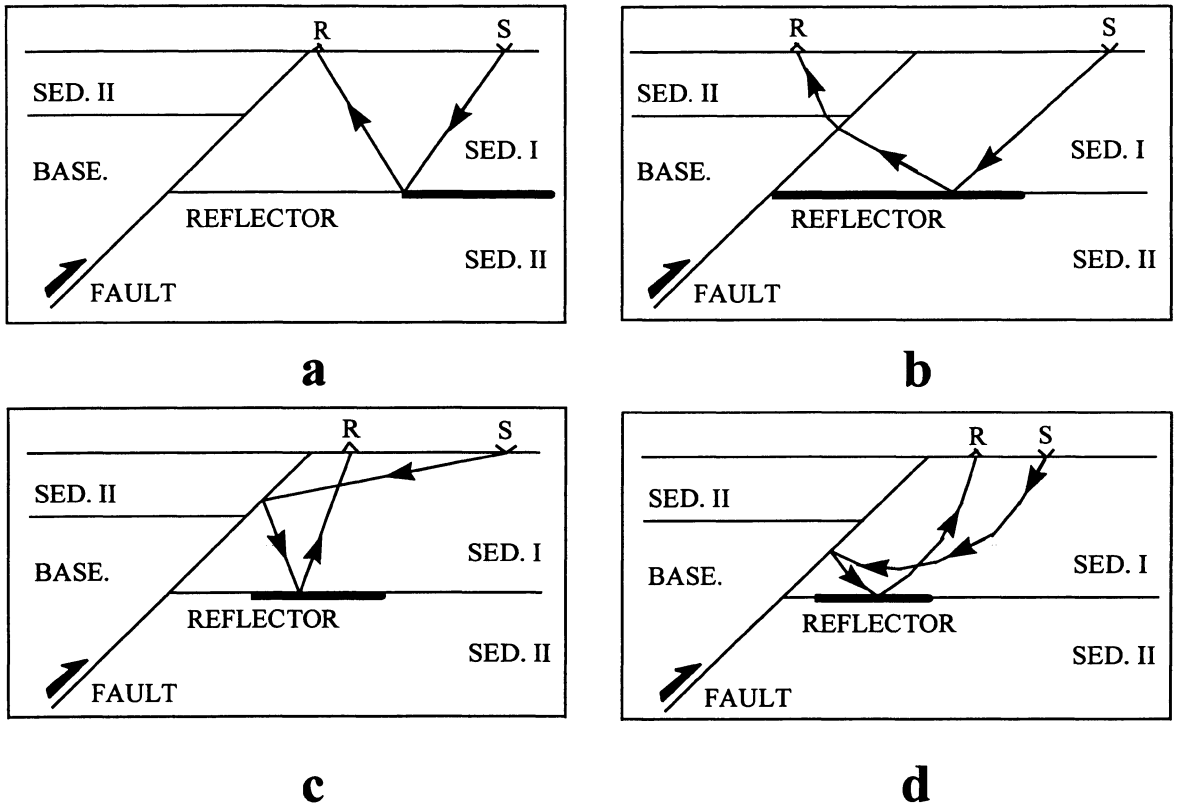

Figure 1. Schematic representation of a generalized overthrust model shows ray paths for conventional primary reflections (a,b) and for fault plane reflections (c and d). Receiver (R); source (S).The reflector separates low speed (SED. I) and high speed (SED. II) sedimentary layers. A thrust fault separates high velocity basement (BASE.) from sediments. Thrust fault dip is taken as 45 deg for convenience of illustration. (a) Primary reflection does not cross fault. (b) Primary reflection crosses fault. (c) and (d) Fault plane reflection does not cross fault for either constant velocity layer (c) or constant velocity gradient layer (d).

other hand, will image the reflector much closer to the fault (Figure 1b). The amplitude of these rays, however, will be diminished severely by the small transmission coefficient due to the large velocity contrast between sediments and basement at the fault.

By moving the source away from the fault, it may be possible to obtain a fault plane reflection that directs energy down to the reflector in the vicinity of the fault and is received on the footwall side of the fault. Figure 1c suggests that this unconventional ray might have large amplitude because of oblique incidence at the fault and might also image close to the fault. Figure 1c also suggests that the price paid is that a source might have to be located a very long distance from the fault in order to produce such a ray. Loss of reflection amplitude due to spherical divergence over such a long ray path might overwhelm the positive effect of a large reflection coefficient at the fault.

Introducing a vertical velocity gradient in the footwall allows the source to be brought closer to the fault (Fig. 1d). It also permits a smaller fault dip because turning of the rays toward normal incidence at the fault expands the angular aperture of possible fault plane reflections. Raypaths will be shorter and spherical divergence less than in Fig. 1c, but the reflection coefficients at the fault and at the reflector will differ from the case of constant layer velocity. In order to investigate the effect of a vertical velocity gradient on amplitudes, a more quantitative description of travel times and amplitude behavior is needed. This can be obtained by ray tracing.

4. Ray Tracing in a Simplified Overthrust Model

The present paper considers the vertical velocity gradient and the acquisition geometry required in order to utilize fault plane reflections. It is a proof of concept study and is not intended to predict the seismic response of a particular overthrust example. We have chosen a simplified overthrust model that varies only in choice of velocity gradient. Thrusts dip at 45 deg or less (Twiss and Moores, 1992), and we have chosen a representative dip of 30 deg. Our model consists of high velocity sediments and basement in the hanging wall and low and high velocity sediments in the footwall. Velocities of 22,000 ft/s for the basement and 21,000 ft/s for the high velocity sediments are taken in broad correspondence, respectively, to the Cambrian igneous rocks underlying the upper Cambrian carbonates of the Anadarko Basin, Oklahoma. Three different vertical velocity gradients, as measured from the surface to a depth of 20,000 ft, are considered: .2, .5, and .7 ft/s per ft , respectively. The steepest gradient results in a velocity of 18,000 ft/s at a depth of 20,000 ft. This is similar to the velocity of the Silurian-Mississippian carbonates in the deep Anadarko Basin (R.E. Schneider, personal communication, 1995). The smaller velocity gradients may be appropriate elsewhere and are considered in this study in order to span the range of ray tracing results for the simplified model. A final example considers the ray focusing due to a synclinal fold beneath an overthrust.

The software used in the study is GX-II (GX Technology, Inc.), a package of seismic ray tracing software for X-windows on workstations. Common shot gather ray tracing is applied to the simplified overthrust model. Amplitude calculation takes into account spherical spreading and the full Zoeppritz equations are used at boundaries. No frictional absorption is introduced and the free-surface effect is disregarded. Vertical component, single receivers are chosen.

5 . Ray Tracing Comparisons

The effect of a vertical velocity gradient on a fault plane reflection in the simplified thrust model is investigated by ray tracing using GX-II. In each case the proximity of the reflection points to the fault, the shape of the event traveltime curve, and the reflection amplitude are considered. Each ray tracing figure shows a very large aperture in order to capture the entire range of behavior of the events. The gain for each synthetic example is constant for all traces, but each example has a different value.

A vertical velocity gradient of .2 ft/s per ft generates a fault plane reflection that images closer to the fault (Fig. 2, coverage D) than a conventional primary reflection (Fig. 2, coverage A and B). The impulse response for the primary reflection produces small amplitudes at receivers in the hanging wall (Fig. 3, event B), but much larger amplitudes are recorded for raypaths entirely within the footwall (Fig. 3, event A). The fault plane reflection loses amplitude because of reflection from the fault, and it has a longer path length than the primary reflection. In comparison to the primary reflection, the fault plane reflection amplitude is so small that it is not even visible on the impulse response (Fig. 3).

An increase in the velocity gradient to .5 ft/s per ft (Fig. 4) results in a large shadow zone for the fault plane reflection producing a gap between coverage D and coverage C along the reflector: only a few rays are recorded in the hanging wall (Fig. 4, coverage D). A number of raypaths are entirely within the footwall (Fig. 4, coverage C) and have oblique reflection at the fault. This suggests that, in comparison to the fault plane reflection for the .2 ft/s per ft case, their amplitudes should be somewhat larger. Indeed, this is the result (Fig. 5, event C), although fault plane reflections are considerably fainter than primary reflections (Fig. 5, event A). This is due, in part, to longer ray paths for the fault plane reflection. A large primary reflection amplitude and 90 deg phase change occur at the P-wave critical angle of approximately 40 deg (distance 87,000 ft in Figure 5).

When the velocity gradient is increased to .7 ft/s per ft, the fault plane reflection becomes a better choice for imaging than the primary reflection for three reasons. The fault plane reflection coverage (Fig. 6) is closer to the fault (coverage C) than that of the primary reflection (coverage A). The reflection coverage also spans more reflector. Fig. 7 shows that amplitudes for the fault plane reflection (event C) become substantially larger than those for the primary reflection (event A). This is because the critical

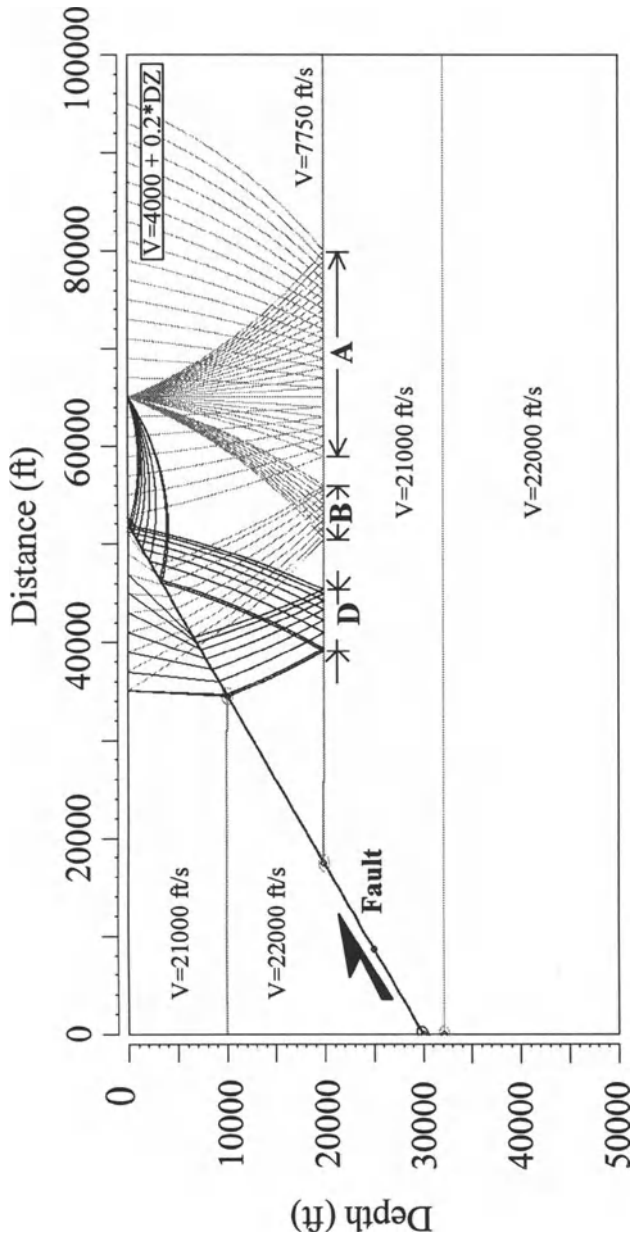

Figure 2. Vertical velocity gradient (.2 ft/s per ft) generates turning rays in the footwall. Fault dip is 30 deg. Primary reflection (coverage B) crosses the fault; reflections for coverage A do not. Ray paths for the fault plane reflection are dark lines with coverage D and all ray paths cross the fault.

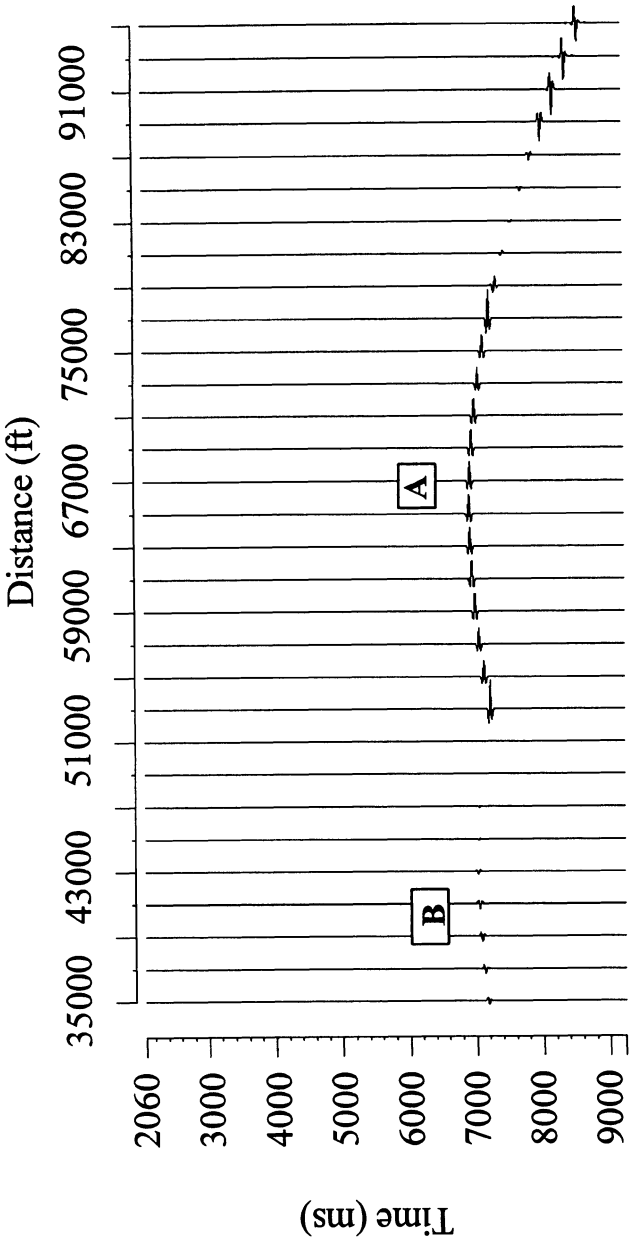

Figure 3. Synthetic traces for raypaths shown in Figure 2. Fault plane reflection is not visible when compared to primary reflection (events A and B). Constant gain record.

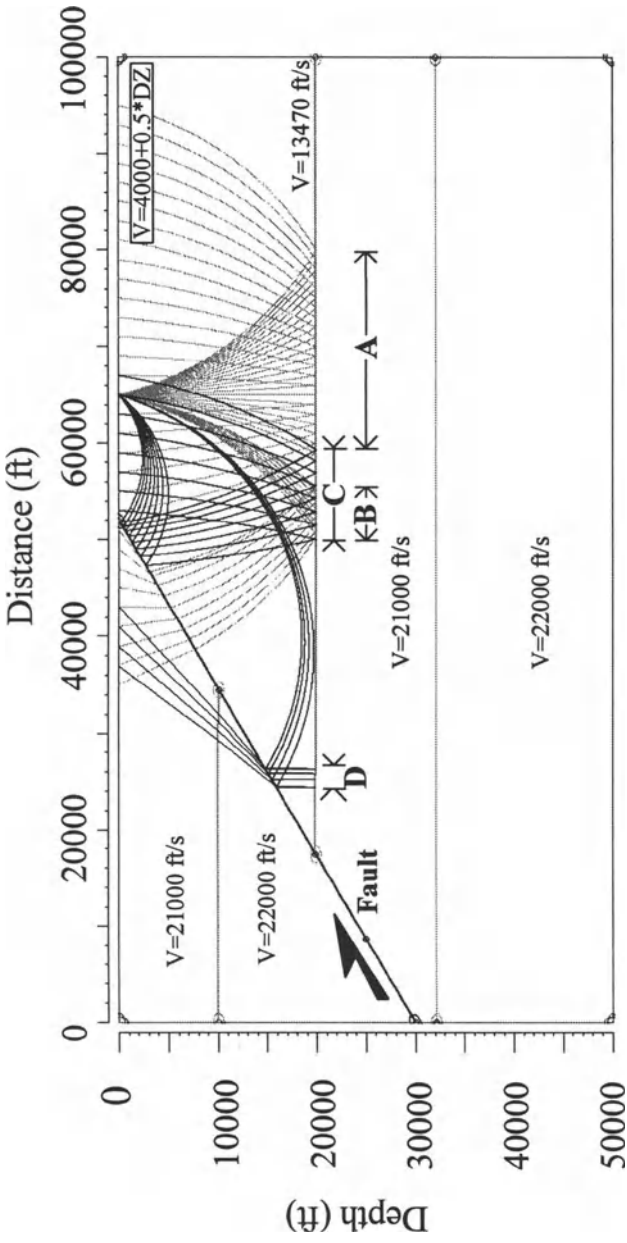

Figure 4. Vertical velocity gradient (.5 ft/s per ft) generates turning rays in the footwall. Primary reflection (coverage B) crosses the fault; reflections for coverage A do not. Ray paths for the fault plane reflection are dark lines. Ray paths for coverage D cross the fault; ray paths for coverage C do not. A shadow zone exists between C and D.

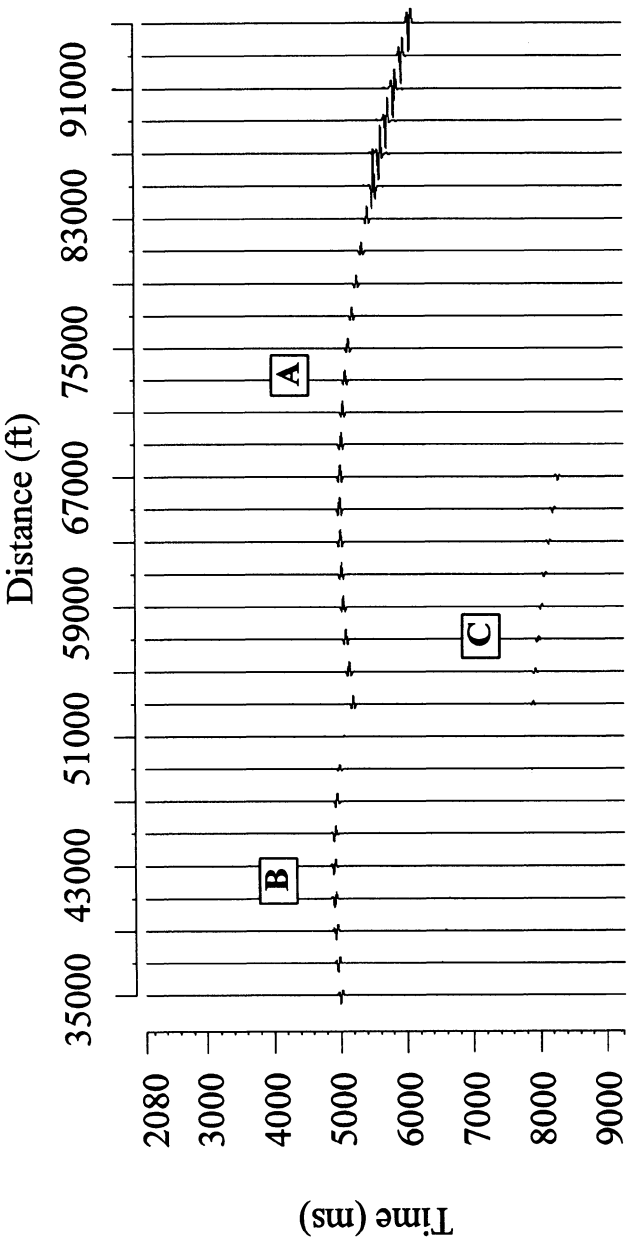

Figure 5. Synthetic traces for raypaths shown in Figure 4. Fault plane reflection (event C) is weak compared with the primary reflection (events A and B) at the same receiver locations.

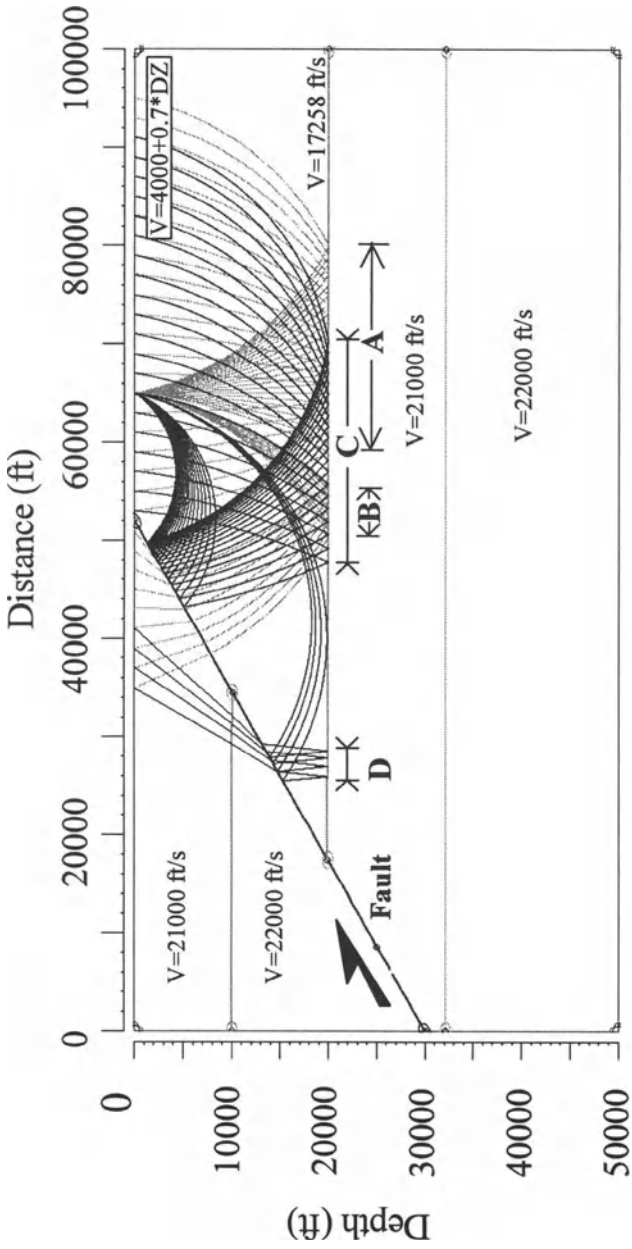

Figure 6. Vertical velocity gradient (.7 ft/s per ft) generates turning rays in the footwall. Primary reflection (coverage B) crosses the fault; reflections for coverage A do not. Ray paths for the fault plane reflection are dark lines. Ray paths for coverage D cross the fault; raypaths for coverage C do not. Fault plane reflection coverage is closer to the fault than primary reflection coverage.

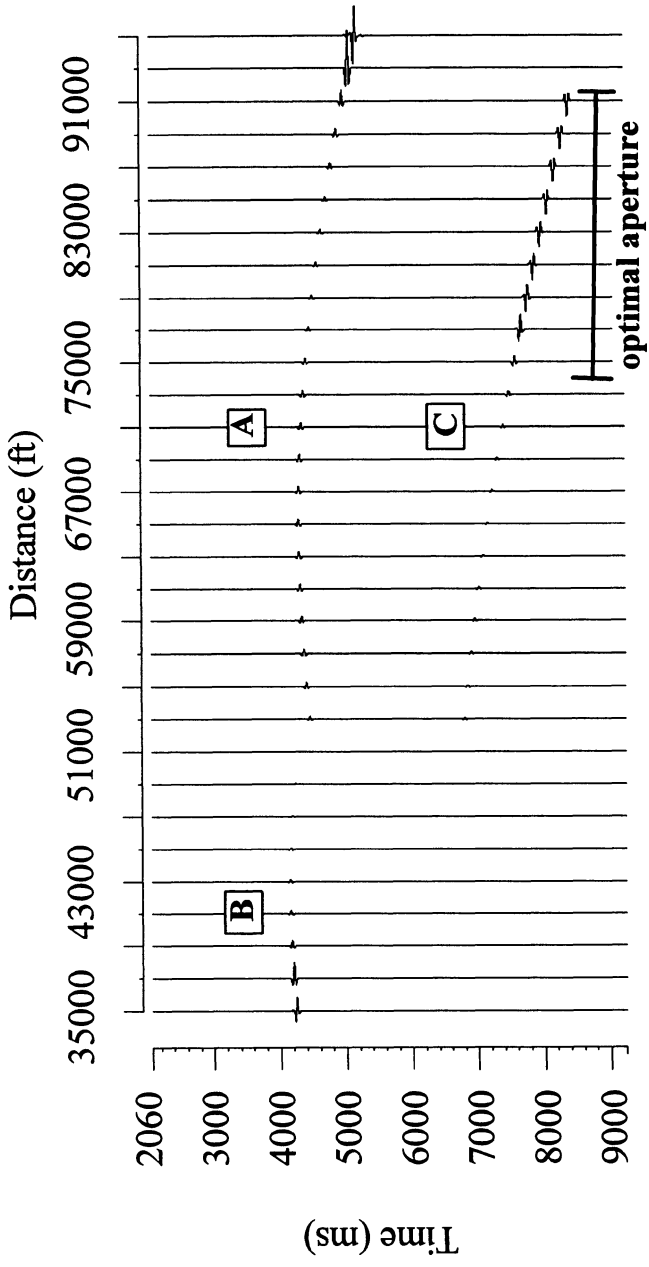

Figure 7. Synthetic traces for raypaths shown in Figure 6. Fault plane reflection (event C) is strong compared with primary reflection (events A and B) and has strongest amplitudes within the optimal aperture shown.

reflection for the fault plane reflection occurs around 79,000 ft, while it occurs at distances greater than 95,000 ft for the primary reflection. This behavior of the fault plane reflection suggests that in the range 73,000-91,000 ft (Fig.7) amplitudes are optimal for this model, and that the fault plane reflection may be useful in imaging subthrust sediments. An extension of the simple overthrust model to include a syncline beneath an overthrust presents a new dimension to the comparison of fault plane reflections and primary reflections (Fig. 8). Focusing by the syncline produces two arrivals for the fault plane reflection; the later and weaker arrival (Fig. 9, event C) reflects very near the fault in the center of the syncline (Fig. 8, coverage C), and the earlier and stronger arrival (Fig. 9, event C′) reflects further from the fault on the shoulder of the syncline (Fig. 8, coverage C′). Despite the much longer travel path for the fault plane reflection, its amplitude between 79,000 and 89,000 ft is twice to three times as large as the primary reflection.

6. Discussion

The ray tracing analysis has borne out the intuitive idea that a fault plane reflection in an overthrust model can image closer to the fault in the footwall and have larger amplitudes than the corresponding primary reflection. A steeper velocity gradient moves reflection coverage closer to the fault and increases amplitude at the receiver. A steeper fault dip would produce the same result as increasing the velocity gradient.

The source location for the present modeling was chosen to give optimal coverage and large amplitudes. The resultant receiver aperture for large amplitude reflections is approximately 20,000 ft and is entirely on one side of the source. Not all source locations, however, generate large amplitudes and coverage near the fault. It is our experience that many combinations of fault dip, source location, and velocity gradient produce poorer results for the fault plane reflection than for the primary reflection. The use of fault plane reflections, consequently, is not a panacea and is unlikely to give improved imaging in many overthrust situations. Nevertheless, a fault plane reflection could be a useful event in some situations. Modeling is necessary to determine these situations and to find an optimal location for receivers.

Useful fault plane reflections require a moderate vertical velocity gradient. This has been distributed across a single, thick layer that is not subdivided into thinner layers in the present modeling. Older, more consolidated sediments are likely to have very small vertical velocity gradients, and the present method may be inapplicable in such geologic circumstances. If layer velocities alternate, large impedance contrasts will decrease the amplitude of a turning ray along its path. This will result in weaker amplitudes for both primary reflections and turning rays; thus, in comparison to the primary reflections, the fault plane reflections might still be useful.

Processing the fault plane reflection will be a challenge. An immediate assistance is that moveout is opposite in sense to traveltimes for some segments of the primary.

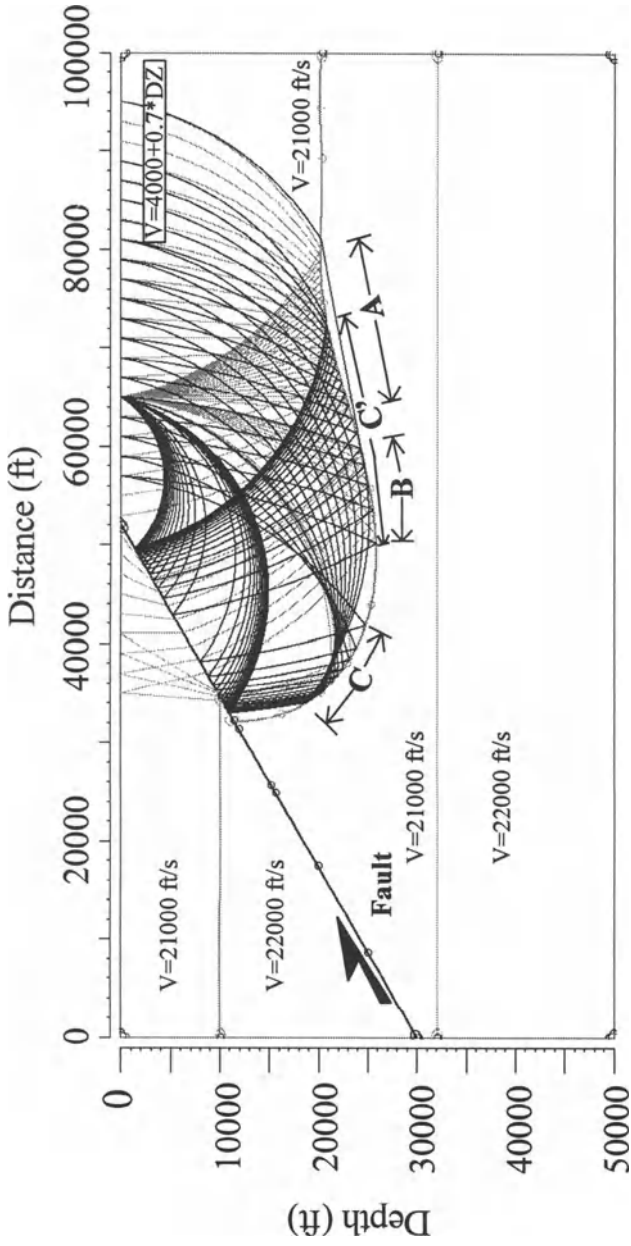

Figure 8. A synclinal fold under a gently dipping fault. Vertical velocity gradient is 0.7 ft/s per ft. The fault plane reflection is focused by the syncline into two segments of reflector coverage, C and C, which are closer to the fault than the primary reflection coverage (A and B).

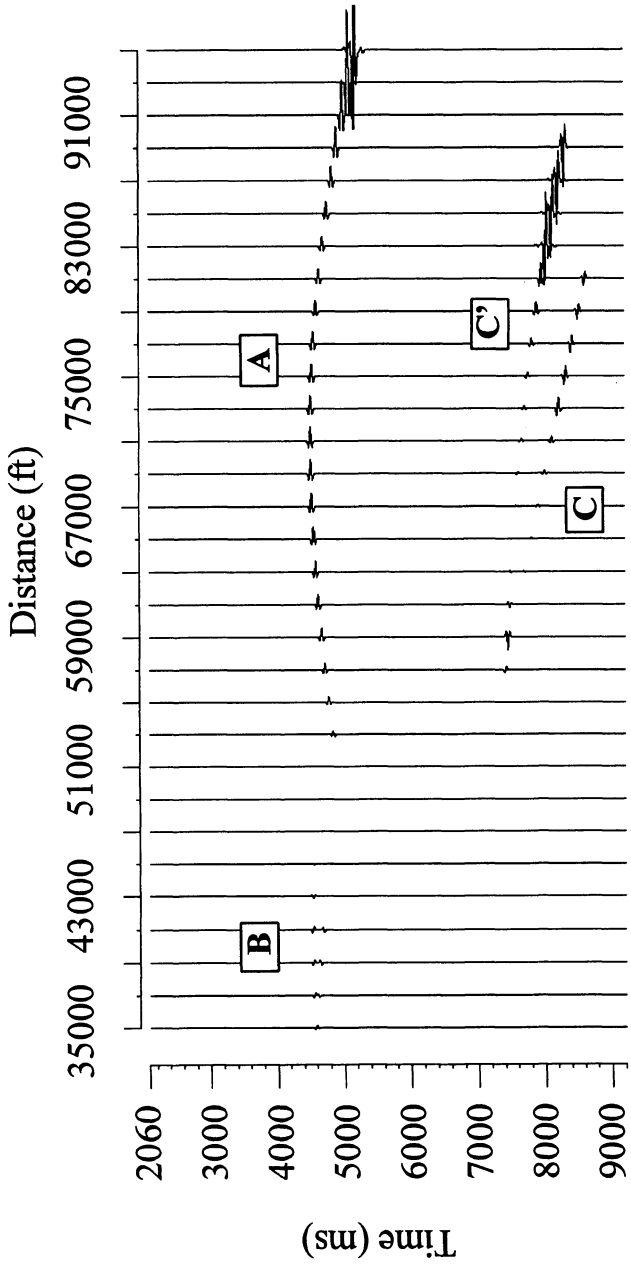

Figure 9. Amplitudes of the fault plane reflection events (C and C) are stronger than primary reflection events (A and B) on many traces.

reflection (Fig. 7: primary reflection A, 53,000–67,000 ft; fault plane reflection C, same interval). Separation of the events by velocity filtering may be possible, but CMP stacking will attenuate the fault plane reflection. Prestack migration of fault plane reflections will require a detailed velocity model, and this requirement is a challenge to present-day processing.

Headwaves along the fault boundary would serve the same purpose as fault plane reflections in imaging closer to the fault. Converted wave primary reflections would also image closer to the fault than a compressional wave primary reflection. Each of these ray types also may hold potential for subthrust imaging.

6. Conclusions

Imaging beneath an overthrust is possible using fault plane reflections in the footwall. A recording geometry different from a conventional split spread is required in order to capture the fault plane reflection. The location of shot point and receivers in this geometry is dependent upon the actual depth model. Model based ray tracing is necessary for designing acquisition geometry to exploit fault plane reflections. It appears that a moderate vertical velocity gradient of .7 ft/s per ft can produce relatively large amplitudes and will be helpful in obtaining reflector coverage near the fault. Conventional stacking of fault plane reflections on CMP gathers will attenuate them. Reverse moveout of fault plane reflections offers encouragement that separating the fault plane reflection from other events by velocity filtering may be possible. Prestack migration of fault plane reflections will require an accurate velocity model.

7. Acknowledgments

The authors thank GX Technology Inc., for their software assistance and J. Pat Lindsey for his suggestions. We also thank Geoff E. Quelch of the Shell Crustal Imaging Facility (SCIF) of the University of Oklahoma for his IBM-RISC 6000 computer systems support. We also appreciate the incisive comments of Don Lawton in reviewing this paper.

8. References

Cook, F.A., Albaugh, D.S., Brown, L.D., Kaufman, S., Oliver, J.E., and Hatcher, R.D., 1979, Thin-skinned tectonics of the crystalline southern Appalachians: COCORP seismic profiling of the Blue Ridge and Piedmont: *Geology* **7**, 563-567.

Iasky, R.P., Young, R.A. and Middleton, M.F., 1991, Structural study of the southern Perth Basin by geophysical methods: *Exploration Geophysics* **22**, 199-206.

Middleton, M.F., 1990, Analysis of wrench tectonics in the Perth and Canning Basins, Western Australia, *Basin and Fuel Report* **No. 3**, 1990, Western Australian Geological Survey, Perth, Australia.

Smithson, S.B., Brewer, J.A., Kaufman, S., Oliver, J.E., Hurich, C.A.,1979, Structure of the Laramide Wind River Uplift, Wyoming from COCORP deep reflection data and gravity data: *Jour. Geophys. Res.* **84**, **B11**, 5955-5972.

Twiss, R.J., and Moores, E.M., 1992, *Structural geology*, W.H. Freeman and Co., 96.

Young, R.A., Stewart, S.C., Seman, M.R., and Evans, B.J., 1990, Fault plane reflection processing and 3D display the Darling Fault, Western Australia: *Tectonophysics* **173**, 107-117.

PART II

ABSTRACTS

PETROLOGY AND TECTONIC SIGNIFICANCE OF THE POLLY WRIGHT COVE PLUTON, BLUE RIDGE PROVINCE, VIRGINIA: AN EXTENSION-RELATED, MULTIPLY-INTRUSIVE MAGMATIC SYSTEM OF ANOROGENIC ORIGIN

W.J. ABBEY, and R.P. TOLLO, *Department of Geology, George Washington University, Washington, DC 20052, e-mail: tollo@acad.ccgs.gwu.edu*
J.N. ALEINIKOFF, *U.S. Geological Survey, Denver, CO 80225, e-mail: jaleinikoff@greenwood.cr.usgs.gov*

The Late Proterozoic Polly Wright Cove Pluton (PWCP) intrudes Grenville-age (1.0-1.1 Ga) basement rocks in the core of the Blue Ridge anticlinorium in central Virginia. The PWCP is part of a regional Late Proterozoic (760-700 Ma) anorogenic supersuite which consists of numerous A-type granite bodies exposed throughout Lauretian terrain in Virginia and North Carolina. The pluton includes four major lithologic phases (from oldest to youngest): (1) fine-grained, biotite granite (present only as xenoliths), (2) medium-grained biotite granite (the most areally extensive lithologic unit), (3) medium-grained biotite leucogranite, and (4) fine- to medium-grained biotite granite (occurs only as dikes). These units are distinguishable in both hand sample and thin section, as well as by their geochemical characteristics. The PWCP granites are metaluminous in composition and have geochemical signatures characteristic of an anorogenic origin including: (1) high Ga/Al and FeO/MgO, (2) marked enrichment of Y, Nb, Zr, Ce and Ga, and (3) low Ba and Sr. The broad range in SiO_2 values (67.1 - 76.5 wt. %), FeO/MgO (12.6 - 41.6), and Ba/Rb (0.34 - 3.50) indicate that fractionation of major minerals was responsible for developing significant compositional variation within the pluton. The late-stage granites (leucogranites and dikes) of the PWCP show a marked depletion in Ba and Sr, as well as an increase in Ga/Al, relative to the older units suggesting that fractionation of alkali feldspar and plagioclase was a major factor controlling differentiation of the PWCP magmatic system. Removal of ferromagnesium silicate minerals is suggested by the range in FeO/MgO and by development of late-stage leucogranite. Additionally, a marked decrease in Ce/Nb relative to Y/Nb in the late stage granites suggests fractionation of allanite. U-Pb isotopic data for zircons from the medium-grained biotite granite yield an upper intercept age of 706 ± 4 Ma, indicating that most of the PWCP was emplaced near the end of the period of regional anorogenic magmatism. The pluton is similar in age to metaluminous granitoids that constitute the southern part of the Robertson River batholith, located 40 km to the north, and it appears to have intruded at the same time as rift-related peralkaline rocks of the Robertson River. A $^{207}Pb/^{206}Pb$ age of 972 Ma from a single xenocrystic zircon preserves isotopic evidence of an inherited component of possible Middle Proterozoic, post-Grenville age. Whereas the supersuite has been indirectly associated with extensional faulting in this region, other studies have linked the PWCP directly to rift-related faulting in the central Virginia Blue Ridge. For this reason, the age of the PWCP has important implications for the timing of extensional tectonics in the region.

BASEMENT-INVOLVED AND DETACHED PHASES OF DEFORMATION IN THE EVOLUTION OF FOLD-THRUST BELTS: EXAMPLES FROM THE SOUTHERN CORDILHEIRA DO ESPINHAÇO AND THE PARAMIRIM DEFORMATION CORRIDOR, BRAZIL

F.F. ALKMIM, and A. DANDERFER Fº, *Departamento do Geologia, Escola de Minas, Universidade Federal de Ouro Preto, 35.400 Ouro Preto, M.G., Brazil; Fax: (55)-31-551-2334*

The southern Cordilheira do Espinhaço in southeastern Brazil, is a Late Proterozoic (Brasiliano/Pan-African) fold-thrust belt that developed along the eastern margin of the N-S trending portion of the São Francisco craton. This N-S-trending and west-verging belt involves both a basement complex, composed of >1.8 Ga crystalline rocks, and Middle to Late Proterozoic metasedimentary units. The Espinhaço fold-thrust belt displays an antiaxial curve in map view, such that the central portion of the belt has propagated further west into the foreland than the northern and southern ends. At its north end, the Espinhaço fold-thrust belt connects to the Paramirim corridor, a deformation belt which trends NNW-SSE and defines the boundary between the E-W trending segment of the São Francisco craton and the N-S trending segment of the craton. The Paramirim corridor, which is doubly vergent, also involves a basement complex and Middle to Late Proterozoic strata. It is composed of two oblique-slip to frontal embryonic fold-thrust belts, which root in a central strike-slip system. The Espinhaço fold-thrust belt and the Paramirim corridor represent inverted segments of a Middle to Late Proterozoic-age passive margin and failed rift, respectively.

Due to at least two Phanerozoic uplift pulses, the whole central to southeastern area of Brazil underwent significant erosion. Exposures at the ground surface today in the Espinhaço fold-thrust belt and the Paramirim corridor. Our results, which define the geometry and kinematics of regional basement-involved structures, show that in both regions, fold-thrust belt deformation developed in two main phases.

In the first phase, deformation was accommodated by movement on detachment faults above the basement-cover contact. This movement resulted in development of duplexes, imbricate fans, and associated flexural to buckle fold trains. All structures formed during this phase have a uniform forelandward vergence. The detachments, at all scales, preferentially developed at interfaces where there was a pronounced rheological contrast, and are found in the foreland and central domains of the fold-thrust belts. Regional detachments occur in metapelitic layers of the Middle Proterozoic Espinhaço Supergroup, and in carbonate beds of the Late Proterozoic São Francisco Supergroup. As shown by previous authors, stress-field geometry during the initial contractional deformation of a sedimentary wedge leads to the generation of a bedding-parallel shear couple, which could have induced formation of the detachments.

In the second phase, basement slices moved along thrust faults and strike-slip faults in the central to foreland segments of the Espinhaço fold-thrust belt and the Paramirim corridor. The faults bounding basement thrust slices commonly represent inverted normal faults. Two distinct styles of basement/cover interaction formed during this phase. (1) Inverted Domino Structure: The first style resulted in formation of domino-like arrays of spaced thrust faults. Faults in these arrays separate unstrained basement slices. The faults either propagate upwards into the overlying cover as out-of-sequence thrusts, or die out in the core of drape folds. As a result, they are overlain by kink folds or monoclines in the cover. (2) Basement-Cored Shear Folding: The second style resulted in formation of zones of pervasive basement shearing, which accommodate development of regional basement-cored antiformal culminations. The contacts between basement and cover around these culminations is a shear zone, and the cover itself deforms by a combination of shear folding and thrusting. Shearing planes in the cover are represented by zones of very intense cleavage. Thrusts within the cover do not cross the basement/cover contact.

Both inverted domino structures and regional basement-cored shear folding generated a very distinctive cover architecture, namely a general synthetic, foreland-directed passive rotation of the involved cover strata. As a consequence of the shear folding process, smaller-order folds in foreland-facing limbs of regional structures have a systematic forelandward vergence. Inverted domino structures are common in the intracratonic Paramirim corridor, whereas basement-cored shear folds and related faults dominate the architecture of the Cordilheira do Espinhaço. During the basement-involved phase of deformation, detachments and associated structures formed during the first phase were faulted and folded, but remnants of first-phase structures can be found in foreland domains, with their original geometries, intact, as documented in the foreland of the Cordilheira do Espinhaço fold-thrust belt.

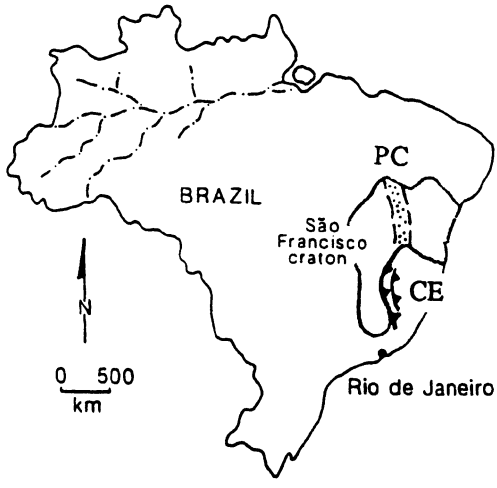

EVOLUTION OF THE LATE PROTEROZOIC BASEMENT IN THE NORTHERN APPALACHIAN OROGENIC SYSTEM AND IMPLICATIONS FOR THE OUACHITA SYSTEM

P.J. BAROSH, *P. J. Barosh, and Associates, 35 Potter Street, Concord, MA 01742, USA, Tel: 508/369-1906*

The evolution of a Post-Grenville, Late Proterozoic basement is clearly revealed in rock well exposed across southern New England. Most of the rock in the southern half of New England is shown to be Precambrian in age on Lyell's 1845 geologic map of North America. A 100 years later these rocks were interpreted to be Paleozoic in age from isolated fossil finds and extrapolation of ages of strata to the north. Today they again are known as Precambrian from detailed stratigraphic studies that show the fossiliferous strata to be in isolated fault slivers or unconformably over a deformed and moderately to highly metamorphosed basement that developed southeast of the cratonic rocks of Grenville age. A regional northward tilt and uplift have brought the basement to the surface in southern New England, whereas in the northern part the rock is largely early and middle Paleozoic in age and in the southern Maritimes late Paleozoic.

This young basement is formed of three tectonic-stratigraphic divisions: a foreland basin that formed as a shelf deposit offshore of the craton, an apparent volcanic arc sequence sliced up in a northwest-dipping suture zone, and a batholithic complex that is considered to have been an extension of what is now northwest Africa. The basinal strata were deposited as thin-bedded limy muds, that commonly contain iron sulfides, and graded-bedded graywacke sands and silts. The arc deposits were a wide variety of thin-bedded commonly laminated, volcaniclastic sands, muds, ash and minor lava. Measured thicknesses of these sequences are 21.7 km and 18.8 km respectively. Both these sequences now contain scattered elongate flow-foliated granitic bodies that invaded thrust faults and numerous pegmatitic lenses. The granodioritic batholith invaded over 2.8 km of strata that were laminated clean sands, volcaniclastic sands and muds, ash, and lava. The batholith is foliated and in folds near the suture, but not to the east of it.

The intrusion of the batholith, 620-630 m.y. marks the main period of collision, underthrusting and metamorphism. This was followed by great uplift and unroofing prior to the initial volcanic deposits in the graben forming the Boston Basin at 595 m. y. Reactivation of the suture zone and other thrust faults combined with uplift deformed the cover rocks at various times during the Paleozoic.

All, but the northwestern part of the northern Appalachian orogen involves this Late Proterozoic basement whose formation and subsequent deformation are the essential features of the orogen's development. This basement largely strikes southwestward beneath coastal plain deposits and is covered along the central and southern Appalachian system. If the northwestern part of the Appalachian belt continues as the Ouachita system of the southern U.S., as is commonly thought, then such a basement should lie buried beneath the coastal plain deposits of southeastern Texas.

THE NORTH-TRENDING SWARM OF MESOZOIC DIKES IN THE SOUTHERN APPALACHIANS: ITS MAP PATTERN AND SIGNIFICANCE FOR MESOZOIC EXTENSION

M.J. BARTHOLOMEW, *Earth Sciences & Resources Institute, University of South Carolina, Columbia, SC 29208, Tel: 803/777-7693, email: jbarth@esri.esri.scarolina.edu*

The N-trending swarm of Mesozoic mafic dikes extends northward from near Charleston, South Carolina, across central North Carolina into SW Virginia. Over most of its extent in the Carolinas, major dikes of this swarm have been traced primarily by magnetic anomalies, whereas in SW Virginia, individual dikes have been mapped on 1:24,000-scale geologic maps by numerous investigators. Within SW Virginia, mapped patterns of this dike swarm include numerous *en echelon* sequences of smaller dikes. These *en echelon* dike sequences consistently defined left-lateral, NE-SW-trending shears and right-lateral, NW-SE-trending shears indicating that the N-trending dike swarm was emplaced with an E-W-oriented σ_3 and a vertical σ_2. The N-trending dike swarm crosses two major Triassic rift basins: the Dan River Basin of southwestern Virginia and adjacent North Carolina, and the Deep River Basin of North Carolina.

The basin-bounding, E-dipping Chatham fault flanks the NW side of the Dan River Basin. Overall, the Chatham Fault trends NE-SW subparallel to the *en echelon* NW-limit of the N-trending dike swarm and is favorably oriented for reactivation as a left lateral strike-slip fault during emplacement of the dike swarm. The Chatham fault has a highly irregular surface trace, thus many short segments trend NW-SE and are favorably oriented for reactivation as right lateral strike-slip faults. The ENE-trending Stony Ridge fault zone serves as the *en echelon* link between the basin-bounding Chatham fault and the Brevard zone which approximately marks the NW-limits of both extensive Mesozoic faulting, documented by Garihan and Ranson (1992), and NW-trending mafic dikes. Fullagar and Butler (1980) reported a mid-Jurassic (180 Ma) Rb-Sr age for the Stony Ridge fault zone.

The basin-bounding, W-dipping Jonesboro fault flanks the SE side of the Deep River basin and is segmented into N-, NE-, and ENE-trending segments. The northern portion of this fault was characterized by normal-oblique movement with an E-W-oriented σ_3 during Triassic extensional development of the basin (Bartholomew and others, 1994). Triassic development of the Deep River Basin, which is the basin closest to the convergent center of the N-trending swarm, and emplacement of the N-trending dike swarm are both characterized by an E-W-oriented σ_3 suggesting sequential emplacement of the N-trending swarm as the basin-forming stress field evolved (inversion of σ_1 and σ_2) followed by Jurassic emplacement of NW-trending dike swarms characterized by a NE-SW-oriented σ_3.

The N-trending swarm ends in central Virginia, but north of these dike patterns also suggest a similar sequential development. NE-trending mafic dikes are subparallel to the basin-bounding fault flanking the NW side of the Culpepper basin of Virginia and Maryland. These NE-trending dikes reflect emplacement within the basin-forming stress field characterized by an ESE-oriented σ_3 and a vertical σ_1 and likely preceded emplacement of NW-trending dikes characterized by a NE-SW-oriented σ_3.

CRUSTAL TECTONIC CONTROLLING METALLOGENIES FROM PALEOZOIC TO TERTIARY IN THE NORTH PATAGONIAN REGION, ARGENTINA

H.G.L. BASSI, *Centro de Investigaciones en Recursos Geológicos, Ramirez de Velasco 847, 1414, Buenos Aires, Argentina*

When comparing alignments of mining districts of the Rio Negro province and the elongation of outcropping granite and metamorphic bodies of precambrian-paleozoic ages strongly similar strikes are found (Figs. 1 and 2).

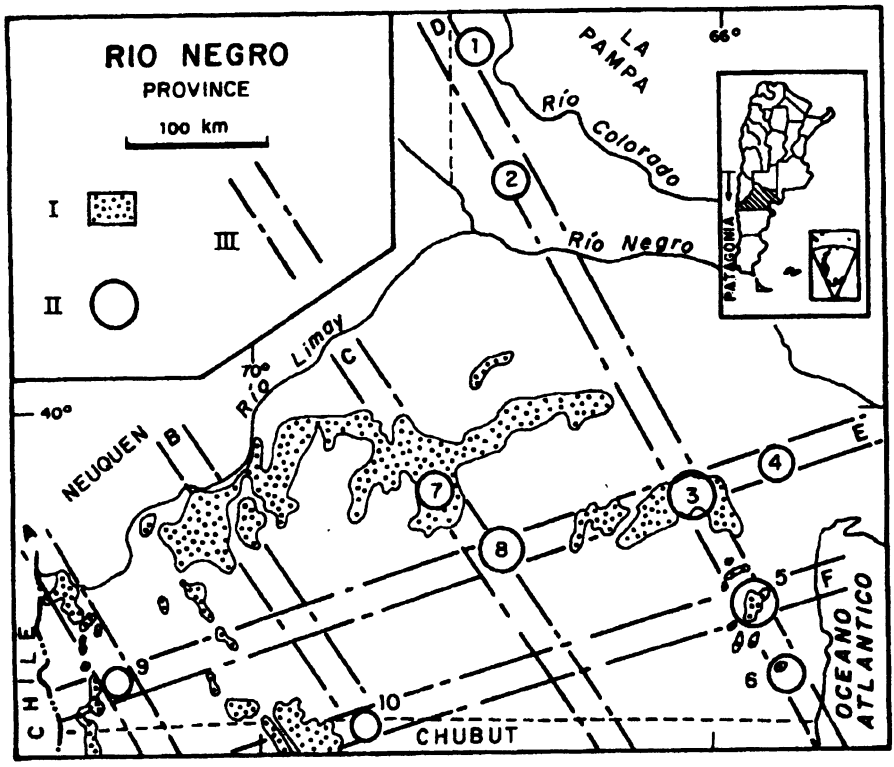

Figure 1. PROVINCE OF RIO NEGRO. INTERPRETATION OF THE METALLOGENIC BELTS. I, basement outcropping bodies (metamorphites-granitoids). II, Mining Districts: 1, Catriel (oil); 2, Lago Pellegrini (bentonite); 3, Valcheta (W, Pb, Cu, F); 4, Gualicho (W); 5, Gonzalito (Pb, W); 6, Sierra Grande (Pb, F); 7, Esperanza (Pb, Mn, F); 8, Choique Mahuida (Pb, Cu, Ba, Mn, Kaolin); 9, María (Pb, Au); 10, Angela (Au, Pb, Zn). III, Metalogenic Belts: A, María; B, Angela; C. Esperanza-Choique; D. Catriel-Sierra Grande; E, María-Gualicho; F, Angela-Gonzalito.

This display is associated to the frequency of strikes shown by megafractures and alignments of more than 150 km length throughout the whole patagonian region (Fig. 3) which extends more than 10^6 km^2.

Such strikes are NNW and ENE, which constitute the main sides of the Patagonian Regmagenic Net, considered as representatives of the crustal fractures (Bassi, 1998).

Such fracturing (proterozoic) modeled the precambrian crust a settled a pattern of periodical tectonic reactivations up to present, which in turn controls the ways of access for differents metallogenies as well as most of the post-precambrian magmatic cycles, mainly the one related to paleozoic granitoids.

Two metallogenic cycles were identified. The first one of high temperature, tungsten bearing and probably of caledonian age. The other, Pb, Ag, Zn, Cu, Barite, Mn, F and Kaolin bearing, ranging from meso to epithermal with ages from Post Jurassic to Tertiary.

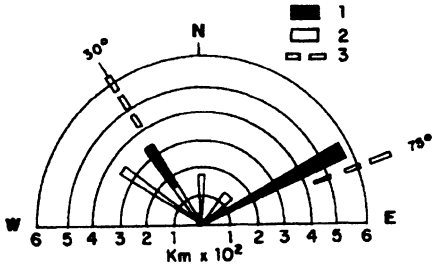

Figure 2. Rio Negro Province. Frequency Diagram. 1, elongation of the basement outcropping bodies; 2, faults (1994, State Geological map 1:750,000); 3, trend of metallogenic belts (without scale).

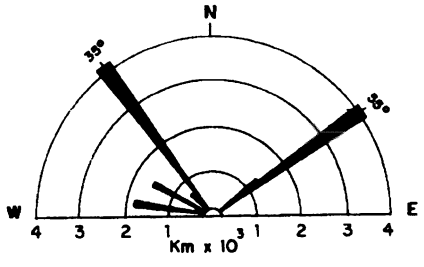

Figure 3. Patagonian Region. Frequency of megafractures and lineaments. (after Bassi, 1988).

Not depending on the age of the genetic cycles, the whole of the know districts arrange themselves following a systematic net, and forming metallogenic belts striking ENE and NNW (Fig. 1).

The know mining districts are always located at the points of intersection of the net lines and may constitute a future prospection tool in the intersections with no mining occurrences as well as along the belts.

References

Bassi, H.G.L. (1988) Hypotheses concerning a regmagenic network controlling metallogenic and other geological events in the South American Austral Cone, *Geologische Rundschau*, 77/2, pp. 491-511, Stuttgart

EARLY PROTEROZOIC DUCTILE REWORKING OF ARCHEAN BASEMENT IN THE CENTRAL LARAMIE RANGE: A COMPLEX RESPONSE TO THE CHEYENNE BELT, TRANS-HUDSON AND CENTRAL PLAINS OROGENS

R.L BAUER, D.A. GRESHAM, and J.D. EDSON, *Department of Geological Sciences University of Missouri, Columbia, MO 65211, U.S.A.*

The central Laramie Range of southeastern Wyoming lies along the southeastern margin of the Wyoming Archean province. The southern margin of the province in this area is defined by the Cheyenne Belt, a suture zone that marks the interface between Archean rocks to the north and early Proterozoic juvenile crust (< 1.8 Ga) to the south. The eastern margin of the Wyoming craton, just east of the central Laramie Range, is buried beneath Phanerozoic cover. However, drill core and geophysical data indicate that this boundary is marked by the southern projection of the early Proterozoic Trans-Hudson orogen (THO), which is generally interpreted as a collisional orogen that formed between the Wyoming and Superior Archean cratons. The THO extends to the south from exposures in Canada, through the Black Hills, to a buried intersection with the Central Plains orogen (CPO). Like the Cheyenne Belt, this northern boundary of the CPO marks the northern limit of juvenile crust younger than 1.8 Ga.

Recent U/Pb apatite dates and thermobarometry by Chamberlain et al. (1993) suggest that the central Laramie Range underwent a near vertical block uplift of ca. 10 km during collision along the Cheyenne Belt. The uplift was accommodated by displacement along the Laramie Peak shear zone that marks the northern boundary between deformed amphibolite facies gneiss of the central Laramie Range and relatively undeformed greenschist facies rocks of the Laramie batholith to the north. The age of uplift is ca. 1.76 Ga (Resor et al., 1994) based on U/Pb sphene ages in a deformed mafic dike within the shear zone.

Our analysis of deformation features in late Archean and Early Proterozoic rocks of the central Laramie Range indicates that intense ductile reworking of this southeastern margin of the Wyoming Archean craton occurred during two events that may be correlated with the Trans-Hudson orogen and the collision that produced the Cheyenne Belt. The dominant Archean rocks include granitic gneiss and infolded supracrustal rocks of the Elmers Rock greenstone belt (Snyder, 1984, 1986). Early Proterozoic mafic and ultramafic dikes and a small granodiorite pluton that intruded the Archean rocks have U/Pb ages of ca. 1.8 Ga (Cox et al, 1993; Snyder et al., 1995). The Proterozoic units cut an early gneissic banding in the Archean rocks, but both the Archean and Early Proterozoic rocks contain at least two generations of folds and deformation fabrics that post-date the prominent banding in the gneiss.

The regional trend of the earliest Proterozoic deformation (D_2) varies from E-W in the southern margin of the central Laramie Range, in the vicinity of the Elmers Rock greenstone belt, to nearly N-S along the eastern margin of the range to the north. The change in trend defines a broad oroclinal bend that closes to the southeast. Rock

fabrics generated during the D_2 event are dominantly L-tectonites in both the E-W and N-S-trending segments. Lineations and fold hinges in the southern area range from westerly plunges in the western part of the area to more northerly plunges and associated reclined fold forms toward the east, approaching the oroclinal hinge of the regional structural trend. The Proterozoic mafic and ultramafic dikes in this area are locally folded on a regional scale about northerly dipping E-W-striking axial planes. A strong L_2 linear fabric, parallel to that in the Archean host rocks, is common within the deformed mafic dikes, but it is quite variably developed even within the same dike. Lineations and fold hinges along the eastern margin of the range, north of the oroclinal bend, plunge moderately to the south. The F_2 folds have upright N-S-striking axial planes and a dominant Z symmetry. Both Proterozoic mafic dikes and a Proterozoic granodiorite pluton, intrusive into the granitic gneiss of this area, contain a strong L_2 linear fabric parallel to that in the Archean host rocks.

Along both the southern and the northeastern study areas, D_2 fabrics are folded by broad open F_3 folds with NW-striking upright axial planes. These folds deform the Proterozoic mafic dikes on a regional scale and have deformed the outline of the granodiorite pluton into an open arc with a NW-striking axial plane. F_3 folding of the L_2 linear fabric produced a complex redistribution of the L_2 lineations within both the Archean and Proterozoic units (Gresham and Bauer, 1994).

Although the Early Proterozoic age of these deformation events is well established, the attribution of these events to Trans-Hudson or Cheyenne Belt/Central Plains orogens is more equivocal. If only the northeastern area is considered, the N-S-trending D_2 features can be readily attributed to E-W shortening during the Trans-Hudson orogen. The F_3 folds could be attributed to later shortening from the south or southwest along the Cheyenne Belt. This scenario is consistent with the relative timing of the Trans-Hudson and the Cheyenne Belt that has been inferred. However, if only the southern area is considered, the E-W-trending D_2 features can be explained as a result of N-S shortening along the Cheyenne Belt followed by younger shortening from the northeast during the Trans-Hudson orogen. This is not consistent with the generally inferred timing of these orogens. It is possible that the oroclinal bend of the D_2 structural trends is due to complex interactions along this southeast corner of the Wyoming craton between convergent island arc sequences accreted from the south along the Cheyenne Belt and concomitant E-W convergence during the Trans-Hudson orogen.

References

Chamberlain, K. R., Patel S.C., Frost, B.R., and Snyder, G.L. (1993) Tectonic reactivation of the Archean Wyoming Province during Proterozoic orogeny: a case for thick-skinned thrust deformation. *Geology*, 21, *995-998.*

Cox, D. M., Chamberlain, KR., and Snyder, G.L. (1993) U-Pb ages of mafic intrusions from the southeast margin of the Wyoming Province: Implications for timing of rifting and deformation. *Geological Society of America, Abstracts with Programs,* vol. 25, p. 24.

Gresham, D.A. and Bauer, R.L. (1994) Evidence for Early Proterozoic timing of widespread ductile deformation in Archean gneiss of the east-central Laramie Range, Wyoming. *Geological Society of America, Abstracts with Prograws*, vol. 26, p. A232.

Resor, P.G, Chamberlain, KR., Frost, C.D., and Snoke, A.W. (1994) U-Pb sphene date of mylonitization associated with the Proterozoic Laramie Peak shear zone, Laramie Mountains, WY. *Geological Society of America, Abstracts with Programs*, vol. 26, p. A465.

Snyder, G..L., (1984) Preliminary geologic maps of the central Laramie Mountains, Albany and Platte Counties, Wyoming: *U.S. Geological Survey Open-Files Report* 84-358 (parts A-M), scale 1:24,000.

Snyder, G..L., (1986), Preliminary geologic maps of the Reese Mountain and part of the Hightower SW 7.5 minute quadrangles (Part A) and parts of the Fletcher Park and Johnson Mountain 7.5 minute quadrangles (Part B), Albany and Platte Counties, Wyoming: *U.S. Geological Survey Open file Report* 86-201, 1:24,000.

Snyder, G.L, Siems, D.F., Grossman, J.N., Ladwig, KR., and Nealey, L.D., (1995), Geological map, petrochemistry, and geochronology of the Precambrian rocks of the Fletcher Park-Johnson Mountain area, Albany and Platte Countries, Wyoming. *U.S. Geological Survey Miscellaneous Investigations Series,* I-2233, 1:24,000.

PROPAGATION OF HIGH ANGLE, DIP-SLIP BASEMENT FAULT ZONES INTO OVERLYING SEDIMENTARY ROCKS

L.A. BOLDT, *School of Geology and Geophysics, The University of Oklahoma, Norman, OK 73019, tel: 405/325-3253, e-mail: lboldt@fault.scif.our.edu*

Some mechanisms by which high angle, dip-slip fault zones in crystalline basement propagate into overlying sedimentary rocks are presented. The study was conducted on a segment of the Uncompahgre Uplift in western Colorado where uplift occurred along faults in the Precambrian basement during Laramide deformation. The basement in this area is composed predominately of granite and gneiss. The structure was mapped at a 1:1000 scale covering an area of about two km^2. This study focuses on the deformation of the Chinle Formation (Triassic), composed of siltstones and shales, which lays directly on the basement, and the overlying, massive aeolian Wingate Sandstone (Triassic).

The basement-sedimentary rock interface in the study area is cut by two nearly E-W striking fault zones (faults A & B, Fig. 1). The northern fault bifurcates along strike from a single fault in the east to two fault segments and an intervening rotated block in the west (compare Figs. 1 & 2). The displacement along fault A occurred across a distinct narrow zone, and is classified as a high angle reverse fault (~70°-80°S). While the sense of displacement on fault B is identical to that of fault A (South block up), the displacement of fault B occurred across a significantly wider zone of unclear inclination. Total throw across both faults A and B and their associated segments is constant at ~150m.

There is a stark contrast in the response of the sedimentary units to uplift along these two fault zones. Above the reverse fault A and its segments, the Chinle Formation is faulted without any apparent loss of throw (faults A_1 and A_2, Fig. 2). The Wingate Sandstone, however, responds in a more complicated manner. Above the single reverse fault A, east of the bifurcation point, the entire Wingate Sandstone is displaced by a single through-going fault that is accompanied by a small amount of folding (fault A, Fig. 1). While the behavior of the Wingate Sandstone above the two individual reverse fault segments, west of the bifurcation, is different (Fig. 2). The discrete displacement at the Chinle-Wingate contact is distributed across a zone that widens up-section producing two distinct monoclines at the top of the Wingate (i.e., these are blind faults).

The sedimentary units over the wide fault zone of fault B (fault B, Figs. 1 & 2) behave in still a different manner. Here the Basement-Chinle contact is again offset, but the Chinle-Wingate contact has little or no fault offset (fault B, Figs. 1 & 2). While the magnitude of throw on this fault is comparable to that of fault A_2, fault B has already gone blind in the Chinle Formation.

This study suggests several factors that control the faulting behavior of sedimentary rocks above basement faults. First, sedimentary units above widely spaced faults tend to accommodate more throw by distributed deformation than the same units above single or closely spaced faults. Secondly, the width of the basement fault zone appears to control the distance the fault propagates into the sedimentary rocks. A narrow fault zone propagates further into the sedimentary sequence as a fault, whereas, a wide fault zone accommodates part of the throw by distribution deformation. Finally, the mechanical properties of the sedimentary rocks will dictate the mechanisms by which the fault throw is accommodated.

Figure 1:Schematic cross section of the east side of the study area

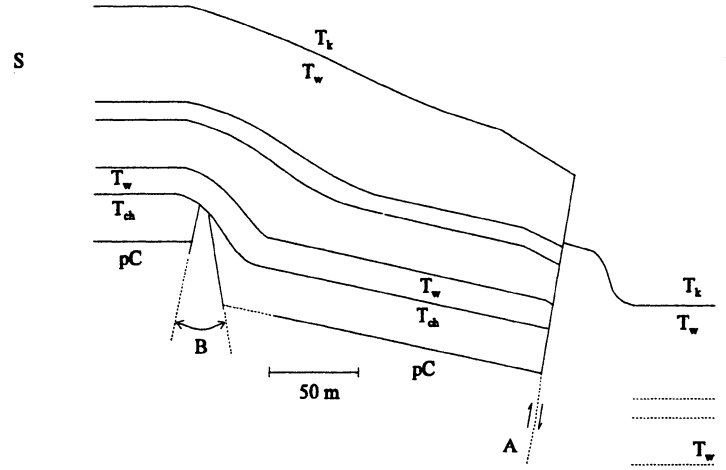

Figure 2: Schematic cross section of the west side of the study area

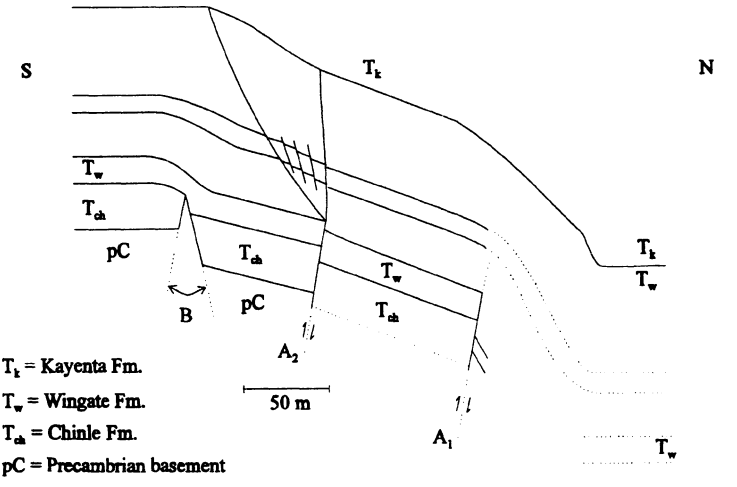

GEOLOGIC PROVINCES OF OKLAHOMA

J.A. CAMPBELL, *Oklahoma Geological Survey, Norman, OK*
R.A. NORTHCUTT, *Independent Geologist, Oklahoma City, OK*

The geologic provinces of Oklahoma are mainly the product of tectonics and attendant sedimentation of Pennsylvanian age. Most boundaries are structural; thus, the provinces map is a generalized tectonic map. Permain and post-Paleozoic strata tend to mask those structures, but most of those strata have been removed by erosion, except in the Anadarko Basin and the Wichita Uplift provinces. The location of most of Oklahoma's oil and gas resources are either influenced by, or are the direct result of Pennsylvanian tectonics and sedimentation patterns. Therefore, the present study also defines provinces in the subsurface on the basis of geological criteria. The authors have attempted to use the originally published names for the recognized provinces. However, we have also used the most *geologically* correct names, i.e., Nemaha Uplift, Nemaha Fault Zone, and Central Oklahoma Fault, in lieu of Nemaha "Ridge."

Oklahoma is separated into five major uplifts and five major basins. Most of these have subprovinces, which sum to 20 additional identified geologic units. The Gulf Coastal Plain is not included in this study because it is a veneer of Cretaceous over that masks significant structures. Faults are the most common boundary element. Although their precise age commonly is known only approximately, their geographic location is less controversial, except in detail. Stratigraphic/structural boundaries are based on less precise geological information. Such boundaries interpreted at the surface are influenced by both geology and geomorphology, and are therefore strongly influenced by the present level of erosion. The major example of a surface stratigraphic/structural boundary is the southwestern limit of the Ozark Uplift in eastern Oklahoma. Stratigraphic/structural boundaries in the subsurface are commonly based on structural or isopachous contours from well or geophysical data, or on a structural trend, as well as the boundary that separates the Marietta Basin from adjacent geologic elements.

Important subsurface boundaries in the Anadarko and Arkoma Basins have been neglected in previous studies: The Anadarko Basin/Shelf boundary is placed at the 700-ft isochore of the Atokan and Desmoinesian Series (Rascoe, 1962), at which there is a marked rate of change of thickening southward into the basin. The northern limit of the Arkoma Basin seems to merge imperceptibly into the southern part of the Cherokee Platform, and has been variously drawn by a number of authors. For the purpose of this study the boundary is modified from the "hinge line" of the Atokan Series (Weirich, 1953). This boundary approximates the striking rate of change of thickness of Atokan strata southward into the Arkoma Basin.

The existing tectonic map of Oklahoma (Arbenz, 1956) is forty years old, and a new one is wanting. This provinces map must suffice until that is accomplished.

Significantly, however, the tectonic map of Texas (Ewing and others, 1990) includes the structurally complex provinces of southern Oklahoma.

The authors are indebted to the numerous earlier studies on which the present mapped boundaries are dependent. They are too numerous to list here.

GEOLOGICAL PROVINCES AND SUBPROVINCES OF OKLAHOMA

Arbuckle Uplift

Arbuckle Mountains	ABM
Tishomingo-Belton Horst	TBH
Pauls Valley-Hunton Horst	PHH
Clarita Horst	CLH
Ada High	ADH
Lawrence Horst	LAH

Nemaha Uplift

Nemaha Fault Zone	NFZ
Central Oklahoma Fault Zone	COF

Ouachita Mountains Uplift

Broken Bow Uplift	BBU
Ouachita Central Region	OCR
Ouachita Frontal belt	OFB

Ozark Uplift

Wichita Uplift

Wichita Frontal Fault Belt	WFB
Criner Uplift	CRU
Waurika-Muenster Uplift	WRU
Marietta Basin	MRB

Anadarko Basin

Anadarko Shelf	
Cimarron Arch	CMA
Cyril Basin	CYB

Ardmore Basin

Arkoma Basin

Franks Graben	FRG
Wapanucka Graben	WPG

Cherokee Platform

Hollis Basin

EVIDENCE FROM THE STRATIGRAPHIC RECORD FOR BASEMENT DEFORMATION IN SOUTHEASTERN NEBRASKA, MIDCONTINENT U.S.A.

M.P. CARLSON, *Nebraska Geological Survey, 113 N.H., University of Nebraska, Lincoln NE 68588-0517, tel. 402-472-7549, email: mpc@unlinfo.unl.edu*

Superimposed on the continental-scale sequence patterns of the Phanerozoic described by Sloss (1963) are stratigraphic features that record local tectonics. For the most part, these tectonic features are the result of regional stress on pre-existing basement fractures causing activity that interrupts the regional stratigraphic record. Facies and local absence of sedimentary units provide evidence for delineating the time and extent of these basement rejuvenations.

The broad facies patterns of the Sauk Sequence were not significantly affected by either local tectonics or the paleotopography present at the surface of the Precambrian. However prior to the deposition of the Tippecanoe Sequence, local uplift in southeastern Nebraska and adjacent areas (Southeast Nebraska Arch) allowed removal of all sediments of the Sauk Sequence. The carbonate, sand, and shale facies of the Tippecanoe Sequence again indicate a broad platform of sedimentation. The unconformities within the sequence are regional with little variation that would indicate the development of local tectonics. Late in the Tippecanoe Sequence, the North Kansas Basin formed allowing greater thicknesses of Silurian-age carbonates to accumulate. Major regional erosion preceded the deposition of the Kaskaskia Sequence; earlier sedimentary units were preserved in the North Kansas Basin.

Several depositional cycles, separated by unconformities, make up the Kaskaskia Sequence. However, the only indication of significant local tectonics is the broad pattern of greater accumulation in the North Kansas Basin. The pre-Absaroka unconformity records significant tectonic activity in midcontinent U.S.A. Many of the local structures represent reactivation of the basement fractures of the Late Keweenawan Midcontinent Rift System. In the southeastern Nebraska area, the Nemaha Uplift emerged separating the older North Kansas Basin into the Forest City Basin to the east and Salina Basin to the west. Both thickness and facies of the initial sediments of the Absaroka Sequence delineate this basin-uplift complex. All earlier sequence sediments were removed from the Nemaha Uplift so Middle Pennsylvanian sediments rest on Precambrian rocks. The later Pennsylvanian and Permain sediments record cyclic eustatic fluctuations of sea level with no significant local tectonics.

No deposits of the Zuni Sequence are present in extreme southeastern Nebraska. However, the anticlines and faults present in the area indicate that some post-Absaroka tectonic activity occurred. More complete stratigraphic sections in adjacent regions suggest that this tectonic activity could equate to that recorded in the late Zuni Sequence. Seismic measurements demonstrate that portions of southeast Nebraska still have tectonic activity.

PETROLOGIC CONSTRAINTS ON THE TECTONIC EVOLUTION OF THE LLANO UPLIFT

W. CARLSON, *Department of Geological Sciences, University of Texas at Austin, Austin, Texas 78712 email: wcarlson@ccwf.cc.utexas.edu*

Tectonic models for the Proterozoic evolution of the Llano Uplift must account for a two-stage metamorphic history characterized by early dynamothermal metamorphism at high pressures that decreases in intensity from southwest to northeast across the uplift, followed by later, largely static, metamorphism at lower pressures resulting from regionally widespread emplacement of granitic intrusions at relatively shallow levels in the crust.

The dynamothermal nature of early metamorphism is evident over much of the uplift in strongly transposed layering and multiple generations of structures and fabrics, but metamorphic conditions during this early event have been largely obscured by later static overprinting that has greatly modified textures, mineral assemblages, and mineral compositions. The most conclusive evidence for high pressures during the early event comes from remnants of eclogitic rocks in the northwestern uplift (Mason County), which preserve the assemblage pyropic garnet + omphacitic clinopyroxene + orthopyroxene + pargasitic amphibole + rutile and yield estimates for equilibration conditions of 750°C at 8-11 kbar. At this locality, partially retrogressed samples display textural features indicative of their high-pressure origin, in particular the partial to complete replacement of omphacitic clinopyroxene by a symplectite of sodic augite + oligoclase. Similar rocks are found in the northern uplift (Whitt Ranch) and the south-central uplift (Oxford), in which later retrogression is more nearly complete; these contain identical symplectitic replacement textures and relict minerals with similar chemistry. Inclusion thermometry at Whitt Ranch yields a lower peak temperature of 585°C, however, and the mineralogy of inclusions in garnet from both Whitt Ranch and Oxford suggests lower peak pressures, in the range 6-8 kbar.

An analysis of growth-zoning patterns in garnet has recently resolved the question of whether these eclogitic remnants are allochthonous bodies that record a pressure-temperature history different from that of their surrounding rocks, or whether the entire uplift experienced early syndeformational metamorphism at high pressures and temperatures. The degree of homogenization of growth zoning during early prograde metamorphism varies systematically across the uplift, both in the eclogitic remnants and in the rocks immediately surrounding them. Garnets of all sizes in the Mason County eclogites and in the surrounding semi-pelitic gneisses were completely homogenized at the peak of early metamorphism; garnets of all sizes in the Whitt Ranch eclogitic remnant and nearby garnet amphibolites are unhomogenized; and garnets in eclogitic rocks at the Oxford locality and in nearby semi-pelitic schists show partial

homogenization that varies systematically with crystal size. These local similarities in degree of homogenization, when combined with regional geographic variations in degree of homogenization, require that the rocks in which the eclogite remnants reside experienced the same thermal history during early metamorphism as the eclogitic rocks themselves, documenting that the Llano Uplift as a whole underwent early metamorphism at moderate to high pressures. This conclusion is corroborated by phase equilibria for high-H-staurolite occurrences in pelitic units and enstatite occurrences in a serpentinized ultramafic body in the southeastern uplift, which together require temperatures near 700°C at pressures in the vicinity of 7 kbar.

Mineral assemblages that preserve a record of early metamorphic conditions are rare. Because of thorough and ubiquitous overprinting, the dominant assemblages throughout the uplift are characteristic of low-pressure (Buchan-series) metamorphism in the middle-amphibolite facies. Deformational fabrics in many rocks are modified by static recrystallization textures, and decussate porphyroblasts of minerals stable at low pressure commonly overgrow metamorphic foliations. These effects are ascribed to widespread recrystallization, accompanied by hydration, during thermal events associated with the emplacement of granitic plutons. Phase equilibria in calc-silicates document static recrystallization driven by the influx of hydrous fluids with oxygen isotopic signatures identical to those of adjacent granitic bodies. Phase equilibria and thermobarometry also document the presence of subtle thermal aureoles surrounding plutons in the southeastern uplift, and indicate equilibration conditions in the range of 475-625°C at 2-3 kbar for localities distributed widely across the uplift. At present, no evidence exists for systematic geographic variations in metamorphic conditions during this episode. This "static event" was neither a single event nor was it entirely post-deformational: crystallization ages for plutons in the uplift span several tens of millions of years, and field evidence suggests that some plutons were intruded in the waning stages of deformation. Nevertheless, late recrystallization throughout the uplift is without doubt thermobarometrically and kinematically distinct from early recrystallization.

Tectonic models for the evolution of the Llano Uplift are therefore constrained by petrologic observations to account for burial to maximum depths of 30-35 km during orogeny, with a decrease in metamorphic intensity from southwest to northeast; and for subsequent uplift to depths of 5-10 km as deformation waned prior to the main pulses of granitic intrusion, with exhumation that was more pronounced in the southwest than the northeast.

PROTEROZOIC EVOLUTION OF THE LLANO UPLIFT, CENTRAL TEXAS: EVIDENCE FOR HIGH-PRESSURE METAMORPHISM FROM THE OXFORD MAFIC BODY

J. DAVIDOW and W. CARLSON *University of Texas at Austin Department of Geological Sciences Austin, Texas 78712 USA*

A unique garnetiferous occurrence of Proterozoic mafic rocks in the south-central Llano Uplift near Oxford in central Texas provides evidence supporting the hypothesis that rocks in the southeast uplift shared the high-pressure metamorphism recorded in remnants of mafic eclogites in the northwest uplift (Mason County eclogite: Wilkerson et al., 1988) and northern uplift (Whitt Ranch metagabbro: Schwarze, 1990). Petrologic features that formed during early high-pressure metamorphism have been partly obscured, however, by late amphibolite-facies retrogression at low pressure, which overprinted many rocks throughout the uplift. Prior to this study of the Oxford body, involvement of the rocks in the southeast portion of the uplift in an early high-pressure metamorphic event had been inferred only on the basis of staurolite textures and chemistry from two localities in the Precambrian Rough Ridge Formation and from regional trends in homogenization of prograde garnet zoning (Carlson and Nelis, 1986; Carlson and Schwarze, 1993; Carlson and Reese, 1994).

Discontinuous outcrops of porphyroblastic garnet amphibolite, mapped by Collins (1978), are exposed in the channel and bank of Lost Hollow Creek near Oxford. The common mineralogy is magnesian hastingsite + oligoclase + quartz + biotite ± almandine-rich garnet (typically strongly resorbed) + ilmenite (typically partly replaced by titanite). Matrix textures are generally foliations defined by aligned amphibole + biotite, layers defined by lack of amphibole + biotite, and fine-grained symplectitic intergrowths of amphibole + plagioclase + augite. Relict garnet porphyroblasts range in diameter from 5 to 2 mm. They are encased by reaction zones (coronas), 5 to 0.5 mm in radial thickness, composed of amphibole + oligoclase to andesine + quartz + ilmenite ± biotite ± magnetite, which lack organization into distinct mineralogical bands. Plagioclase compositions adjacent to garnet are andesine and become steadily more sodic toward the matrix. Inclusions in garnet occur as polymineralic assemblages of ilmenite ± apatite ± titanite ± quartz ± andesine ± epidote ± amphibole and as monomineralic inclusions of andesine, quartz, epidote, apatite, ilmenite, magnetite, and titanite. Garnet-hornblende thermometry (Graham and Powell, 1984) on one polymineralic inclusion of quartz + ferro-tschermakite near the rim of a highly resorbed garnet crystal records a minimum prograde temperature of 620 ^{0}C.

Although these rocks lack appropriate assemblages for thermobarometry to characterize their early history, they exhibit a striking textural and chemical affinity with the eclogitic remnants at Whitt Ranch in the northern portion of the uplift, which present more definitive evidence of having undergone an early, high-pressure metamorphism. Matrix symplectites, garnet compositions, and inclusion suites in garnet are similar in both occurrences. Garnet resorption mineralogy is similar in both

occurrences, although the coronas in the Whitt Ranch rocks are highly organized into mineralogical bands. Carlson and Johnson (1991) have shown that the Whitt Ranch coronas formed by a diffusion-controlled reaction. It is possible that the unorganized coronas in the Oxford rocks formed by a different mechanism, or formed initially by a similar mechanism but were later modified.

Preliminary results from an investigation of garnet zoning profiles in a suite of centrally sectioned crystals, following the method described by Carlson and Schwarze (1993), indicate that the degree of homogenization of growth zoning experienced by garnets in the Oxford body is intermediate between the completely homogenized garnets in the northwest Mason County and the unhomogenized Whitt Ranch rocks. Thermometry on mineral assemblages in these occurrences indicates peak temperatures in the early high-pressure event of ~750 ^{0}C for the Mason County and ~585 ^{0}C for the Whitt Ranch rocks. The peak temperature experienced by the Oxford body is likely bounded by these values.

These three mafic occurrences document a regional gradient in early peak metamorphic conditions across the uplift that is consistent with Schwarze's (1990) suggestion that peak conditions during Proterozoic continental collision were greatest in the southwest and decreased toward the northeast, along a northeast-trending line parallel to the bulk tectonic transport direction.

References

Carlson, W.D. and Reese, J.P. (1994) Nearly pure iron staurolite in the Lano Uplift and its petrologic significance. American Mineralogist, 79, 154-160.

Carlson, W.D. and Schwarze, B.T. (1993) Petrologic and tectonic significance of geographic variations in garnet growth zoning in the Liano Uplift. GSA Abstracts with Programs, 25, 101-102.

Carlson, W.D. and Johnson, C.D. (1991) Coronal reaction textures in garnet amphibolites of the Llano Uplift. American Mineralogist, 76, 756-772.

Carlson, W.D. and Nelis, M.K. (1986) An occurrence of staurolite in the Llano Uplift, central Texas. American Mineralogist, 71, 682-685.

Collins, E.W. (1978) Precambrian geology of the Grape Creek area, Llano County, central Texas, 122 p., Master's thesis, University of Texas, Austin, Texas.

Graham, C.M. and Powell, R. (1984) A garnet-hornblende geothermometer: calibration, testing, and application to the Pelona Schist, Southern California. Journal of Metamorphic Geology, 2, 13-21.

Schwarze, E.T. (1990) Polymetamorphism in the Llano Uplift: Evidence from geothermobarometry and compositional zoning in garnet, 275 p., Master's thesis, University of Texas, Austin, Texas.

Wilkerson, A., Carlson, W.D., and Smith, D. (1988) High-pressure metamorphism during the Llano orogeny inferred from Proterozoic eclogite remnants. Geology, 19, 391-394.

DIKES IN THE PRECAMBRIAN OF THE EASTERN ARBUCKLE MOUNTAINS

R.E. DENISON, *The University of Texas at Dallas, Richardson, TX 75083*

There are four main types of dikes found in the massive Precambrian rocks of the eastern Arbuckle Mountains (1) diabase, (2) rhyolite porphyry, (3) microgranite porphyry and (4) granite. Three of these dike types give crucial information in the understanding the Cambrian opening of the southern Oklahoma aulacogen and later Paleozoic geologic history. Some of the older dikes define an earlier zone of weakness that may have controlled the location and N60°W direction of the rift.

Four massive granitic units are the framework rocks for the Cambrian opening. Numerous diabase dikes cut the host granitic units as well as fewer but conspicuous rhyolite and microgranite porphyry dikes. One suite of diabases is near the age of the host granites and another was emplaced during and are the manifestation of the Cambrian opening. The dikes suites cannot be separated in the field or by petrography (they are simple plagioclase + pyroxene + iron oxide ± olivine rocks). Both diabase suites have a very strong N60°W strike direction. There are a few (<10) dikes of a distinctive microgranite porphyry that form prominent dikes that can be traced for several miles along strike. These dikes are 1,350-1,400 Ma old, cutting the oldest granites but not the youngest. A few dikes of brick red rhyolite are Cambrian in age and probably represent feeders for the widespread rhyolite flows in the aulacogen to the south. Both the microgranite porphyry and rhyolite dikes have a preferred N60°W strike. There are also some granite dikes near the age of the host granites that do not show any systematic strike or dip.

The diabase dikes are most numerous adjacent to the rift margin and are common for a distance of about 8 km from the margin. The microgranite porphyry dikes are rather evenly spaced through the older granitic host rocks in the west. The rhyolite dikes are found within about 10 km of the rift margin. It is believed that the rhyolite and an undetermined portion of the diabase dike swarm reflect the Cambrian rifting that occurred during the opening of the Ouachita depositional basin to the southeast. The strike direction of the Precambrian dikes is one of the few demonstrations of preferential weakness in any basement rocks of the southern interior. By the Late Cambrian transgression any volcanics fed by the dikes had been eroded. The aulacogen received an exceptionally thick section of lower and middle Paleozoic rock. During intense Pennsylvanian deformation the N60°W dike direction was reactivated as the regional structural grain.

NEOPROTEROZOIC CONTINENTAL-SCALE TRANSPRESSION MEGAZONE IN EASTERN BRAZIL

I. ENDO, *Federal University of Ouro Preto, Department of Geology, Campus Morro do Cruzeiro, 35400-000, Ouro Preto, MG, Brazil; e-mail: issamu@degeo.ufop.br*
R. MACHADO, *São Paulo University, Institute of Geosciences, Cidade Universitária, 01498-970, São Paulo, SP, Brazil*

The Transatlantic megashear system (TATLmss) is a northeast-trending continental-scale transpression megazone which exhibits coeval Neoproterozoic structural and tectonic evolution. On the Brazilian platform it is 900 km wide and 3600 km long and extends northeastward into the African continent and southwestward into Argentina, Uruguay and Paraguay.

We propose a new interpretation for the Brazilian Neoproterozoic structural and tectonic framework. This tectonic model eliminates the major geometric and kinematic problems of the Brazilian structural provinces, providing an evolutionary model that explains in an integrated way the coexistence of the circumscribed fold-thrust belts around the São Francisco Craton as well as transcurrent shear belts in outer zone (Fig. 1). We hope that this model will serve as a working hypothesis for future field and geodynamic studies of the region.

The internal geometry and kinematic of the transpression megazone - TATLmss - display consistent manifestation of regional right-handed transpressional tectonic regime in which the deformation is accommodated by several shear belts of different orders. Where exposed the TATLmss comprises low to high grade metamorphic and mylonitic belts with aggregated reworked Archean to Paleoproterozoic rocks. We briefly describe these shear belts that are represented, in map view, by the axes of internal zones which corresponds to the loci of intense deformation, rooting into large positive flower-like structure of complex anatomy (Figs. 1 & 2). The bold numbers corresponds to descriptions of the map.

The first-order shear belts of the TATLmss are: **(1)** Atlantic (ASB): The ASB is composed by two sets of right-handed transpressional shear systems which extends over 3000 km. Its sinusoidal trace follows parallel the eastern Brazilian Atlantic margin with NE-SW direction [1,2]. These systems are: **(1a)** Paraíba do Sul Shear System (PSSS) and **(1b)** Dom Feliciano Shear System (DFSS); **(2)** Transbrazilien (TBSB) [2]: The TBSB is a NE-trending dextral shear belt that extends up to 3150 km. Most of TBSB is covered by Phanerozoic sediments of Paranà and Parnaíba basin. The second-order shear belts are: **(3)** Campo do Meio (CMSB) [2]: The CMSB is a NW-trending sinistral transpressional shear belt; **(4)** Paramirim (PMSB) [2]: The PMSB is a sinistral transpressional shear belt with NW-SE trend; **(5)** Senador Pomeu (SPOSB) [2]: The

SPOSB is sub-parallel to TBSB with dextral shear sense; (**6**) Pernambuco (PESB): The PESB is oriented in E-W direction with dextral shear sense; (**7**) Patos (PASB): The geometry and kinematic of PASB is similar to PESB.; (**8**) Tocantins (TOSB) [2]: The TOSB is a N-trending structure with dextral shear sense; (**9**) Tentugal (TESB) [2]: The TESB is a NW-trending belt with sinistral shear sense; (**10**) Sarandi del Yi (SDYSB) [2]: The SDYSB is a dextral NW-trending connective belt between PSSS and DFSS.

One of the illustrative geologic transects across the ASB was described by Machado & Endo [8] (Fig. 2). They found three important structural settings corresponding to kinematic partitioning of the displacement field: (i) internal, (ii) intermediate and (iii) external zone. The internal zone comprise a domain of intense deformation with dominant strike-slip transpressional component and vertical planar rock fabric of high metamorphic grade. Geophysical anomalies are associated with these zones and significant volumes of synkinematic granitic bodies are intruded in the later phase. In the intermediate zone the basement blocks are generally involved in the deformation which is partitioned between strike-slip and thrust-fault components mechanically coupled and in the external zone the deformation is typically due to contractional component.

Important subsurface magnetic gravimetric anomalies [3,4,5] are usually related to axis of that systems or belts. They also show regional divergent metamorphic polarity [6] and double structural vergency [7,8] which are features compatible with large positive flower-like structure. Moreover, reactivation processes in several Phanerozoic cycles are a pervasive phenomena whose manifestation is indicated by transtensional sedimentary basins and alkaline intrustions.

According to these model the São Francisco Craton represents a suggestive brittle "megaporfiroclast" surrounded by, and probably three-dimensionally braided, Neoproterozoic mobile belts in the interior of the TATLmss.

Finally, our proposition states that TATLmss represents, in the transpression model, a mobile zone situated between two rigid blocks. This zone is called Atlantic Tectonic Province (ATP) [1] and adjacent rigid blocks are represented by the Amazon and Congo cratons. The former, on the Brazilian platform, is called Amazon Tectonic Province (AmTP) [9,1].

References

[1]Machado, R. and Endo, I. (1993) IV Simp. Nac. E st. Tect. SBG/Núcleo Minas Gerais, Bol 12, p. 189-191.

[2]Endo, I. And Machado, R. (1993) IV Simp. Nac. E st. Tect. SBG/Núcleo Minas Gerais, Bol 12, p. 356-359.

[3]Haraly, N.L.E.I. And Hasui, Y. (1981) Simp. Geol. Centro-Oeste, SBG/Goiânia., p. 53-72.

[4]Schobbenhaus, C., Campos, D.A., Derze, G.R. and Asmus, H.E. (1984) *Mapa geológico do Brasil e área oceânica adjacente.* MME/DNPM.

[5]Shukowsky, W., Mantovani, M.S.M., and Hallinan, S.E. (1993) *I Simp. Intern. Del Neoproteroxóico*-Cambrioco de la Cuenca del Plata, Uruguay, vol. 2, Doc 32.

[6]Cordani, U. G., Brito Neves, B.B., Fuck, R.A., Porto, R., Tomaz Fº, A. and Cunha, F.M.B. (1984) *Ciência-Técnica-Petróleo, PETROBRÁ,* nº15, 70p.

[7]Egydio Da Silva, M. (1987 *Unpubl. PhD Thesis,* IG/USP, 141p.

[8]Machado, R. and Endo, I. (1993) *III Simp. Geol. Sudeste.,* Rio De Janeiro - RJ.

[9]Braun, O. P. G. (1982) *Photogrammetria*, 37:77-108.
[10]Almeida, F. F. M., Hasui, Y., Brito Neves, B.B. Fuck, R. A. (1981) *Earth Sci. Rev.*, 17:1-29.
[11]Almeida, F. F. M. and Hasui, Y. (1984) *O Pré-Cambriano do Brasil*, Ed. Edgard Blücher Ltda. São Paulo-SP, 378p.

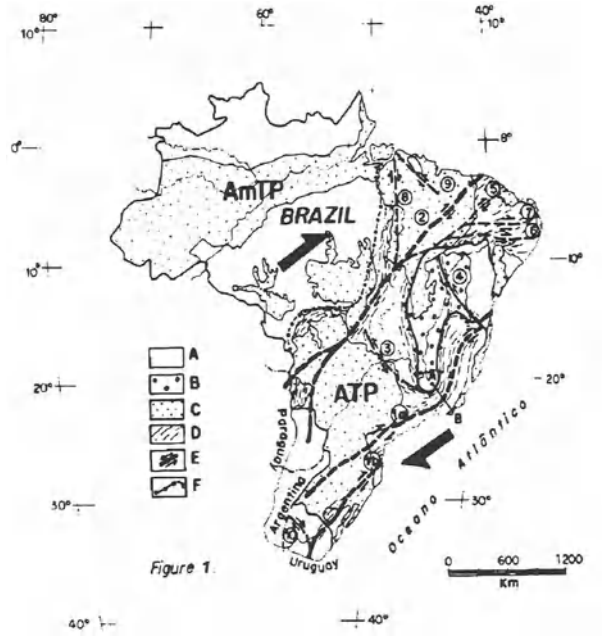

Figure 1: Selected structural and tectonic elements showing a suggestive coeval evolution across the Transatlantic Megashear System. A- Basement, B- Neoproterozoic cover, C- Phanerozoic Cover, D- Foliation trend, E- Axial zone: site of intense deformation, F- Limit between Amazon (AmTP) and Atlantic (ATP) Tectonic Province (Mod, from [3,4,10,11]).

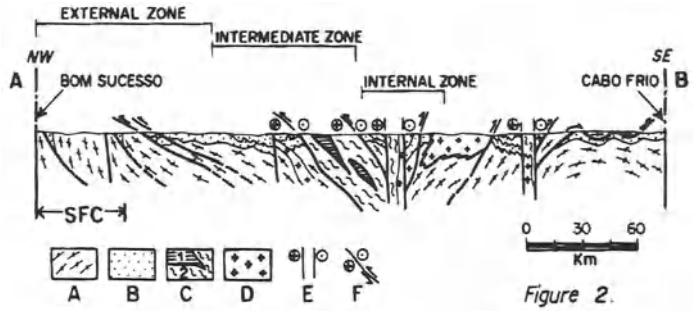

Figure 2: Transect across the Atlantic Shear Belt - ASWB - between Bom Sucesso and Cabo Frio Localities. A- Basement, B- Meso to Neoproterozoic cover, C- Granulites and Charnockites [1] and mylonitic rocks [2], D- Granitic batolith E- Dextral strike-slip shear zone, F- Reverse shear zone with dextral strike-slip component. SFC- São Francisco craton (after [8]).

MULTIPLE REACTIVATIONS OF MAJOR FAULT ZONES IN THE NORTHERN READING PRONG, USA

A.E. GATES, and R. COSTA, *Dept. of Geology, Rutgers University, Newark, NJ 07102*

Fundamental zones of crustal weakness that were established in the northern Reading Prong during Grenville orogenesis were reactivated during every subsequent tectonic event. The rocks in these fault zones contain complexly overprinted mylonites, cataclasites, and breccias with distinct kinematics and mineralizations. By studying the similarities and differences of rocks from three separate fault zones across the eastern Pennsylvania, New Jersey, and the southeastern New York part of the Reading Prong, the tectonic succession and a relative chronology can be determined. In addition, new indicators of multiple reactivations can be identified.

The NE-striking composite Morgan Hill and related shear zones in Easton, PA is the westernmost of the three zones. A period of major reverse movement at peak Grenville metamorphic conditions is represented by a 2 to 3 km-wide mylonite zone in all lithologies. Locally crossing the reverse zone are thin 10 to 100 m wide NW-striking sinistral strike-slip shear zones. These faults appear to have been active late in the Grenville event and are best represented by quartz-magnetite mylonites that formed at the brittle-ductile transition. These two shear zones are fragmented, overprinted and obliterated by major normal movement on NE-striking zones. Well developed S-C mylonites in granitic and serpentinite (calc-silicate) rocks show consistent normal offset. These zones are bounded by mineralized pockets of fault breccia for which shear sense and age cannot be determined. All previous zones were fragmented and offset by Taconian thrust faults and possible Alleghanian thrust faults.

The NE-striking Reservoir fault zone extends from central New Jersey through southern New York. It has peak to late Grenville S-C mylonites that show reverse movement in New York but these rocks were fragmented and removed during late to post Grenville dextral strike-slip shearing. Cataclasites and marginal mylonites of this event are well mineralized with halogen-bearing amphiboles. These rocks were dominantly fragmented and removed during Taconian(?) reverse faulting and Alleghanian dextralreverse faulting. The Reservoir fault is seismically active.

The NE-striking Ramapo fault is the easternmost of the three zones. The Ramapo fault has been shown to have undergone Grenville reverse movement, late-post Grenville dextral strike-slip movement, Taconian reverse movement, Acadian-Alleghanian reverse movement, Mesozoic normal faulting, and it is currently seismically active. The Taconian reverse movement formed the most pervasive mylonites. However, these mylonites show many brittle pull-apart amphiboles and feldspars with equivocal shear sense as well as folds in the flow fabric. There are "V"

fractures in the pull apart grains with two distinct sets of mineral overgrowths. These textures can be used to identify remylonitization of mylonites.

Among the three faults as many as 7 phases of reactivation can be identified. The weak zones between relatively rigid crustal blocks exhibit multiple and intense deformational episodes because they absorb the majority of strain in a tectonic event. The crystalline rocks between the faults show relatively little post peak Grenville deformation. The rigid blocks simply adjusted to the renewed stresses along their boundaries. Depending upon stress and metamorphic conditions, the previously formed mylonites and cataclasites were either fragmented or resheared during reactivation.

STRUCTURAL EVOLUTION OF CIMA TERMINE AREA, VAL VENOSTA (NORTHERN ITALY)

G.0. GATTO, *Dipartimento di Geologia, Paleontologia e Geofisica, Universita' di Padova, Corso Garibaldi 37, 1-35137, Italy, tel. 39-49-664828.*

N. MINZONI, *Dipartimento di Scienze Geologiche e Paleontologiche, Universita' di Ferrara, Corso Ercole I dEste 32, 1-44100, Italy, tel. 39-532-210341.*

In the Alpine chain, the Austroalpine domain represents the Mesozoic African margin which, during Alpine orogenesis, overrode the European domain. In both margins the collision caused the emplacement of several Europe-verging nappes.

In the Cima Termine area, the nappe consists of pre-Mesozoic (Precambrian and Variscan) crystalline rocks and Mesozoic terrigenous and carbonate sequences.

During the main Alpine tectonics, the Mesozoic sequences were overthrust by the crystalline rocks. The sedimentary succession was also detached from the crystalline basement and stacked in several small tectonic units characterized by metric to hectometric isoclinal recumbent folds.

The deformation developed by flat-ramp-flat geometry, with the formation of hinterland-dipping duplexes evolving in a wide stacked imbricate antiform.

Structural analysis indicates that tectonic transport was towards north-westerly areas. Slaty cleavage and very low-grade Alpine synkinematic metamorphism may be observed along the overthrusting surfaces. Some field data suggest that the main overthrusting surfaces were formed by the re-use of Mesozoic growth faults.

ON FRACTURE DEVELOPMENT IN ROCK SUBJECTED TO COMPRESSION

L.N. GERMANOVICH, K.K. LEE, J-C ROEGIERS, *School of Petroleum and Geological Engineering, The University of Oklahoma, Energy Center, T301, 100 East Boyd, Norman, OK 73019-0628, 405-325-2907, leonid@rmg.uoknor.edu*
A.V. DYSKIN, *The University of Western Australia, Nedlands, Western Australia, 6009,61-9-380-3987*

This paper describes an experimental study involving laser-induced cracking of transparent blocks made of PMMA and polyester casting resin. Disc-shaped cracks were introduced into the cylindrical and rectangular specimens by focusing a Nd-YAG laser beam. The PMMA samples were frozen in a dry ice-bath at a temperature of -72 ^{0}C or in liquid nitrogen (-198.5 ^{0}C) to make them brittle. Similarly, the resin samples were cooled in the freezer, at -20 ^{0}C, prior to testing. Besides being transparent, such a material also exhibits elastic and strength properties similar to rocks. The samples were subsequently loaded uniaxially to observe internal 3-D crack propagation in compression. The whole process took no more than 2 minutes in order to maintain the frozen condition of the samples, which did not exhibit any noticeable residual strain. This technique was then expanded to induce several cracks of given sizes and at given locations, allowing the study of 3-D crack interaction in compression.

This study demonstrated that 3-D crack growth in compression qualitatively differs from the 2-D case. Unlike 2-D cracking, where extensive growth of branches leads to sample splitting, there are intrinsic limits on 3-D growth of wing cracks produced by a single pre-existing crack. Although wings branched from the initial crack, they, at most, grew to a size comparable to the initial crack dimensions (Fig. la) which is insufficient to cause overall failure. The whole process then ended up in an explosion-like failure not related to the laser-induced cracks; when the applied load reached the compressive strength of the material (Fig. lb). Moreover, cracks did not propagate further even when they were located near a free surface.

However, when two cracks were suitably located with respect to each other, new large cracks were produced as a result of the combined action of wing cracks originating from the initial flaws. This is probably the result of remote tensile stresses induced by the interaction of the propagating wing cracks. A macro fracture can indeed be produced if these wings grow in approximately the same plane, but not otherwise.

In multicrack situations with high crack densities, either new cracks are initiated or wings of some existing cracks are made to grow further. In this case, the crack density is a key factor in the mechanism of fault nucleation. In dense crack populations, the combined action of crack-induced tensile stresses can produce large fractures (Fig. 2a) or make some of the wing cracks grow further, creating fault-like structures (Fig. 2b). On the other hand, in low density crack populations, the cracks

practically grow independently (Fig. 2c). Indeed, in dense crack populations, such as in rock samples, the probability of having at least two closely located and properly arranged cracks is rather high.

In rock, even though the 3-D flaw splitting the sample eventually becomes 2-D-like, the initial stage of its development is qualitatively different from the 2-D case. A mechanism of fault nucleation, i.e., the transition between the (micro) scale of the initial 3-D cracks (Fig. la) and the resulting large-scale 2-D-like structure (Fig. 2a) could be based on the tensile stresses generated by micro-scale wing cracks in the direction perpendicular to the loading.

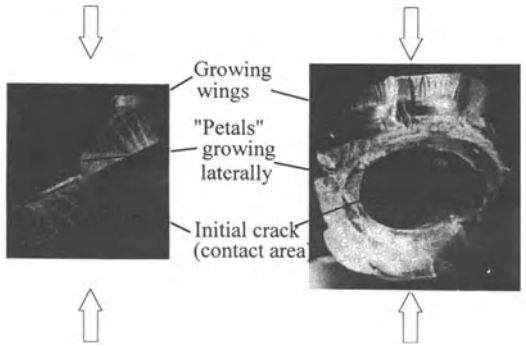

(a)

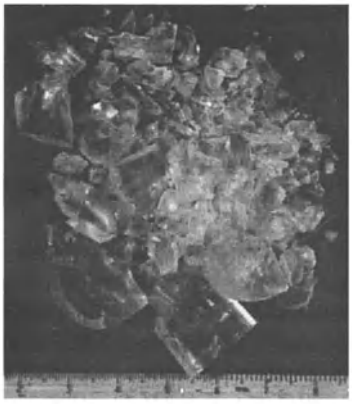

(b)

Figure 1

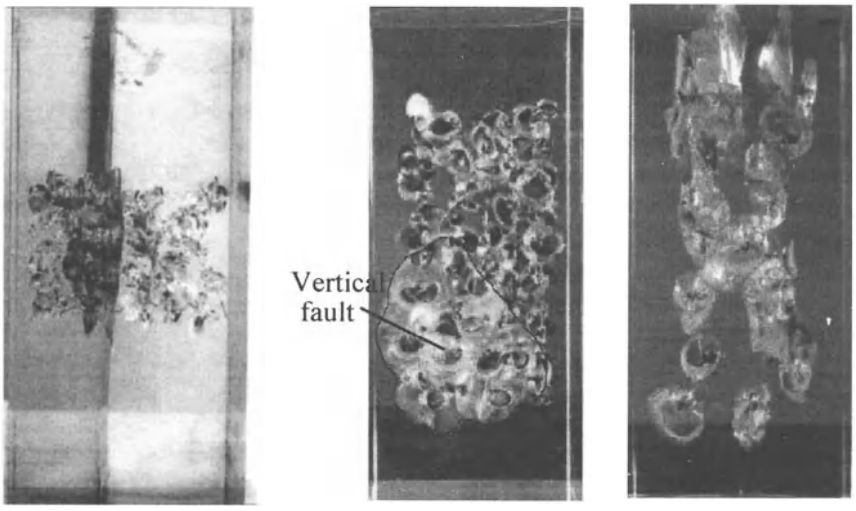

a b c

Figure 2

THE CHARACTERISTICS AND TECTONIC EVOLUTION OF THE BASEMENT OF THE COLLISION OROGENIC BELT ON THE SOUTHEASTERN MARGIN OF THE YANGTZE PLATE

X. GUIZHONG and W. YIFEN, *Institute of Geology, Chinese Academy of Sciences, Beijing 100029, China, tel. 86-01-2027766, fax. 86-01-491 9140*

The collision orogenic belt on the Southeastern margin of Yangtze plate is a narrow but long region northeast-trending, passing through North Jiangxi, South Anhui and West Zhejiang Provinces and extending about 700km long and 150-200km wide. This region is bounded by the Pingxiang-Jiangshan-Shaoxing deep-seated fault zone on the south, and the Jiangnan deep-seated fault zone on the north. Its southeast boundary is adjacent to the Huaxia craton.

The basement of the collision orogenic belt is composed of Middle Proterozoic low-grade metamorphic rocks. The formation of the basement was closely related to Precambrian paleoplate activity. The available data suggested that there are three sets of NE-striking ophiolitic melanges distributed along deep-seated fault zones of the basement from north to south. They are Tunxi-Shexian, Zhangshudun-Zhongcun and Jiangshan-Shaoxing ophiolitic melange zones. The outcrop of ophiolite represents the location of interaction between paleo-marine and paleo-continental crusts, and thus is a most important geological evidence in the discussion of tectonic evolution of the basement. The formation of the basement of the orogenic belt is composed of the products of a Middle Proterozoic trench-arc-basin system which developed in the southeastern margin of the Yangtze plate. The Tonggu-Jingdezhen-Ningguo deep-seated fault and Yingtan-Dexing-Anji deep-seated fault divided the system into Yongxiu-Qimen paleoshelf area, Wanzhai-Tunxi paleo-back-arc basin, the Henfeng-Jiande paleo-island arc and Jiangshan-Shaoxing trench areas from north to south.

The basement has different names in different areas: the Shuangqiaoshan group in northern Jiangxi, the Shangxi group in southern Anhui and the Shuangxiwu group in western Zhejiang. They formed at the same time but in different tectonic environments, and many kinds of deformation made them a complex structural-lithological association. The facies, lithology, rock association and metamorphic grade of Shuangqiaoshan Group vary from area to area. In the paleoshelf area north of Tonggu-JingdezhenNingguo deep-seated fault, it is mainly composed of a series of low-grade metamorphic rocks, including phyllites, slates and tuffaceous slates. In the paleo-back-arc basin area south of the fault, with a relatively high-grade metamorphism, it mainly consists of chlorite-sericite-schists, garnet-sericite-schists, quartzschists, tuff and tuffaceous phyllites, but includes considerable metamorphosed basic lavas, minor acid lavas and ultrabasic rock blocks. They belong to the products of back-arc basin. The Shangxi Group, mainly distributed in the southern Anhui area north of Tonggu-

Jingdezhen-Ningguo deep-seated fault is a series of low-grade metamorphic rocks, including feldspar-quartz sandstones, carboneous slates, siliceous slates and minor tuffaceous slates. To the south of the fault, the Shangxi Group consists of sedimentary flysh and contains a large amount of metamorphic basic lavas, a minor amount of acid lavas and volcanic clastics. The provenances of these rocks belong to back-arc basin. The Shuangxiwu group, distributed with a narrow outcrop in the western Zhejiang area, is a series of low-grade metamorphic rocks. Near the north side of Pingxiang-Jiangshan-Shaoxing deep-seated fault, it is a suite of marine metamorphic volcanic-sedimentary rocks, in which volcanic rocks are mainly spilites but include minor keratophyres and quartz-keratophyres. In the Fuyang and Zhangcun areas, it is composed of continental metamorphic andesites, rhyolites, volcanic clastics, sandstones, conglomerates and mudstones. These rocks are the products of volcanic arc.

Tunxi-Shexian ophiolitic melange zone is well developed, 50 km long and 5 km wide. It is mainly composed of serpentized dunites, scapolite-peridotites, pegmatic gabbros, gabbros, diorites, quartzdiorites, pilites, quartz-keratophres, tuffaceous phyllites and slates. It can be considered that the melange would occur north of the Wanzhai-Tunxi paleo-back-arc basin in last Middle Proterozoic. Zhangshudun--Zhongcun ophiolitic melange zone distributed along the west side of Yingtan-Dexing-Anji deep-seated fault, this zone strikes NE, and is 110km long and 8-15 km wide. There are 250 little rootless basic and ultrabasic rock blocks to be mapped. The peridotites, including orthopyroxene-pedotites and minor dunite, represent the hard-melted or unmelted materials in primitive mantle, and then were mixed into Shuangqiaoshan group by high-pressure ductile deformation. The cumulatic rocks are mainly composed of pyroxene-peridotites, pyroxenites and gabbros, and have layered or banded structures due to the fractional crystallization. The metamorphic volcanic rocks are marine tholeiites. Jiangshan-Shaoxing ophiolitic melange zone is distributed along Jiangshan-Shaoxing deep-seated fault with 45 km long and 0.5-7 km wide. The peridotites, pyroxenites, amphibolites and gabbros are isolated and enclosed by schist and quartz-diorites, appearing as a mylonitic belt with several hundred kilometers long. The provenance of muscovite-schists and muscovite-quartz-schists accompanied with these blocks should belong to trench flysh sediments. We consider that Tunxi-Shexian and Zhangshudun-Zhongcun ophiolitic melange should be the products of the back-arc basin. And Jiangshan-Shaoxing ophielitic melange could be the product of the subduction zone.

The collision orogenic belt of the southeastern margin of Yangtze plate underwent the following tectonic evolution process. Before Middle Proterozoic, Yangtze paleocraton was isolated from Huaxia paleocraton by a wide ocean. From Middle Proterozoic, as a marine plate north of Huaxia paleocraton subducted to the south side of Yangtze paleocraton, the continental margin disintegrated gradually so that a trench-arc-basin system formed. This system continued to the last Middle Proterozoic. These two plates collided to form Jinning orogenic belt before 900 Ma. Since the crust became thick and the partial melting took place in the deep crust, collisonal granodiorites formed. At the same time, the high-pressure metamorphic rocks related to collision formed in northeastern Jiangxi ophiolitic melange zone. In Sinian, a series of rift basins formed on the orogenic belt due to postorogenic stress relaxation.

REVISED GRANITE-GABBRO AGE RELATIONSHIPS, SOUTHERN OKLAHOMA AULACOGEN U.S.A.

W.E. HAMES, *Department of Geology, Auburn University, Auburn, AL 36849 tel: (205) 844-4282; email: hameswe@mail.auburn.edu*;
J.P. HOGAN, and M.C. GILBERT, *School of Geology and Geophysics, University of Oklahoma, Norman, OK 73069-0628, tel: (405) 325-3253; email: jhogan@ou.edu, mcgilbert@ou.edu*

Igneous activity associated with formation of the Cambrian Southern Oklahoma Aulacogen is compositionally bimodal consisting of mafic and felsic volcanic and plutonic rocks. The aulacogen is floored by an extensive substrate of layered anorthositic gabbro, the Glen Mountains Layered Complex. The layered complex was intruded by a suite of hydrous gabbros, characterized by primary amphibole and biotite, that form small plutons of the Roosevelt Gabbro Group of which the Mount Sheridan Gabbro is typical. Overlying this mafic substrate is a voluminous pile of felsic volcanics, comprised predominantly of rhyolite flows with minor tuffs and agglomerates, of the Carlton Rhyolite Group. Intrusive into the base of this volcanic pile are a series of laterally extensive but thin, amphibole-biotite alkali feldspar granite sheets of the Wichita Granite Group, of which the A-type Mount Scott Granite sheet is typical. Cross-cutting these units are a suite of basaltic dikes and rare "rhyolite" dikes that represent the final stages of igneous activity.

Contacts between the older Glen Mountains Layered Complex and the younger Roosevelt Gabbros are well exposed in several locations and permit straightforward determination of relative age relationships. Similarly contact relationships between Carlton Rhyolite and Wichita Granite repeatedly demonstrate the intrusive nature of the granites. However, rare "rhyolite" dikes cross-cutting granite also permit the presence of younger rhyolite flows. In contrast, the nature of some contacts between mafic and felsic igneous rocks have long been the source of considerable debate in the Wichita Mountains.

The contact between the two underlying gabbro units and overlying Mount Scott Granite is regionally sharp but locally complex. This contact is well marked by the trace of the tree line along the lower slopes of the eastern Wichita Mountains and can be followed for several 10's of kilometers demonstrating the relatively shallow dipping to sub-horizontal nature of this contact on a regional scale. Details of the contact are typically obscured by talus from the overlying granite cliffs. Where exposed the granite-gabbro contact is comprised of hybrid granitoid rocks commonly containing abundant amphibole and a texturally and compositionally diverse suite of enclaves. Where the granite is in contact with the Glen Mountains Layered Complex, a well developed igneous breccia, composed of angular enclaves with sharp contacts, formed in the basal portion of the younger Mount Scott Granite sheet. Within this breccia are

readily identifiable xenoliths and plagioclase xenocrysts derived from underlying anorthositic gabbro of the Glen Mountains Layered Complex. In addition, the underlying anorthositic gabbro displays evidence of high temperature alteration and partial melting (?) that may be related to contact metamorphism during intrusion of the granite. The intrusive nature of other members of the Wichita Granite Group into the Glen Mountains Layered Complex can also be shown elsewhere (e.g., Quanah Granite).

Contact relationships between Mount Scott Granite and members of the Roosevelt Grabbro Group are more enigmatic. Hybrid igneous rocks are spatially associated with these contacts as well but also may locally be surrounded entirely by granite. These hybrid rocks contain a diverse suite of enclaves some of which have more irregular shapes. Both the Sandy Creek and Mount Sheridan Gabbros exhibit regular and systematic compositional and mineralogic variation towards more felsic rock types as the contact with the overlying Mount Scott Granite is approached. Evidence of hydrothermal alteration or contact metamorphism of the underlying Mount Sheridan Gabbro by the overlying Mount Scott Granite, where suggested, is unclear.

The complexity of this contact coupled with poor exposure has contributed greatly to sustaining ambiguity in the relative age relationships of these two units. Mount Sheridan Gabbro has previously been interpreted as being considerably older than the Mount Scott Granite by most workers, based on a presumed consanguineous relationship to the Glen Mountains Layered Complex, although some have suggested a coeval relationship with Mount Scott Granite, based on the inference that the hybrid rocks formed as a result of magma mingling, and a few have postulated a younger age. A single crystal laser $^{40}Ar/^{39}Ar$ study of igneous amphibole and biotite from Mount Sheridan Gabbro and amphibole from Mount Scott Granite was undertaken to explore this ambiguity. Amphibole (SQ-1-266.5) was separated from drill core of Mount Scott Granite taken below the depth of alteration of magnetite to hematite (see Price et al., this volume) and yielded an age of 539+2 Ma which is currently interpreted to represent the crystallization age for this granite sheet. Amphibole and/or biotite were separated from three samples of Mount Sheridan Gabbro: (1) Amphibole from a late stage pegmatitic dike related to Mount Sheridan Gabbro (JH-8-94) yielded an age of 535+8 Ma; (2) amphibole separated from a sample of gabbro just below the contact with the overly Mount Scott Granite (JH-38-93) yielded an age of 533+2 Ma; and (3) primary magmatic biotite from gabbro sampled in a quarry 10's of meters below the contact with the overlying granite (JH-36-93) yielded an age of 533+4 Ma. Amphibole from the pegmatite has a small component of excess argon; the other samples do not exhibit evidence for additional argon components or disturbance of their $^{40}Ar/^{39}Ar$ systematics. The close agreement of age determinations from both amphibole and biotite are consistent with quick cooling of this shallow level intrusion and are interpreted as the crystallization age of the Mount Sheridan Gabbro.

New crystallization ages for Mount Sheridan Gabbro and Mount Scott Granite indicate a close temporal relationship, as well as spatial relationship, for mafic and felsic magmatism during formation of the Southern Oklahoma Aulacogen. These results suggest that compositional variation in Mount Sheridan Gabbro towards more felsic rock types, as contacts with overlying Mount Scott Granite are approached, result from

assimilation of Mount Scott Granite and fractional crystallization rather than simple fractional crystallization of a pristine basaltic liquid. Finally, this study demonstrates that advection of thermal energy and new material from the mantle into the continental crust was a significant component of lithospheric extension throughout the development of the Southern Oklahoma Aulacogen.

LATE PRECAMBRIAN STRIKE-SLIP FAULT SYSTEM OF THE WICHITA-AMARILLO MOUNTAINS AS DELINEATED BY DETAILED AEROMAGNETIC DATA

B.W. HAWLEY, and S.P. GAY, JR., *Applied Geophysics, Inc., Salt Lake City, UT 84111, tel.801-328-8541*

Detailed aeromagnetic data, extending from the eastern terminus of the Wichita structural system westward across southern Oklahoma and the Amarillo uplift to the Texas-New Mexico line, reveal a series of long linear faults that evidently formed by regional strike-slip movement in the Proterozoic era. The faulting may represent offset within the existing North American craton, but could also represent the suturing of another continental segment to the craton. Later Paleozoic southwest-northeast compression of these pre-existing wrench faults produced thrusting that is obvious in present-day surface and subsurface geology.

The eastern terminus of this great strike-slip fault system may never be deciphered, as it plunges tens of thousands of feet beneath stacked Ouachita thrusts. What happened at the western end, in New Mexico, may be deciphered in the future, but cannot be mapped from the very sparse geological and geophysical data that exists there at the present time. This represents a very interesting and challenging problem in understanding the structural makeup of North America.

CRUSTAL GROWTH DURING CONTINENTAL RIFTING: AN EXAMPLE FROM THE SOUTHERN OKLAHOMA AULACOGEN

J.P. HOGAN and M.C. GILBERT, *School of Geology and Geophysics, University of Oklahoma, Norman, OK 73019, tel. (405) 325-3253; email: jhogan@ou.edu, mcgilbert@ou.edu*
J.E. WRIGHT and M. DEGGELLER, *Department of Geology and Geophysics, Rice University, Houston, TX 77005, tel. (713) 285-5130; email: jwright@owlnet.rice.edu*

The Southern Oklahoma Aulacogen (SOA) is one of several aulacogens that formed within the North American craton during breakup of the Laurentian Supercontinent in Late Proterozoic to Cambrian time. Lithospheric extension that formed the SOA was accompanied by voluminous bimodal igneous activity. Following cessation of rift-related igneous activity, isostatic adjustment of the crust resulted in accumulation of 4-5 km of Paleozoic sediments within an intracratonic basin that developed over the subsiding aulacogen. Uplift by block faulting, accompanied by erosion, during the late Paleozoic Ouachita Orogeny, and again in the Cretaceous and late Cenozoic, exposed the Cambrian igneous basement. The absence of significant Mesozoic and Cenozoic deformation within the mid-continent ensure preservation of the rift assemblage. Subsequent erosion has exposed the volcanic and plutonic rocks that floored this aulacogen such that the present erosional surface is not far below the erosional surface in Cambrian time. Integrated petrologic and geophysical investigations of these igneous rocks and the underlying crust suggest a significant amount of new material can be added to the crust during periods of lithospheric extension.

Igneous activity associated with rifting appears to have occurred in two distinct events separated by a period of uplift and erosion. The earlier episode of magmatism was dominantly mafic. This activity is represented by the Late Precambrian to Cambrian Raggedy Mountains Gabbro Group which consists of extensive (>1000 km^2; ~3-4 km thick) layered anorthositic gabbro intruded by small (~10 km^2) gabbro plutons characterized by primary biotite and amphibole. The later episode of magmatism was dominantly felsic. The A-type Carlton Rhyolite, a thick (~1 .4 km) areally extensive (~44,000 km^2) sequence of subaerial rhyolite flows and minor tuffs and minor agglomerates, rest unconformably on the older extensive substrate of layered gabbro. Intrusive into the base of this volcanic pile are a series of penecontemporaneous thin (~0.5 km) but laterally extensive (~20-55 km in length) A-type sheet granites of which the Mount Scott Granite sheet is typical. Numerous basaltic dikes and rare porphyritic microgranite or "rhyolite" dikes crosscut members of the Wichita Granite Group and represent the final stages of igneous activity. Evidence for coeval mafic and felsic magmatism within the rift is scarce and spatially restricted in occurrence.

Geochemical and isotopic characteristics of A-type felsic magmatism accompanying formation of the SOA are in marked contrast to those expected for typical crustal melts and require derivation from more primitive mantle-like sources. The granites have low Yb/Ta, Y/Nb, and Ce/Nb ratios that are more typical of Ocean Island Basalts (OIB) than of average Continental Crust or Island Arc Basalt (e.g., Eby, 1990). In addition, the absence of a Ta-Nb anomaly in the primordial mantle normalized trace element plot for Mount Scott Granite is also consistent with derivation from a source with OIB-like characteristics. Calculated initial $^{81}5r/^{86}5r$ for Mount Scott Granite at 525 Ma range from 0.7030-0.7043 (n=6) and for Carlton Rhyolite 0.7018-0.7054 (n=3). Epsilon Nd $_{(525\ Ma)}$ values for Mount Scott range from +3.4 to +3.7 and for Carlton Rhyolite +2.9 to +3.5 and are indicative of a primitive source for these magmas with minor crustal assimilation.

Mount Scott Granite and Canton Rhyolite exhibit geochemical and isotopic compositions that are similar in many respects with mafic magmatism associated with the rifting event as represented by basaltic dikes of the Late Diabase Dike suite. Incompatible trace element ratios (e.g. Rb/Nb, La/Nb, Zr/Nb, etc.) for Late Diabase and Mount Scott Granite are comparable. In particular calculated initial $^{87}Sr/^{86}Sr$ for samples of Late Diabase at 525 Ma range from 0.7033-0.7041 and epsilon Nd $_{(525\ Ma)}$ values range from +2.8 to +4.3 (n=4) both of which are nearly indistinguishable from those of the granites and rhyolites. These similarities suggest a closely related origin for mafic and felsic magmas associated with formation of the Aulacogen. The extreme scarcity of igneous rocks corresponding to intermediate magma compositions makes direct derivation of large volumes of felsic liquids (e.g., Carlton Rhyolite, Mount Scott Granite) by extended fractional crystallization of a basaltic magma (e.g., Late Diabase Dikes) unlikely as the dominant process by which these melts formed. We suggest A-type felsic melts are likely to have formed as the result of partial melting at depth of mafic rocks that were intruded during the initial stages of rifting.

Incompatible trace element ratios (e.g., Rb/Nb, La/Nb, Zr/Nb, etc.) for Late Diabase are intermediate between depleted upper mantle and an enriched plume source suggesting these mafic melts may have been derived by interaction between a hot-spot and asthenospheric and/or lithospheric mantle components (Weaver et al., 1991). Impingement of a mantle plume at the base of an already extending lithosphere could provide the additional heat required to partially melt previously intruded mafic rocks. Uplift and doming of the crust during rifting, as recorded by the unconformity separating the earlier and later magmatic episodes, the subaerial nature of Carlton Rhyolite, and the lack of rift-related sedimentation, is consistent with a high-heat flow regime for this crustal column. Thus rather than being sourced by remelting of older continental crust, A-type felsic magmas associated with continental rifting, such as Carlton Rhyolite and Wichita Granites, may be derived later in the rifting cycle by partial melting of mantle-derived magmas intruded into the middle to lower crust earlier in the rifting cycle. Large volume of mafic and felsic igneous rocks, both with primitive sources, are associated with formation of the SOA. Thus the amount of new material added to the crust during lithospheric extension is substantial and should have important

consequences for modeling the time-intergrated geochemical evolution of crust and mantle reservoirs.

References

Eby, G.N., 1990, The A-type Granitoids; A review of their occurrence and geochemical characteristics and speculation on their petrogenesis: Lithos, v 26, 115-134.

Weaver, B.L., Gilbert, M.C., and Lambert, D.D., 1991, Trace element and isotopic geochemistry and petrogenesis of mafic igneous rocks from the Southern Oklahoma Aulacogen: Geol. Soc. Amer. Abstr. with Progs., v. 23, A103.

INTEGRATED PETROLOGIC AND SEDIMENTOLOGIC STUDIES OF A LATE NEOPROTEROZOIC RIFT BASIN WITHIN THE GRENVILLIAN BASEMENT OF VIRGINIA

F.E. HUTSON, *Department of Geological Sciences, The University of Texas at Austin, Austin, TX 78712, tel.512-471-1177; e-mail: hutson@maestro.geo.utexas.edu*
R.P. TOLLO, *Department of Geology, George Washington University, Washington, DC 20056, tel.202-994-6960, e-mail: tollo@acad.ccgs.gwu.edu*

Integrated studies of late Neoproterozoic clastic sediments and anorogenic granitoids exposed within 1.0 Ga basement rocks of the Blue Ridge anticlinorium of central Virginia enabled us to: 1.) determine the spatial relationship of rift-related plutonism, volcanism, and sedimentation; 2.) place relatively tight age constraints on the temporal relationship between magmatic and depositional processes in this extensional setting; and 3.) use both the sedimentary and igneous rocks as a probe of the basement.

Late Neoproterozoic metasedimentary rocks of the Mechum River Formation (MRF) nonconformably overlie ~1.0 Ga basement rocks and ~0.73 Ga anorogenic granitoids of the Robertson River Igneous Suite (RRIS) in the Blue Ridge anticlinorium of central Virginia. The MRF and RRIS are spatially and temporally correlative to rift sequences exposed throughout the southern Appalachians and, on a much larger scale, to sequences exposed on all margins of Laurentia. These sedimentary and igneous rocks are interpreted as part of a ~0.7 Ga extensional event that preceded a ~0.6 Ga rift event that led to the opening of the Iapetus Ocean.

The MRF is composed of conglomerates, sandstones, and mudstones that are variably deformed and have been metamorphosed under upper greenschist facies conditions. The metasediments are exposed in a 100 km long by 0.5-3 km wide belt that has been down-faulted into the core of the Blue Ridge anticlinorium. The MRF experienced the effects of multiple Paleozoic tectonic events; nevertheless, it retains identifiable features associated with many modern rift basins. These include areal dimensions, grain size trends, facies patterns, sedimentary petrology, and structural geology. For example, the present length and structurally restored width of the MRF outcrop belt is broadly equivalent in dimensions to many East African rift basins. Additional evidence includes increasing grain size towards the margins of the MRF belt and depositional environments that range from alluvial fan to lacustrine. A major identifying characteristic of many but not all rift basins is the presence of magmatic rocks, commonly volcanics, which are associated with the sediments. Prior to our studies, no volcanic rocks had been found within the MRF and the relationship of the ~0.73 Ga anorogenic granites of the RRIS to the MRF sediments was unclear.

Field, petrographic, and geochemical studies of rocks from the RRIS, MRF, and a limited number of samples from the Grenvillian basement enabled us to identify the source of some clasts within conglomerates of the MRF and demonstrate that rocks previously mapped as MRF clastic rocks are felsic volcanic rocks. Clast count data indicate a large proportion of the clasts are composed of relatively undeformed granitoids, which is in direct contrast to the lithologic character of the presently exposed Grenvillian basement that is dominated by orthogneisses. Point count data from the clasts overlap data from the RRIS but these data are not clearly distinguishable from Grenvillian granitoids. However, elevated concentrations of high field strength elements (HFSE) and light rare earth elements (LREE) were found for clasts that are similar in petrography to members of the RRIS. This same pattern of geochemical enrichment also is typical of the RRIS. In addition, a local nonconformable relationship was recognized between the RRIS and the MRF. The combination of field, petrographic, and geochemical evidence strongly supports the derivation of many of the MRF clasts from the RRIS. A detailed study of the MRF sub-basin that contains rocks previously mapped as sediments revealed the presence of rhyolites and associated volcaniclastic rocks. The evidence of a volcanic origin for these presumed clastic rocks includes: 1.) the presence of euhedral grains of feldspar and quartz, volcanic rock fragments, and spherulites contained within a very fine-grained, white matrix and 2.) whole-rock geochemical data that display highly elevated concentrations in HFSE and LREE. These rhyolites can be clearly differentiated from sedimentary rocks, including samples of the MRF. More importantly, there is a strong geochemical correlation between these rhyolites and subvolcanic rocks of the RRIS, the latter of which are in close proximity to the MRF sub-basin.

U-Pb isotopic dating of specific units of the RRIS combined with the data outlined above, make it possible to demonstrate a direct link between anorogenic magmatism and extensional sedimentation. In addition, we are able to constrain the maximum depositional age of the MRF to 0.73 Ga and further demonstrate that sedimentation and volcanism were occurring at 0.7 Ga. We suggest that truly integrated studies of basement terranes can provide valuable information on both the early and later history of a basement terrane.

STRUCTURAL IMPRINT OF THE WICHITA MOUNTAINS FRONTAL ZONE ON OVERLYING SEDIMENTS

A.C. LAMBERT, *Phillips Petroleum Company, Bartlesville, OK 74004 te.l 918 661-0423*
R.A. YOUNG, *School of Geology and Geophysics, University of Oklahoma, Norman, OK 73019, tel 405 325-5753; email: ryoung@ou.edu*

The Wichita Mountains Frontal Zone (WMFZ) of southwestern Oklahoma is the boundary between the Wichita Mountains Uplift and the Anadarko Basin. The WMFZ has been explored by reflection seismic surveys conducted by the oil industry and by university research consortia studying sedimentary structures and their relationship to the deep crust, respectively. Direct examination of the rocks comprising the WMFZ is not possible due to the thick cover of overlying Permian strata.

The last period of major tectonism affecting the WMFZ was uplift in the Pennsylvanian. Minor adjustments have occurred since then, however, Holocene surface faulting at the southern boundary of the WMFZ along the Meers fault being the most cited. The present study of the northern boundary of the WMFZ deduces the orientation of axes of five broad folds by correlating dip measurements from the few existent exposures with mapped outcrop patterns. Near surface seismic data observed on five lines parallel to local dip show subtle flexures corresponding to the fold axes. A pattern of rectangular drainage characterizes this area, and axes of synclines are the location of major streams.

A set of thrust faults divides the WMFZ into basement blocks. Several of these faults can be followed to the surface where they coincide with mapped features. Reactivation of the Elk Creek fault after Pennsylvanian tectonism has resulted in normal faulting with basin upward relative movement, as for the Meers fault. Differential compaction at depth affects outcrop patterns on the surface, and differential erosion correlates with extrapolation of faults toward the surface.

PLASTIC DEFORMATION AS A FACTOR OF MATERIAL TRANSFORMATION OF ROCKS (SOUTHERN TIEN SHAN)

M.G. LEONOV, *Geological Institute, Russian Academy of Sciences*

1. To make an analysis of factors controlling metamorphic transformation is the essential task of geology. A most disputable problem is the one concerning the structural control of metamorphic processes. The solution of the problem concerning the role of the dynamic factor in the material evolution of rocks remains highly disputable. New data on Southern Tien Shan make it possible to cast another look into the relation between structural (plastic deformation) and material (metamorphism) transformation of rocks.

2. Study of Southern Tien Shan zones of greenschist metamorphism reveals the following peculiarities of structural and material transformation (Konygin, Leonov, 1987; Leonov, Kozhukharova, 1992; Leonov, 1988; and others).

(a) Irregular intensity. According to the existing notion of metamorphic facies, the extent of transformation of a substance varies from an initial catogenesis to high-temperature grades of the greenschist and epidote-amphibolite facies, and from low-pressure series of the greenschist facies to high-pressure ones of the glaucophane-greenschist facies. Besides the qualitative irregularity which shows in a spotted-mosaic distribution of corresponding mineral paragenesis, there is also the quantitative criterion of the irregularity of secondary material transformation: the content of metamorphic minerals may vary (0 to 100 percent) in a volute of rock. The results of the quantitative evaluation of deformation obtained by Lukianov (1980) prove an essential heterogeneity of a plastic deformation. It varies from zero to 500-1000 percent.

(b) Spatial irregularity. The extent of structural and material transformation varies within a wide range: from a thinsection to a fold belt on the whole. Generally, it is an intricate spotted-mosaic or a band-loop combination of more or less intensely transformed (structurally or materially) volute (body) of rocks. As for the metamorphism, it is not controlled by any lateral or vertical zoning. Equally, the intensity of plastic deformation considerably varies vertically or laterally.

(c) Structural and a material transformation are correlated: zones of the most intense material change coincide with those of the most intense plastic deformation and v.v. the irregularity of epigenesis-metamorphism reflects the irregular intensity of plastic deformation.

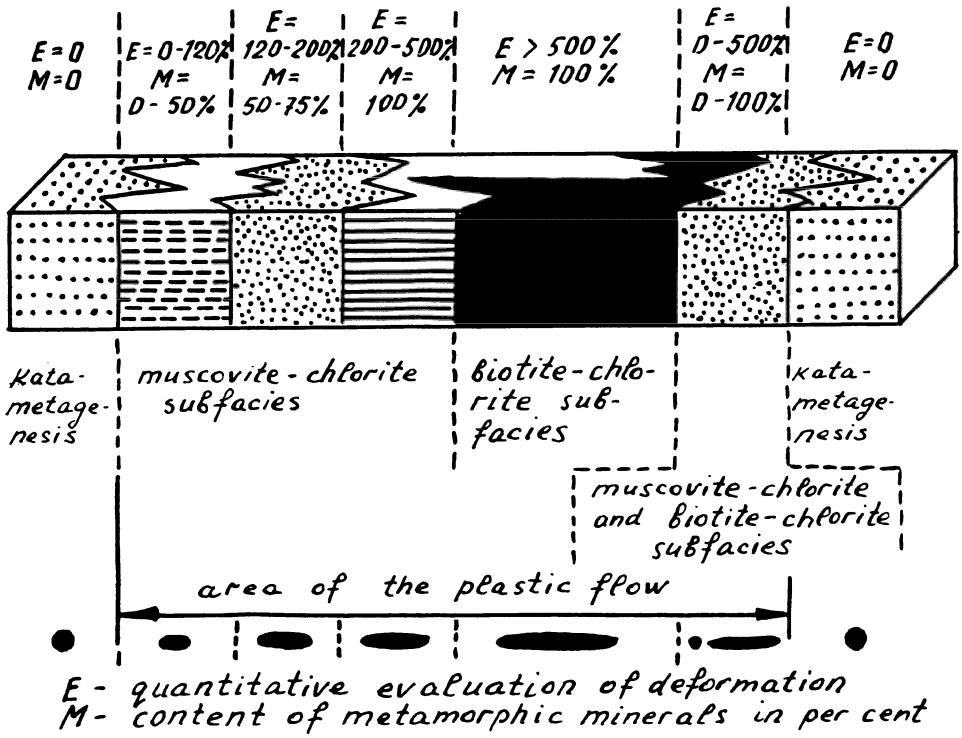

Correlation between metamorphic facies, the content of metamorphic minerals and the quantitative evaluation of plastic deformation (Kurganack's zone of plastic flow, Southern Tien Shan).

3. According to the present-day notions, the irregularity of metamorphic manifestation ought to reflect the irregular spatial distribution of thermodynamic parameters, first of all temperature and lithostatic pressure. Consequently, to explain the existing pattern of the metamorphic process we should point to either the mechanism of P and T-changes or some other factor favoring the material transformation of rocks.

4. In the studied regions, areas of more intense metamorphism are at the same time areas of more intense plastic deformation. There is a paragenetic liaison between these phenomena which is fixed at different scaile levels. Stemming from this it should be logical to assume that the plastic deformation is the factor somehow influencing the course of metamorphic reactins.

5. This conclusion is confirmed by data of mechanochemistry that studies chemical and physical change of a substance under the influence of mechanical energy. Experimental investigation in the field of mechanochemistry (Avvakumov, 1986; Bridgmen, 1955; Peters, 1966; Scheinike, 1987; and many others) allow us to consider the following postulates as proved:

(a) the influence of mechanical energy on solid bodies may cause all types of chemical reactions known in the chemistry of solid bodies;

(b) the increase of chemical activity of a substance with a supply of mechanical energy promotes a decrease of temperature and: lithostatic pressure as

compared with those necessary for petrochemical transformation proceeding in static condition;

(c) the important mechanochemical effects are typical of substances with well-defined plastic characteristics; the amount of the substance that took part in a reaction is proportional to deformation, and the plastic deformation is the most effective mean of mechanical activity of solid bodies, petrochemical reaction may develop in the plastic flow regime as self-stimulating.

6. The peculiarities of greenschist metamorphism of S. Tien Shan, and analysis of mechanochemical data prove that a plastic deformation is a real factor of metamorphic transformation. This type of metamorphism is "mosaic". Genetically it is dynamo-relaxational.

EVOLUTION OF PROTEROZOIC GRANITOIDS, EASTERN ARBUCKLE MOUNTAINS, OKLAHOMA

E.G. LIDIAK, *Department of Geology & Planetary Science, University of Pittsburgh, Pittsburgh, PA 15260, U.S.A., tel. 412-624-8871; email: egl@vms.cis.pitt.edu*

The midcontinent region of the United States in early and middle Proterozoic time was the site of widespread anorogenic igneous activity, which in Missouri, Kansas, Oklahoma, and adjacent areas occurred about 1,340-1,400 Ma ago. Granitoids in the Arbuckle Mountains of eastern Oklahoma have been included as part of the anorogenic suite. However, recent detailed geochemical and mineralogical data reveal that the granitic plutons within the Arbuckles may have formed in a different tectonic environment. The data are consistent with plutonism occurring during convergent tectonism along the southern margin of the midcontinent craton about 1,375-1,400 Ma ago. The main evidence for convergence comes from the formation of calc-alkalic magmas by possible interaction between a subducted slab and the overlying crustal wedge. Following or during the waning stages of active subduction, calc-alkalic magmatism gave way to potassic "post-orogenic" magmatism.

Major and trace element geochemistry indicate that the main middle Proterozoic plutons (Burch granodiorite, Troy and Tishomingo granites) evolved independently from their respective source regions. Linear co-variance of elements suggests that mafic and felsic members of each pluton are related by separation of early formed minerals. Modeling of possible source regions of the granitoids is poorly constrained because the composition of the 1.9 Ga lower and middle crust beneath the Arbuckles is unknown. However, LILE and REE compositions of the Burch granodiorite can be closely approximated by assuming equilibrium batch melting (EBM) of about 20% average graywacke or about 30% EBM of partly hydrated lower crustal sialic granulite. Troy granite compositions are consistent with their derivation from about 20% EBM of an equal mixture of sialic amphibolite-grade and granulite-grade gneisses. The high LILE and REE compositions of the Tishomingo granite require a source region that is geochemically more evolved than most lower crustal sources, possibly a mixture of sialic amphibolite-grade gneisses and lower Proterozoic felsic basement rocks.

SEISMIC IMAGING BENEATH THRUST BLOCKS

Z. LIU, *School of Geology and Geophysics, University of Oklahoma, Norman, OK 73019, tel. 405-325-4424*
R.A. YOUNG, *School of Geology and Geophysics, University of Oklahoma, Norman, OK 74004, tel. 405-325-5753; email: ryoung@ou.edu*

Seismic images of structures beneath basement overthrust blocks are difficult to obtain. Conventional CMP profiling uses ray paths that are transmitted across the large velocity contrasts presented by crystalline basement/sediment boundaries. These contrasts shield sub-thrust features from illumination by scattering the incident wavefield. Conventional survey apertures may be too short to record events from more steeply dipping sub-thrust boundaries. In addition, the large velocity decrease and the extreme lateral velocity variation across such boundaries render CMP stacking ineffective.

The use of turning ray paths that undershoot the basement block is examined in the present work. Turning rays have been used quite effectively for sub-salt imaging in the Gulf of Mexico, and the possibility of applying these methods to sub-thrust imaging is investigated.

SEISMICITY AND TECTONIC RELATIONSHIPS OF NORTH CENTRAL OKLAHOMA

K.V. LUZA, *Oklahoma Geological Survey, Norman, OK, 73019-0628, tel.(405) 325-3031*

In central Oklahoma, particularly near the axis of the Nemaha uplift, the basement-rock surface slopes gently southward. It is approximately 1,220 m below the surface near the Kansas border and is 2,440 m deep near Oklahoma City. Denison (1966, 1981) classified the central Oklahoma basement rocks into the following four units: (1) Washington Volcanic Group, (2) Spavinaw Granite Group, (3) Osage Microgranite, and (4) Central Oklahoma Granite Group. The isotopic ages range from 1,150 to 1,270 million years, and these ages, when considered with analytical variations, indicate a main period of thermal activity about 1,200 million years ago.

A total-intensity aeromagnetic map for the Enid and Oklahoma City 10° x 20° Quadrangles was prepared from the U.S. Department of Energy's National Uranium Resource Evaluation (NURE) data by Noel F. Rasmussen. Five dominant high and low anomalies feature the Lamont Ring Complex (high), Central Oklahoma metamorphics (low), Tulsa Mountains (high), and Greenleaf and Osage Island maxima (highs). Six major fault zones were identified: (1) north-south Nemaha, (2) east-west Garfield-Noble. (3) southwest-northeast Osage, (4) southwest-northeast Cushing, (5) Hughes County, and (6) Creek County fault complexes.

In 1977, the Oklahoma Geological Survey began to operate a 10-11 statewide network of seismograph stations. From 1882 through 1976, Oklahoma had approximately 130 known earthquakes. Over 880 additional earthquakes were located in Oklahoma from January 1, 1977, to December 31, 1994. The pre-1977 earthquake data, when combined with the 1977-94 earthquake data, produce at least one seismic trend in north-central Oklahoma. A 40-km-wide by 145-km-long zone extends northeastward from near El Reno toward Perry. The El Reno-Perry trend cuts diagonally across the Nemaha-Uplift structures at about a 30° angle. The southern end of this trend, the El Reno-Mustang area, appears to be more active than the middle and northern parts. The recent as well as the historic earthquake data seem to support this observation. The Canadian County earthquakes appear to coincide with the breakover from shelf to basin. Lower Paleozoic faults that probably were initiated when the Anadarko basin began to develop in Middle Cambrian time. However, most of these structures are not manifested in upper Paleozoic rocks.

It is not clear what the earthquake activity between El Reno and Perry represents. The earthquake zone may be the result of a coincidental plot of earthquake epicenters and/or related to some unknown northeast-trending structure(s). There are no known major Paleozoic structures in the vicinity of the zone. However, an

interpretation of the aeromagnetic data suggest northeast-southwest-trending Precambrian features near of the El Reno-Perry trend.

References

Denison, R. E., 1966, Basement rocks in adjoining parts of Oklahoma, Kansas, and Arkansas: unpublished Ph.D. dissertation, University of Texas, Austin, 292 p.

Denison, R. E., 1981, Basement rocks in northeastern Oklahoma: Oklahoma Geological Survey Circular 84, 84 p.

DISTRIBUTION OF PHANEROZOIC FAULTING AND FOLDING, SEISMICITY, AND ORE DEPOSITS IN THE MIDCONTINENT REGION, UNITED STATES: A REFLECTION WIDESPREAD PROTEROZOIC RIFTING IN THE NORTH AMERICAN CRATON?

S. MARSHAK and T.S. PAULSEN, *Department of Geology, University of Illinois, 1301 West Green Street, Urbana, IL 61801; tel.217-333-7705, email: smarshak@uiuc.edu*

Most of the Midcontinent region in the United States is a continental interior platform, where Precambrian basement is almost completely covered by a veneer of Phanerozoic sedimentary strata. To structural geologists accustomed to working in orogens, continental-interior platforms appear, at first glance, to have been undeformed during the Phanerozoic. Yet on closer examination the Midcontinent does contain a fascinating history of Phanerozoic tectonism; this history is recorded by structural features that differ markedly in style from the more dramatic features of orogens. Structural features of the Midcontinent can be divided into two general categories: (1) epeirogenic features (basins, domes, and arches of regional extent) whose development, though affecting regional patterns of stratigraphic thickness and facies, has resulted only in regional bedding dips of less than a few degrees; and, (2) fault and fold zones, which are belts of relatively localized deformation in which faulting has displaced stratigraphic contacts and/or bedding has been significantly bent or tilted. In this paper, we speculate on the question of fault and fold zones originated.

Many fault and fold zones, such as the Midcontinent rift and the Rough Creek graben, are known to be multiply reactivated rifts (e.g., Cannon, 1994). Here, we suggest that many, if not most other Midcontinent fault and fold zones also originated as rifts in the Proterozoic, but that their rift origin is more obscure simply because of later inversion and because of lack of data about structure character at depth. Our basis for this statement is as follows: (1) Rock is much weaker under tension, so initiation of faults in a strong cratonic region is easier if the structures form under tension than if they form under compression. Had differential stresses in the Midcontinent been sufficient to initiate thrusts in intact craton during the Phanerozoic, strain in the cover strata probably might be greater than is observed; (2) Fault and fold zones throughout the Midcontinent parallel known Proterozoic rift faults and dike trends that have been mapped both in the Midcontinent and along the western margin of the North American craton. Known rifts and Midcontinent fault and fold zones cluster in three dominant trends (approximately E-W, NW-SE and NNE-SSW) as has been recognized by numerous previous authors. (3) The structural style exhibited by Midcontinent fault and fold zones resembles examples of known rifts that have been inverted in transpression (cf. Mitra, 1993). Specifically, the zones contain steep, basement-penetrating faults, and local development of flower structure geometries and *en echelon* subsidiary fault arrays.

Folds in these zones, in general, are forced folds draped over the edge of fault blocks. In this regard, Midcontinent structures resemble Laramide structures of the Colorado Plateau, or subdued versions of Rocky Mountain basement-cored uplifts. In some locations, the local map pattern of structures in Midcontinent fault and fold zones strongly resembles the map pattern of normal faults linked by transfer faults, as is typical of contemporary rifts. For example, recent remapping of the LaSalle belt in the interior of the Illinois basin (Nelson, 1993) suggests that it is composed of approximately N-trending faults that terminate at NW-SE trending zones. Though the deep structure of this belt is unknown, the pattern strongly suggests that the N-trending faults originated as normal faults in a rift, and the NW-SE trending zones were transfer zones. Some of the NW-trending zones, in fact, lie directly along strike of known transfer faults in the Midcontinent rift; (4) Where deep drilling data or seismic-reflection data are available (e.g., Rough Creek graben; Missouri fault belt), they demonstrate that there are abrupt stratigraphic thickness changes across Midcontinent fault and fold zones, compatible with a normal faulting origin, even if the present offset of contacts is in a reverse sense. The magnitude of displacement on the basement/cover contact differs from that of younger units, indicating that the faulting was active in the Precambrian (e.g. Sims, 1990).

Where data are available, it is clear that Midcontinent fault and fold zones have been reactivated several times during the Phanerozoic, and that the sense of slip in successive events is not necessarily the same. A recent study of Devonian reactivation on structures in the Illinois basin, for example, suggests that movement occurs both during times of continental-margin collisional orogeny, and during times when collision was not occurring (Nelson and Marshak, 1995). Fault and fold zones have been able to survive as long-lived weaknesses, because they have not been annealed by subsequent metamorphism and transposition. Considering that the proposed rift trends roughly define a mutually orthogonal system, we concur with proposals that the Midcontinent is, effectively, divided into blocks that move slightly relative to one another (Shurr et al., 1994) in response to changes in the intracratonic stress field. The sense of movement at a given time depends on the configuration of the stress field. Thus, during one deformation event, the NNE-trending faults are reactivated as normal or reverse faults and the NW-trending faults are transform faults, while during other events the roles of the structures reversed. For example, as pointed out by Thomas (1991), during early Paleozoic and during Mesozoic rifting along the eastern margin of the continent, the NNE-trending structures were reactivated as rifts and the NW-trending structures became transform faults. One of the largest of the NW-trending structures is the Transamerican continental weak zone (Paulsen and Marshak, 1994; Marshak and Paulsen, 1994), which, because it has controlled rifting and transform geometry, influenced the geometry of Phanerozoic structures in marginal orogens, and today can be traced diagonally from Carolina to Idaho and Washington. In fact, this structure may serve as a pinning point to define the fit between Australia-Antarctica and North America in the Late Proterozoic.

The pattern of contemporary seismicity suggests that it is strongly controlled by the pattern of fault and fold zones in the Midcontinent. Presumably, the faults remain

today as weak zones, capable of being reactivated even though the continent is not subjected to collisional stress. Particularly active seismic zones occur at the intersection of NNE-trending fault zones with E-W or WNW-trending zones. The activity of these fault intersections may occur because the intersections are particularly weak (due to cross-cutting faults), because the intersections are weakened by higher heat flow (related to alkalic intrusion), because intrusive masses in these intersections create local stress concentrations, or because fluids have greater access to these regions due to greater fracturing. Localization of ore deposits at fault-zone intersections, further suggests that these locations are zones of enhanced permeability. Our proposal of a rift origin for most Midcontinent fault and fold zones can be tested by seismic-reflection and drilling studies. Our proposal implies that, considering the areal extent of fault and fold zones, rifting was widespread throughout North America during the Proterozoic. In this context, the aulacogens of the Cordillera need not be failed arms of three-armed rifts, but rather are merely earlier rifts truncated by the terminal Proterozoic rifting event. Further, our proposal suggests that previously unrecognized Proterozoic/early Paleozoic rift basins may underlie Midcontinent fault and fold zones; the presence of such rifts may explain widespread subhorizontal reflectors in deep seismic-reflection profiles.

References

Cannon, W.F., 1994, Geology: v.22, 155-158.

Nelson, WJ., 1993, Illinois State Geological Survey Bulletin 100.

Marshak, S., and Paulsen, T., 1994, Geological Society of America Abstracts with Programs, v. 26, p. A-192.

Mitra, S., 1993, American Association of Petroleum Geologists Bulletin, v.77, 1159-1191.

Paulsen, T., and Marshak, S., 1994, Geology, v.22, 15-18.

Nelson, WJ., and Marshak, S., 1995, Geological Society of America, Memoir, *in press.*

Sims, P.K., 1990, United States Geological Survey Map I-i 853A.

Shurr, G.W., Hammond, R.H., Bretz, R.F., 1994, Geological Society of America, Special Paper 287, p. 237-256.

Thomas, W.A., 1991, Geological Society of America Bulletin, v.103, 415431.

THE VARISCAN GEODYNAMIC CYCLE IN THE SARDINIAN-CORSICAN MASSIF

N. MINZONI, *Dipartimento di Scienze Geologiche e Paleontologiche, Universita' di Ferrara, Corso Ercole I d' Este 32, I-44100, Italy, tel. 39-532-210341.*
M. MINZONI, *Via Zappaterra 48, Ferrara, 1-44100, Italy, tel. 39-532-94180*

The most recent data indicate that the Variscan geodynamic cycle in the Sardinian-Corsican Massif developed as follows.

From early to middle Cambrian, a terrigenous shelf and carbonate succession were deposited on a Precambrian metamorphic basement in SW Sardinia. From mid-Cambrian to early Ordovician, extensional tectonics affected the whole Sardinian-Corsican area, with the deposition of shallow-water terrigenous sequences and emplacement of alkaline granitoids.

The geodynamic regime suddenly changed from early-middle Ordovician times. Compressional and extensional tectonics contemporaneously developed with the formation of open folds in SW Sardinia ("Sardinia Phase" auct.) and effusion of "bimodal" volcanics in central Sardinia and deposition of thick flysch-like terrigenous successions in northern areas of the island.

Several data indicate that the mid-Ordovician extensional tectonics developed with increasing intensity from central Sardinia northwards and that the middle-late Ordovician flysch-like sediments of northern Sardinia represent the basinward equivalent of epicontinental sequences deposited in southern Sardinia and northern Corsica.

The Silurian-mid-Devonian was characterized by sedimentation of black shales and carbonate sequences.

Variscan orogenesis developed from late Devonian to early Carboniferous. Several data indicate that the Variscan chain was formed by subduction processes followed by continental collision, with migration of Barrovian metamorphism and deformation from northern Sardinia southwards

These data suggest the following conclusions.

Only from the middle-late Ordovician onwards did a basinal area form in northern Sardinia. An oceanic suture line has recently been recognized in this area.

Radiometric dating indicates a Precambrian age (950 Ma) for the ultrabasic protoliths. However, the present data suggest that the ocean opened during the middle-late Ordovician. Therefore, the mid-Ordovician "bimodal" volcanics of central Sardinia must be related not to subduction processes (as proposed by several Authors) but to the extensional tectonics that caused the continental break-up marking the opening of the oceanic area in northern Sardinia. Moreover, extensional tectonics developed

contemporaneously with compressional tectonics. Since these phenomena are characteristic of wrench dynamics, the oceanic basin in northern Sardinia may be considered a transtensional area, probably related to strike-slip mega-faults. The geometric complexity of the Variscan chain in Europe and its unusual width may be the result of space-time opening of several oceanic areas caused by wrench dynamics.

THE INFLUENCE OF STRUCTURAL POSITION AND LITHOLOGY ON THE FRACTURE DISTRIBUTION IN THE EAST KAIBAB MONOCLINE, SE UTAH: IMPLICATIONS FOR FLUID FLOW PROPERTIES

P.N. MOLLEMA, A. AYDIN, and D.D. POLLARD, *Rock Fracture Project, Department of Geological and Environmental Sciences, Stanford University, Stanford, CA 94305*

The fracture distribution in the Paleozoic and Mesozoic sediments exposed in the East Kaibab monocline, Utah, has been documented for the purpose of developing a conceptual model for the spatial distribution of the fractures, understanding the mechanical evolution of the monocline, and evaluating the effects of the fractures on the fluid flow properties of the rocks.

The trend of the monocline is north with bedding dipping to the east, up to 60°. The width of the monocline is 4 to 5 kilometers. Using aerial photos and field mapping, the fractures were characterized on the basis of type (opening, closing, or shearing modes), geometry and spatial distribution in three cross sections through the monocline: Hackberry Canyon, Five Mile Spring area and Buckskin Gulch. The relation between these characteristics and structural position in the monocline, defined by curvature of the layers, position and distance with respect to the underlying basement structure and proximity to possible splays to branches of a basement fault was studied. The influence of sedimentary features (lithology, bedding, dune boundaries, and cross bedding) on the localization of fractures was studied by comparing outcrops of different lithologies in the same structural position. Four structural domains are defined from west to east across the monocline on the basis of recurrent fracture assemblages: (1) systematic joints at high angle to the monocline trend and discontinuous joints at high angle to the systematic set; (2) bedding plane faults and associated tail cracks; (3) major faults striking parallel to the fold axis and deformation bands; (4) a systematic joint set parallel to the monocline and joints at high angle to the systematic set.

The shape of the fold in the Hackberry Canyon and Five Mile Spring area show a broad concave upward bend of relatively low (negative) curvature on the west part and a narrow concave upward bend of high (positive) curvature on the east side. The Buckskin Gulch profile is more symmetric and has an overall lower curvature. The style of deformation in the Buckskin Gulch is different from the other profiles by the intense jointing and faulting over a 1.5 km wide area in domain (3), the lack of bedding plane faults on the west limb and the presence of low angle thrusts and compaction bands in domain (4). The difference in shape of fold, lower curvature and style of deformation in the Buckskin gulch with respect to the other two cross sections could be explained by a more proximate location to the basement fault. The occurrence of shallow dipping thrusts in the Buckskin Gulch can be indicative for buckling whereas

the lack of thrusts and high curvature in the other two cross sections suggests that bending is more important there. Assuming that the Navajo formation in the Hackberry Canyon initially behaved as a single distribution in a ideally elastic flexed plate. The location of faults observed in the steeply dipping layers of the Navajo in the Hackberry Canyon agrees with the location of high shear stresses in a flexed plate with clamped edges. The widespread occurrence of the bedding plane faults through almost the whole thickness of the Navajo does not agree with the location of high horizontal compressive stresses predicated with a plate model.

The style of the monocline parallel faults varies along the strike of the monocline but localization of deformation bands next to faults can be separated from fracture localization due to folding by detailed mapping.

The implications of the conceptual model of fracture distribution in the monocline for fluid flow properties are a strong directional permeability in each domain, with the direction of maximum and minimum permeability varying from domain to domain. Domain (3) would be most influenced by the presence of fractures and typically flow would be inhibited across the fault zones that are perpendicular to the monoclinal axis and would be enhanced vertically and parallel to the monocline along joints and slip planes.

EVOLUTION OF GRENVILLE TECTONIC PROVINCES, SOUTHEASTERN LLANO UPLIFT, CENTRAL TEXAS

S. MOSHER amd R.C. ROBACK, *University of Texas at Austin, Department of Geological Sciences, Austin TX 78712.*
J.F. REESE, *Idaho State University, Department of Geology Pocatello, ID 83209*

Grenville-aged orogenesis along the southern margin of Laurentia as recorded in the Llano uplift of central Texas includes extensive plutonism, regional polydeformation, and dynamothermal and static metamorphism that occurred from 1.32 to 1.07 Ga. Multidisciplinary geologic studies in the southeastern Llano uplift have delineated the following tectonic domains: a polydeformed, highly transposed supracrustal sequence (Packsaddle domain) that is situated between a lesser deformed tonalitic to dioritic island arc terrane (Coal Creek domain) and a polydeformed granitic gneiss terrane (Valley Spring domain).

The Coal Creek domain is a structural and lithologic province that displays, in contrast to the rest of the uplift, well preserved cross-cutting igneous relationships, and an older structural and metamorphic history. The domain consists dominantly of a cogenetic 1275 to 1292 Ma dioritic to tonalitic metamorphosed igneous suite intruded into 1303 to 1324 Ma mafic to tonalitic gneisses (all ages reported herein are U-Pb zircon from this study and Walker, 1992). Metamorphism and deformation of tonalitic gneisses occurred between 1282 and ca 1303 Ma, and a younger metamorphism of the domain is directly dated at 1256 Ma. A large tectonic slice of serpentinized harzburgite and numerous smaller serpentinites are spatially associated with the domain. The lithologic association of the Coal Creek domain, as well as common Pb and Nd isotopic signatures, differ from the dominantly granitic and metasedimentary domains to the north. The Coal Creek domain also preserves a metamorphic and structural history that is, in part, unique to that of the rest of the uplift. We consider the Coal Creek domain to represent part of an island arc that is allochthonous to the ancient Laurentian continental margin. The boundary between the Coal Creek and Packsaddle domains is a wide mylonite zone containing proto- to ultramylonitic granitic sills ranging in age from 1251-1238 Ma.

Metasedimentary, metavolcanic, and metaplutonic rocks of the Packsaddle domain have undergone five phases of outcrop to regional scale folding that resulted in the formation of five penetrative metamorphic foliations. Complete transposition of the original layering concurrent with amphibolite facies metamorphism has obscured original contact relationships and most protoliths. Mylonites that predate most of the folding have been recognized. Tectonic transport as indicated by asymmetry of porphyroclasts and fold vergence is towards the northeast. Late stage to post-contractional N-S extension is locally observed. Regional deformation is bracketed by

sills dated at 1238 Ma which are affected by the last four phases of folding, and an undeformed, regionally extensive rhyolitic dike dated at 1098 Ma that cross cuts all structures. At the northern boundary of the Packsaddle domain, the youngest identified deformed metamorphic rock (1216 Ma) is involved in a ductile shear zone that places Packsaddle domain on granitic gneiss of the Valley Spring domain. Orthogneisses of the Valley Spring domain range in age from 1232-1288 Ma. Complex U-Pb zircon systematics from a granitic (ortho?) gneiss as old as 1360 Ma record the presence of yet older crust. These oldest gneisses may be correlative with the southern Granite-Rhyolite terrane of Laurentia.

High to medium pressure regional metamorphism was synchronous with deformation throughout most of the uplift. The highest pressure and temperature conditions are recorded by medium T eclogites in the western uplift. Pressures and temperatures generally decrease to the northeast in the direction of tectonic transport. Regional metamorphic and structural features were overprinted by a low pressure, mid-amphibolite facies, static metamorphism associated with late syn- to post-tectonic granite plutons dated at 1135-1070 Ma. Local penetrative ductile deformation of the older of these plutons suggests their emplacement during the waning stages of orogenesis.

Grenville orogenic activity in central Texas spanned at least 250 Ma and involved collision of a long-lived (60 Ma) island arc terrane (Coal Creek domain) with a continental block (Valley Spring domain) that may represent the southern margin of Laurentia. Timing of this collision is bracketed between 1275 and 1133 Ma.

References

Walker, N. (1992) Middle Proterozoic geologic evolution ot Llano uplift, Texas: Evidence from U-Pb zircon geochronometry, *Geological Society of America Bulletin* 104, 494-504.

ANATOMY OF THE GRENVILLE OROGEN IN WEST TEXAS

K.C. NIELSEN and K. SOEGAARD, *Programs in Geosciences, University of Texas/Dallas, Richardson, TX, 75083-0688, tel. 214-883-2406; email: knielsen@utdallas.edu*
M.E. BICKFORD, *Department of Geology, Syracuse University, Syracuse, NY, 13244-1070, tel. 315-443-2672; email: mebickfo@suvm.acs.syr.edu*

Exposures of Precambrian basement rocks near Van Horn, Texas provide an important transect across the Grenville age deformational front. To the south, metamorphic rocks of the Carizzo Mountain Group (CMG) are interpreted to be an allocthonous package of ~1350 Ma rift-related rocks. The CMG has been subdivided into three structural domains. In the northwest portion of the mountains a large east-west trending, reclined synform characterizes the hanging wall of the Streeruwitz thrust. The southern limb of this synform has been truncated by the Mineral Creek fault zone (MCfz), a 350 meter thick imbricate package characterized by mylonitized rhyolite. The central domain is in the hangingwall of MCfz and contains large (5 km wavelength) tight, inclined folds with subhorizontal axes. These folds are cut by several northerly directed thrust faults. In the southeast domain, southerly trending structures suggest a zone of refolding plunging beneath the Paleozoic cover. The CMG is translated towards the NNW on the Streeruwitz thrust. In the foreland, sedimentary rocks of the Allamoore Fm. record shallow marine carbonate deposition associated with (andesitic) volcanism of 1250 Ma. Initial deformation is documented in the Tumbledown Fm, a volcaniclastic package containing megabreccias of the Allamoore Fm. This initial deformation is interpreted to reflect a transtensional setting between 1250-1100 Ma. Deformation within the Tumbledown Fm. includes penetrative cleavage and complex conical folds. Post-dating these events is the development of a large alluvial fan comprised of coarse conglomerate and siltstone, the Hazel Fm. The source of these sediments are the Allamoore and Tumbledown Fm. and a granitic/rhyolite basement of ~1100 Ma, not the CMG. This observation suggests continued strike slip deformation and basement uplift in front of the advancing Streeruwitz thrust. The Hazel alluvial fan is deformed into large kink folds which are subsequently overridden by complex thrust sheets. The thrust sheets are folded and klippe of CMG are emplaced during this final stage of deformation. Recurrent motion has occurred along many of the basement faults in the foreland area. Isotopic data suggests two distinct stages of deformation, an early stage ~1250 Ma and a younger stage between 1100-1000 Ma. Between these two events is a regional igneous event of ~1100 Ma, possibly coincident with rifting in the midcontinent.

HALOKINETIC ASSOCIATED CRUSTAL STRETCHING IN THE SOUTHERN RED SEA: NEW OBSERVATIONS OF THE BASEMENT AND SEDIMENTARY COVER FROM REFRACTION CONSTRAINED REFLECTION SEISMIC STRATIGRAPHY

J.D. PIGOTT, E.S. GEBRETSADIK, and A. ALAHDAHL, *School of Geology and Geophysics, University of Oklahoma, Norman, OK 73019, U.S.A.*

Much tectonic speculation of Red Sea rifting has been founded upon the assumed structural styles interpreted from exclusively either solid earth geophysical surveys or poor resolution single channel reflection seismic profiles. The problem of seismically imaging the basement and its associated structures has been compounded by significant wavelet attenuation and multiple generation contributed by the overlying salt.

We report new structural-stratigraphic interpretations based upon an integration of seismic refraction, reflection, and geological borehole control. Conventional industry acquired multifold reflection seismic profiles including and extending from offshore Eritrea (>2000 line kms) across the Red Sea axial trough into offshore Yemen (>1000 line kms) were depth constrained using published sonobouy refraction surveys (11 stations). The major sequences were geologically controlled using forward seismic modeled synthetics from proprietary borehole (4 wells) density and sonic logs. Attenuation of multiples was conducted using post-stack Fourier division wavelet processing.

The integrated seismic stratigraphy of the Southern Red Sea reveals the following structural-stratigraphic highlights: basement controlled horsts, non-basement controlled salt mobilization accentuated horsts, basement controlled grabens, non-basement controlled salt withdrawal grabens, salt-swells in phase with tilted basement block apexes, counter-regional faulting, eustatic controlled sequence boundaries, and non-eustatic halokinetic controlled sequence boundaries.

Differences in directly observed basement-influenced stretching occurs in four zones, beginning from the axial trough outward: Zone 1- maximum crustal attenuation in the axial trough with magmatic extrusion; Zone 2- high crustal stretching with imbricate en echelon tilted basement blocks with eroded distal corners; Zone 3- moderate crustal extension with high angle fault bounded horsts and grabens; and Zone 4- minimum crustal extension on the rift flanks. These zones of structural style resulted from the first phase of rifting (25.2 Ma). A second pulse of rifting (post salt or 5.2 Ma) is revealed by basement influenced high angle extensional faults which cut post-salt sediments. A third phase of on-going crustal extension is a product of halokinesis which only affects post-salt sediments.

Our observations suggest Southern Red Sea rifting to be described as a multi-phased crustal attenuation model, halokinetic influenced, with structural features supportive of a pure shear regional extension model with local transfer zones of simple shear.

PARTIAL MELTING OF MOUNT SCOTT GRANITE AT 850° C AND 500 BARS

J.D. PRICE, J.P. HOGAN, G.B. MORGAN VI, D. LONDON, and M.C. GILBERT, *School of Geology and Geophysics, University of Oklahoma, Norman, Oklahoma 73019, tel. 405-325-3253; email: jprice@geophysics.scif.ou.edu.*

Fluorine and water influenced the emplacement characteristics of the Cambrian, Mount Scott A-type granite, Wichita Mountains. Feldspar geothermometry temperatures of 640°C are unreasonably low for a dry solidus. Emplacement as a shallow, high aspect ratio sheet (length/thickness ~110) indicates low melt viscosity. Both suggest possible volatile activity. However, the granite offers little evidence of high H_20 content. It contains few miarolitic cavities, pegmatites, or aplites. Biotite chemistry and fluorite grains point to F as a significant player in emplacement and crystallization history.

Partial melting experiments were conducted to clarify $T\text{-}XH_2O\text{-}XF_2$ phase relationships at possible conditions of emplacement (850°C, 500 bars). The Mount Scott granite has abundant kspar + quartz, lessor plag + amphibole + biotite + magnetite + hematite, minor apatite + titanite + zircon + fluorite, and scarce ilmenite + pyrite. Plagioclase ($An_{5\text{-}17}$) is far less abundant than microperthitic alkali feldspar; much of the kspar occurs as ovoid-shaped phenocrysts. The rock is metaluminous (A/NCK = 0.9) and low in CaO (1.24 wt%). Fresh material was obtained from drill core [see Price *et al.*, this issue] 25 feet below the weathered zone (depth = 123-125 feet). Sample powders were dried overnight at 110°C. Run times were 10 days at 850°C and 500 bars, using Au capsules in cold-seal reaction vessels. Bulk composition of the sample controlled O_2. The sample charges were: (1) powder only; (2) powder with 10 wt% added H_20; (3) powder with 5 wt% added cryolite, Na_3AlF_6; and (4) powder with added H_20 and Na_3AlF_6. Although the addition of Na_3AlF_6 changes the bulk composition, Mount Scott granite may have lost F through an alkali-fluoride *(e.g.,* cryolite was identified as a vapor-deposited phase in similar experiments [Manning, 1981]).

Charge 1 (powder only): yielded 5% melt, indicating the "dry" solidus temperature is slightly lower than 850°C at 500 bars. Melt forms an intergranular film (~1 μ thick) adjacent to newly crystallized ternary feldspar Na-rich) and alkali feldspar similar to those seen in the rock. Because of the small size of the melt pools, the glass was not analyzed. Phases differed slightly from the starting composition. Biotite is notably absent, supplying water for melting.

Charge 2 (powder with 10 wt% added H_20): produced 67% melt. This glass contained 3.0 ± 0.5 wt% H_20 and was largely comprised of feldspar components. It contained higher percentages of CaO and lower percentages of FeO (total iron), $Ti0_2$, F, and Na_2O

than the Na_3AlF_6-added charges. The run gave the assembly of quartz + feldspar + amphibole + titanite + magnetite + ilmenite. Again, biotite is notably absent. Feldspar is ternary and strongly resorbed, appearing as if the K-rich perthitic lamellae had been removed leaving behind the Na-rich component to readjust to the melt. Amphibole EDS analyses are calcic; these grains are skeletal and tubular.

Charge 3 (powder with added Na_3AlF_6): resulted in 45% melt. Analysis revealed low water concentrations. The glass contained higher percentages of the added components and TiO_2, and lower CaO and BaO. Phases included quartz + kspar + biotite + fluorite + fayalite + magnetite + ilmenite. Fluorite is present as small, round crystals. Amphibole was absent in the F-added charges, and supplied water to the melt. Spongy textured magnetite was present and was rimmed by fayalite. Ilmenite appeared stable. The presence of quartz + ilmenite + magnetite reacting to form fayalite indicates lowering fO_2 during the run.

Charge 4 (powder with 10 wt% added H_20 and 5 wt% added Na_3AlF_6): yielded >90% melt. Glass composition was comparable to charge 3, although containing higher TiO_2. This melt had a higher percentage of water (3.7 ± 0.5 wt%) than charge 2. The charge contained biotite, fluorite, and rare oxide. As in charge 3, amphibole was absent. EDS analysis of biotite grains revealed Ca, possibly resulting from unresolvable inclusions of fluorite. Most fluorite grains occurred near biotite as small (1-5μ), rounded blobs. Crystallization of abundant fluorite depleted CaO from the melt. The A/NCK ratio of these melts approached those of the whole-rock composition (0.90), as opposed to the more aluminous melt in charge 2. Charge 3 and charge 4 (recalculated on an anhydrous basis) contained 2.4 wt% F in the melt.

These experiments provided the following conclusions. Kspar, quartz, and biotite appear to melt first in a "dry" sample. With excess H_20, kspar and biotite disappear first, and remaining plagioclase feldspar readjusts to a ternary composition. Addition of F leads to an instability in calcic plagioclase, produces fluorite, and shifts the minimum melt composition away from quartz in this system. Increasing melt F and alkalinity stabilize biotite. For uncertain reasons, additional F appears to lower fO_2. Magnetite reacts with Na, Al, F enriched melt to form fayalite, a phase not seen in the Mount Scott granite. Additionally, H_20-saturation in charge 2 and charge 4 results in an HS-bearing(?) vapor with a quench pH = 2, the result of sulfide dissolution. None of the melts contained detectable amounts of S.

Based on the results of these experiments, Mount Scott granite contained less than 3 wt% fluorine during emplacement. Most notably, lower concentrations of F are necessary to stabilize the magmatic plagioclase. The results also indicate lower H_20 concentrations than examined in this study. Further investigation is warranted as to the phase relationships and melt chemistry with smaller percentages of H_20 and F_2, at lower T, and at different (controlled) fO_2.

References

Manning, D.A.C., 1981, The effect of fluorine on liquidus phase relationships in the system Qz-Ab-Or with excess water at 1 kb, *Contributions to Mineralogy and Petrology,* 76, 206-215.

Price, J.D., Hogan, J.P., Payne, J., and Gilbert, M.C., Investigation of the Mount Scott Granite Drill Core, Wichita Mountains, Oklahoma, *12th International Conference on Basement Tectonics,* in press.

INVESTIGATION OF THE MOUNT SCOTT GRANITE DRILL CORE, WICHITA MOUNTAINS, OKLAHOMA

J.D. PRICE, J.P. HOGAN, J. PAYNE, and M.C. GILBERT, *School of Geology and Geophysics, University of Oklahoma, Norman, Oklahoma 73019, tel. 405-325-3253; email: jprice@geophysics.scif.ou.edu.*

A drilling investigation of the epizonal, Cambrian, Mount Scott A-type granite, produced 287 feet of continuous drill core. The drilling project aimed to characterize the contact zone between this unit and one of the underlying host units, the Sandy Creek gabbro. The drill hole location is 5 meters from the contact with the Sandy Creek gabbro, and it was anticipated that the hole would intercept the contact at depth. The drill failed to encounter the Sandy Creek gabbro, nor is there direct evidence of Sandy Creek gabbro in the core. The core is homogenous with respect to primary silicate mineralogy, feldspar chemistry, and mineral texture. Two-feldspar geothermometry on samples from 287, 114, and 17 feet yields temperatures of ~640 + 50 ^{0}C. Samples from 287 feet contain a sodic amphibole not generally seen in the Mount Scott, but common to the younger, nearby Quanah granite.

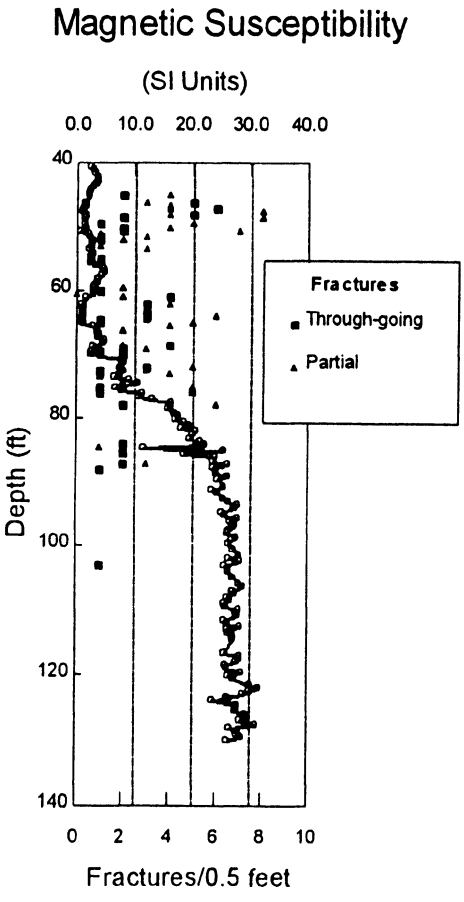

The core is comprised of a *fractured zone* from the surface to 70 feet, where it grades over a length of 30 feet into a more *competent zone* (fig. 1). The fractured zone is marked by healed and incompletely healed through-going and partial fractures, ranging in scale from microscopic to macroscopic. Fractures typically lack visible offset. Hematite, produced by oxidation of primary titanomagnetite, is more abundant in the fractured zone. Hematite in the competent zone is mostly in fractures within magnetite and along grain margins. The darker rock color of the fractured zone reflects this change in oxide mineralogy. Cathodoluminescence indicates a larger ferric component in the feldspars of this upper zone. The magnetic susceptibility quantifies this change (Fig. 1): the fractured-zone ranges from 2 to 5 SI units grading into competent zone ranges of 25 - 30 SI units.

Figure 1. Magnetic susceptibility and fracture density of the SQ core.

Both zones preserve evidence of primary and secondary sulfide phases. Many of the through-going fractures are coated with a hematite stain but contain abundant green-colored, circular areas (0.5-2 mm diameter) with small pyrite grains The presence of secondary sulfides and oxides points to a complex history of fluid-rock interaction.

GEOLOGICAL AND GEOPHYSICAL EXPLORATION FOR URANIUM MINERALIZATION ON EI-EREDIYA PROSPECT AREA, CENTRAL EASTERN DESERT, EGYPT.

S.I. RABIE, A.A.A. MEGUID, and A.S. ASSRAN, *Nuclear Materials Authority, P.O.Box 530 Maadi, Cairo, Egypt*

Ground geologic, structural, radiometric, magnetic and horizontal-loop electromagnetic data (surface and mining) have been applied to follow the surface and downward extension of the uranium mineralizations showings of El -Erediya prospect area, located in the Central Eastern Desert, Egypt.

El-Erediya uranium mineralization are associated with jasperoid silica veins hosted in El-Erediya granite which represent one of the later phase plutons of the Egyptian granitoids (550-590 Ma). The silica veins fills tensional fractures related to ENE normal faulting and to its feather fractures. Geologic and structural investigation of the area indicate a supergene origin for silica veins and uranium mineralization. Firstly a silica rich solution altered the granite and leached its uranium and precipitates it in open ENE fractures with some iron sulfides. A second phase of uranium mobilization and concentration was accompanied with tectonic rejuvenation of ENE fractures where uranium gets more concentrated in a second jasperoid silica solution which cements the brecciated early silica veins and the contact granite. A third remobilization process are indicated by surface leaching and alteration of the early formed pitchblende and iron sulfides and redistribution of secondary uranium mineralizations and hematitization along different fractures and alteration zones.

The integration of the results obtained from the magnetic data, led to the construction of a basement tectonic map closely correlative to the geological map for the area under consideration . The interpretation of the horizontal-loop electromagnetic data of the surface profile (00 NS) and the mining profiles indicate the deduction of conductive zones. These zones are mainly associated with the jasperoid veins, shear and fault zones. The conductive parameters such as location, width, dip, depth and conductivity thickness were estimated for each conductive zone, as averaged from the utilized four frequencies.

NATURE AND AGE OF DUCTILE DEFORMATION ASSOCIATED WITH THE "ANOROGENIC" TOWN MOUNTAIN GRANITE, LLANO UPLIFT, CENTRAL TEXAS.

R.M. REED, R.C. ROBACK, and M.A. HELPER, *Department of Geological Sciences University of Texas, Austin, TX 78712*

1.07-1.13 Ga granites comprise almost half of the rocks in the Proterozoic (Grenvillian) Llano Uplift of central Texas and thus have contributed significantly to the evolution of basement along the southwestern margin of Laurentia. Intrusions of Town Mountain Granite in the Llano Uplift have previously been described as "anorogenic", but recent work has shown that deformation accompanied and/or postdated intrusion of some granites.

The Wolf Mountain intrusion (WMI) of the northcentral Llano Uplift is a chevron-shaped (phacolithic) granitic body that occupies the hinge of a southeast-plunging syncline. A foliation in the WMI is parallel to the axial plane of this syncline. This foliation has a magmatic component defined by alignment of microcline megacrysts which has been overprinted by moderate amounts of high-temperature, solid-state deformation. Folding while the intrusion was not completely crystallized has resulted in complex internal structures including transtensional dikes, deformed magmatic enclaves and xenoliths, and convolute boundaries between granitic phases. A preliminary U-Pb zircon age of ca 1.13 Ga has been obtained for a small body associated with the WMI Deformation within the Grape Creek Pluton (GCP) of the southeastern Llano Uplift is more focussed than deformation in the WMI. A >400 meter-wide shear zone has formed an augen gneiss with zones of mylonite from an isotropic, porphyritic, very coarse-grained granite. The shear zone strikes N5OW and dips moderately to the northeast with a down-dip stretching lineation. Deformation and grain-size reduction are accomplished by high-temperature recrystallization of feldspars and quartz. Sigma-type recrystallized tails on feldspar porphyroclasts and an S-C fabric indicate reverse (top-to-the-southwest) sense of shear. A preliminary U-Pb zircon age of ca 1.13 Ga has been obtained for the GCP.

The Midway granite sill of the northeastern Llano Uplift has undergone pervasive recrystallization to form an augen gneiss. Foliation within the granite gneiss trends WNW and dips to the SW with a shallow SE-plunging stretching lineation. Kinematic indicators show a combination of right-lateral and thrust motion. Early dikes that intrude the country rock are folded, boudinaged, or mylonitized. Late dikes are undeformed, showing deformation was syn-plutonic.

The foliation in the WMI is parallel to the axial plane of the syncline it occupies and also to the late-stage foliation in the surrounding country rock. While the foliation within the GCP is similar in orientation to foliation within the WMI, the northeast dip and southwest transport directions are opposite those in nearby metamorphic rocks. Foliation in the MSG and that in surrounding country rocks are parallel.

Geologic evidence for syn- to post-emplacement deformation suggests that early intrusions of Town Mountain Granite were synchronous with the waning stages of Grenvillian orogenesis. As a whole, the Town Mountain Granite suite appears to be late syn- to post-orogenic and not anorogenic.

Information on Geochronological Samples: The Grape Creek Pluton sample location is located approximately 5.9 kilometers WSW of the town of Sandy, Texas on the Granite Knob Ranch. The sample was taken from within the shear zone.

The other date given is for an unnamed dike-like body of medium-grained pink granite that occurs on a northwest trend passing through the town of Llano, Texas. As stated above, this body is thought to be related to the main Wolf Mountain Intrusion.

U-Pb zircon geochronology was done by Robert C. Roback.

INTERDEPENDENCY OF MECHANICAL AND CHEMICAL PROCESSES DURING THE EVOLUTION OF CHLORITIC BRECCIA, SACRAMENTO MOUNTAINS, SE CALIFORNIA

J. SCHWEITZER, *Department of Geosciences, University of Tulsa, 600 S. College Ave., Tulsa, OK 74104-3189, tel. 918-631-2090*

Complex interaction between brittle deformation and mineralizing fluids resulted in the formation of the chloritic breccia zone that is found in crystalline footwall rocks of the Sacramento Mountains detachment fault (SMDF). The Sacramento Mountains, located in southeastern California, is one of a line of metamorphic core complexes in western North America that extends from Canada into Mexico. Similar to other core complexes, the Sacramento Mountains is characterized by upper plate Tertiary sedimentary and volcanic rocks separated from lower plate intrusive rocks (predominantly granite and granodiorite) by a low angle extensional fault. Chloritic breccia is found in the crystalline footwall rocks in most metamorphic core complexes and is characterized by 1) the disruption of preexisting rock textures due to brittle deformation and 2) a green color due to secondary chlorite and epidote.

In the Sacramento Mountains, the chloritic breccia zone is variably developed for approximately 100 m below the SMDF. The most deformed zones, such as immediately adjacent to the SMDF, consist mostly of green to green-blue microbreccia. Within the microbreccia, preexisting rock fabrics are destroyed and the protolith is generally unidentifiable. Angular to rounded clasts up to 10 cm across, but most commonly < 1 cm, are found in an aphanitic matrix. Microstructural examination reveals that the clasts include fragments of the protolith, monomineralic aggregates, or pieces of an older microbreccia. Textures range from matrix-supported to clast-supported, although the former is more common. The matrix is composed of abundant cryptocrystalline epidote and lesser amounts of chlorite, hematite and quartz.

In less deformed portions of the chloritic breccia zone, two common fracture sets are observed on the both the micro- and mesoscale:

The Type A fracture set consists of a subplanar brittle shear zones (BSZ) and oblique fractures that extend both above and below the BSZ boundary. In outcrop, BSZs typically have shallow to moderate dips. They contain fine-grained gouge of variable thickness, consisting of angular to subrounded, fine- to very fine-grained wall rock fragments in a microcrystalline matrix of cryptocrystalline epidote plus varying quantities of quartz, feldspar, hematite, chlorite, and sericite. Oblique fractures are oriented from 40 to 65 degrees to BSZ boundaries and are usually decorated with cryptocrystalline epidote.

The Type B fracture set is a set of moderately to steeply dipping conjugate fractures, with an acute angle of intersection ranging from 50 to 65 degrees. These fractures are typically decorated with cryptocrystalline epidote plus chlorite and hematite, and are usually found in rocks with previously developed Type A sets. Fine-

grained gouge is rare, and where it is found, there is typically little apparent offset across the fracture. Type B fracture sets generally cross-cut and offset BSZs, or may curve into parallelism and merge with them.

Rocks in the chloritic breccia zone have experienced both replacement alteration and open-space alteration. Replacement alteration affected most of the feldspar, amphibole, and biotite in the zone and occurred throughout its history. Three generations of open-space alteration have been recognized in these rocks: phase 1: precipitation of cryptocrystalline epidote, phase 2: precipitation of cryptocrystalline epidote and chlorite, and phase 3: precipitation of calcite.

Stage 1 in the evolution of chloritic breccia was the initiation and development of Type A fracture sets in response to tectonic stresses that locally exceeded the rock strength. The formation of the fractures allowed the influx of mineralizing fluids that precipitated cryptocrystalline epidote (alteration phase 1) in the fractures and voids between rock fragments in the BSZs. Cementation of the gouge with epidote resulted in strain hardening within the BSZ and subsequent fracturing of the gouge zone and wall rock. This resulted in progressive thickening of the BSZs and reworking of older cemented cataclasite. In high strain areas, cyclic fracturing, cataclasis, and cementation produced localized zones of microbreccia.

Stage 2 was the development of Type B fracture sets at high angles to the BSZs. Disruption of Type A structures by multiple generations of Type B fractures also resulted in local development of microbreccia. In addition, there is evidence that cataclasite development continued in some of the BSZs during the development of Type B fractures. Incursion of fluids into the system resulted in deposition of chlorite and epidote (phase 2 alteration) along Type B fractures, within voids in some BSZs and in veins that crosscut Types A and B fracture sets. This alteration phase continued after the cessation of cataclasis. All of the deformation fabrics found in the lower plate rocks are locally cross-cut by calcite veins with that have grains that show no evidence of strain, indicating that the third phase of alteration postdated significant deformation events.

In the Sacramento Mountains within the chloritic breccia zone, the most intensely deformed rocks were also the most highly altered. The positive correlation between the intensity of mechanical disruption and chemical alteration reflect that the two were interdependent during chloritic breccia evolution.

FACTORS AFFECTING LIMITING ANGLES FOR FAULT REACTIVATION IN BASEMENT ROCKS

T.B. SCOTT, JR. *School of Geology and Geophysics, The University of Oklahoma, Norman, OK, 73019-0628.*

The reactivation of a preexisting weakness in a rock, such as a fault or fracture, depends upon the relationship between the coefficient of sliding friction of the surface, the internal coefficient of friction for the country rock and the orientation and magnitudes of the superimposed stress fields. Handin (1969) demonstrated that a set of 'limiting' angles for reactivation of a preexisting sawcut rock sample subjected to triaxial stresses are related the geometry created by superimposing a Mohr stress circle, at the point of failure, over the sliding friction line for a given rock type. Samples with sawcut angles outside of the limiting angles cannot be reactivated but will fracture across the preexisting plane to form a new shear failure surface. Samples with favorably oriented sawcuts will be reactivated when the shear and normal stresses exceed a given value. This effect has been documented in laboratory testing for a wide range of rock types. Laboratory testing of sawcut samples suggests that the angles for the reactivation of faults in basement blocks may be significantly different than those for rocks in the shallow crustal regime. High porosity rocks, such as sandstones, generally have a narrow set of limiting angles due their lower strength (Scott and Nielsen, 1981). Limiting angles for fault reactivation of low porosity rocks, typical of basement lithologies, are generally wider - around from 50° to 470° of the principal directed stress. Two notable exceptions will dramatically affect this pattern of limiting angles. The presence of abnormally high fluid pressures within the fault gouge zone and the presence of clays in a gouge will significantly expand the range of limiting angles for fault reactivation of basement rocks.

LEAD ISOTOPE MAPPING OF CRUSTAL RESERVOIRS WITHIN THE GRENVILLE SUPERTERRANE: CENTRAL AND SOUTHERN APPALACHIANS

A.K. SINHA, *Department of Geological Sciences, Virginia Polytechnic Institute and State University, Blacksburg, VA 24061.*

Geodynamic models for the crustal evolution of the earth are best constrained by recognizing terranes associated with both the accretion and separation of continental plates. In older mountain belts that have experienced multiple episodes of metamorphism and structural reorganization, terrane boundaries are usually not recognizable. However, recent advances in interpreting isotope characteristics of crustal blocks permits separation of distinct crustal reservoirs that may represent terranes.

The Grenville orogen is a globe-encircling belt that is marked by either clearly identifiable reactivated older crust or blocks dominated by addition of juvenile magmas. The timing of linkages of terranes, with implications regarding juxtaposition of isotopically distinct reservoirs, is still a matter of debate. However, the lead isotopic characterization of crustal reservoirs show that measurable isotopic differences may be related to differences in crustal histories, thus leading to delineation of distinct terranes.

New whole rock Pb isotope data are presented from basement rocks of Grenville age. Samples from nine major basement rocks, extending from Pennsylvania to Georgia have been utilized to delineate isotopic crustal reservoirs. Utilizing Pb isotope correlation diagrams, three distinct isotopic reservoirs can be recognized. The three groups are subdivided on the basis of inferred μ ($^{238}U/^{204}Pb$) of the Grenville age rocks, as well as evidence of an Archean component in two of the blocks. On the basis of only 94 analyses, the three groups are: (i) Carvers Gap Gneiss and Stage Road Layered Gneiss; (ii) Blue Ridge, Baltimore Gneiss, State Farm Gneiss, and Pine Mountain Gneiss; and (iii) Tallulah Falls, Sauratown Mountain, Corbin and Honeybrook Uplands. It is suggested that Grenville age tectonic processes juxtaposed these isotopic reservoirs, leading to the development of the Grenville Superterrane.

PETROLOGY AND GEOCHEMISTRY OF A LATE PROTEROZOIC ANOROGENIC SUPERSUITE, LAURENTIAN APPALACHIANS, VIRGINIA AND NORTH CAROLINA: IMPLICATIONS FOR MAGMA-GENERATION ASSOCIATED WITH CRATONIC EXTENSION

R.P. TOLLO, *Department of Geology, George Washington University, Washington, DC 20052; e-mail: tollo@acad.ccgs.gwu.edu*
F.F. HUTSON, *Department of Geological Sciences, The University of Texas at Austin, Austin, TX 78712; email: hutson@maestro.geo.utexas.edu*

The magmatic record of rift-related processes operative along incipient continental margins often is obliterated or modified by subsequent compressional tectonic events. Nevertheless, analysis of such igneous rocks is important in determining the nature of sources and melt-generating processes involved in large-scale cratonic rifting. Magmatic activity associated with regional extension produced more than 20 granitoid plutons within the Laurentian Appalachians of Virginia and North Carolina. The plutons and associated volcanic rocks constitute a supersuite that spans an age range of at least 760-700 Ma and defines a period of magmatism that preceded development of oceanic crust by about 130 m.y. Plutons constituting the supersuite, which includes granitoids of the Crossnore Complex and Robertson River Igneous Suite, among others, are variable in size, typically elongate, and range from monzogranite to alkali feldspar syenite. Most plutons record a sequence of multiple intrusions that, in the large Robertson River batholith, spanned at least 35 m.y. The plutonic and associated volcanic rocks of the supersuite display many petrologic characteristics of A-type granitoids including (1) metaluminous to (relatively rare) mildly peralkaline bulk compositions, (2) high (relative to well-documented I-, S-, and M-types) Zr, Nb, Ga, Y, REF (not Eu), Fe/Mg, and Ga/Al, and (3) common occurrence of hypersolvus feldspar assemblages, Fe-rich ferromagnesian silicates, fluorite, and REF-bearing accessory phases including allanite. Intrapluton compositional variation is locally significant and reflects both source- and fractionation- (dominantly feldspar and/or accessory minerals) related mechanisms, locally modified by Fluid-driven, late- and post-magmatic processes. Trace element data from the most thoroughly studied plutons indicate that the peralkaline rocks are not petrologic derivatives of the more abundant metaluminous types. Moreover, comparison with other well documented suites suggests that the peralkaline rocks exhibit source-related characteristics similar to ocean-island basalts whereas metaluminous types display characteristics similar to bulk continental crust. Results of experimental investigations by other workers in which A-type metaluminous granite liquids were produced through melting of charnockitic rocks representative of the Grenville-age basement of the Virginia Blue Ridge support derivation of the metaluminous magmas from sources of similar composition. Sm-Nd isotopic data for

the Robertson River Igneous Suite have epsilon-Nd values (calculated for crystallization ages of 730 Ma as indicated by U-Pb isotopic analyses of zircon) ranging from -0.1 to +2.1 and model ages from 1.1 to 1.3 Ga. These model ages overlap with the age range of basement in the Blue Ridge. Epsilon-Nd values increase with decreasing age within the suite. Older metaluminous units have epsilon-Nd values indicative of interaction with evolved crust (-0.1 to +1.4) but the younger peralkaline units show more positive epsilon-Nd values (+1.8 to +2.1) that suggest either a change in source characteristics or degree of crustal contamination with time. Collectively, these data indicate that abundant metaluminous magmas associated with the earliest stages of Laurentian rifting were produced dominantly through melting of local continental crust and that such melts diversified in composition largely through crystal fractionation. Coeval peralkaline magmas, produced during the waning stages of this period of regional magmatic activity, were generated through melting of more geochemically primitive sources; however, the magmas evolved compositionally through similar mechanisms. The mode of occurrence, type and range of compositions, and inferred petrogenesis of the supersuite are similar to those of anorogenic, encratonic granitoids documented worldwide. The Laurentian Appalachian supersuite represents a significant, long-lived, temporally episodic period of magmatism that ended with encratonic rifting but not development of oceanic crust. As such, the rocks are indicative of processes operative during the earliest, pre-drift stages of Laurentian extension.

THE ROLE OF RECURRENT TECTONICS IN THE FORMATION OF THE NEMAHA UPLIFT AND CHEROKEE-FOREST CITY BASINS AND ADJACENT STRUCTURAL FEATURES IN EASTERN KANSAS AND CONTIGUOUS STATES, USA

F.W. WILSON and P. BERENDSEN, *Kansas Geological Survey, University of Kansas, Lawrence, KS 66074, tel. 913-864-4991, e-mail: pieter_berendsen@msmail.kgs.ukans.edu*

We elaborate on an old hypothesis suggesting that once the early-formed crust of the Earth attained sufficient buoyancy, thickness, and strength to react in brittle fashion, it was broken into semi-rectangular blocks by tensional stresses, perhaps associated with development of its equatorial oblateness. The roughly orthogonal fractures bounding the crustal blocks are spaced more or less evenly by dissipation of stresses between adjacent megafractures, depending upon the strength of the local crust. We further propose that once the primordial crust was broken, the fractures became the loci of stress relief for whatever combinations of horizontal, vertical, and shear stresses acting on them throughout geologic time. Because the through-crustal fractures (including the outlines of meteorite impact craters of whatever age) continue to be active, they propagate upwards to the present surface through succeeding layers and are manifested by stream patterns which reflect faults, flexures, and joints; outcrop anomalies; and even subtle tonal changes on remotely-sensed images. Examples are the Chesapeake, Bolivar-Mansfield faults, (Wilson and McCauley, 1989) which have been mapped in Missouri and are traced on trend into the Kansas subsurface by means of major stream lineaments or divides and other more subtle features. Other northwest- and northeast-trending structural zones are likewise recognized (Blair and others, 1992). The pattern or mapped faults and the interpretation of stream patterns suggests that many are wrench faults, and reversed movement at various times depending on the direction of applied horizontal compressive stresses and the orientation of the resisting or passive blocks. We postulate that the stresses originated at the eastern margins of the North American craton during continent-continent collisions beginning during Grenvillian or earlier times, and continued during the Taconian, Acadian, Appalachian-Alleghenian. Major episodes affected the midcontinent during the Ouachitan-Wichitan-Marathon orogenies, and with somewhat lesser effects during later geologic times to the present. The stresses are assumed to have been transmitted primarily via Precambrian basement rocks and the overlying Cambro-Ordovician through Mississippian carbonate rocks.

Our analysis and interpretation of the tectonic history of Eastern Kansas and surrounding states begins with the period after emplacement of the mafic igneous rocks of the Midcontinent Rift at about 1,100 Ma. The Ozark Dome to the east in Missouri is an older, positive structural element. Extending westerly from the Ozark dome the Chautauqua Arch and Central Kansas Uplift are probably also pre-rift positive structural

elements. The area northwest of the Ozark dome was a broad peneplaned surface of low relief which was cut by the newly-formed Midcontinent Rift. North of the Fall River Tectonic Zone (FRITZ) considerable thicknesses of clastic sediments were deposited in rift-flanking basins. The Forest City Basin, containing about 4,000 feet of Cambro-Ordovician through Permian sedimentary rocks, is separated from the younger Cherokee Basin by a low Pennsylvanian divide known as the Bourbon Arch. The basins are bounded on the west by the Nemaha Uplift and on the east by the Ozark Dome.

As the major collisional forces rotated to the SW and closer to the referenced area, it caused closure of and considerable thrusting toward the W, NW, and finally N, during the formation of the Ouachitas-Wichitas. We postulate that these stresses caused the entire width of the NNE-trending Nemaha Uplift (not just the prominent Humboldt Fault on its east flank) to be activated as a massive left-stepping, left-lateral wrench fault zone. The Nemaha Uplift was finally overtopped by relatively undisturbed early Permain sediments of about the same age as the last strata cut by a series of en echelon faults, indicating left-lateral, northerly-directed faulting, in north-central Oklahoma.

The NE-trending Webb City-Osceola lineament parallels the east edge of the Cherokee-Forest City basins and continues to the SW as the Miami Trough in extreme SE Kansas and NE Oklahoma (Brockie and others, 1968). Other NE-trending structural elements include a subtle lineament near the center of the Cherokee-Forest City basins, which we term the Chanute-Kansas City Trend. This lineament is marked by low monoclinal folds and short segments of streams and appears to have had an influence upon the distribution of oil and gas in the area. The Lampe-Mansfield structural zone in western Missouri and northern Arkansas is marked by a series of NE-trending faults.

The NW-trending FRITZ is the southernmost important structural zone and passes through the Tri-State lead-zinc district (Bendelari Trough). Mafic rocks and rift-related clastic sedimentary rocks occur at the basement surface only north of the FRITZ. To the north the Neosho River lineament coincides with a prominent NW trending stream segment by the same name. It is prolonged southeastward from its intersection with the Chanute-Kansas City lineament as a narrow, linear stream divide which seems to coincide with the Nashville-Carthage Sag in Missouri. North of this, at approximately the same spacing, are a discontinuous series of NW trending streams which seem to trace the trend of the Bolivar-Mansfield Fault in Kansas. Still further north in Kansas, again at the same spacing, is the prologation of the Kansas City-Centerview trend in Missouri. On it is the enigmatic McLouth oil and gas field which is associated with complex geophysical anomalies. A prominent NW-trending lineament and geophysically defined gravity anomaly, referred to as the Missouri gravity low (Arvidson and others, 1982), offsets and separates and Iowa and Kansas segments of the Mid-continent Rift and is traced to the SE through Missouri and beyond.

We believe we have demonstrated the importance of recurring tectonics along preexisting basement fracture systems in the formation of the Nemaha Uplift, the Ozark dome, and the Cherokee-Forest City basins in eastern Kansas and western Missouri. These tectonic episodes coincided with major continent-continent collisional events at

the eastern and southeastern margins of the continent and follow closely the outline of epeirogenic events described by Ham and Wilson (1967).

References

Arvidson, R.E., Guinness, E.A., Strebeck, J. W., Davies, G. ZF., and Schulz, K.J., 1982: EOS, v. 63, p. 261-265.

Blair, K.P., Berendsen, P., and Seeger, C.M., 1992: U.S. Geological Survey, Miscellaneous Field Studies Map, Map MF-2125_C (With text).

Brockie, D.C., Hare, E.H., Dingess, P.R., 1968: in Ore deposits of the United States, 1933-1967, J. D. Ridge, ed.: AIME, New York, p. 400-430.

Ham, W.E., and Wilson, J.L., 1967: American Journal of Science, v. 265, p. 332-407.

Wilson, F.W., and McCauley, J.R., 1989: U. S. Geological Survey Open-File Report 89-169, p. 45 (Abstract).

COCORP SOUTHWESTERN OKLAHOMA SIESMIC LINES REVISITED

R.A. YOUNG, *School of Geology and Geophysics, University of Oklahoma, Norman, OK 73019, tel 405-325-5753; email:ryoung@ou.edu*
A.C. LAMBERT, *Phillips Petroleum Company, Bartlesville, OK 74004, tel. 918-661-0423*

The Consortium for Continental Reflection Profiling (COCORP) seismic reflection lines 2-2A and 5-5A were acquired in 1979 and 1980 in order to probe the deep crustal structure of the Wichita Mountains and the adjacent portions of the Hardeman basin, to the south, and the Anadarko basin to the north. The interpretation of these lines by Brewer et al. (1983) has remained the standard for discussion of crustal structure in this area. The mid-crustal features at depths of 2-10 km in the Wichita Mountains Frontal Zone (WMFZ), however, were indistinctly imaged by the COCORP lines because acquisition and processing focused on deeper features. A subsequent program of oil industry-sponsored seismic investigation along short lines oriented perpendicular to the local structural trend greatly improved the image of the WMFZ. Many people familiar with the COCORP lines have not seen the lines owned by Seismic Exchange, Inc., though, as the latter have not been published.

The present study examines three of the SEI lines that fall within 3 miles of COCORP lines 2-2A and 5-5A. Unpublished COCORP line drawings are remarkable in identifying many of the mid-crustal features seen much more clearly on the SEI data. A rapid change in configuration of basement blocks and Pennsylvanian sediments along strike is evident. The clarity of the seismic data details layering within the igneous basement, block rotations and indications of overturned folds, major depositional centers and a half graben developed in the "granite wash", and syntectonic depositional features.

Proceedings of the International Conferences on Basement Tectonics

1. R. Mason (ed.): *Basement Tectonics 7.* Proceedings of the Seventh International Conference on Basement Tectonics, held in Kingston, Ontario, Canada, August 1987. 1992 ISBN 0-7923-1582-0
2. J. Bartholomew, D.W. Hyndman, D.W. Mogk and R. Mason (eds.): *Basement Tectonics 8 – Characterization and Comparison of Ancient and Mesozoic Continental Margins.* Proceedings of the Eighth International Conference on Basement Tectonics, held in Butte, Montana, USA, August 1988. 1992 ISBN 0-7923-2088-3
3. M.J. Rickard, H.J. Harrington and P.R. Williams (eds.): *Basement Tectonics 9 – Australia and Other Regions.* Proceedings of the Ninth International Conference on Basement Tectonics, held in Canberra, Australia, July 1990. 1992 ISBN 0-7923-1559-6
4. R.W. Ojakangas, A.B. Dickas and J.C. Green (eds.): *Basement Tectonics 10.* Proceedings of the Tenth International Conference on Basement Tectonics, held in Duluth, Minnesota, U.S.A., August 1992. 1995 ISBN 0-7923-3342-9
5. O. Oncken and C. Janssen (eds.): *Basement Tectonics 11 – Europe and Other Regions.* Proceedings of the Eleventh International Conference on Basement Tectonics, held in Potsdam, Germany, July 1994. 1996 ISBN 0-7923-3797-2
6. J.P. Hogan and M.C. Gilbert (eds.): *Basement Tectonics 12 – Central North America and Other Regions.* Proceedings of the Twelfth International Conference on Basement Tectonics, held in Norman, Oklahoma, U.S.A., May 1995. 1998 ISBN 0-7923-5192-4

KLUWER ACADEMIC PUBLISHERS – DORDRECHT / BOSTON / LONDON